GRUMMAN AEROSPACE CORPORATION

REPORT RM-799

AERODYNAMIC HEATING RATE DISTRIBUTIONS INDUCED BY TRAILING EDGE CONTROLS ON HYPERSONIC AIRCRAFT CONFIGURATIONS AT MACH 8

August 1984

RESEARCH & DEVELOPMENT CENTER

NASA TM-87453

DRH/LANGLEY

REPORT RM-799

AERODYNAMIC HEATING RATE DISTRIBUTIONS INDUCED BY TRAILING EDGE CONTROLS ON HYPERSONIC AIRCRAFT CONFIGURATIONS AT MACH 8

August 1984

prepared by

Louis G. Kaufman II
Aerosciences Directorate

Grumman Aerospace Corporation
Research and Development Center
Bethpage, New York 11714

and

Charles B. Johnson
Langley Research Center
National Aeronautics and Space Administration
Hampton, VA 23365

Approved by: Richard A. Scheuing
Richard A. Scheuing, V.P.
Director, R&D Center

N85-22370 #

ABSTRACT

Aerodynamic surface heating rate distributions in three dimensional shock-wave boundary-layer interaction flow regions are presented for a generic set of model configurations representative of the aft portion of hypersonic aricraft. Heat transfer data were obtained using the phase change coating technique (paint) and, at particular spanwise and streamwise stations for sample cases, by the thin-wall transient temperature technique (thermocouples). Surface oil flow patterns are also shown. The good accuracy of the detailed heat transfer data, as attested in part by their repeatability, is attributable partially to the comparatively high temperature potential of the NASA-Langley Mach 8 Variable Density Tunnel. The data are well suited to help guide heating analyses of Mach 8 aircraft, and should be considered in formulating improvements to empiric analytic methods for calculating heat transfer rate coefficient distributions.

CONTENTS

ILLUSTRATIONS

ILLUSTRATIONS (continued)

ILLUSTRATIONS (continued)

ILLUSTRATIONS (continued)

ILLUSTRATIONS (continued)

ILLUSTRATIONS (continued)

1. INTRODUCTION

Thermal loads on the surfaces of high speed vehicles can be changed greatly when shock waves interact with the boundary layer flows over these surfaces. The resulting surface heating rate distributions may be far different from those anticipated neglecting shock-wave boundary-layer interactions. Such interactions are recognized widely as an important problem area in the design of high speed aircraft, and have prompted many investigations of shock-induced separated flows (e.g., Ref. 1-3). An empirical base is being established to develop simple analytic methods that can be used to estimate effects of three-dimensional shock-wave boundary-layer interactions. The data described herein are part of this empirical base, which can be used to compare experimental results with results calculated using existing analytic methods (Ref. 4 and 5).

The particular problem addressed in this report is three-dimensional flow separation caused by trailing edge controls on basic configurations representative of wing and fuselage sections of hypersonic aircraft. Impingement of a shock wave, caused by a trailing edge control, on the boundary layer on an adjacent surface can result in extensive regions of increased thermal loads, which are much larger than predictable using either inviscid or two-dimensional flow analyses (Ref. 5-8). The increased thermal loads can compromise an aircraft design. Although these effects are important to the design of high speed aircraft, there were few data of general applicability to three-dimensional separated flows and no completely satisfactory analytic methods for predicting general three-dimensional, inviscid-viscid, interaction flow effects (Ref. 9-11).

The character of the boundary layer is one of the most important factors influencing interactions between shock waves and boundary layers (Ref. 12). Wind tunnel models of complete aircraft configurations frequently have laminar or transitional boundary layers, unlike the actual flight configurations which have predominately turbulent boundary-layer flows over their surfaces. This discrepancy, caused by the limitations of hypersonic wind tunnels on model size, make questionable the validity of extrapolating small scale model data to full scale flight vehicles.

An experimental program was designed to increase the data base required to understand three-dimensional flow interactions - those pertinent to elevon deflections on high speed aircraft. Instead of a complete configuration, a simple "wing-elevon" model was used to simulate the wing trailing edge control, and aft fuselage portion of a "typical" hypersonic aircraft. (See Fig. 1 and Ref. 5). The chord of the semispan wing-elevon model was several times larger than that which could be used for a complete aircraft configuration in the same wind tunnel. Therefore, chord-length Reynolds numbers comparable to those anticipated for flight vehicles could be achieved and more detailed data could be obtained in the interaction flow region.

Fundamental shapes (planar and cylindrical surfaces) were chosen to make the data as generally applicable as possible and to increase their usefulness in guiding analyses of three-dimensional interaction flow regions with a minimum of extraneous effects. Sharp leading-edge flat-plate wings with leading-edge sweep angles of 0^{o}, 50^{o} and 70^{o} were tested at 0^{o} angle of attack. Regions of boundary-layer transition on these wings are parallel to the sharp leading edges, and frequently are as extensive as the upstream length of laminar flow for the flow conditions considered herein (Ref. 13). For the 70^{o} swept wings, the boundary layer at the elevon hinge line location is turbulent on the inboard portion of the wing (near the root chord) and transitional or laminar on the outboard portion (near the wing tip), (Ref. 14). The character of the boundary layer has a strong influence on flow separation (Ref. 12) and so wing sweep affects separated flow regions strongly. Planar and cylindrical center bodies were used to provide data for basic three-dimensional interaction flows (Ref. 5).

Experiments were conducted in the NASA Langley, Mach 8, Variable Density Tunnel to obtain fundamental three-dimensional interaction flow data for conditions simulating flight of hypersonic aircraft. The root chord Reynolds numbers were approximately 20 million (comparable to Mach 8 flight of: a Shuttle at 110,000 ft altitude, a research airplane at 80,000 ft, or a missile at 50,000 ft). Presented in this are sample photographic data (frames from oil flow and phase change coating motion pictures), and surface heating rate distributions, obtained using both the phase change coating (paint) technique and the transient temperature thin wall (thermocouple) technique, for many wing-trailing-edge-control model configurations.

The same basic model has been used in the Langley 20-in. Mach 6 Tunnel to

obtain photographic, pressure and heating rate data (Ref. 15). The Mach 6 data and the present Mach 8 data substantially enlarge the data base required to understand three-dimensional interaction-flow effects on high speed aircraft. The high temperature potential of the Mach 8 tunnel enables obtaining quite accurate heat transfer data; the data presented herein should be used to improve empiric analytic methods that have been proposed for predicting three-dimensional interaction-flow effects (Ref. 4 and 5).

2. SYMBOLS

g	width of gap between end plate and inboard edge of elevon, in.
HL	hinge line
h	heat transfer coefficient, BTU/ft^2 sec°R
M	Mach number
P	ratio of surface pressure to free-stream pressure, p/p_∞
p	pressure, psia
Re_c	Reynolds number based on free-stream conditions and wing root chord length (25.25 in.)
T	temperature, °R
T/C	thermocouple
t	time, sec
x	surface streamwise distance measured downstream from the wing apex (or wing leading edge for the unswept wing), in.
y	spanwise distance measured outboard from the inboard location of the trailing edge control, in.
z	distance measured upward from wing surface, in.
γ	ratio of specific heats for air (taken as 1.4 herein)
ϵ	elevon deflection angle, deg
θ	elevon shock-wave angle, deg
Λ	wing sweepback angle, deg
ρ	density of silicone rubber portions of model, kg/m^3

Subscripts:

aw	adiabatic wall
i	initial
inv	value calculated for inviscid flow, neglecting separation
pc	phase change of paint coating
0	stagnation conditions of free-stream tunnel flow
1	local undisturbed flow conditions over wing surface
∞	free-stream flow conditions

3. EXPERIMENTAL PROGRAM

3.1 MODEL DESIGN CRITERIA

The half model used for these experiments is representative of the aft portion of a winged flight configuration with trailing-edge controls (Fig. 1 and Ref. 15). This approach has the advantage that, for a given test facility, the wing chord for the model can be several times larger than that for a corresponding complete aircraft configuration. More detailed data may be obtained in the interaction flow region, the resulting larger root-chord Reynolds number more nearly equals that for flight vehicles, and the character of the boundary layer on the model surfaces resembles closely that expected for flight vehicles. Simulating the character of the boundary layer is particularly important in regions where separated flow may occur (Ref. 1, 7 and 12). On a swept wing, the boundary layer ahead of the trailing edge control may be characteristically turbulent on the inboard portion of the wing and laminar on the outboard portion, resulting in a complex flow structure with significant effects on surface loads (Ref. 13 and 14).

3.2 TWO TYPES OF 3-D INTERACTION FLOWS

Two types of 3-D interaction flows are depicted in Fig. 2. For small elevon deflection angles the elevon-generated shock emanates from the hinge line, whereas for large deflection angles the flow separates from the wing surface upstream of the hinge line and a shock emanates from the separation line (Fig. 2). In both of these cases, the extent of the disturbance on the adjacent end-plate (fuselage) surface is far larger than would be anticipated using inviscid-flow analyses (Ref. 5). The extent of the disturbed flow on the end plate surface is shown by oil-accumulation lines indicated in Fig. 2.

A similar 3-D interaction flow problem that has received much attention is that caused by fin generated shock waves incident to a boundary layer on an adjacent surface (Ref. 4 and 16). The prime difference is the existence of a boundary layer on the wing surface upstream of the elevon. The similarity in these 3-D interaction flows prompted the use of data from both types of flows in developing methods for estimating 3-D interaction flow effects (Ref. 4 and 5).

3.3 MODEL DESCRIPTION

Three half wing models were fabricated to investigate wing sweep effects. The flat plate wings have leading edge sweepback angles of 0, 50, and 70° and all have machined sharp (11.2^{o}) leading edges. The stainless steel half wing models have attachable stainless steel center bodies (simulating aft fuselage sections) and various trailing edge controls. Both a planar (end plate) and a cylindrical center body are attachable to the half wings. Thus, data could, and were, obtained both without and with inboard body effects.

The end plate has a machined sharp leading edge and a sweepback angle of 70^{o}. It is aligned in the free stream direction and may be set either flush to or with a 1/4 in. (0.635 cm) gap from the inboard side of the trailing edge control. The cylindrical body, when attached to the wing, is adjacent to the inboard side of the trailing edge control.

The wings have attachable trailing edge controls, either elevons or spoilers. There are two different chord length ("long" and "snort") elevons that can be set at (flow compression) deflection angles from 0 to 30^{o} in 5^{o} increments. There are two spoilers ("high" and "low") that are attachable at the elevon hinge line location.

A sketch of a wing-elevon-end plate model configuration is shown in Fig. 3. The coordinate system used herein is indicated in the same figure. Note that "x" is the streamwise distance measured from the wing apex on the surface of the wing and elevon. Thus, the"x" value of a location on the elevon surface does not vary with elevon deflection angle. Outlines of wing-elevon-end plate configurations are shown in Fig. 4. The "long" chord elevon is shown, the "short" chord elevon has the same span but a chord length of 3.5 in. instead of 5.5 in.

The wings, elevons, and end plate have replaceable stainless steel and silicone-rubber inserts. The stainless steel inserts were instrumented with thermocouples to enable obtaining accurate and detailed heating rate distributions along specific streamwise and vertical lines on wing-elevon model configurations using the thin-wall transient-temperature technique. Thermocouples were closely spaced along streamwise lines on the wing and elevon inserts (at y = 2.375 in.), and along a vertical line on the end plate

insert (at x = 24.25 in.). The locations are indicated by dot-dash lines in Fig. 4. The silicone rubber inserts were used to obtain surface heating rate distributions using the phase change coating technique. These surface heat transfer results are compared with the thermocouple results at the same spanwise and chordwise stations.

The cylindrical center body, sketched in Fig. 5 and shown in the photograph in Fig. 6, is used only on the 70^{o} swept wing. The ridge line of the cylinder is at a 10^{o} angle from the flat plate wing surface.

High and low spoilers, with forward faces at the same location as the elevon hinge line, were used on all three half wing models. The high spoiler extends one inch above the wing surface, the low spoiler extends 0.64 inches above the flat plate wing surface (the same ratio as the elevon chord lengths: 3.5/5.5 = 0.64/1.0). The stainless steel spoilers are not instrumented.

The model configurations tested are indicated in Table 1. The gap between the end plate and the inboard edge of the trailing edge control is 1/4 in. In other cases, the trailing edge control was sealed to the center body. In all cases, the control was sealed to the wing surface.

Table 1 Model Configurations

Wing Sweep, deg	Center Body	Controls
0	None	Elevons & spoilers
	End plate	Elevons & spoilers
	End plate with gap	Elevon
50	None	Elevons & spoiler
70	None	Elevons & spoilers
	End plate	Elevons & spoilers
	End plate with gap	Elevons
	Cylindrical	Elevons & spoilers

3.4 TUNNEL & FLOW CONDITIONS

The experiments were conducted in the NASA Langley Mach 8 Variable Density Tunnel in Hampton, VA. It is a blowdown wind tunnel with a closed circular test section 18 in. in diameter. The tunnel can provide Mach 8 free stream flows for unit Reynolds numbers ranging from 0.20 to 9.5 million per foot.

The tunnel has a model injection system in a vacuum chamber beneath the test section (Fig. 7 and 8). Full injection to tunnel centerline takes 0.8 sec, but the model passes through the tunnel wall shear layer, where it experiences nonuniform flow heating, in just 0.2 sec.

In order to have high Reynolds number flows, the highest tunnel operating stagnation pressure (approximately 2600 psia) was used for all these test runs. Nominal values of the tunnel stagnation and free stream flow conditions are listed in Table 2. The Reynolds number is for a root chord of 25.25 in.

Table 2 Tunnel Flow Conditions

p_o	≈	2600 psia
T_o	≈	1500 °R
M_∞	≈	8
p_∞	≈	0.266 psia
T_∞	≈	109 °R
Re_c	≈	20×10^6

3.5 TEST PROCEDURE

For each tunnel run, the tunnel flow was established before injecting the model into the test section. Strip recorders were used to monitor and record tunnel stagnation conditions. These values varied slightly from run to run but remained essentially constant during each tunnel run. Strip recorders were also used to monitor several thermocouple temperature-time readings when the thermocouple instrumented inserts were used. Closed circuit television was used to monitor the profile schlieren image for all thermocouple test

runs. Closed circuit television was also used to monitor all phase change coating and oil flow test runs. These monitoring devices were used in determining when the model should be ejected from the tunnel flow.

There are a total of 60 thermocouples in the wing, elevon and end plate inserts. Temperatures were recorded 40 times per second for each thermocouple. These temperature-time traces were used in the thin-wall transient-temperature technique (Ref. 17) to obtain accurate aerodynamic heating rate distributions along a streamwise line on the wing and elevon surfaces and along a vertical line on the end plate surface.

The model configurations tested and the type of data obtained on each are indicated in Table 3. In addition to the data indicated in Table 3, profile schlieren photographs were obtained for thermocouple-instrumented, wing-control configurations without center bodies.

Surface flow streamline shapes, the extent of separation, and the location of reattachment were determined using motion pictures of a splattering of oil droplets on the model surfaces. Motion picture cameras and a closed circuit television camera were mounted to view the model in the tunnel test section (Fig. 9). The model was prerubbed with silicone oil. Then a mixture of titanium dioxide, silicone oil and a small percentage of oleic acid was splattered on the model surfaces. The model was then injected into the established Mach 8 tunnel flow and the movement of the oil droplets monitored and recorded, on motion picture film, until a steady flow pattern was firmly established. The model was then ejected from the tunnel flow. Still photographs were taken of the final oil flow pattern, which was also traced on paper overlayed on the model surfaces after the test run.

The same cameras (Fig. 9), with color motion picture film, were used to obtain surface heating rate distributions using the phase change coating technique (Ref. 18 and 19). A thin coating of temperature sensitive paint was sprayed on the model (different phase change temperature paints for the wing, elevon and center body were used). Grids were then scribed on the painted model surfaces and surface temperatures were recorded. The tunnel flow was established and the model injected into the flow. The progression of the melt line with time was monitored, using the television cameras, and recorded by the motion picture cameras. The model was ejected from the tunnel flow once all the paint on the silicone rubber inserts had melted.

Table 3 Mach 8 Test Configurations & Data

Wing L. E. Sweep	Trailing Edge Control	Center Body			
		None	End plate	E. P. Gap	Cylinder
0	0L	P,T	0,P		
	5L	P,T	0,P		
	10L	0,P,T	0,P		
	15L	0,P,T	0,P		
	20S	0,P	0,P		
	20L	T			
	25S	0,P	0,P	0,P	
	30S	0,P			
	LoSp	0,P	0,P		
	HiSp	0,P	0,P		
50°	0L	P			
	10L	P			
	20S	P			
	HiSp	0,P			
70°	0L	P	0,P	T	0,P,T
	5L	P	0,P,T		0,P,T
	10L	P	0,P,T		0,P,T
	15L	P	0,P,T		0,P,T
	20S	0,P	0,P	P	0,P
	20L	0,P			T
	25S	P	P		0,P
	30S		0,P	0,P	
	LoSp	0,P	0,P		0,P
	HiSp	0,P	0,P		

Control key: Number with "L" or "S" indicates deflection angle and "Long" or "Short" elevon. Low Spoiler and High Spoiler are denoted by LoSp and HiSp.
Data key: O = Oil flow, P = Phase change, T = Thermocouple

4. EXPERIMENTAL RESULTS

The trailing edge control (elevon angle or spoiler height) is dominant in affecting the surface aerodynamic heating rate distributions for given free stream flow conditions. Therefore, results are grouped for each trailing edge control. Variations in surface heating rate distributions caused by different center bodies and wing sweep are described for each trailing edge control. Data obtained for a particular configuration are usually presented in proximity. For each trailing edge control, results obtained on the wing and elevon surfaces are presented before showing the same type of data results on the end plate or cylindrical center body surfaces.

For each trailing edge control and wing sweep, data are presented, when available, for: no center body, cylindrical center body, end plate with gap, and end plate. Oil flow results are shown prior to the phase change coating and thermocouple results. Tracings of melt lines from many motion picture frames of the phase change coating on a configuration are superimposed to obtain isotherms, contours of equal aerodynamic heating rates, for the configuration. When available, these are compared with heating rate distributions obtained using the thermocouple generated data for selected configurations.

Data presented for various model configurations are indicated in Table 4. Sample frames of the oil flow and phase change coating motion pictures are presented only for selected configurations. Results based on examination of the color motion pictures for all of the configurations are included in the discussion of the experimental results. Constant aerodynamic surface heat transfer coefficient contours, hereafter referred to simply as "contours", are presented for all configurations for which they were obtained.

The true view of the elevon surface is shown instead of projecting the deflected elevon surface onto the plane of the wing. The projection of the trailing edge control on the center body is indicated. In certain instances, the words "hot" and/or "cold" are shown on the contour plots to indicate regions of relatively high and/or relatively low surface heating.

4.1 NO TRAILING EDGE CONTROL

The phase change coating faded gradually and evenly over the entire

Table 4 Configuration Data Figure Numbers

TRAILING EDGE CONTROL	WING SWEEP 0°	50°	70°	CENTER BODY NONE	CYLINDER	E.P.w GAP	END PLATE	FIGURE NUMBERS
None	X			X			X	10-13
		X		X				14
			X	X	X	X	X	15-23
5° Long	X			X			X	24-28
			X	X	X		X	29-38
10° Long	X			X			X	39-44
		X					X	45
			X	X	X		X	46-54
15° Long	X			X			X	55-60
			X	X	X		X	61-69
20° Short	X			X			X	70-75
		X		X				76
			X	X	X	X	X	77-84
20° Long	X			X				85
			X		X			86
25° Short	X			X		X	X	87-97
			X	X	X		X	98-101
30° Short	X			X				102-104
			X			X	X	105-112
Low Spoiler	X			X			X	113-120
			X	X	X		X	121-135
High Spoiler	X			X			X	136-143
		X		X				144,145
			X	X			X	146-152

surface. The all melted stage was attained 6.10 sec after injecting the model into the tunnel flow. This corresponds to an aerodynamic heat transfer coefficient of 0.0047 BTU/ft^2 sec ^{o}R (Fig. 10). The phase change coating and thermocouple results for the same configuration are compared in Fig. 11.

When the end plate was added to the configuration, oil flows indicated all streamwise flow on the wing, elevon and end plate surfaces. Phase change data for this configuration are given in Fig. 12 and 13. Regions of relatively high and low aerodynamic heating rates are indicated by "hot" and

"cold". Phase change results for the 50° swept wing are shown in Fig. 14. Phase change results for the 70° swept wing are given in Fig. 15.

Oil flows for the 70° swept wing with the cylindrical center body showed an outboard deflection of the surface streamlines on the inboard portion of the wing (Fig. 16). Oil accumulated along the shoulder of the cylindrical body, but was swept off the ridge line (Fig. 17). Phase change results for the same configuration are given in Fig. 18 and 19. As might well be expected, highest heating occurred along the ridge line of the cylindrical body. The paint did not melt on the vertical sides of the cylindrical body (Fig. 20). Phase change and thermocouple results on the wing and elevon surfaces are compared in Fig. 21.

All surface flow was streamwise with the end plate on the 70° swept wing. Phase change coating and thermocouple data are given in Fig. 22 and 23. Oil flows for this configuration indicated streamwise surface streamlines on the end plate, wing and elevon surfaces. Phase change results for the end plate moved 1/4 in. away from the elevon are essentially the same as for the end plate adjacent to the elevon, as would be expected.

4.2 5° LONG ELEVON

Phase change coating results indicate somewhat higher heating rates on the outboard portions of the slightly deflected elevon (Fig. 24). Heating rates from the phase change and thermocouple test runs are compared in Fig. 25. They agree.

Oil flows of the wing and elevon surfaces show all streamwise flow with the end plate attached to the unswept wing. However, there is an oil accumulation line on the end plate surface (Fig. 26). This line is at a considerably higher angle then the inviscid shock wave angle for a 5° deflection, indicating a larger region of disturbed flow on the end plate surface than would be calculated using inviscid flow theory. Phase change coating results for this configuration are given in Fig. 27 and 28.

Heating rate distributions for the 5° elevon on the 70° swept wing are shown in Fig. 29. In this case, higher heating occurred on the inboard portion of the elevon.

Results of oil flow motion pictures show regions of high shear on the wing and elevon surfaces when the cylindrical center body is attached (Fig.

30). An oil accumulation line is apparent on the planar surface of the cylindrical body close to the elevon (Fig. 31). Highest heating occurs along the ridge of the cylindrical center body (Fig. 32 and 33). Phase change coating and thermocouple data on the wing surface are compared in Fig. 34.

The cylindrical center body was replaced by the end plate. Oil flows indicated all streamwise flow on the wing, elevon and end plate surfaces. Unfortunately, the top camera was not in clear focus. It appears, however, that the elevon and wing surface heat transfer coefficients were approximately 0.0045 BTU/ft^2 sec °R for both surfaces (Fig. 35). Heating rates on the end plate surface are indicated in Fig. 36. Thermocouple data for the wing, elevon and end plate surfaces are given in Fig. 37 and 38. The paint results on the wing surface are approximately 10% too high (compare Fig. 35 and 37).

4.3 10° LONG ELEVON

Oil flows showed no indication of separation caused by the 10° elevon. All surface streamlines were streamwise. There were, however, uneven heating rates on the elevon surface (Fig. 39). Thermocouple data for the wing and elevon are compared with the phase change data in Fig. 40.

The end plate slightly changed the oil flow pattern. High shear was evidenced in the wing-end plate corner (Fig. 41 and 42). An oil accumulation line formed far outboard of the projection of the elevon induced shock wave (Fig. 42). Surface heating rate distributions are shown in Fig. 43 and 44.

The 50° swept wing exhibited a far different surface heating pattern (Fig. 45). This discrepancy is yet to be explained. Surface heating rate distributions on the 10° elevon and 70° swept wing configuration are shown in Fig. 46.

Regions of relatively high shear on the wing and 10° elevon surfaces, with the cylindrical body attached to the wing, are shown in Fig. 47. Oil accumulation lines on the cylindrical body surface are shown in Fig. 47 and 48. Surface heating rate distributions for the same configuration are shown in Fig. 49 and 50. The phase change coating results are compared with thermocouple results in Fig. 51.

Oil flows indicated streamwise flow on the 70° swept wing, 10° elevon and end plate surfaces. Bad light reflections made the phase change contours

nearly indistinguishable (Fig. 52). Thermocouple results are plotted in Fig. 53 and 54.

4.4 15° LONG ELEVON

Oil flows on the unswept wing and 15° elevon showed strictly streamwise flow and no separation ahead of the hinge line. Heating distributions obtained using the phase change coating technique are shown in Fig. 55, and compared with thermocouple data in Fig. 56.

Planform and profile sketches of oil flow motion pictures with the end plate on the unswept wing - 15° elevon are shown in Fig. 57 and 58. In regions of high shear the oil is wiped clean off the surface. The oil accumulation line on the end plate surface indicates a far more extensive region of disturbed flow than predicted by inviscid flow theory. Phase change coating surface heating rate distributions for this configuration are indicated in Fig. 59 and 60. In Fig. 60, contours 6 and 7 near the elevon are coincident with contour 5.

Phase change results for the 15° elevon on the 70° swept wing are shown in Fig. 61. Oil flows indicate purely streamwise flow and no regions of separated flow. Sketches made from oil flow motion pictures for the 70° wing-15° elevon-cylindrical body configuration are shown in Fig. 62 and 63. Again, a high shear region was observed at the wing-body junction. Surface heating rate distributions obtained from phase change coating motion pictures are shown in Fig. 64 and 65. Thermocouple heat transfer rate data along a streamwise line on the wing and elevon surfaces are indicated in Fig. 66.

Planform oil flows exhibited streamwise flow on the wing and elevon surfaces when the end plate was attached to the model. There was no evidence of separated flow. However, on the end plate surface, distinctive oil accumulation lines were observed (Fig. 67). Heating rates along a streamwise line on the wing and elevon surfaces are indicated in Fig. 68 and heating rates along a vertical line on the end plate surface are indicated in Fig. 69.

4.5 20° SHORT ELEVON

Oil flow on the unswept wing and 20° short elevon configuration showed simply streamwise flow and no evidence of separation. Phase change surface heat transfer rate distributions are shown in Fig. 70.

Oil flows exhibit high shear in the corner region between the wing-elevon and end plate (Fig. 71 and 72). A photograph of the end plate surface taken after the oil flow test run is shown in Fig. 73. Phase change heat transfer rate distributions on the unswept wing, elevon and end plate surfaces are given in Fig. 74 and 75.

Phase change data for the 20° short elevon on the 50° and 70° swept wings are shown in Fig. 76 and 77. The heating rates are very similar for both configurations. Oil flows showed all streamwise flow with no separation for both configurations.

Oil flows for the 70° swept wing, 20° short elevon and cylindrical center body configuration are shown in Fig. 78 and 79. Some oil accumulated at the center of the hinge line and there was a distinctive streamwise band of oil on the elevon surface downstream of the hinge line (Fig. 78). Surface streamlines on the cylindrical surface are sketched in Fig. 79. Phase change surface heating rate distributions for this configuration are given in Fig. 80 and 81.

The 70° swept wing with the 20° short elevon was tested with the end plate placed 1/4 in. away from the elevon. Phase change data results for this configuration are presented in Fig. 82 and 83.

The 70° wing was also tested with the end plate adjacent to the 20° short elevon. Oil flows showed no evidence of separation on the wing surface. Bad light reflections prevented good views of the aft portion of the elevon surface. The same problem occurred for the phase change coating results. The few results that were discernable are shown in Fig. 84.

4.6 20° LONG ELEVON

The 20° longer chord elevon was also tested on the unswept and 70° swept wings. The 70° wing had the cylindrical center body adjacent to the elevon. Streamwise distributions of heating rates along a line on the wing and elevon surfaces, obtained from thermocouple data, are given in Fig 85 and 86.

4.7 25° SHORT ELEVON

Small "bubbles" of separated flow were observed on the unswept wing just ahead of the 25° elevon (Fig. 87). The heating rate distributions had somehwat higher values in these same regions. As a check on the reliability

(accuracy and repeatability) of the phase change coating technique, two repeat tunnel runs were made for this model configuration. Isotherms, prepared independently for all three tunnel runs, were all very similar. A composite of the three sets of contours of constant heat transfer coefficient values is shown in Fig. 88. Heat transfer coefficients obtained on the wing and elevon surfaces along a streamwise line at the y = 2.375 in. spanwise station are shown in Fig. 89.

Small bubbles of separated flow just ahead of the hinge line were also observed when the end plate was attached to the model 1/4 in. away from the elevon (Fig. 90). Surface streamline on the end plate are shown in Fig. 91. Heating rate distributions on the wing, elevon and end plate surfaces for this configuration are indicated in Fig. 92 and 93. In Fig. 93, contour 6 near the elevon is coincident with contour 5. No separation bubbles were observed when the end plate was adjacent and sealed to the 25° short elevon, and the heating rate distributions were somewhat different (Fig. 94-97).

Oil flows on the 70° swept wing, 25° short elevon and cylindrical center body configuration are shown in Fig. 98 and 99. Surface aerodynamic heating rate distributions for the same configuration are shown in Fig. 100 and 101.

The 25° short elevon was also tested on the 70° swept wing with the end plate attached. Unfortunately, bad light reflections obliterated the wing, elevon and aft portion of the end plate surface. Only the forward portion of the end plate surface was clearly discernible; heat transfer coefficient values on the forward portion of the end plate surface were approximately 0.0050 BTU/ft^2 sec°R for this configuration.

4.8 30° SHORT ELEVON

Oil flows for the 30° elevon on the unswept wing indicate separated flow ahead of the elevon (Fig. 102 and 103). Surface heating rate distributions are indicated in Fig. 104. No thermocouple data were obtained for configurations with the 30° elevon.

Sketches of oil flows obtained on the 70° swept wing, 30° short elevon and end plate, with a 1/4 in. gap between the elevon and end plate, are shown in Fig. 105 and 106. Two oil accumulation lines on the end plate surface are apparent. Note that "streamlines" in the oil flow sketches means "surface streamlines." There are distinctive regions of separation and surface flow

disturbance on the wing, elevon and end plate surfaces. Phase change coating heat transfer results are shown in Fig. 107 and 108. The phase change coating chosen for the elevon surface was too high and therefore no melt on the elevon surface was observed within a reasonable amount of time.

Separated flow regions are delineated by the oil accumulation lines sketched in Fig. 109 and 110 for the 70° wing, 30° elevon and end plate sealed to the elevon. A photograph of the oil flow in the interaction region is shown in Fig. 111. The smearing of the oil accumulation line may indicate unsteady flow in this region. Severe light reflections obliterated most of the configuration during the phase change coating test run, only the forward portion of the end plate surface was clearly discernable in the motion pictures (Fig. 112).

4.9 LOW SPOILER

Sketches of the oil flow pattern and the phase change coating heat transfer rate distribution on the unswept wing with the low spoiler are given in Fig. 113 and 114. The oil accumulation line coincides with the narrow band of isotherms separating high and low heating rates on the wing surface. No thermocouple data were taken with either the low or high spoilers attached to the wings.

Oil flows on the unswept wing and end plate surfaces, with the end plate adjacent to the low spoiler, are sketched in Fig. 115 and 116. A frame from the motion picture of the run (Run No. 119) is shown in Fig. 117, and a photo of the end plate taken after the test run is shown in Fig. 118. Surface heat transfer rate distributions obtained by the phase change coating technique for this configuration are shown in Fig. 119 and 120.

A sketch and photograph of the oil flow on the 70° swept wing with the low spoiler are shown in Fig. 121 and 122. Phase change results for the same configuration are given in Fig. 123 and a frame of the motion picture is shown in Fig. 124. There is a definite similarity in the oil flow and phase change coating patterns on the wing surface.

Sketches of oil flow on the 70° wing and cylindrical body surfaces are shown in Fig. 125 and 126. A photograph of the oil flow on the wing and cylindrical body surfaces is shown in Fig. 127. Surface heat transfer rate contours are sketched in Fig. 128 and 129, and a frame from the phase change

coating test run is shown in Fig. 130. Again, the oil flow and phase change patterns are quite similar (Fig. 127 and 130).

Oil flows on the wing and end plate surfaces are sketched in Fig. 131 and 132. A frame from the color motion picture of the oil flow is shown in Fig. 133. Phase change heating rate distributions for the same configuration are shown in Fig. 134 and 135.

4.10 HIGH SPOILER

The high spoiler caused the greatest disturbance of any of the trailing edge controls tested. The surface oil flow pattern observed on the unswept wing is shown in Fig. 136. Surface heating rate distributions are indicated in Fig. 137.

Sketches of oil flow patterns on the end plate and unswept wing surfaces, with the high spoiler attached, are shown in Fig. 138 and 139. A photograph of the flow is shown in Fig. 140. Surface heating rate contours are sketched in Fig. 141 and 142. A frame from the motion picture is shown in Fig. 143.

Surface streamlines on the 50° swept wing with the high spoiler are sketched in Fig. 144. Surface heating rate distributions are given in Fig. 145.

The oil flow pattern on the 70° swept wing surface is given in Fig. 146 and the surface heating rate distribution for the same configuration is indicated in Fig. 147. The extent of separation is much more extensive on the outboard portion of the wing where the boundary layer is transitional or laminar prior to separation (Ref. 14 and 20).

Surface oil flow patterns observed when the end plate was attached to the 70°wing with the high spoiler are shown in Fig. 148 and 149. A frame from the oil flow motion picture is shown in Fig. 150. Heat transfer coefficient rate contours on the surfaces of the 70° swept wing and end plate are shown in Fig. 151 and 152. Note that in Fig. 151 contours 3 and 4 are nearly coincident.

5. CONCLUDING REMARKS & RECOMMENDATIONS

Surface oil flow and heat transfer coefficient contours are presented for hypersonic free stream flow (Mach 8) over a generic set of wing-elevon-body configurations. The shock-wave boundary-layer interactions result in complex surface flow patterns in the three-dimensional interaction flow regions. Salient aspects of the flows and certain anomalies are described. Effects of wing sweep, trailing edge control, and inboard body may be ascertained readily by comparing the pertinent, quantitative, data presented in the figures.

Generally, the thermocouple and phase change coating heat transfer data agree quite well. The data are repeatable from run to run, and thereby pass the most stringent test for reliability. Surface oil flow and phase change coating patterns are quite similar for the same model configuration, and adequately delineate the surface regions affected by the trailing edge control.

There is no flow separation from the wing surface for trailing edge elevons having 20° deflection angles or less. The 25° elevon causes little flow separation. Heat transfer to the wing surface in the separated flow region ahead of the 30° elevon is twice as large as for attached flow. As expected for turbulent boundary layer separation (Ref. 1), the heat transfer to the wing surface in the turbulent separated flow region upstream of the spoilers is much greater then for attached flows. The effective dividing streamline angle in the two dimensional flow region is approximately 11° for the low spoiler and 11.5° for the high spoiler, in general agreement with data from many sources (Ref. 14 and 20).

The end plate and cylindrical center bodies substantially alter the heating distributions on the wing and elevon surfaces; they do not necessarily increase the maximum heat transfer rate coefficient observed on the elevon surface. As expected, the center bodies inhibit inboard venting of separated flow and usually increase the length of separation, particularly on the inboard portion of the wing. This effect is most pronounced for the end plate sealed to the trailing edge control.

Wing sweep affects both magnitude and distribution of heat transfer rate coefficients on the wing and elevon surfaces. Depending on sweep, elevon deflection angle and center body, maximum heating may occur along the edges of

the elevon, in the middle of the elevon, or elsewhere on the elevon surface. The extent of separation is fairly constant ahead of the spoilers on the umswept and 50° swept wings, for which the boundary layers were turbulent prior to separation. However, the extent of separation is much more extensive on the outboard portion of the 70° swept wing, where the boundary layer is transitional or laminar prior to separation (Ref. 14 and 20). In all cases, the surface oil flow and phase change coating patterns are quite similar for the same configuration.

The region on the adjacent aft fuselage section affected by the trailing edge control is much larger than would be anticipated using inviscid flow analyses. Deveikis (Ref. 21) observed this same phenomenon for end plates (fences) on a large flat plate - ramp model. He also observed that the streamlines on the end plate surface more closely parallel the oil accumulation line than the elevon surface (Fig. 26 and 58). As examples: for a 5° elevon, the area downstream of the oil accumulation line is more than twice as large as that downstream of the projection of the 5° elevon inviscid shock location on the end plate (Fig. 26); for a 15° elevon, the end plate area affected by the elevon is more than five times as extensive as the area downstream of the projection on the end plate surface of the inviscid flow shock wave emanating from the elevon hinge line (Fig. 58 and 60). Wing sweepback reduces the aft fuselage (end plate) area affected by the trailing edge control (Fig. 58 and 67). The affected area on the cylindrical center body is quite similar to that on the end plate center body.

The phase change coating technique discloses local regions of nigh heat transfer rates that may be missed by even extensive arrays of thermocouples, and the phase change and thermocouple heat transfer rate data agree. More detailed analyses should be made to determine center body and wing sweepback effects on maximum heating rates to the elevon surface. Nevertheless, results presented herein enlarge the data base required to refine empiric analytic methods for estimating surface heating rate distributions in complex interaction flow regions. The results should be compared with analytic results, calculable using methods such as those presented in Ref. 4 and 5.

6. REFERENCES

1. Korkegi, Robert H., "Survey of Viscous Interactions Associated with High Mach Number Flight", AIAA J, Vol 9, No. 5, May 1971.

2. Reding, J.P. and Ericsson, L.E., "Flow Visualization Reveals Causes of Shuttle Nonlinear Aerodynamics," J Aircraft, Vol 19, No. 11, Nov 1982.

3. Ryan, Bertha M., "Summary of Aerothermodynamic Interference Literature," Naval Weapons Center, China Lake, CA, Tech Note 4061-160, April 1969.

4. Hayes, James R., "Prediction Techniques for the Characteristics of Fin Generated Three Dimensional Shock Wave Turbulent Boundary Layer Interactions," AFFDL TR 77-10, Wright-Patterson AFB, OH, May 1977. (Available from DTIC as AD A042 024).

5. Kaufman, Louis G. II and Johnson, Charles B., "Methods for Estimating Pressure and Thermal Loads Induced by Elevon Deflections on Hypersonic Vehicle Surfaces with Turbulent Boundary Layers," NASA TM 83130, Sept 1981.

6. Goldberg, Theodore, J., "Three-Dimensional Separation for Interaction of Shock Waves with Turbulent Boundary Layers," AIAA J, Vol 11, No. 11, Nov 1973.

7. Korkegi, Robert H., "Comparison of Shock-Induced Two-and Three-Dimensional Incipient Turbulent Separation," AIAA J, Vol 13, No. 4, April 1975.

8. McCabe, A., "The Three-Dimensional Interaction of a Shock Wave with a Turbulent Boundary Layer," Aeronautical Quarterly, Vol XVII, Part 3, Aug 1966.

9. Peake, David J., Rainbird, William J., and Atraghji, Edward G., "Three-Dimensional Flow Separations on Aircraft and Missiles," AIAA J, Vol 10, No. 5, May 1972.

10. Whitehead, Allen H. Jr., Sterrett, James R., and Emery, James C., "Effects of Transverse Outflow from a Hypersonic Separated Region," AIAA J, Vol 10, No. 4, April 1972.

11. Small, William J., Kirkham, Frank S., and Fetterman, David E., "Aerodynamic Characteristics of a Hypersonic Transport Configuration at Mach 6.86," NASA TN D-5885, 1970.

12. Chapman, Dean R., Kuehn, Donald M., and Larson, Howard K., "Investigation of Separated Flows in Supersonic and Subsonic Streams with Emphasis on the Effect of Transition," NACA Report 1356, 1958.

13. Whitehead, Allen H., Jr. and Keyes, J. Wayne, "Flow Phenomena and Separation over Delta Wings with Trailing-Edge Flaps at Mach 6," AIAA J, Vol 6, No. 12, Dec 1968.

14. Kaufman, Louis G. II and Freeman, L. Michael, "Separation ahead of Steps on Swept Wings," J Aircraft, Vol 13, No. 12, Dec 1976.

15. Kaufman, Louis G. II and Johnson, Charles B., "Pressure and Thermal Distributions on Wings and Adjacent Surfaces Induced by Elevon Deflections at Mach 6," NASA TP 1356, March 1979.

16. Korkegi, Robert H., "On the Structure of Three-Dimensional Shock-Induced Separated Flow Regions," AIAA J., Vol 14, No. 5, May 1976.

17. Haslett, Robert A., et al, "Interference Heating due to Shock Impingement," AFFDL TR 72-66, Wright-Patterson AFB, OH, July 1972.

18. Jones, Robert A. and Hunt, J. Larry, "Use of Fusible Temperature Indicators for Obtaining Quantitative Aerodynamic Heat Transfer Data," NASA TR 230, 1966

19. Johnson, Charles B. and Kaufman, Louis G. II, "Heat transfer Distributions Induced by Elevon Deflections on Swept Wings and Adjacent Surfaces at Mach 6," NASA TM 74045, Aug 1978.

20. Kaufman, Louis G. II and Freeman, L. Michael, "Separation Ahead of Controls on Swept Wings," Air Force Systems Command, Wright Patterson AFB, OH, ARL-TR-75-0134, June 1975.

21. Deveikis, William D., "Effects of Flow Separation and Cove Leakage on Pressure and Heat-Transfer Distributions Along a Wing-Cove-Elevon Configuration at Mach 6.9," NASA TP 2127, June 1983.

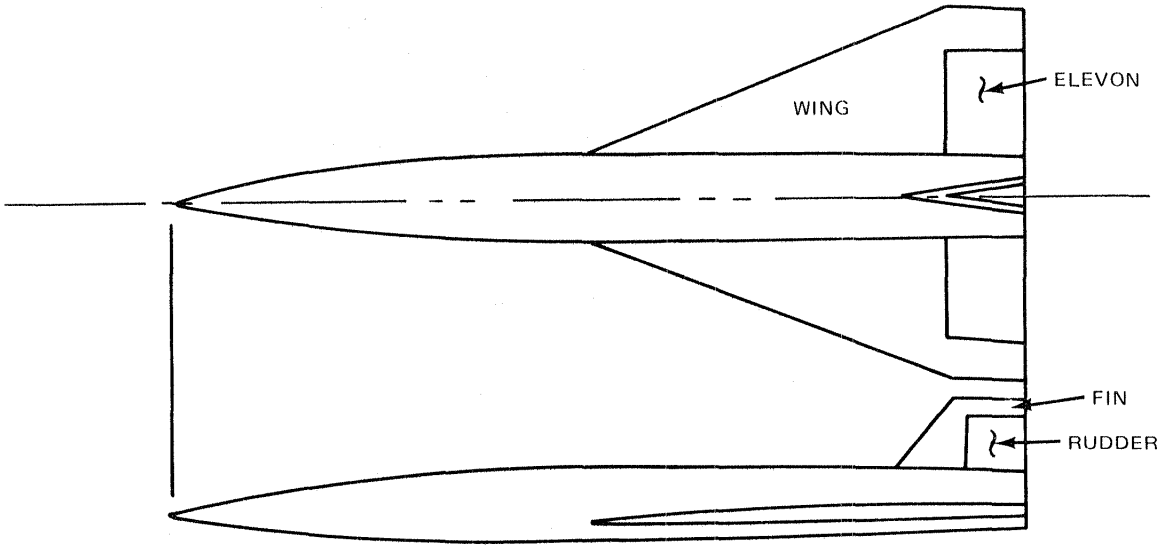

CONCEPTUAL HYPERSONIC AIRCRAFT CONFIGURATION

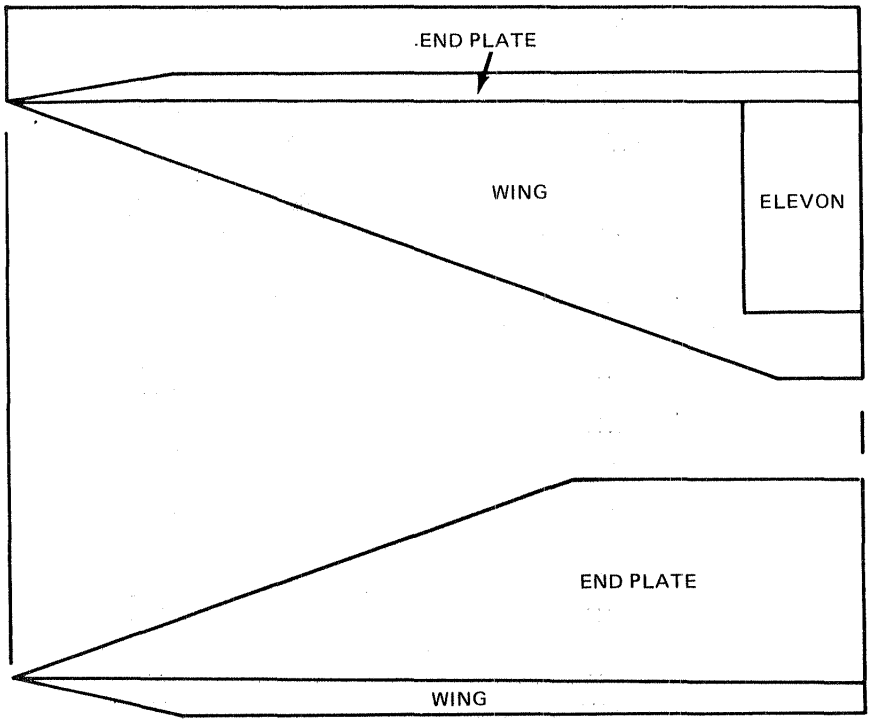

"WING-ELEVON" MODEL CONFIGURATION

R84-1080-001(T)

Fig. 1 Outlines of Conceptual High Speed Aircraft Configuration "& Wing-Elevon" Wind Tunnel Model Representative of Aft Portion of Such an Aircraft

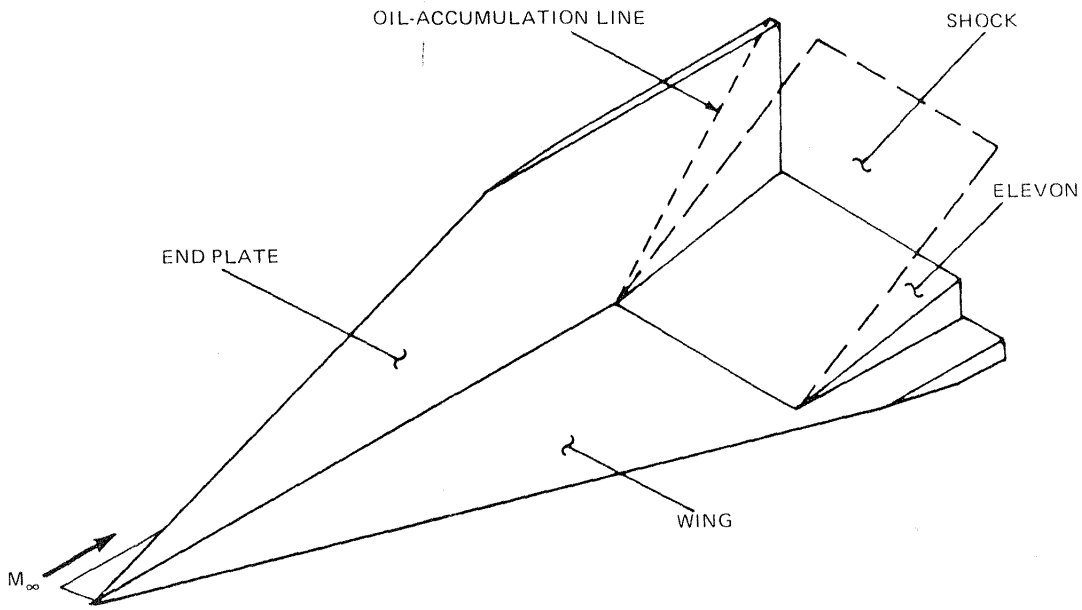

a. NO SEPARATION UPSTREAM OF ELEVON HINGE LINE

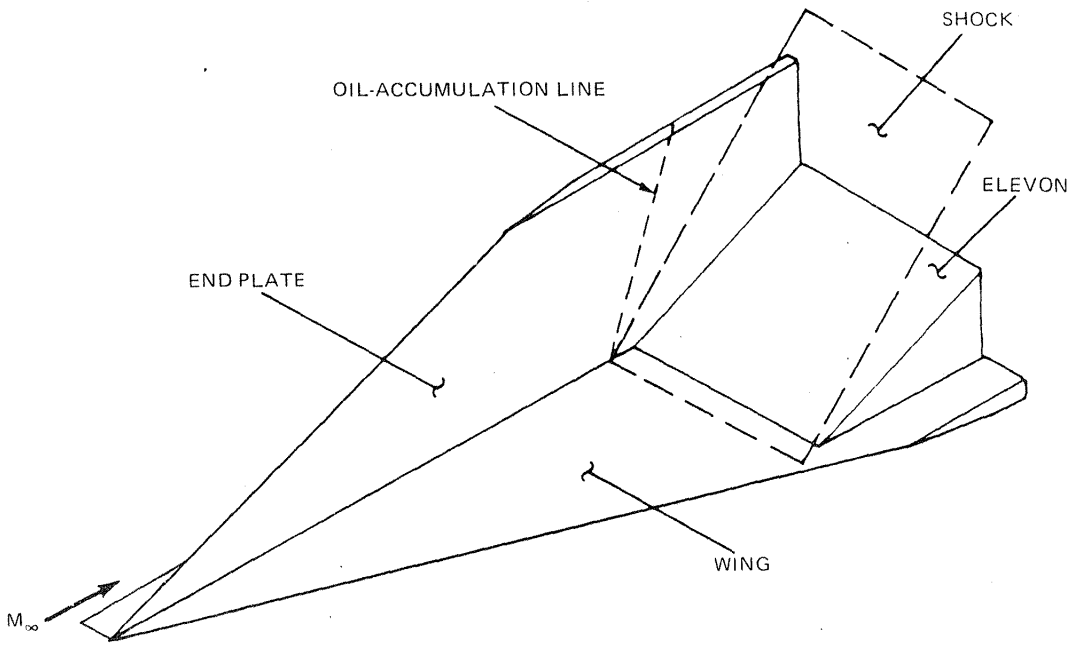

b. SEPARATED FLOW UPSTREAM OF ELEVON HINGE LINE

R84-1080-002(T)

Fig. 2 Two Types of 3-D Interaction Flow Models for Turbulent Boundary Layers Upstream of Trailing Edge Elevons

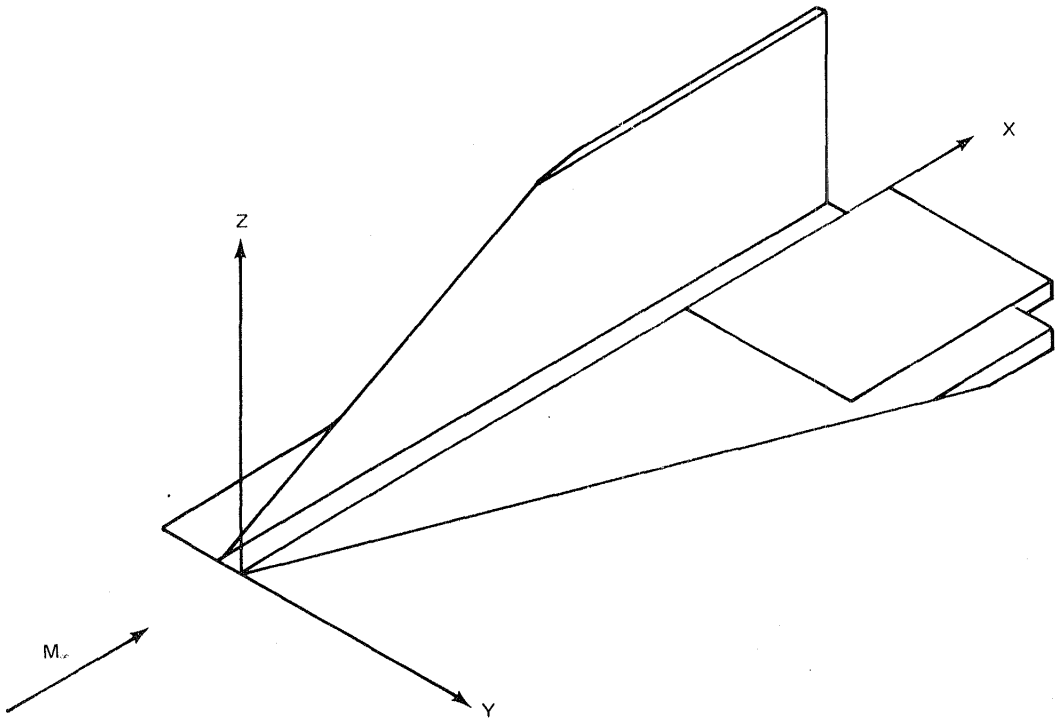

R84-1080-003(T)

Fig. 3 Sketch of a 70° Swept Wing-Elevon-End Plate Model Configuration & Coordinate System

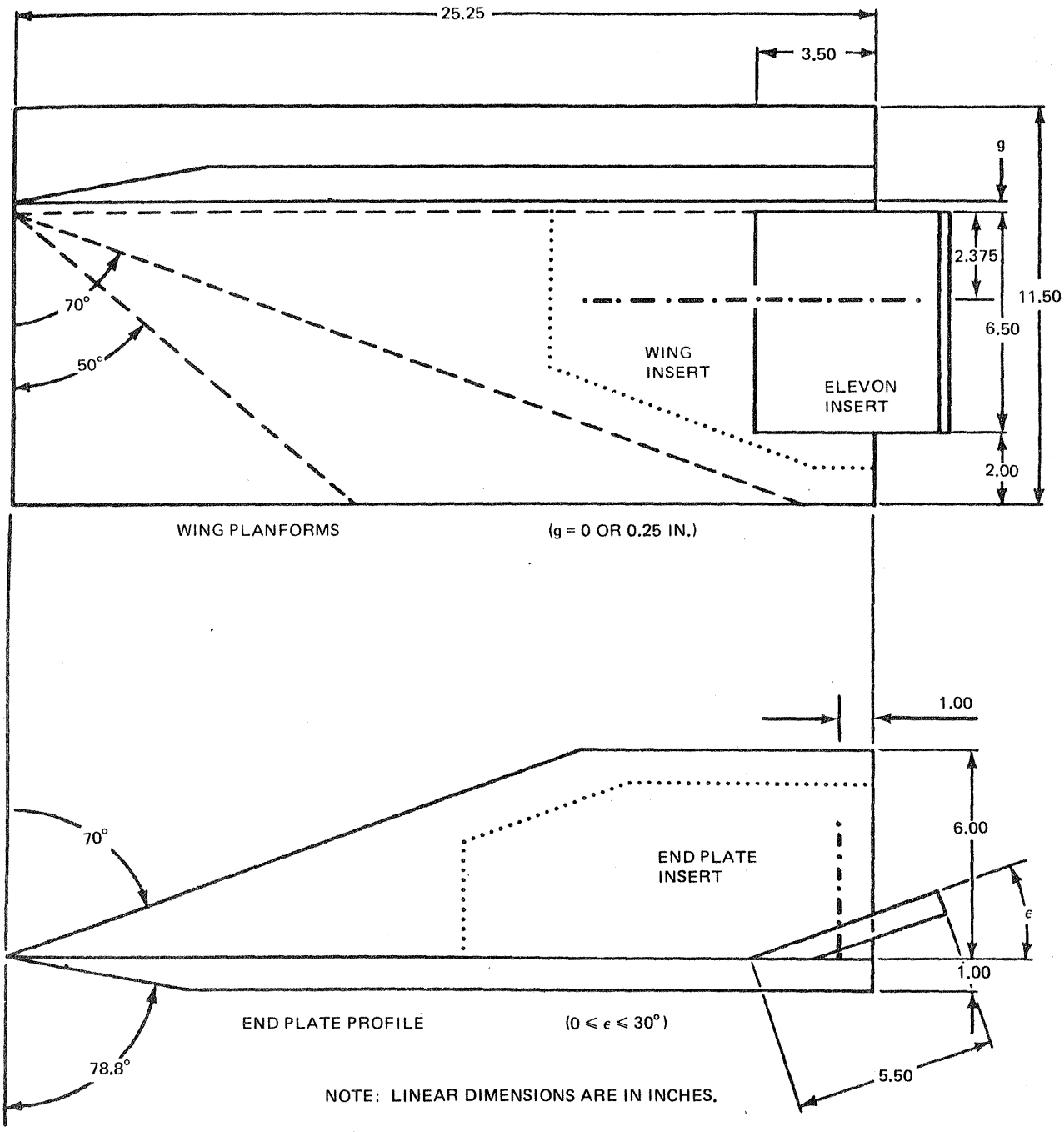

Fig. 4 Wing & Plate Planforms for Wing Elevon Model

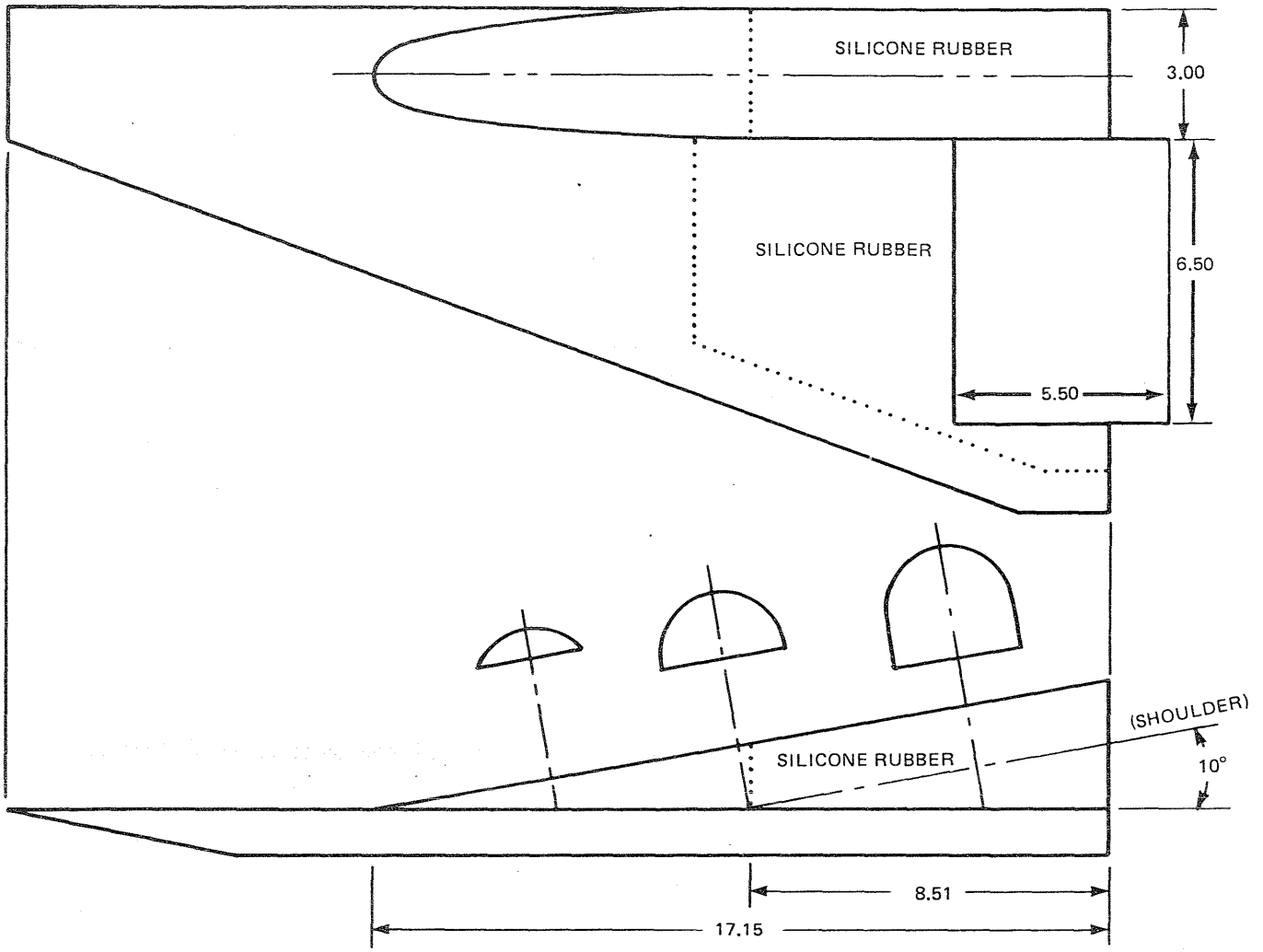

R84-1080-005(T)

NOTE: LINEAR DIMENSIONS ARE IN INCHES.

Fig. 5 Cylindrical Body Attached to 70° Wing

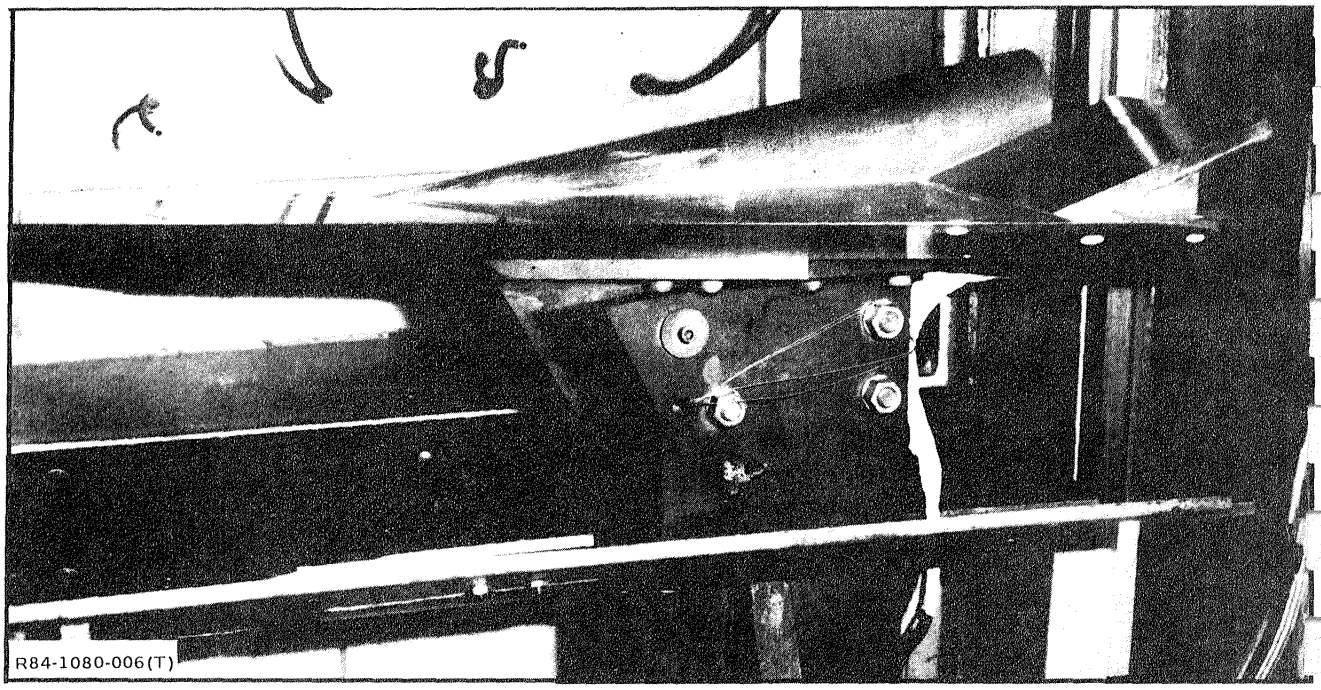

Fig. 6 Photograph of 70° Wing-Long Elevon-Cylindrical Center Body Model Configuration Installed in Injection Chamber Beneath Test Section

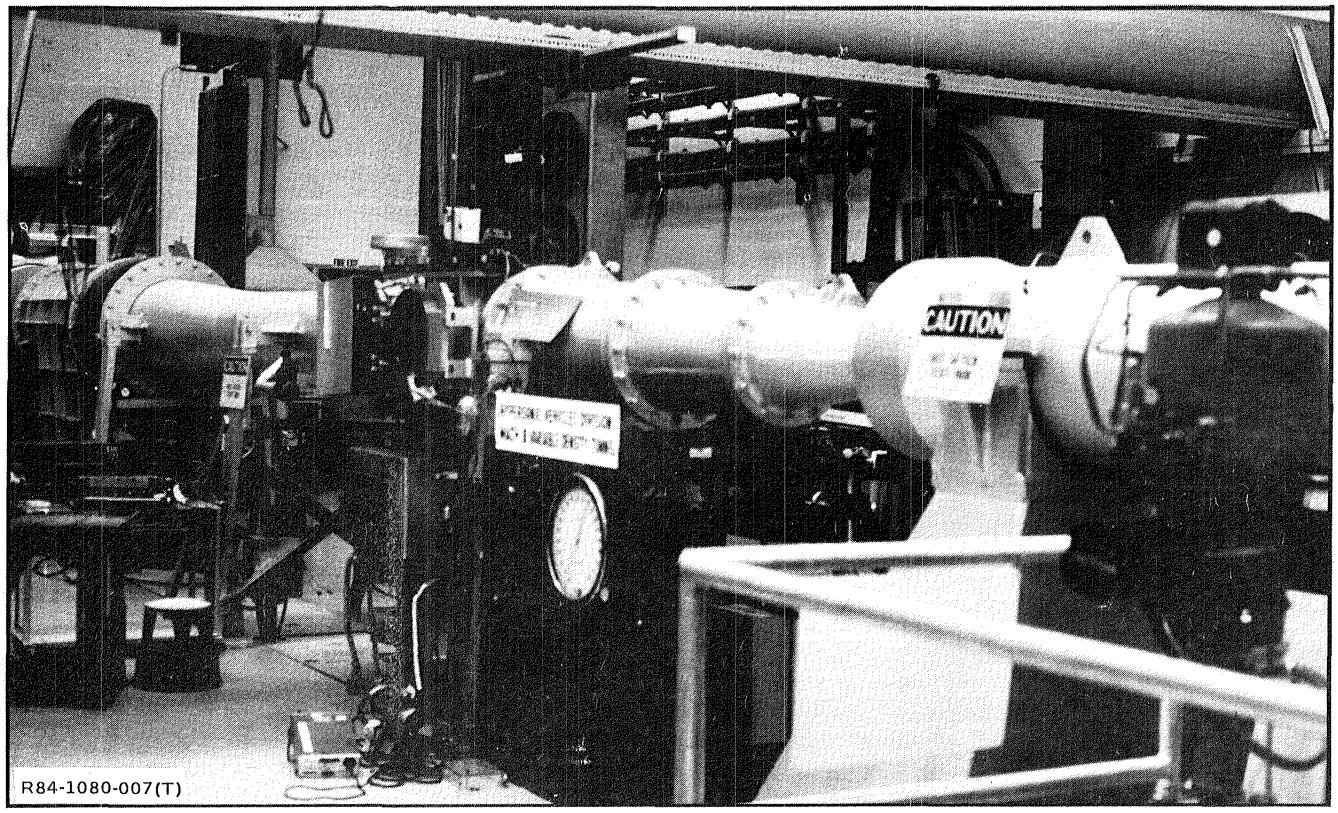

Fig. 7 NASA Langley Mach 8 Variable Density Tunnel

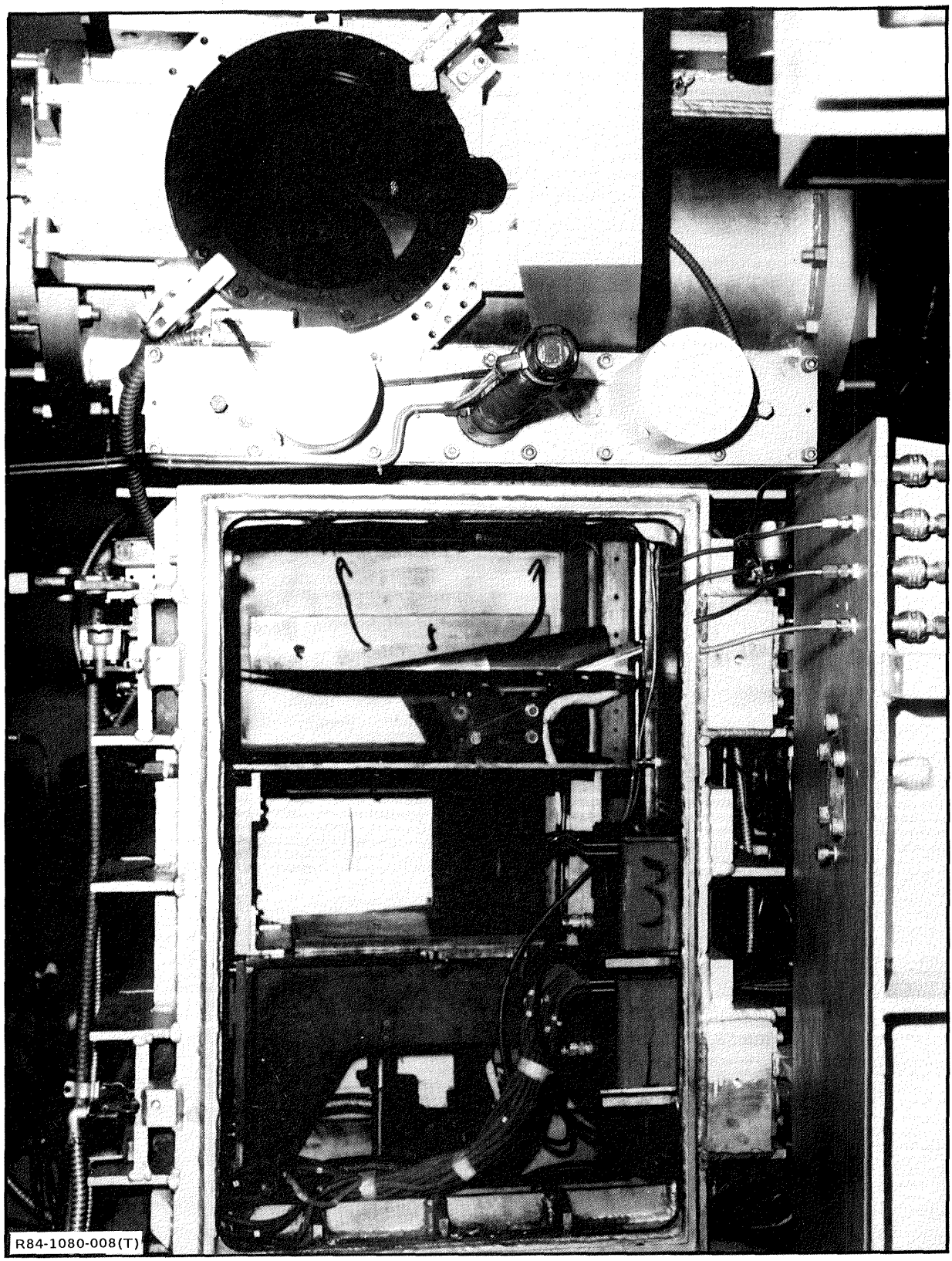

Fig. 8 Wing Elevon Model Mounted on Injection System Beneath Test Section

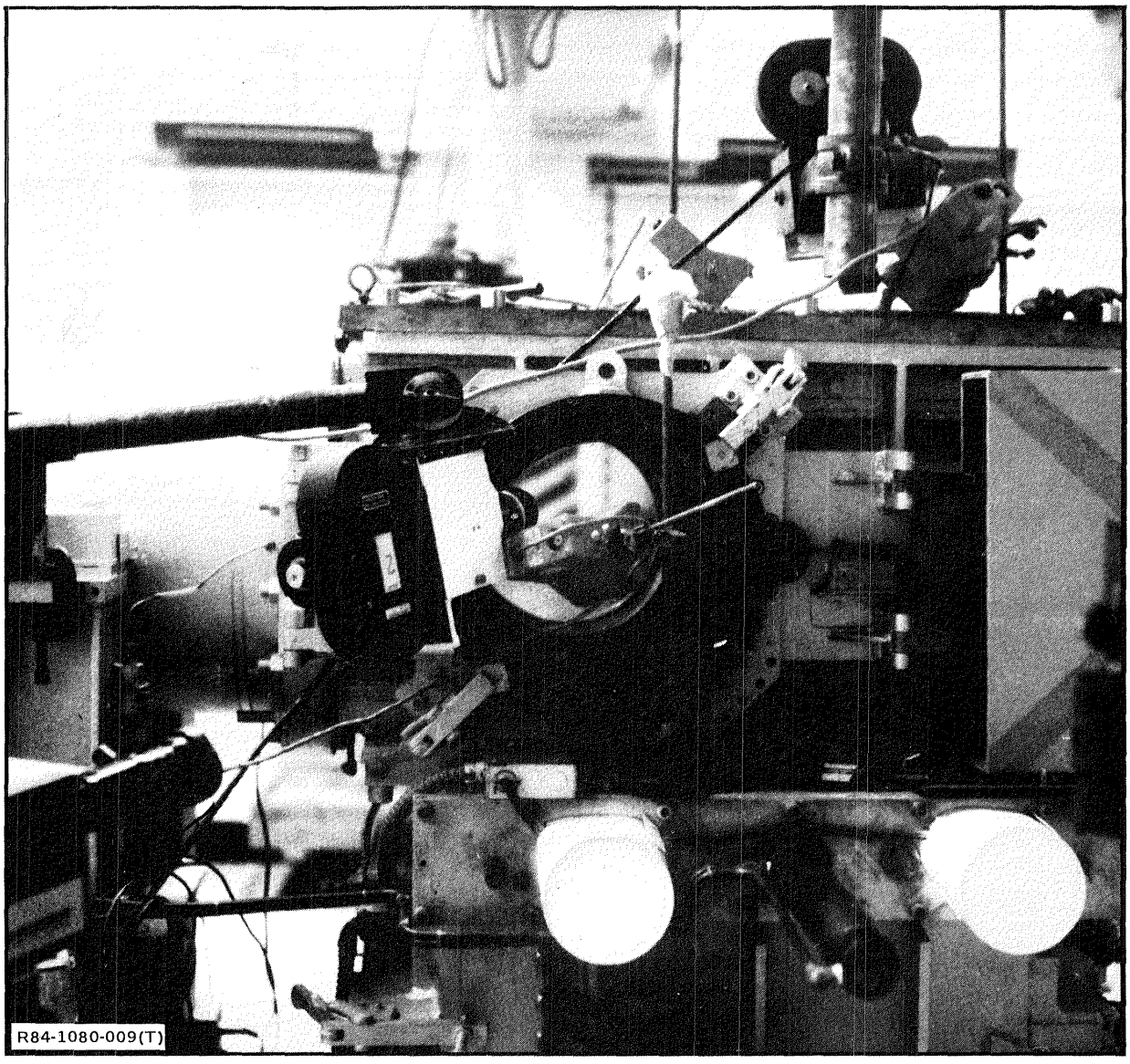

Fig. 9 Setup of Cameras & Lights for Oil Flow & Phase Change Coating Experiments

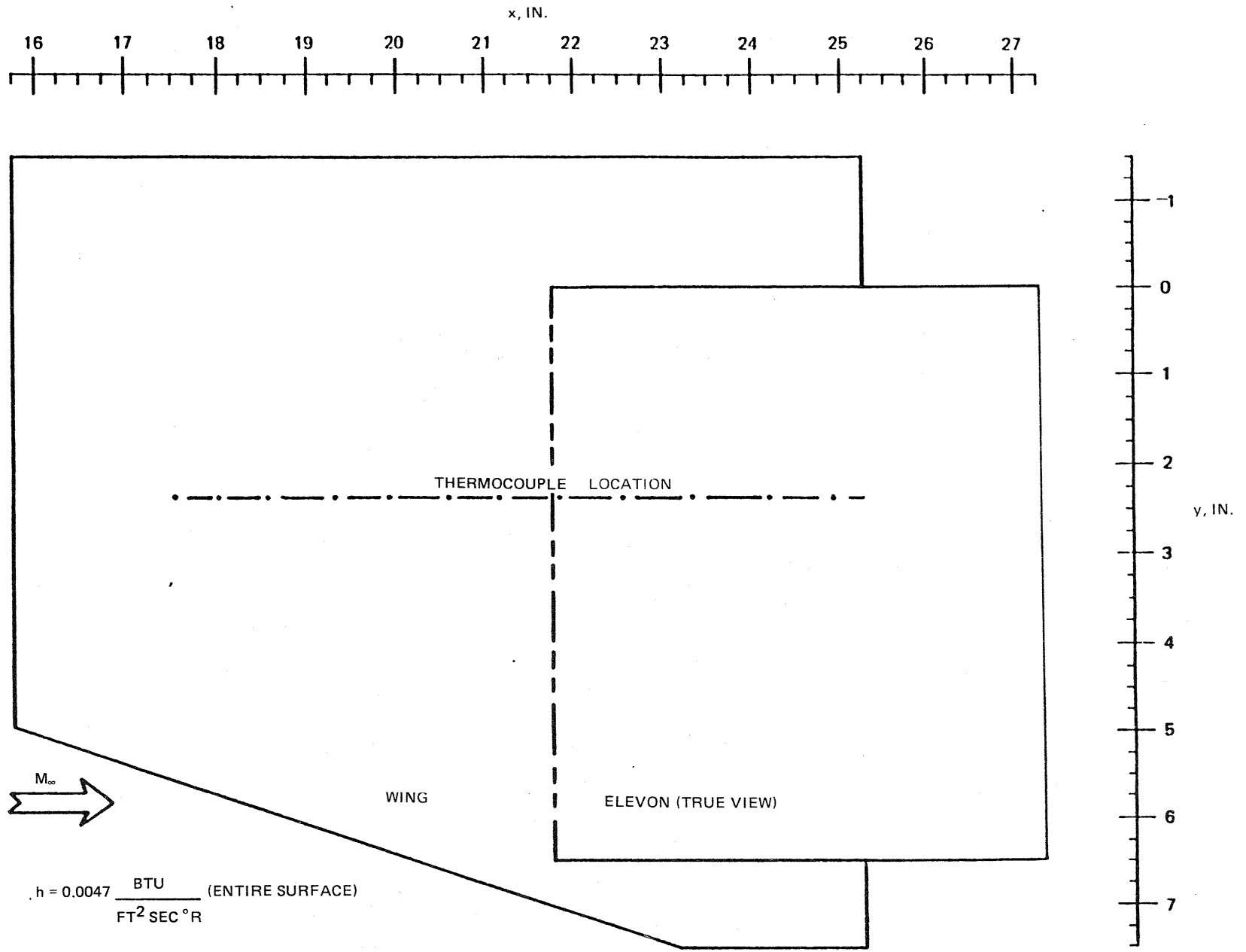

Fig. 10 Undeflected Long Elevon — Planform Phase Change Results, Unswept Wing, No Center Body

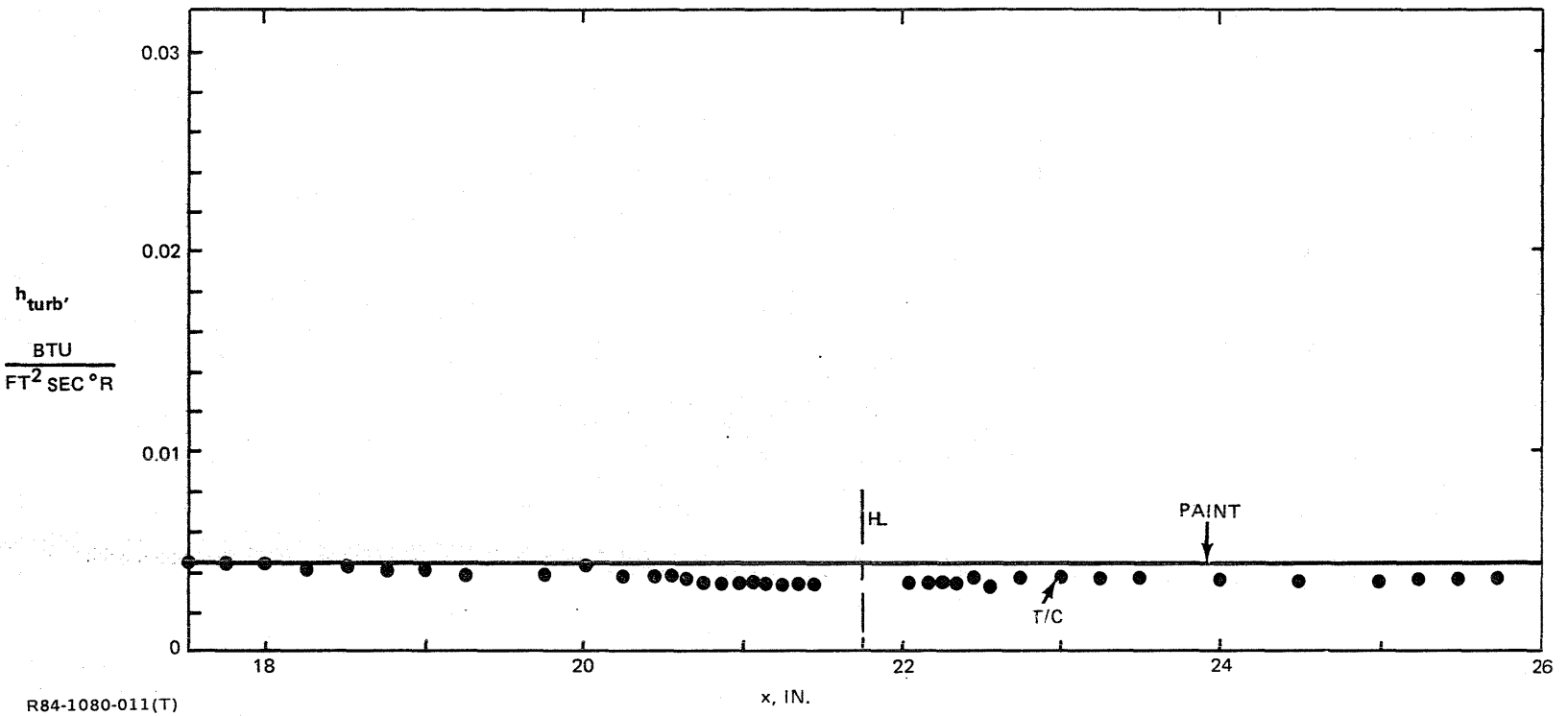

Fig. 11 Undeflected Long Elevon — Comparison of Phase Change & Thermocouple Data, Unswept Wing, No Center Body

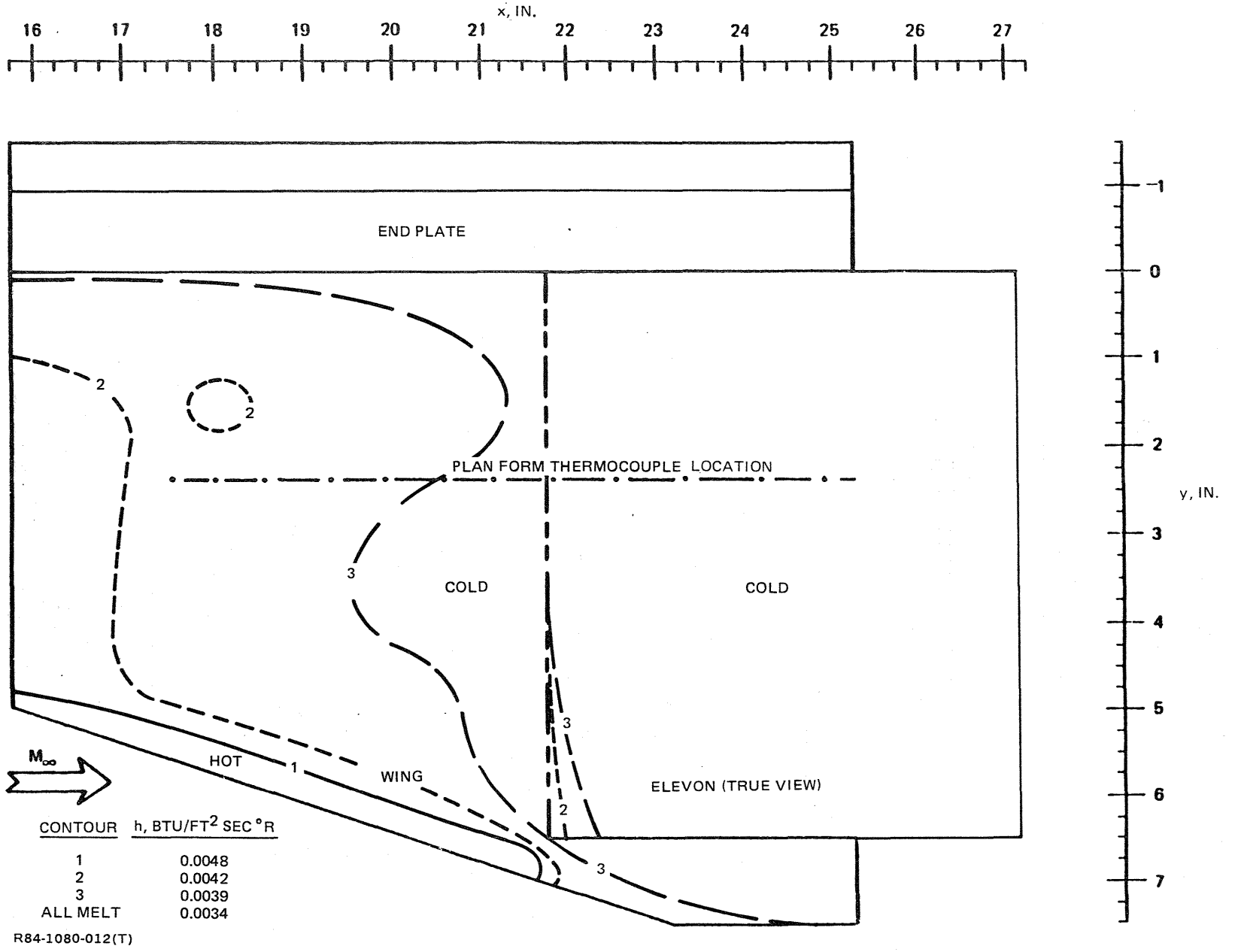

Fig. 12 Undeflected Long Elevon — Planform Phase Change Results, Unswept Wing, End Plate

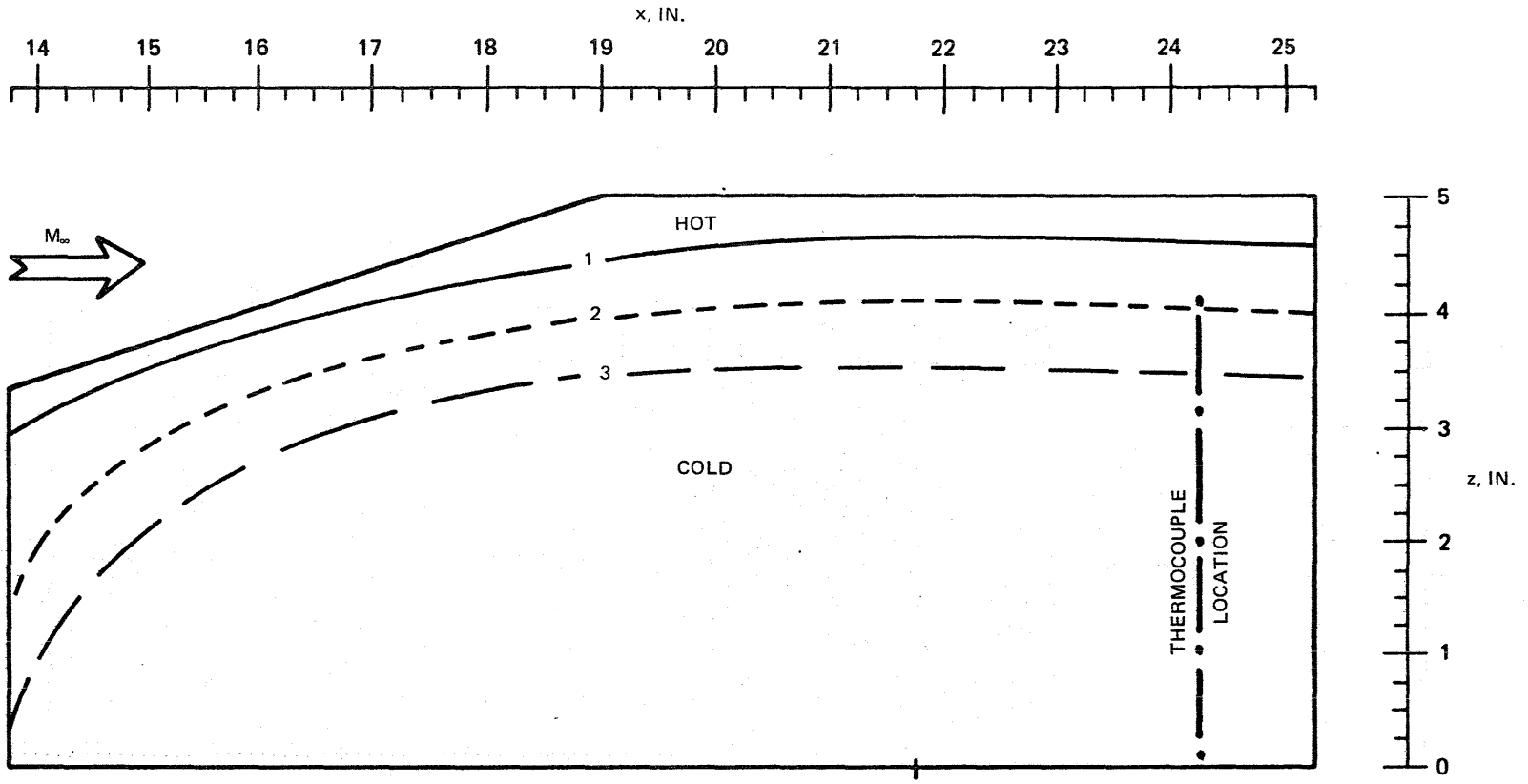

CONTOUR	h, BTU/FT^2 SEC °R
1	0.0048
2	0.0042
3	0.0039
ALL MELT	0.0034

R84-1080-013(T)

Fig. 13 Undeflected Long Elevon – Profile Phase Change Results, End Plate on Unswept Wing

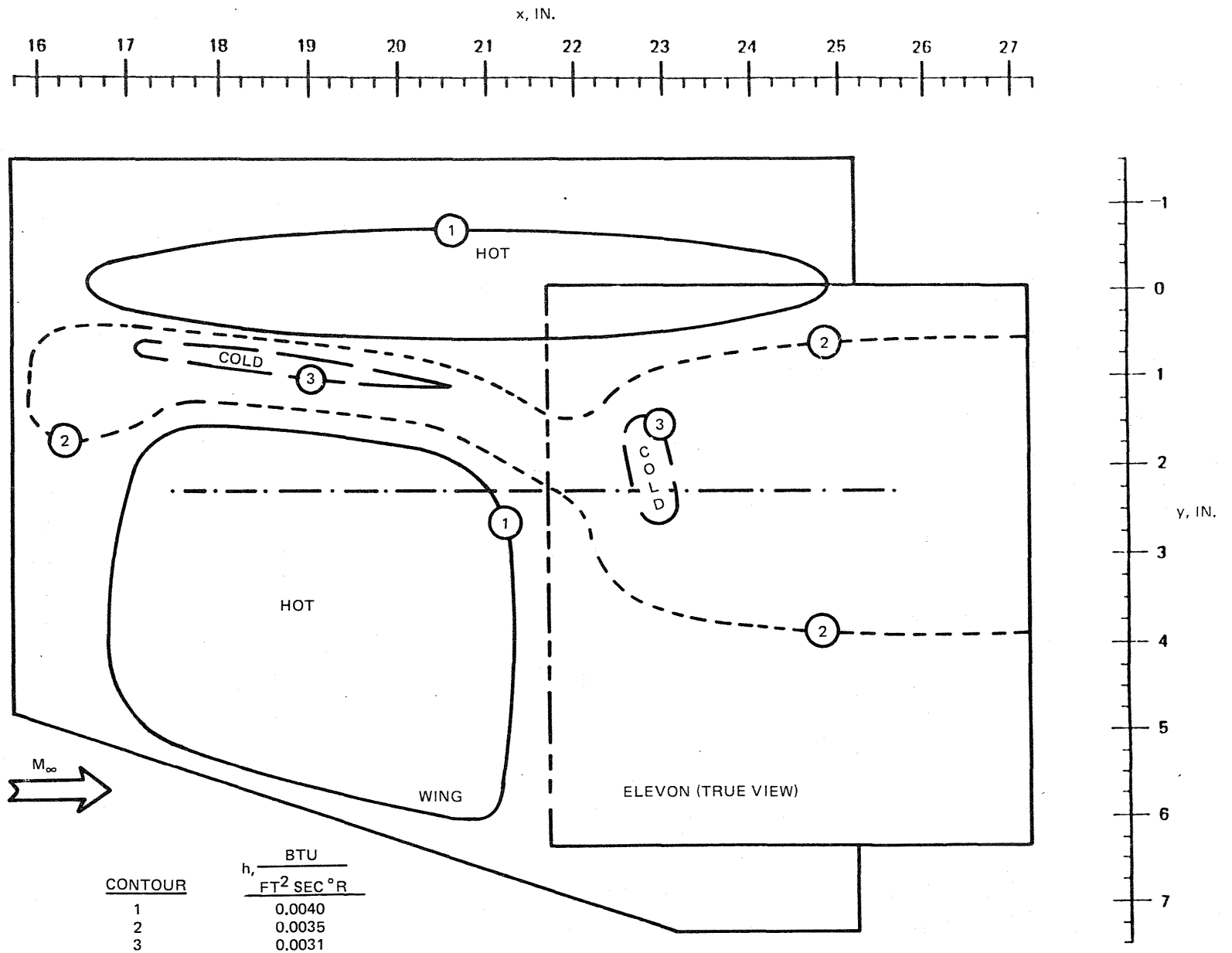

CONTOUR	h, BTU / FT^2 SEC °R
1	0.0040
2	0.0035
3	0.0031
ALL MELT	0.0029

R84-1080-014(T)

Fig. 16 Undeflected Long Elevon — Planform Phase Change Results, 50° Swept Wing, No Center Body

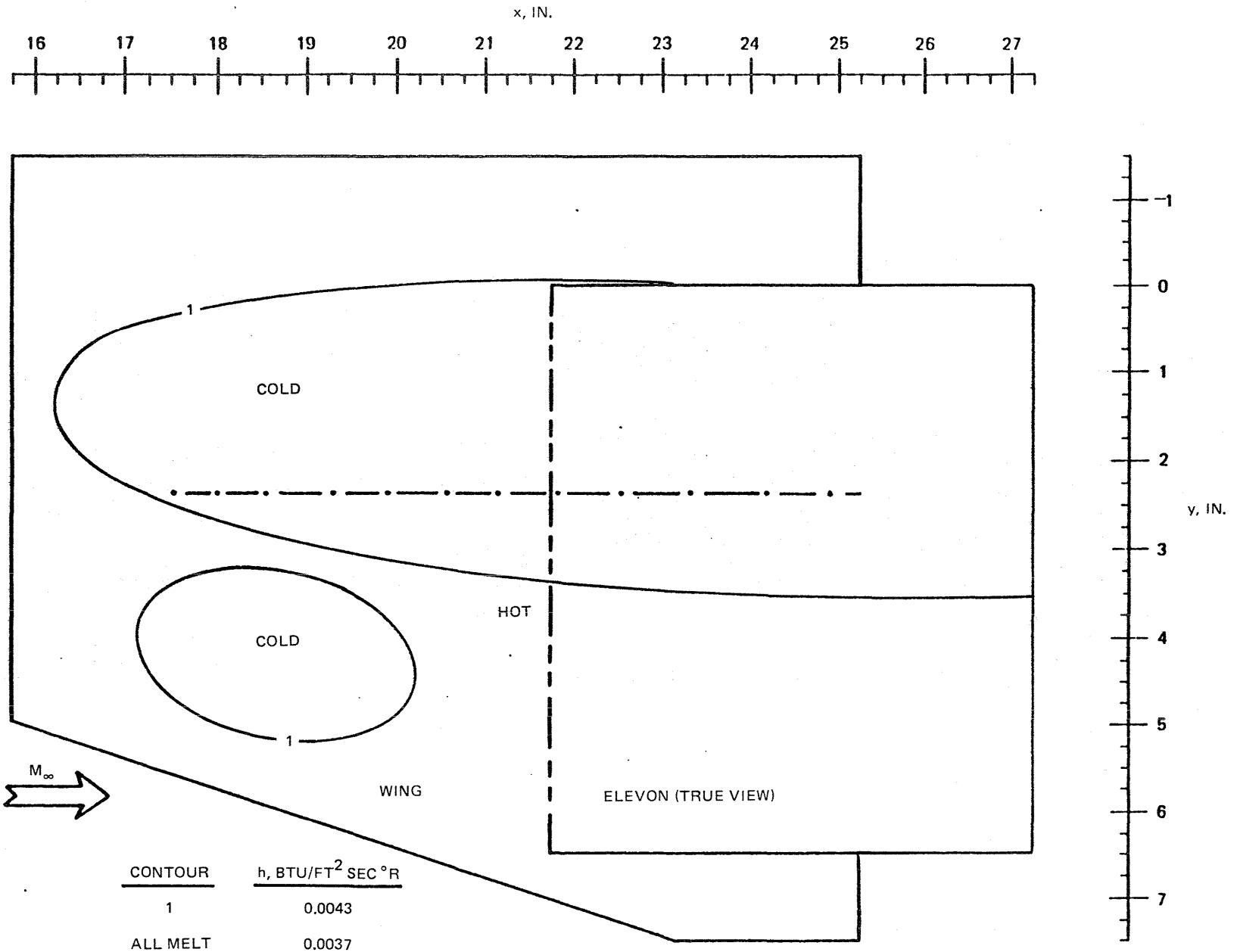

Fig. 15 Undeflected Long Elevon – Planform Phase Change Results, 70° Swept Wing, No Center Body

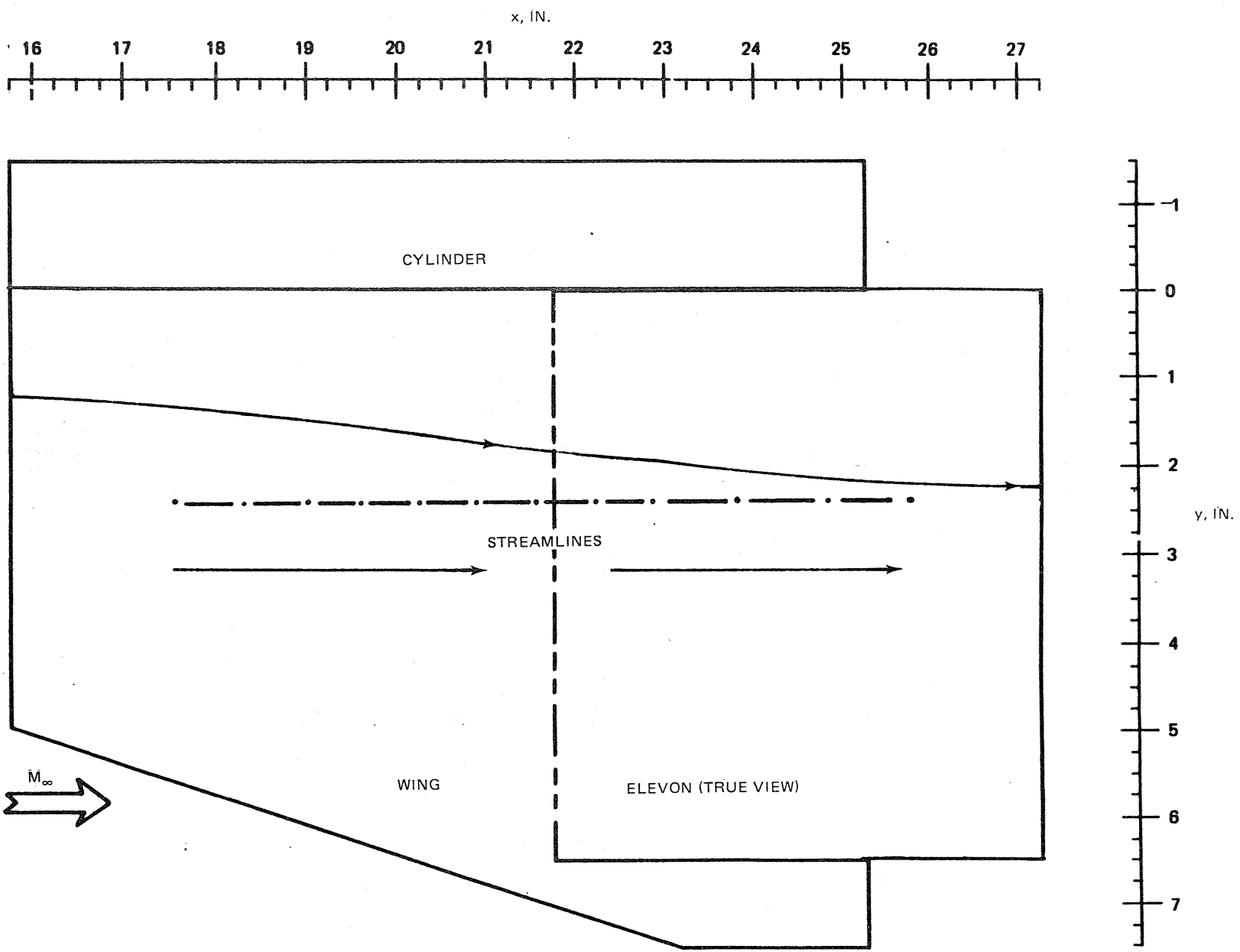

R84-1080-016(T)

Fig. 16 Undeflected Long Elevon — Planform Oil Flow Results, 70° Swept Wing, Cylindrical Center Body

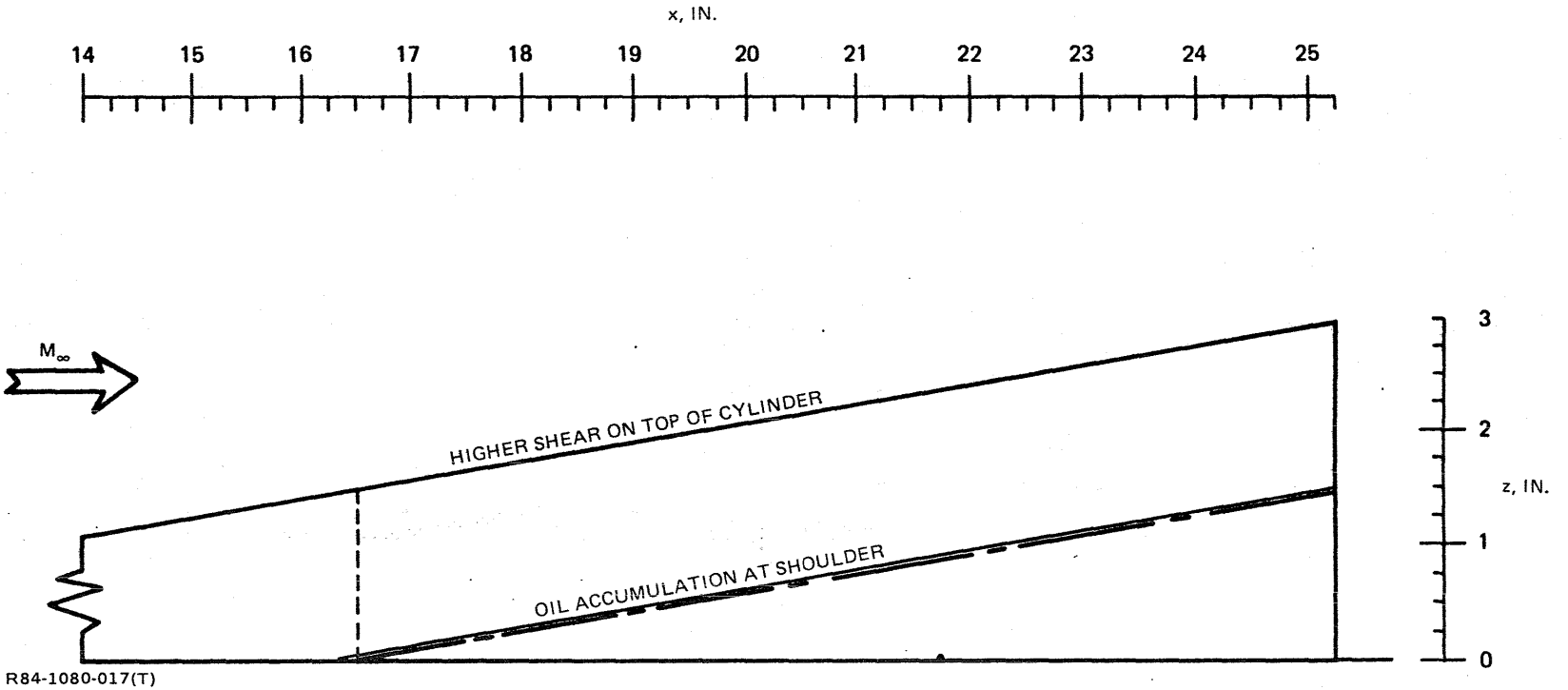

Fig. 17 Undeflected Long Elevon – Profile Oil Flow Results, Cylindrical Center Body, 70° Swept Wing

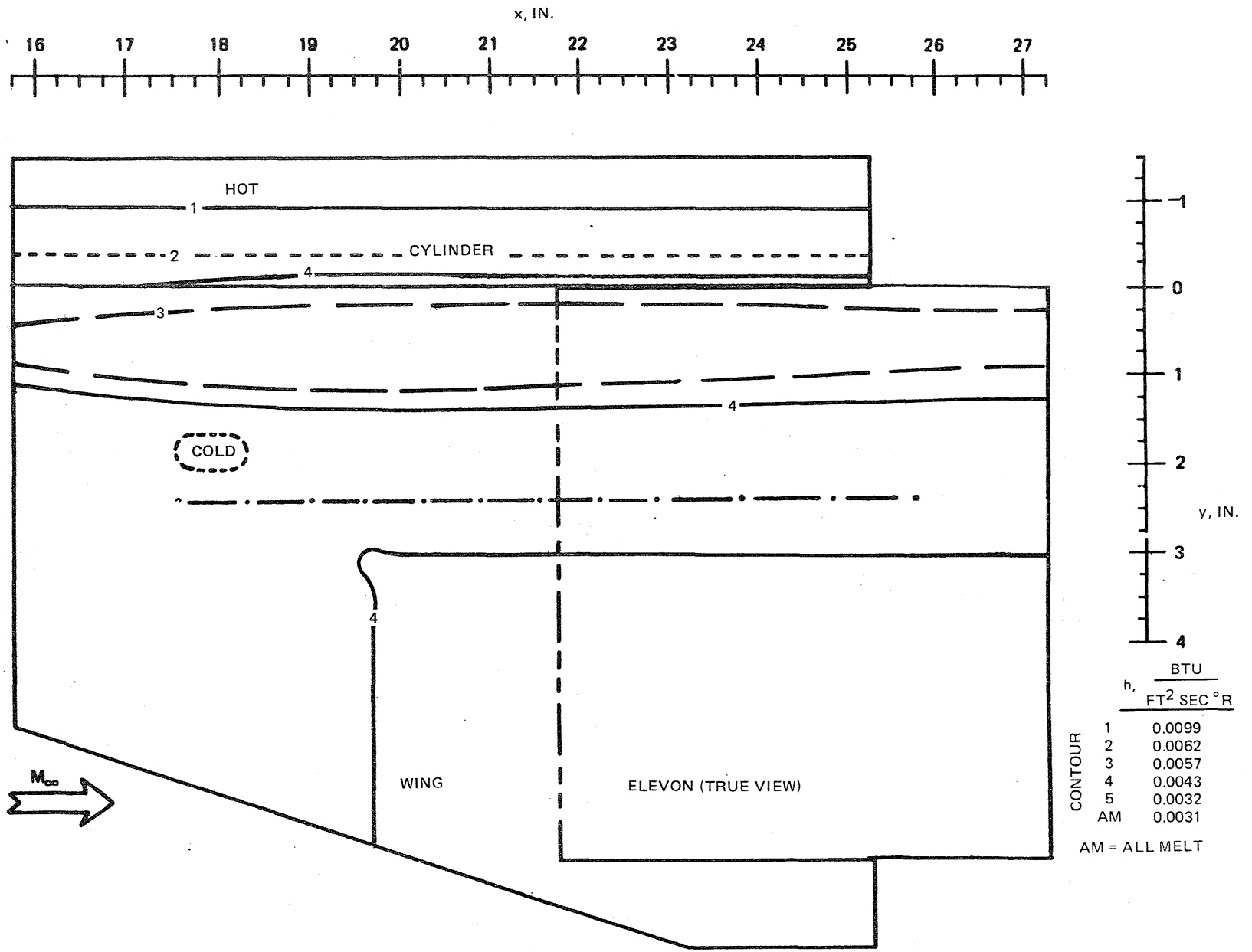

Fig. 18 Undeflected Long Elevon — Planform Phase Change Results, 70° Swept Wing, Cylindrical Center Body

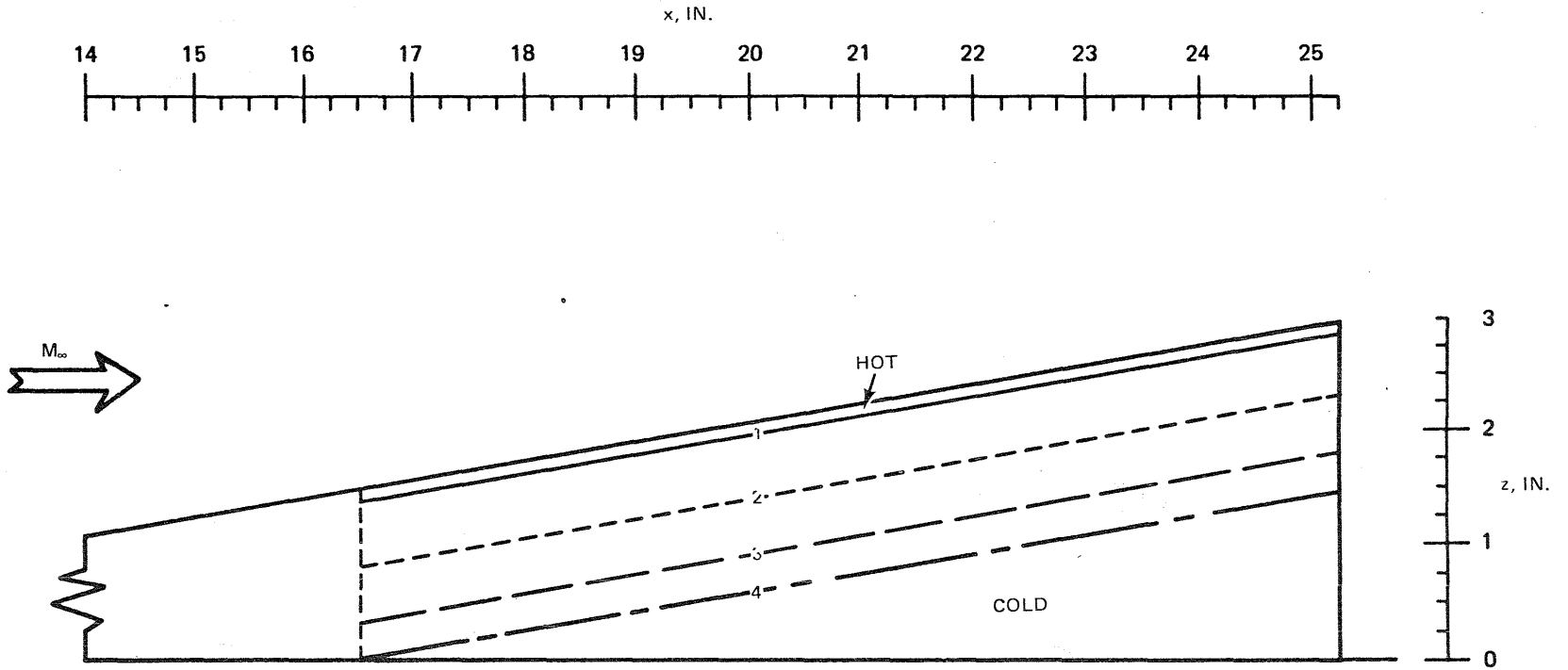

CONTOUR	h, BTU/FT^2 SEC °R
1	0.0094
2	0.0061
3	0.0045
4	0.0031
ALL MELT	0.0030

R84-1080-019(T)

Fig. 19 Undeflected Long Elevon – Profile Phase Change Results, Cylindrical Center Body, 70° Swept Wing

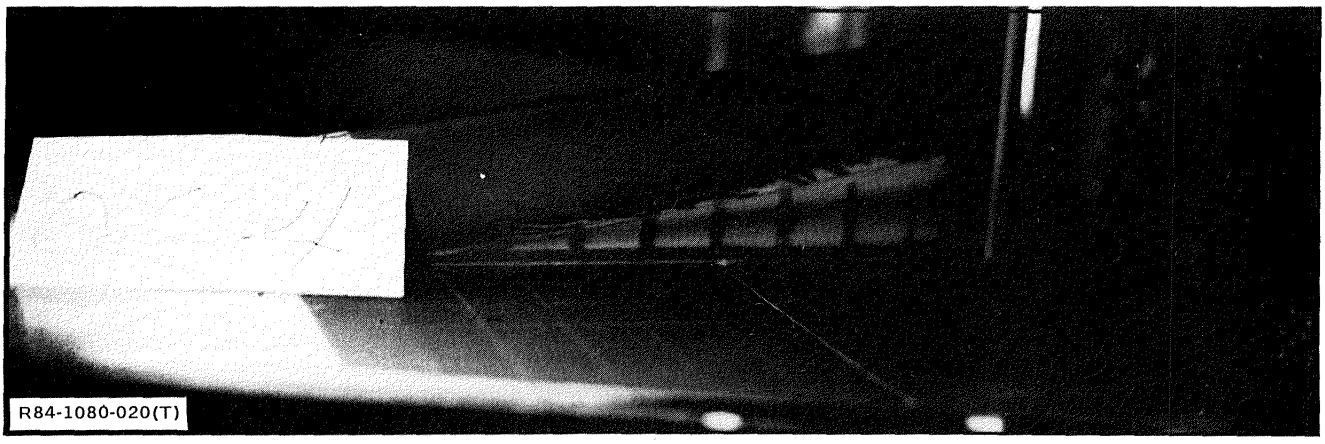

Fig. 20 Undeflected Long Elevon – Photograph of Model After Phase Change Test Run, 70° Swept Wing, Cylindrical Center Body

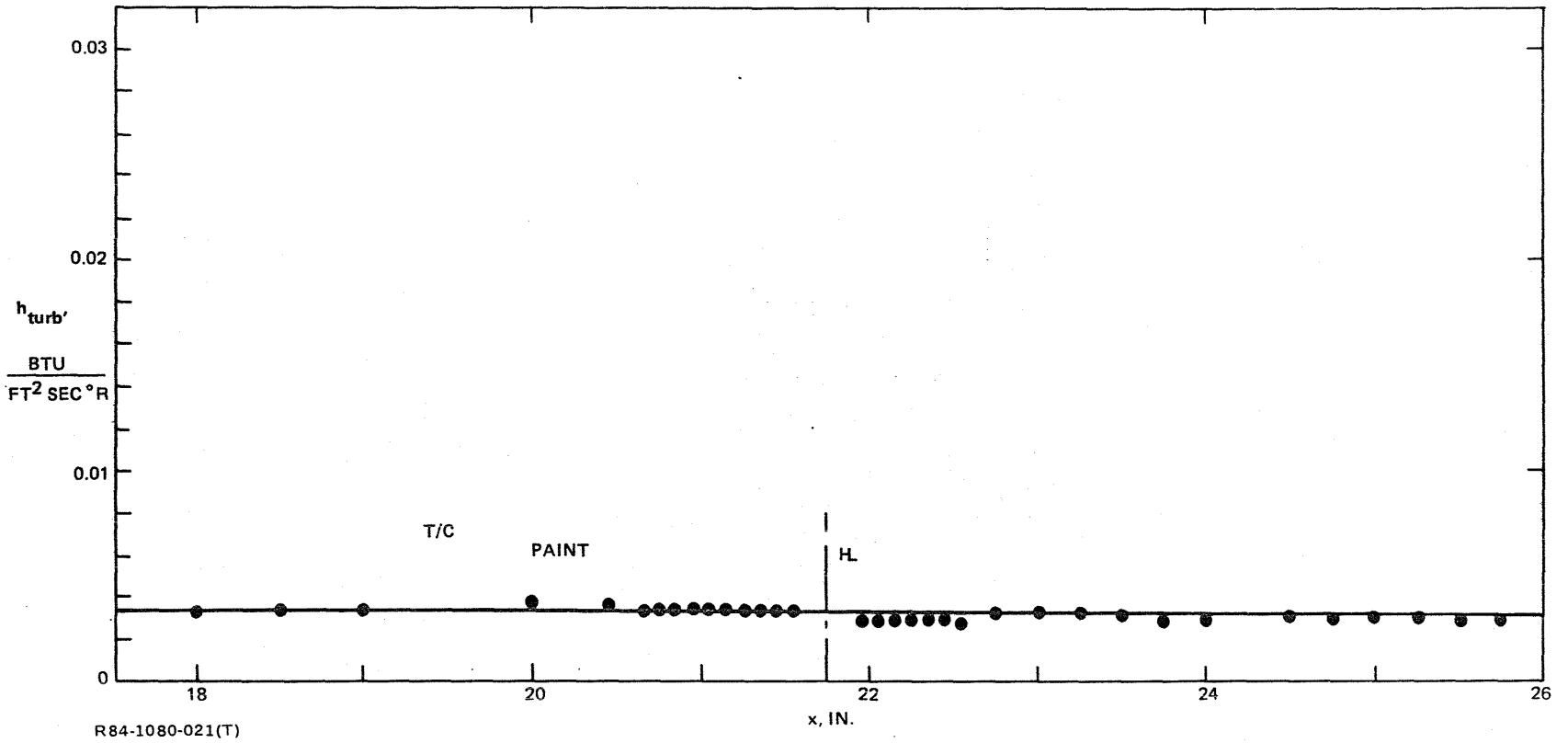

Fig. 21 Undeflected Long Elevon – Comparison of Phase Change & Thermocouple Data, 70° Swept Wing, Cylindrical Center Body

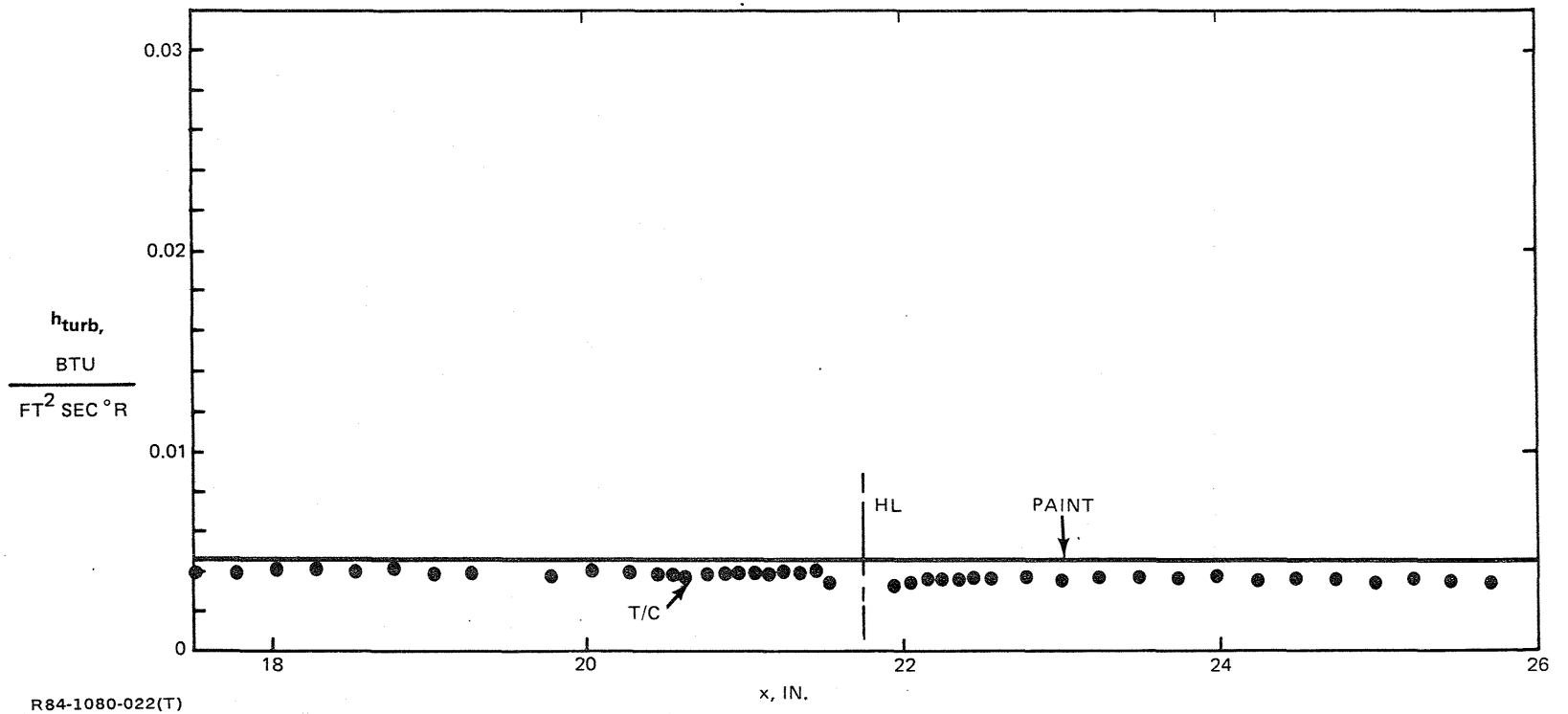

Fig. 22 Undeflected Long Elevon – Comparison of Phase Change & Thermocouple Data, 70° Swept Wing, End Plate Positioned ¼ in. Inboard of Elevon

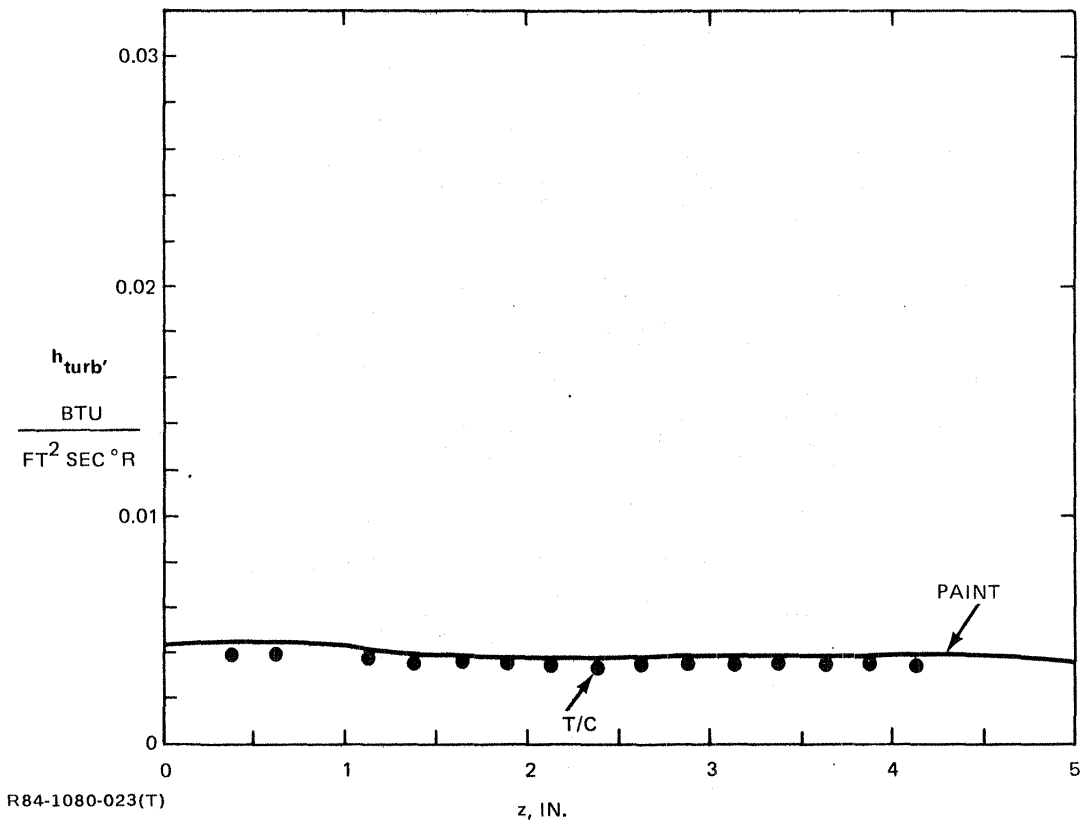

Fig. 23 Undeflected Long Elevon — Comparison of Phase Change & Thermocouple Data, End Plate Positioned ¼ in. Inboard of Elevon, 70° Swept Wing

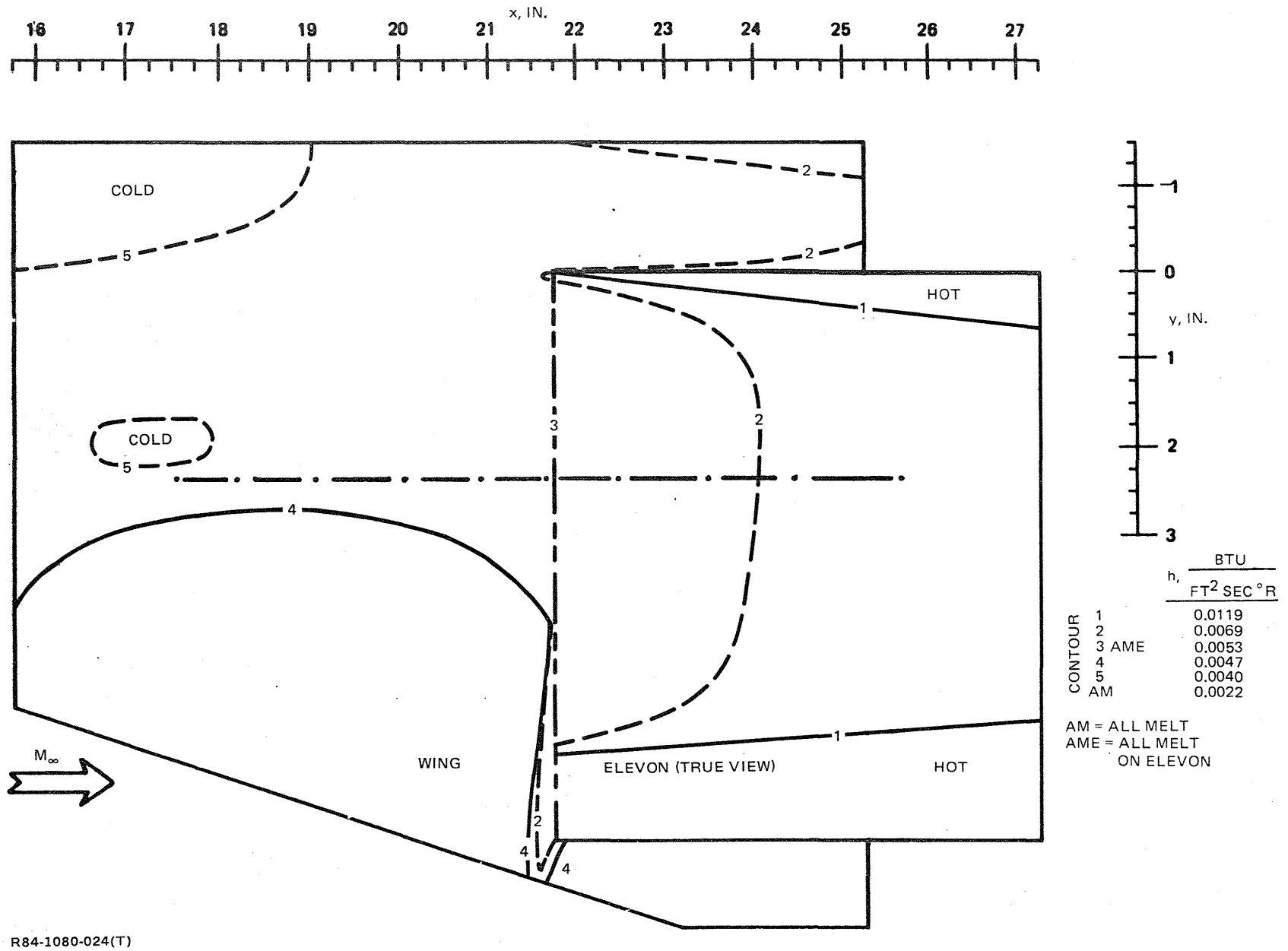

Fig. 24 5° Long Elevon – Planform Phase Change Results, Unswept Wing, No Center Body

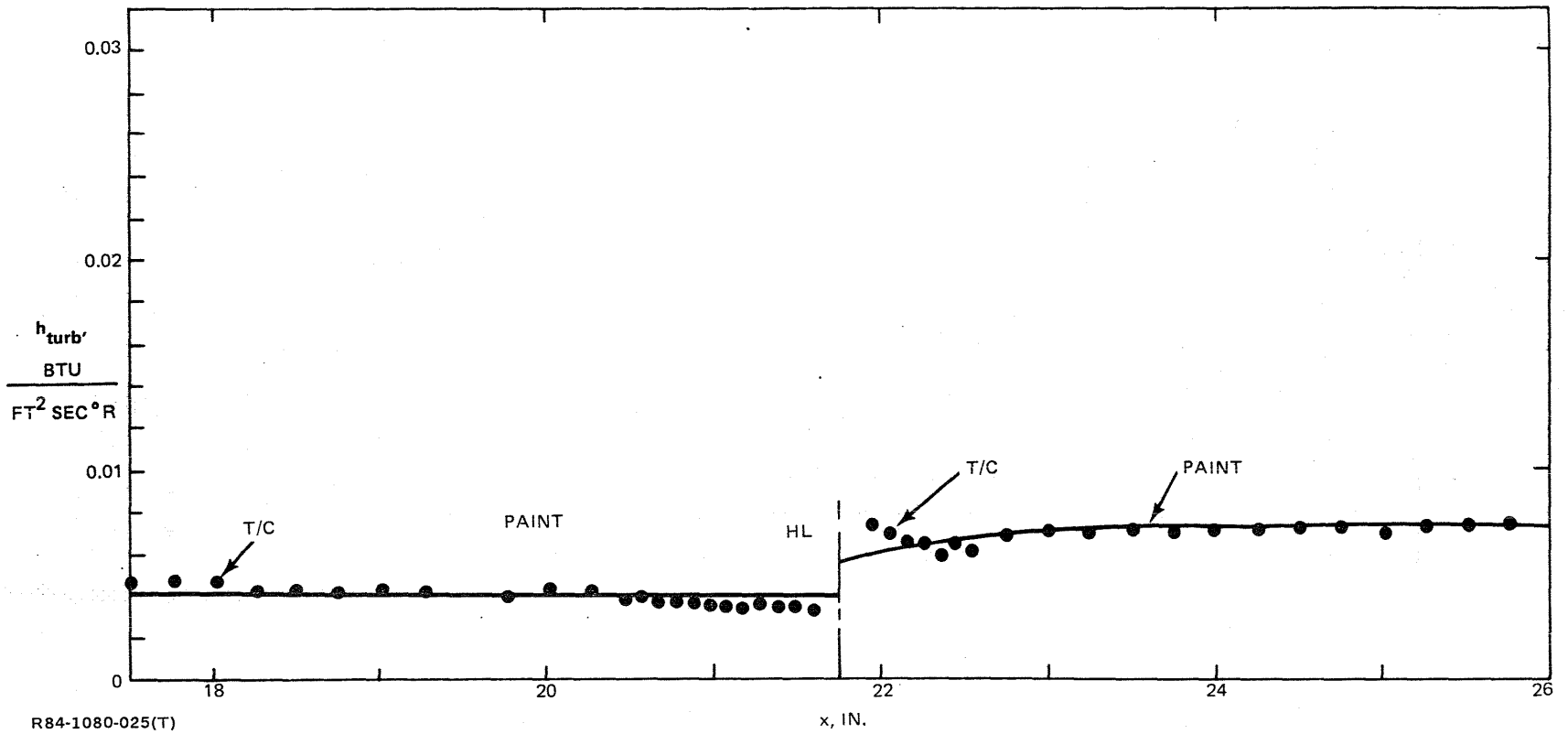

Fig. 25 5° Long Elevon — Comparison of Phase Change & Thermocouple Data, Unswept Wing, No Center Body

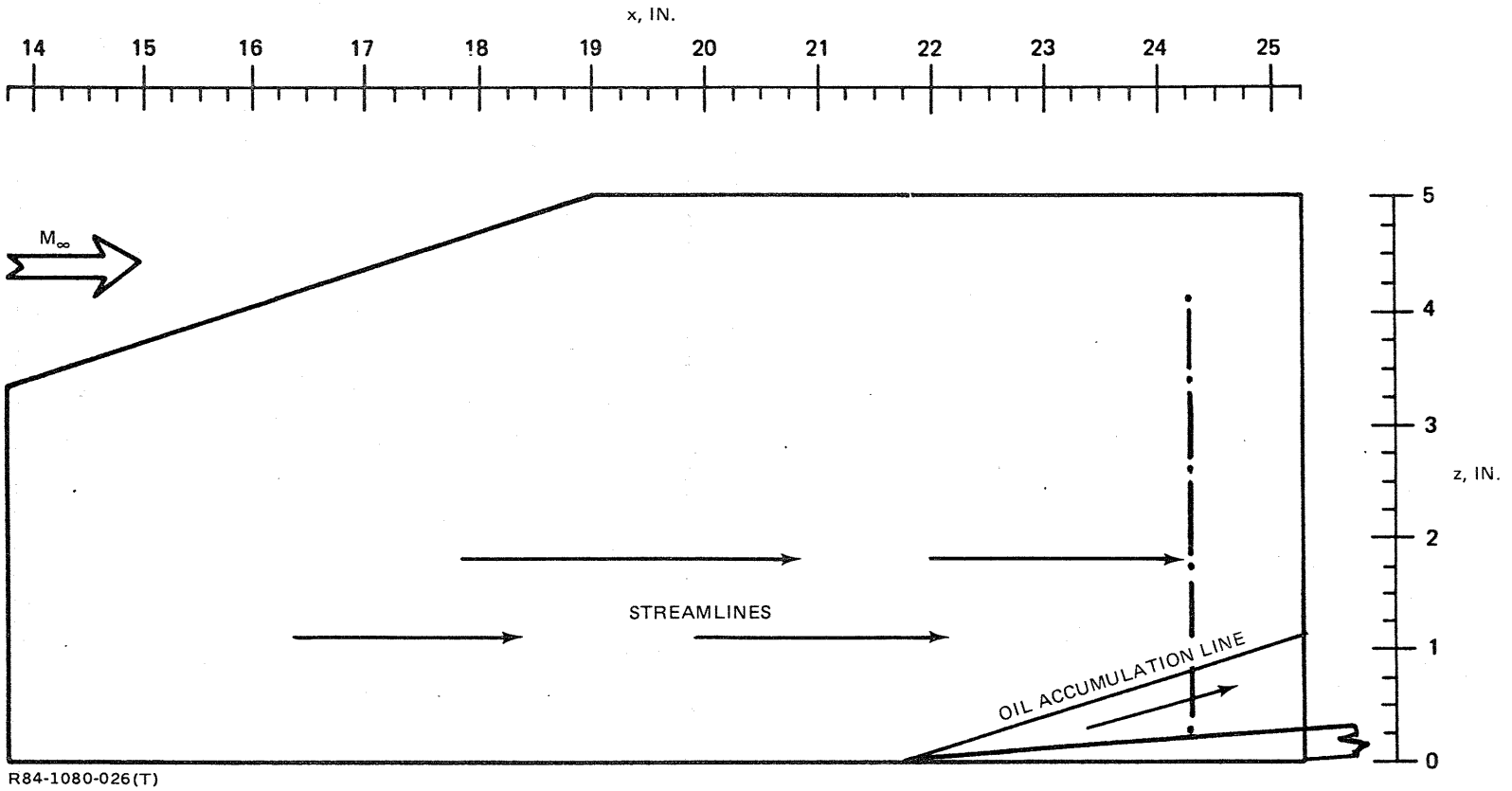

Fig. 26 5° Long Elevon – Oil Flow Pattern on End Plate Surface, Unswept Wing

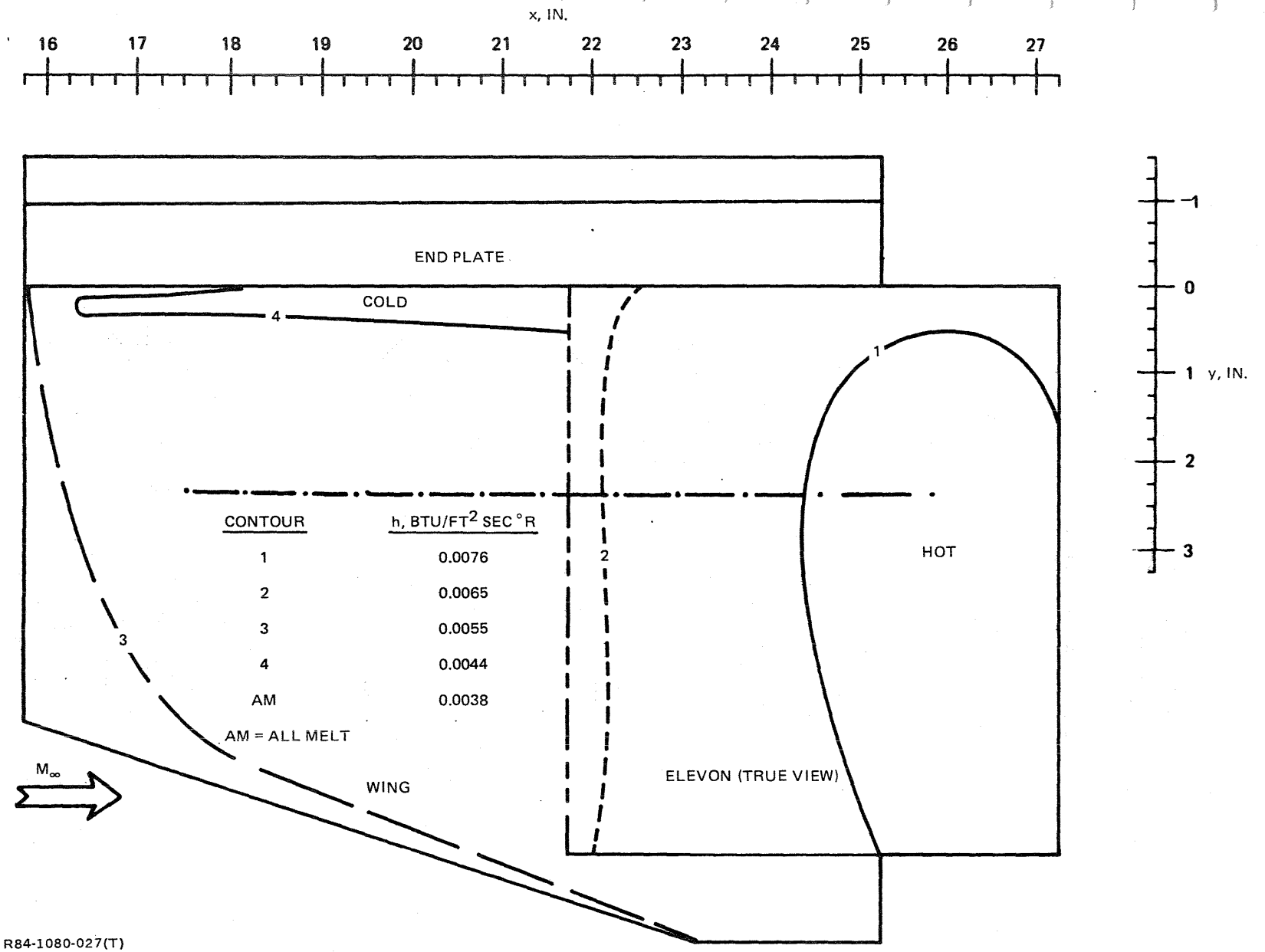

Fig. 27 5° Long Elevon — Planform Phase Change Results, Unswept Wing, End Plate

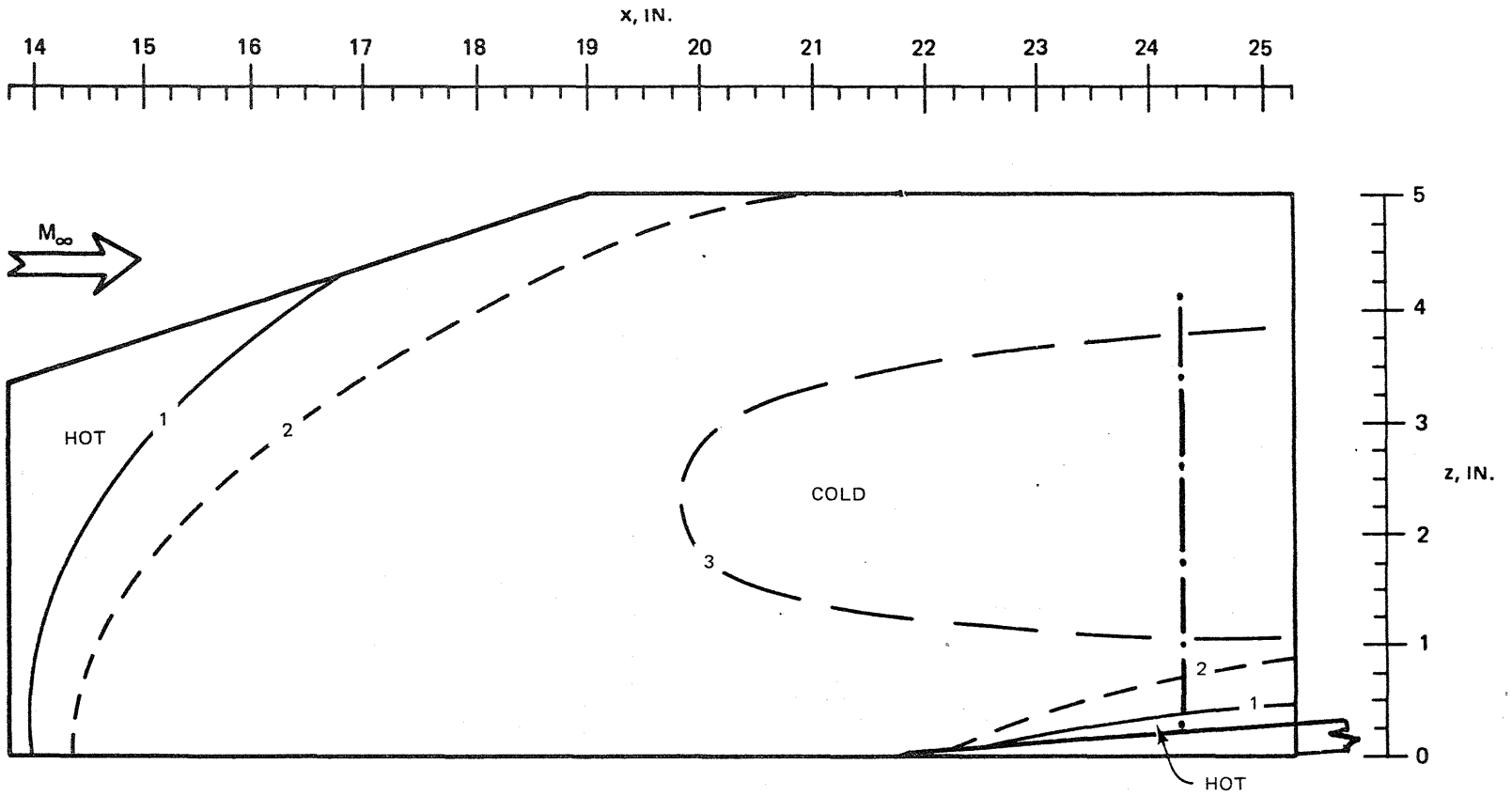

CONTOUR	h, BTU/FT^2 SEC °R
1	0.0055
2	0.0044
3	0.0038
ALL MELT	0.0036

R84-1080-028(T)

Fig. 28 5° Long Elevon — Profile Phase Change Results, End Plate, Unswept Wing

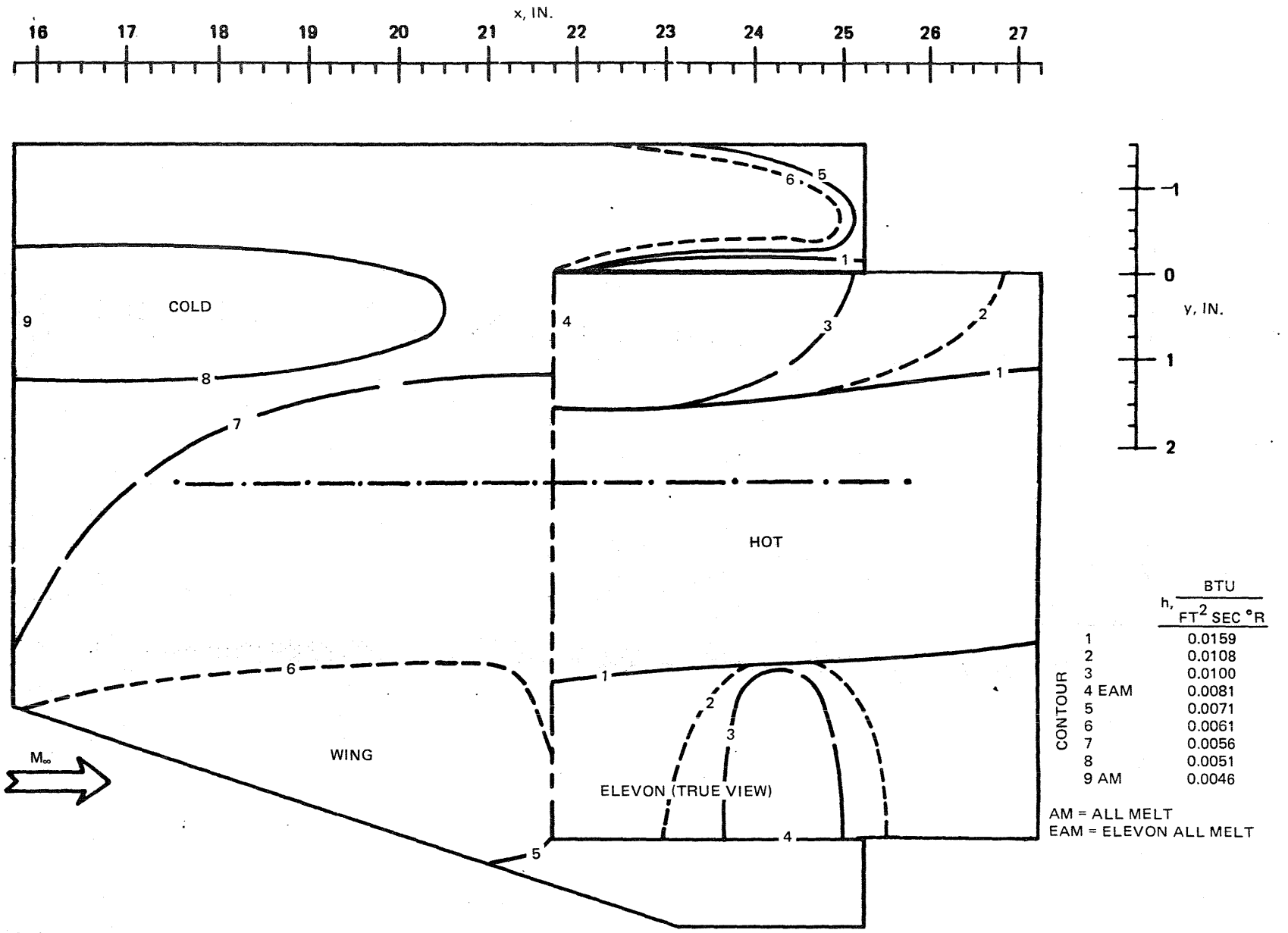

Fig. 29 5° Long Elevon — Planform Phase Change Results, 70° Swept Wing, No Center Body

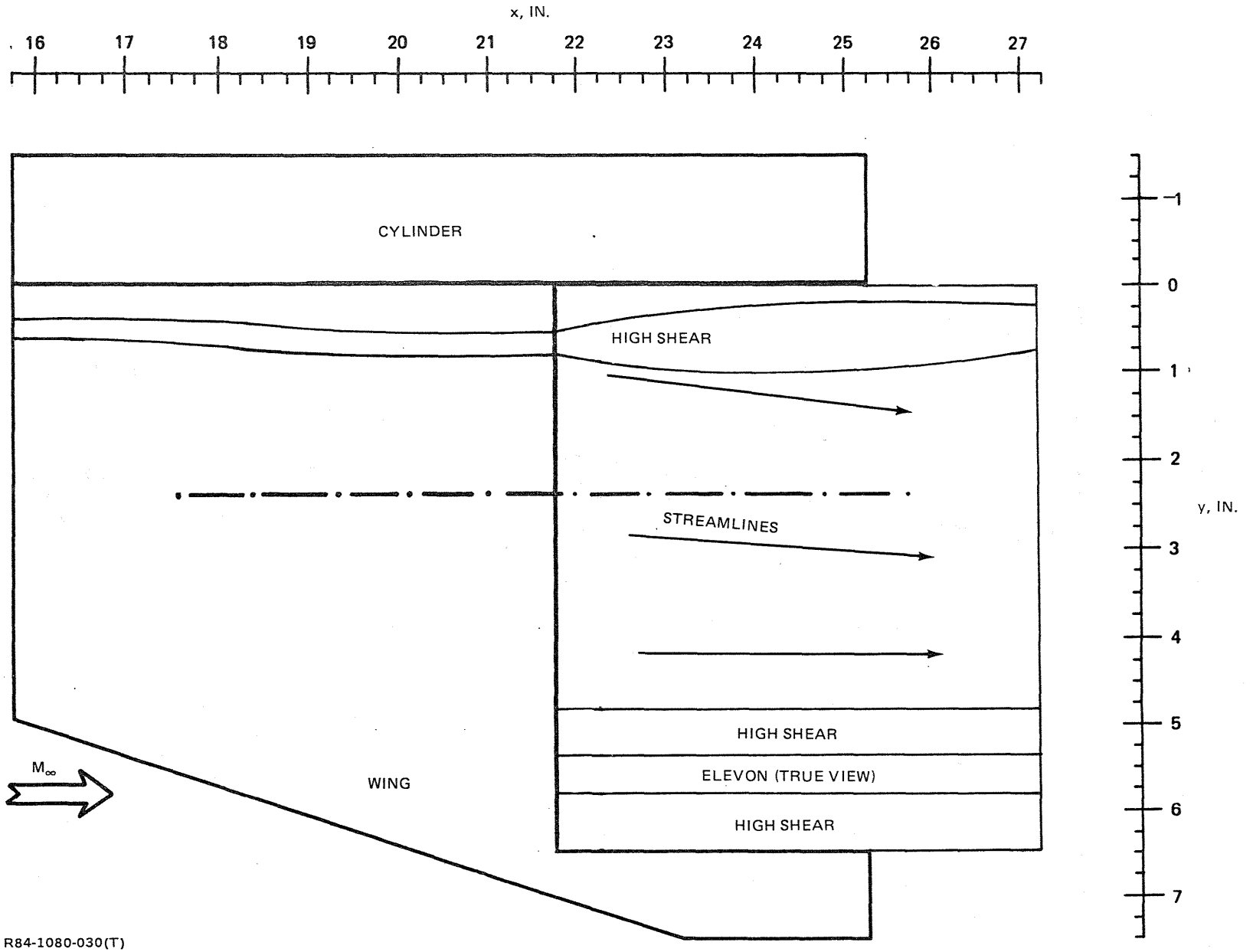

Fig. 30 5° Long Elevon – Planform Oil Flow Results, 70° Swept Wing, Cylindrical Center Body

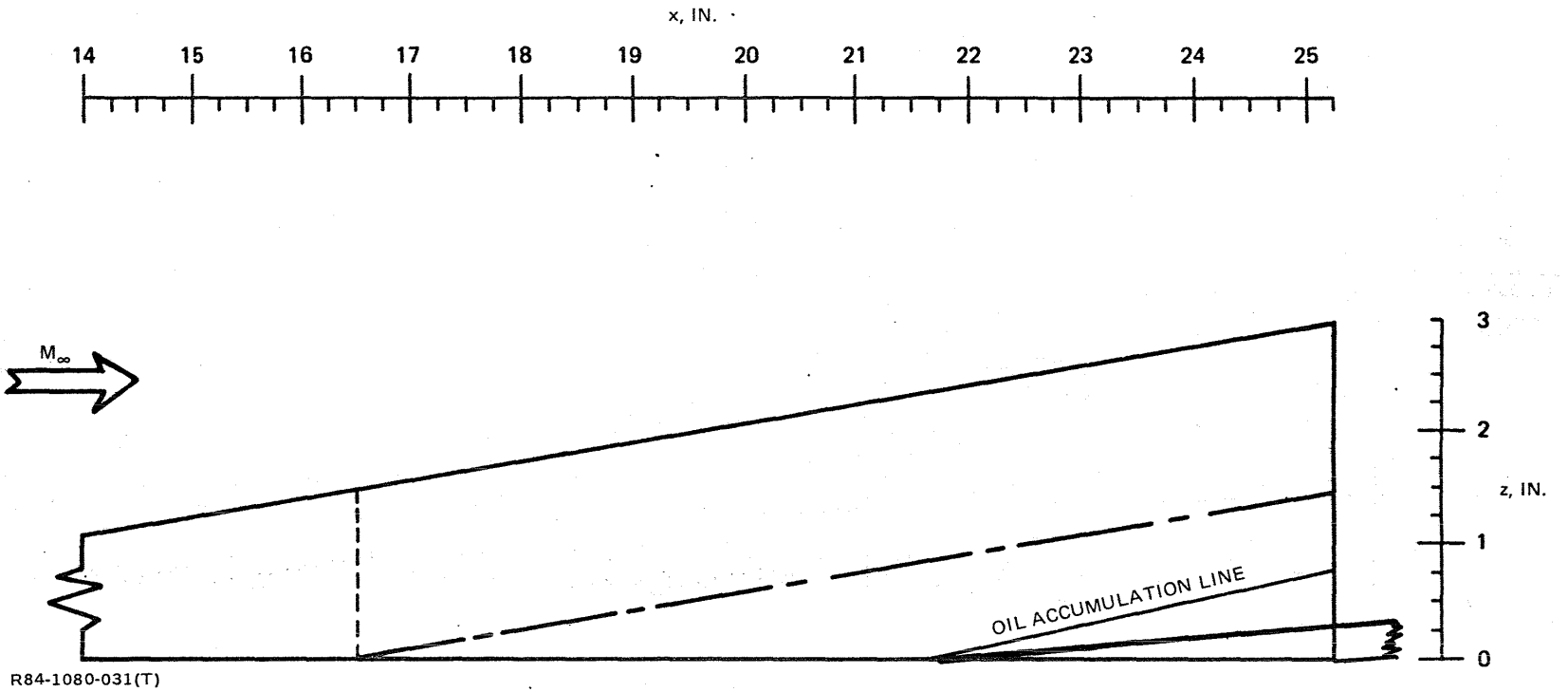

Fig. 31 5° Long Elevon — Oil Accumulation Line on Cylindrical Center Body, 70° Swept Wing

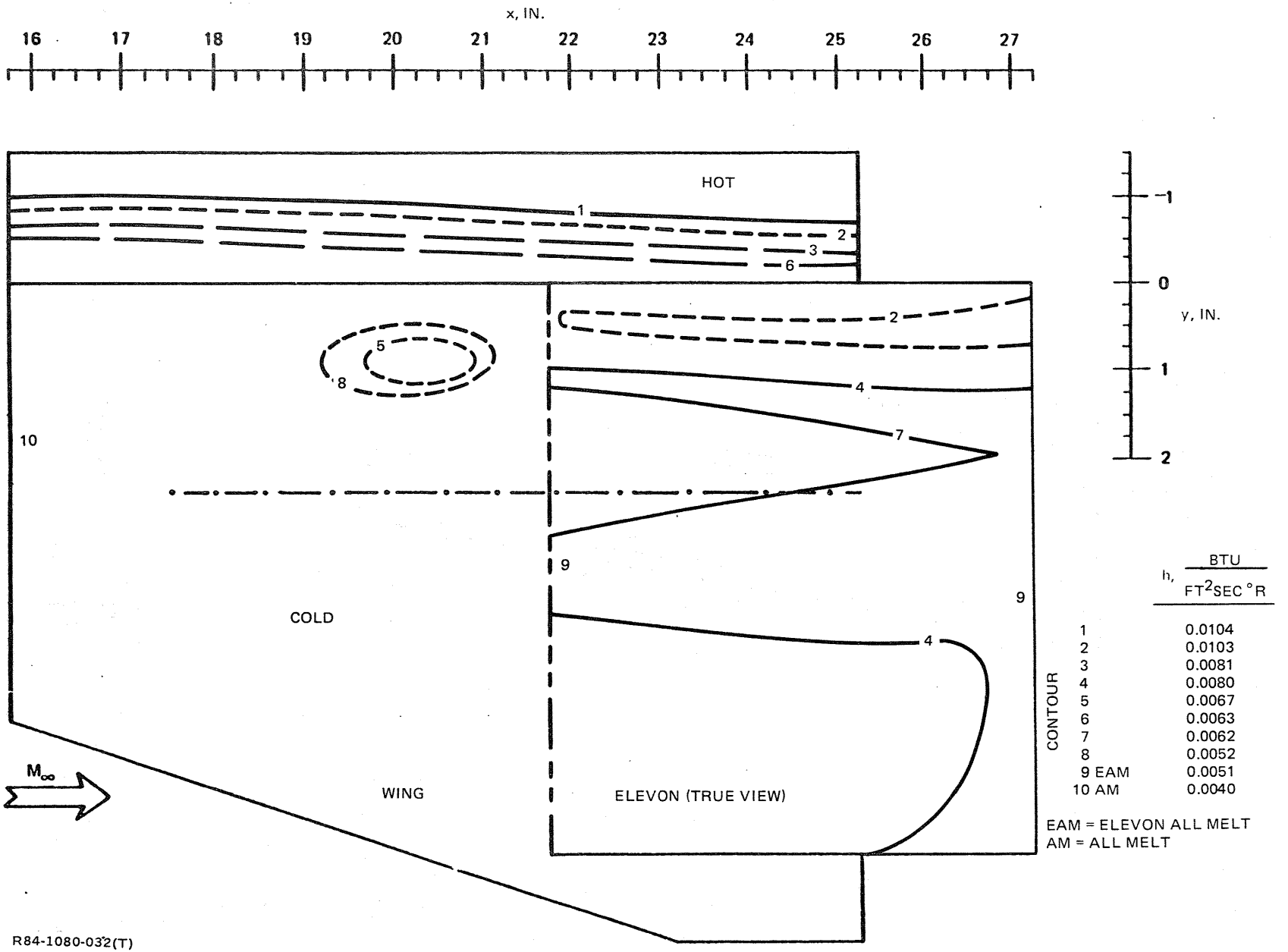

Fig. 32 5° Long Elevon – Planform Phase Change Results, 70° Swept Wing, Cylindrical Center Body

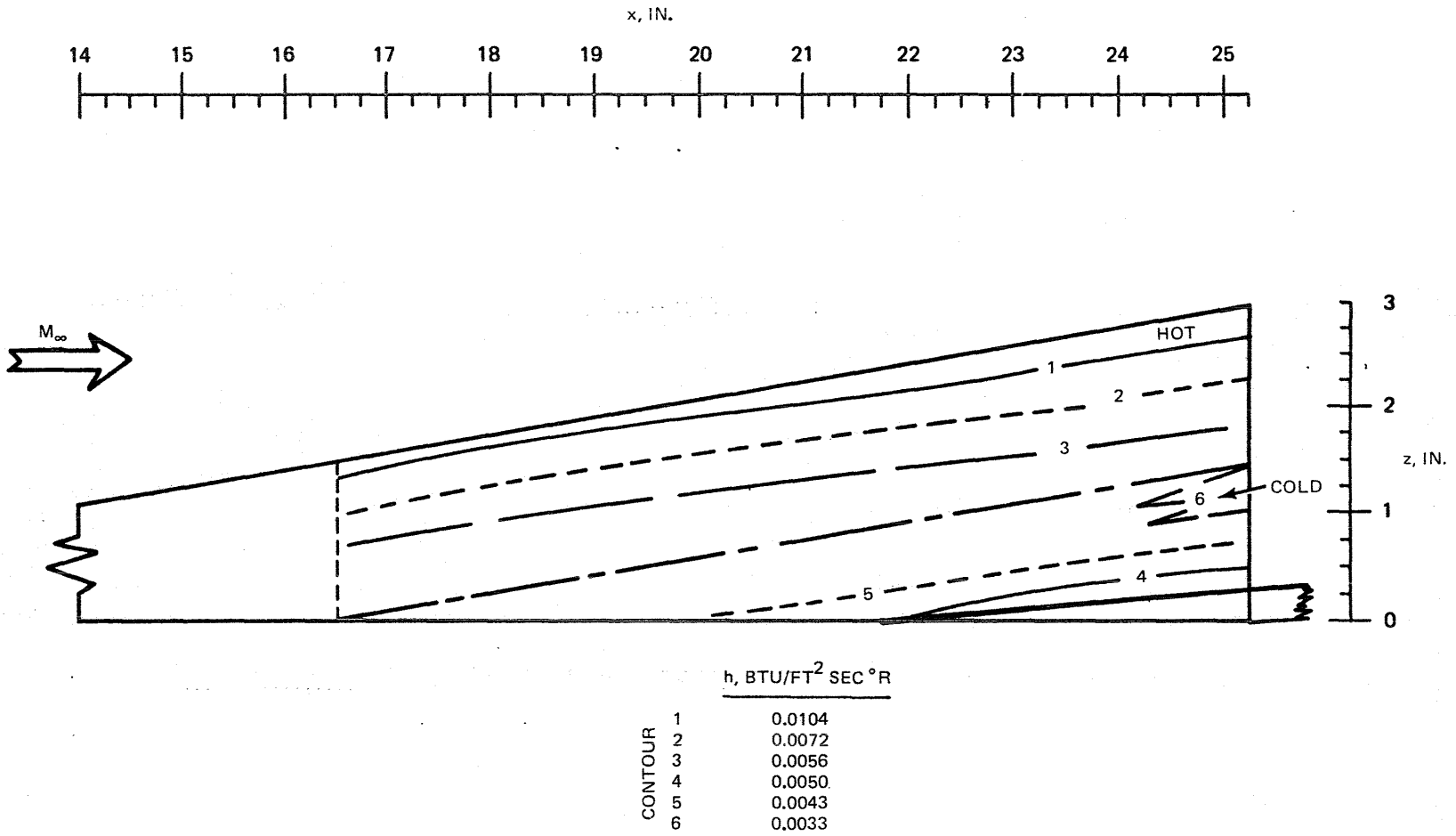

R84-1080-033(T)

Fig. 33 5° Long Elevon – Profile Phase Change Results, Cylindrical Center Body, 70° Swept Wing

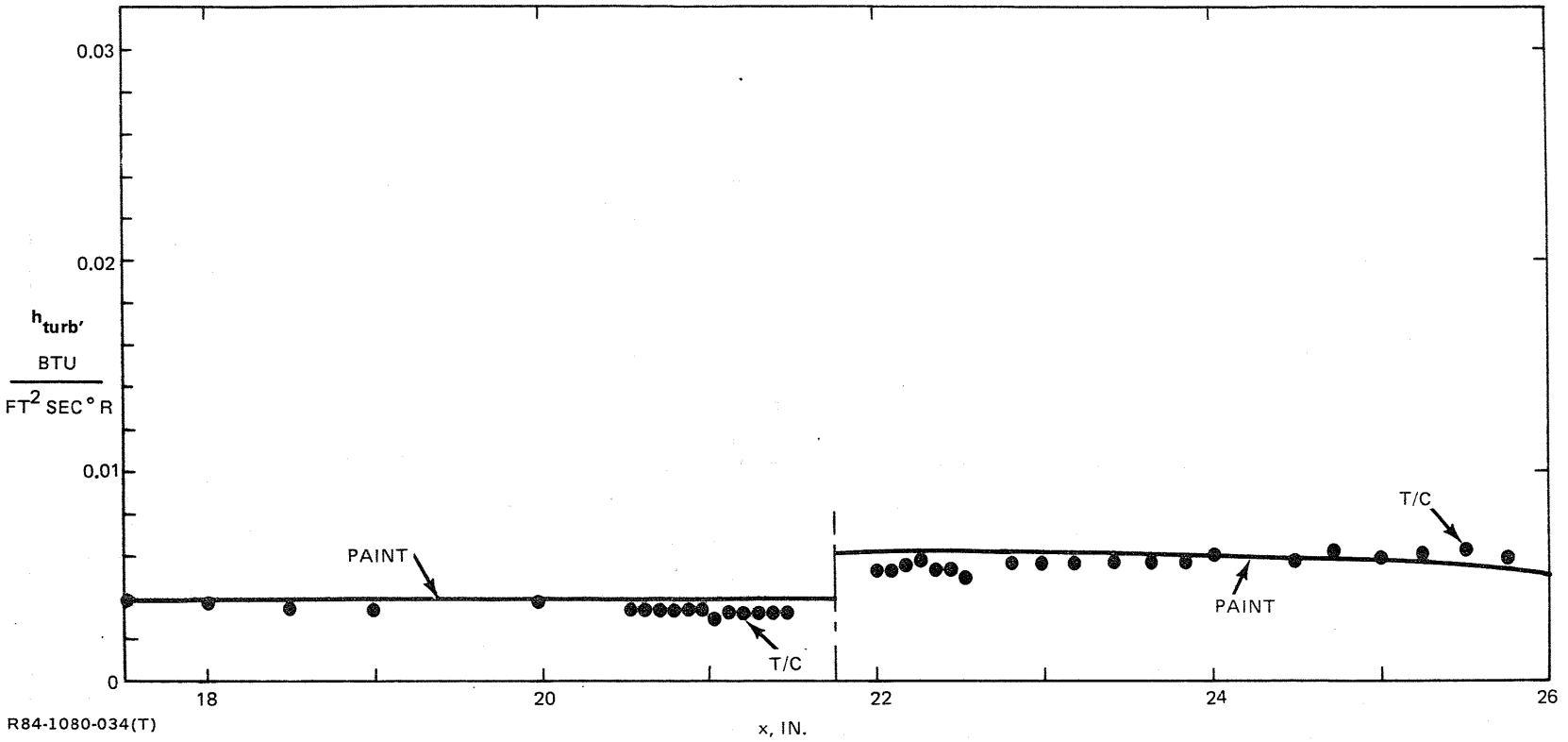

Fig. 34 5° Long Elevon – Comparison of Phase Change & Thermocouple Data, 70° Swept Wing, Cylindrical Center Body

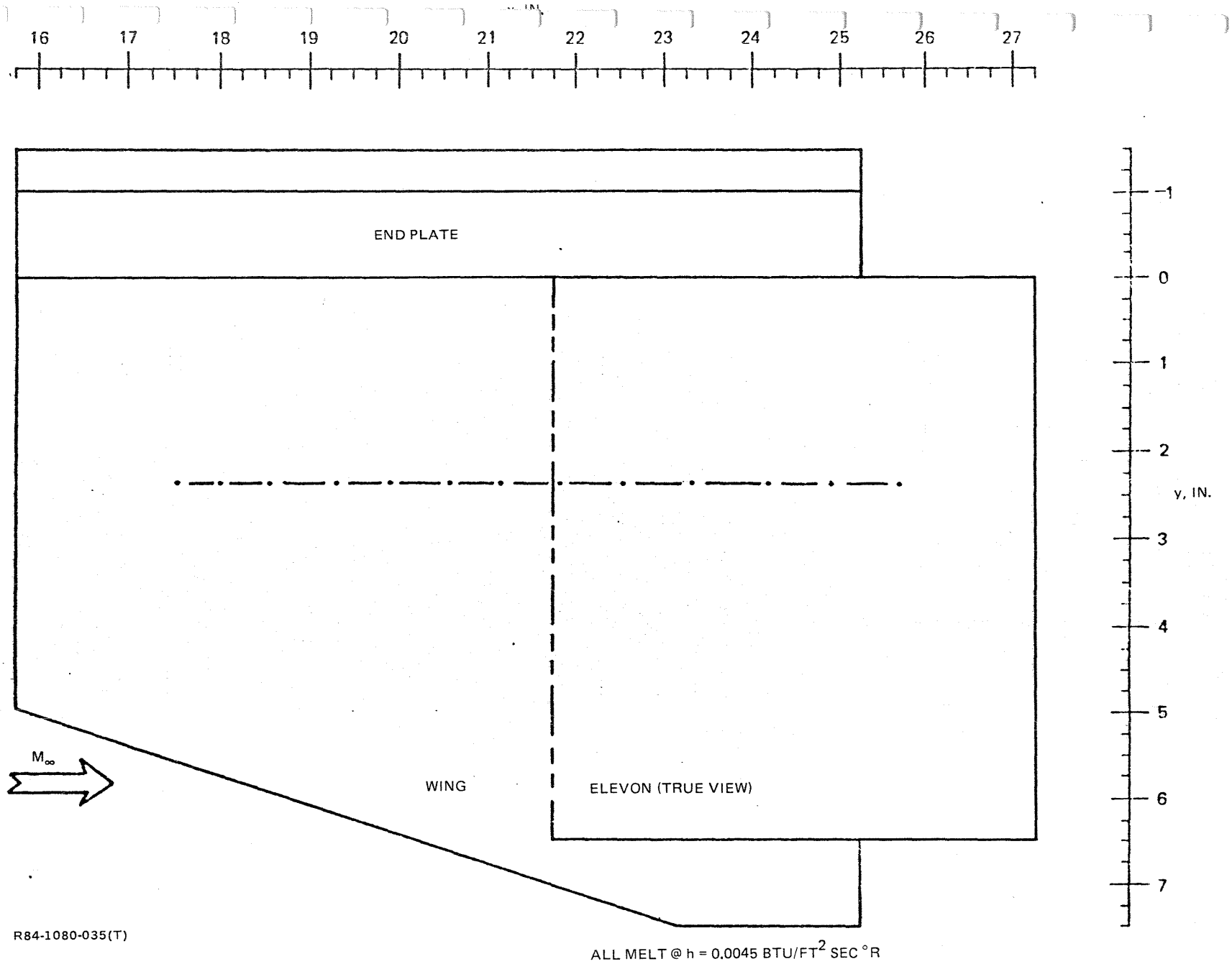

Fig. 35 5° Long Elevon — Planform Phase Change Results, 70° Swept Wing, End Plate

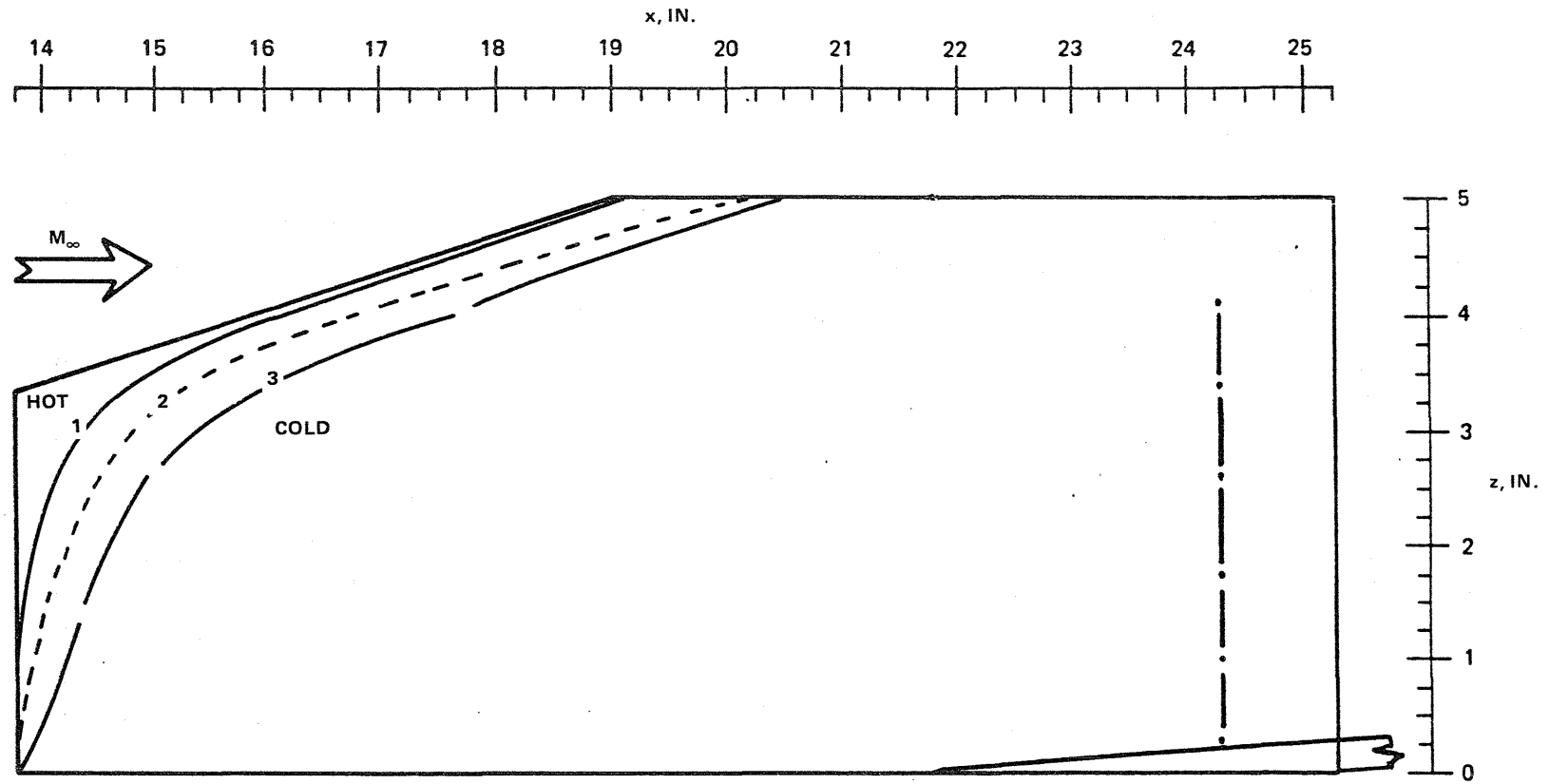

CONTOUR	h, BTU/FT^2 SEC °R
1	0.0050
2	0.0046
3	0.0044

R84-1080-036(T)

Fig. 36 5° Long Elevon – Profile Phase Change Results, End Plate, 70° Swept Wing

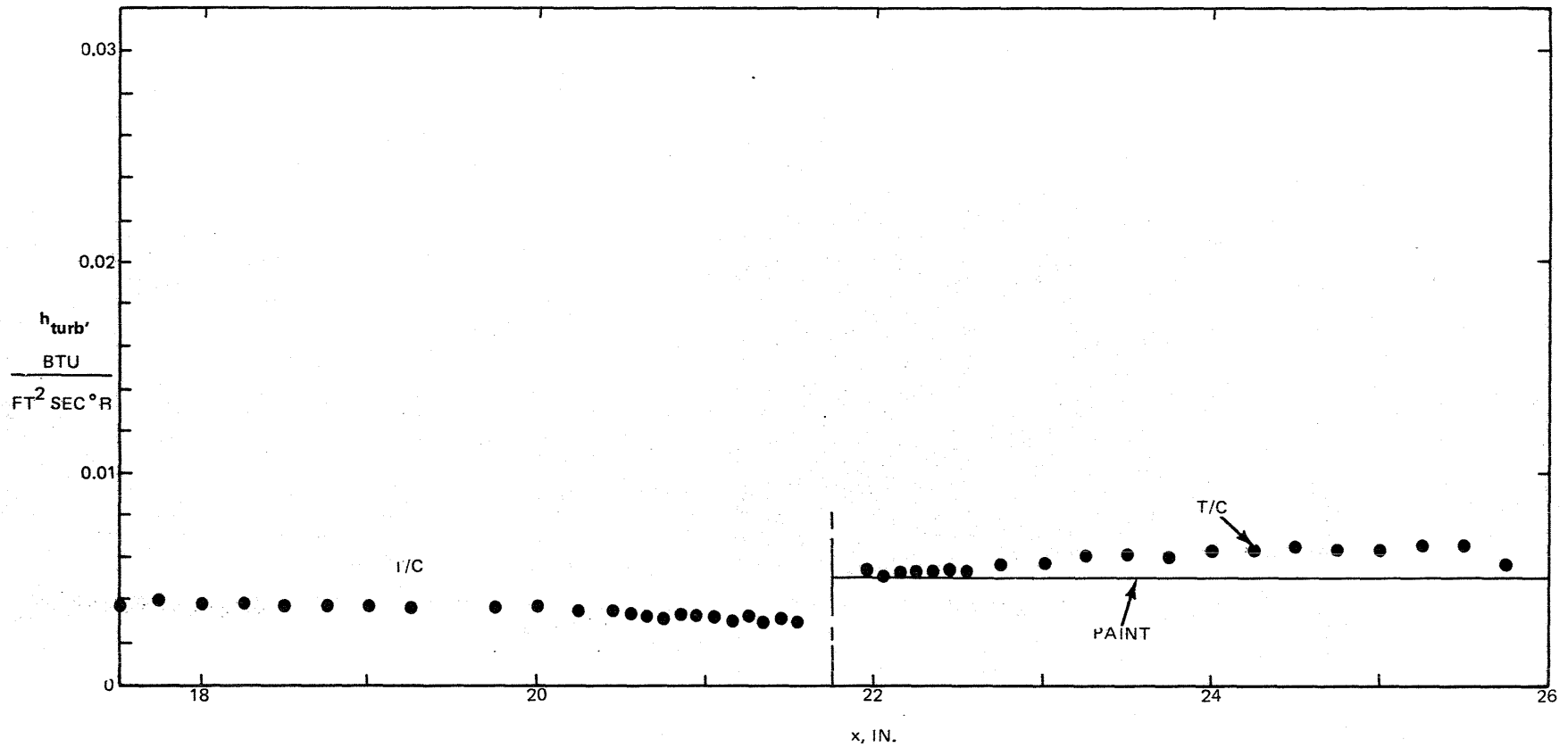

R84-1080-037(T)

Fig. 37 5° Long Elevon — Comparison of Phase Change & Thermocouple Data, 70° Swept Wing, End Plate

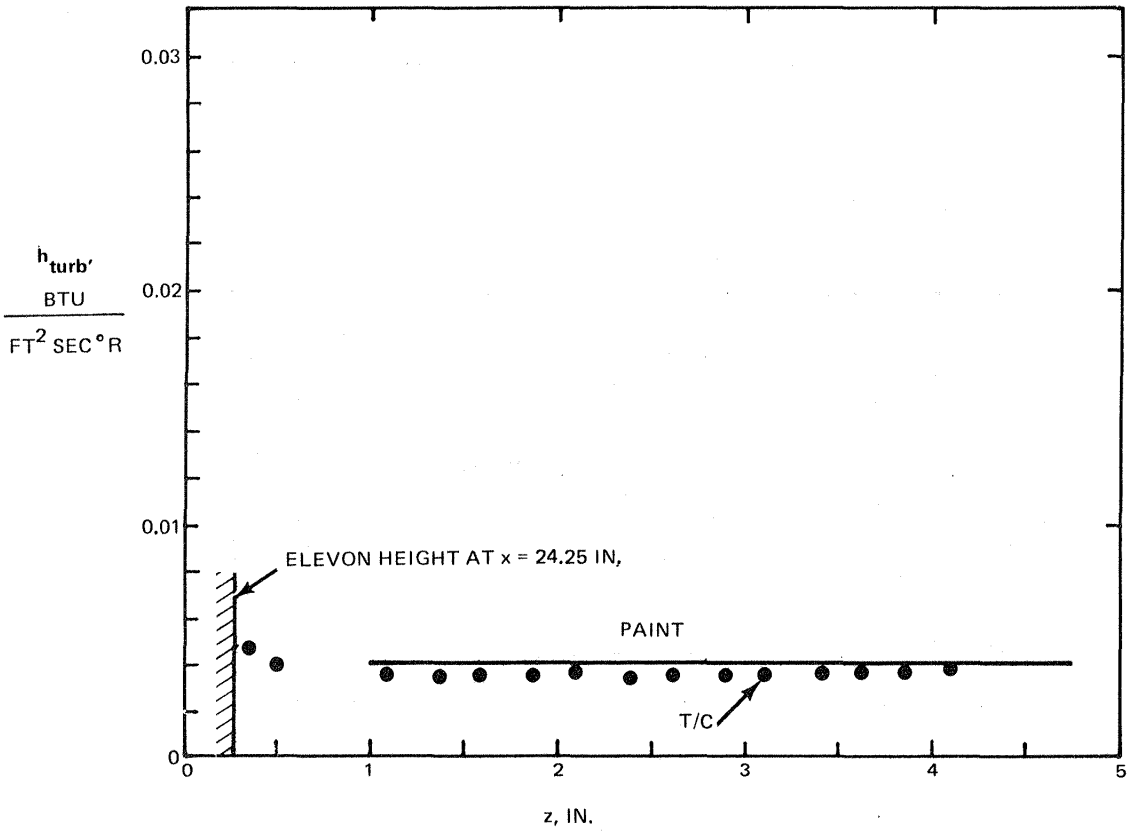

R84-1080-038(T

Fig. 38 5° Long Elevon — Comparison of Phase Change & Thermocouple Data, End Plate, 70° Swept Wing

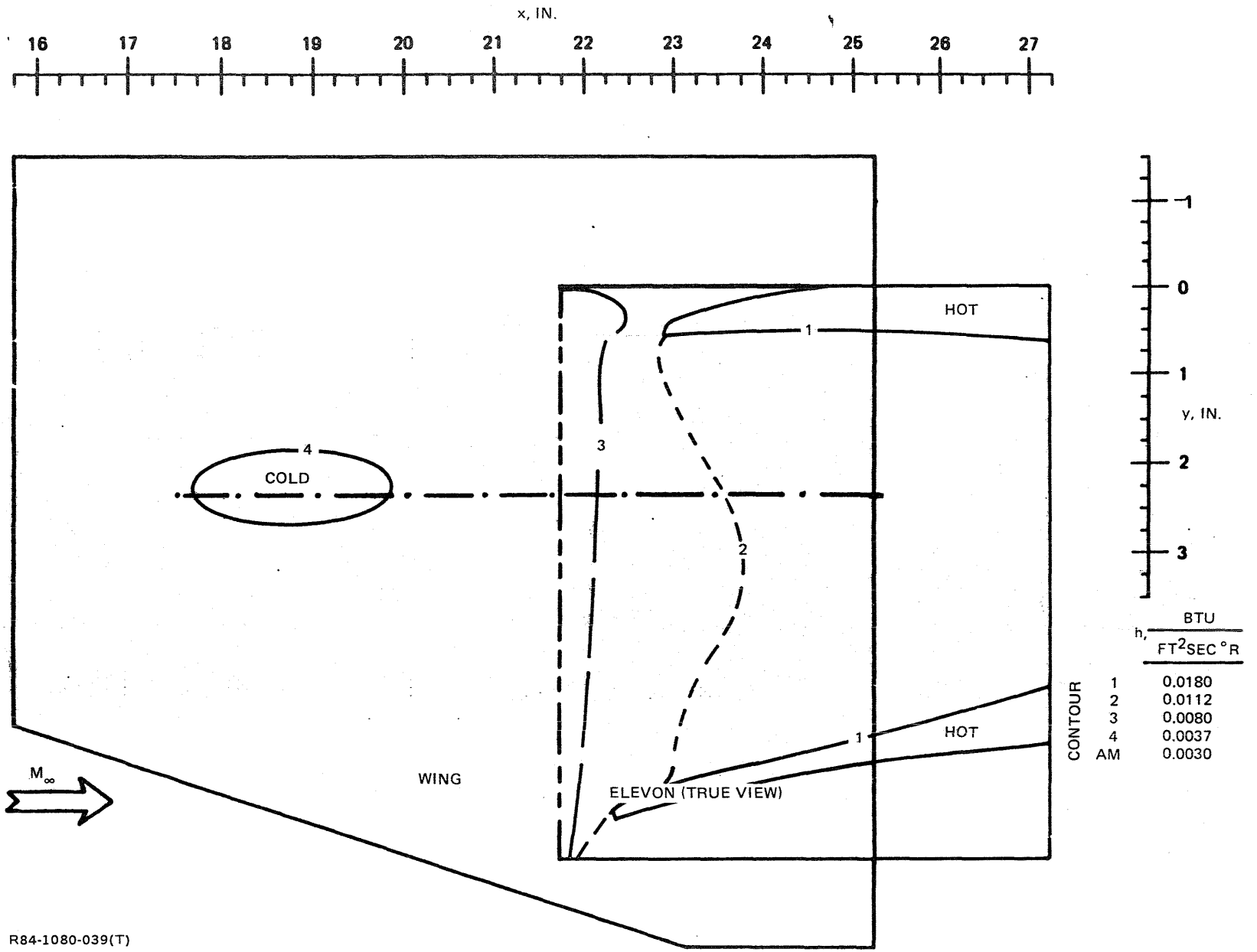

Fig. 39 10° Long Elevon — Planform Phase Change Results, Unswept Wing, No Center Body

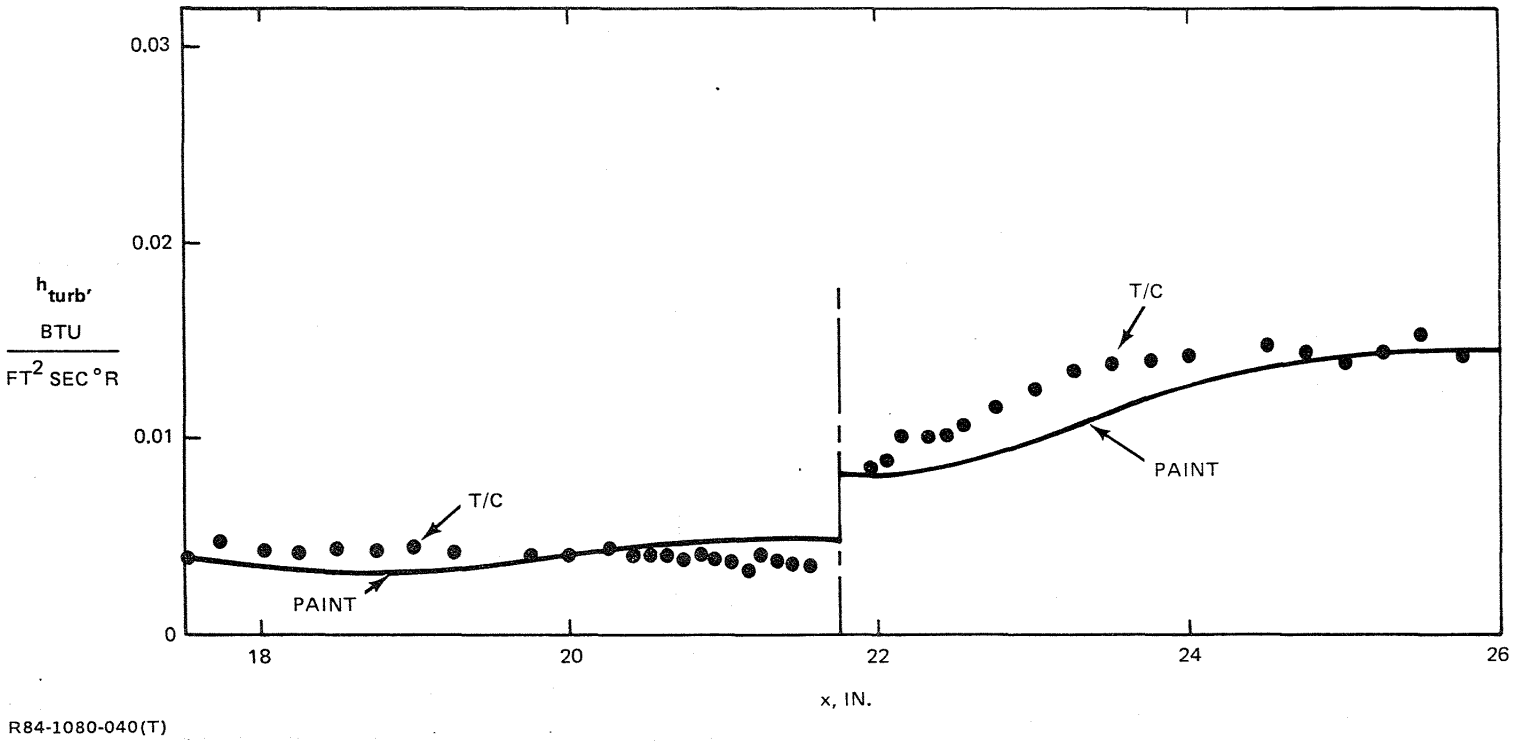

R84-1080-040(T)

Fig. 40 10° Long Elevon — Comparison of Phase Change & Thermocouple Data, Unswept Wing, No Center Body

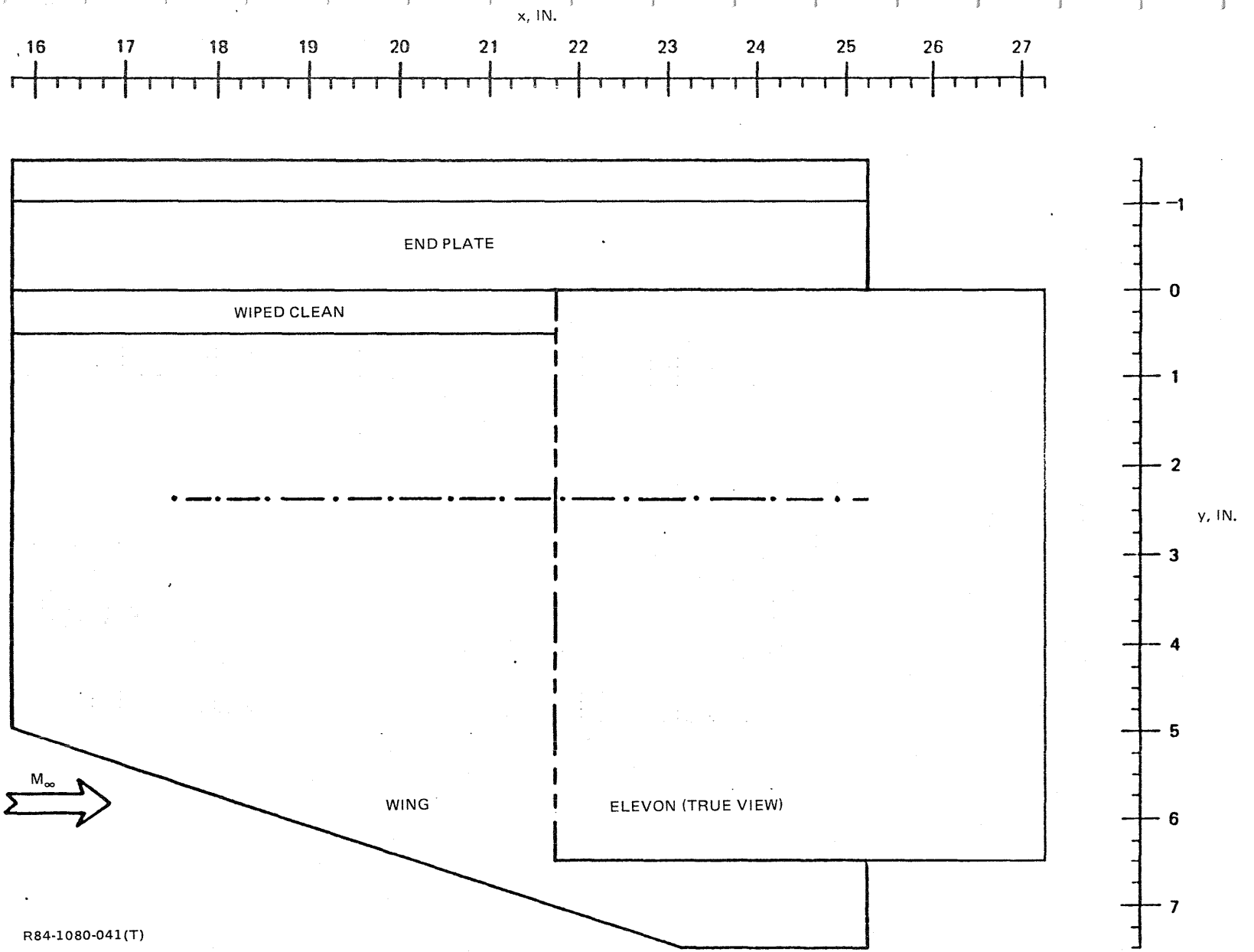

Fig. 41 10° Long Elevon – Planform Oil Flow Results Indicating Region of High Shear, Unswept Wing, End Plate

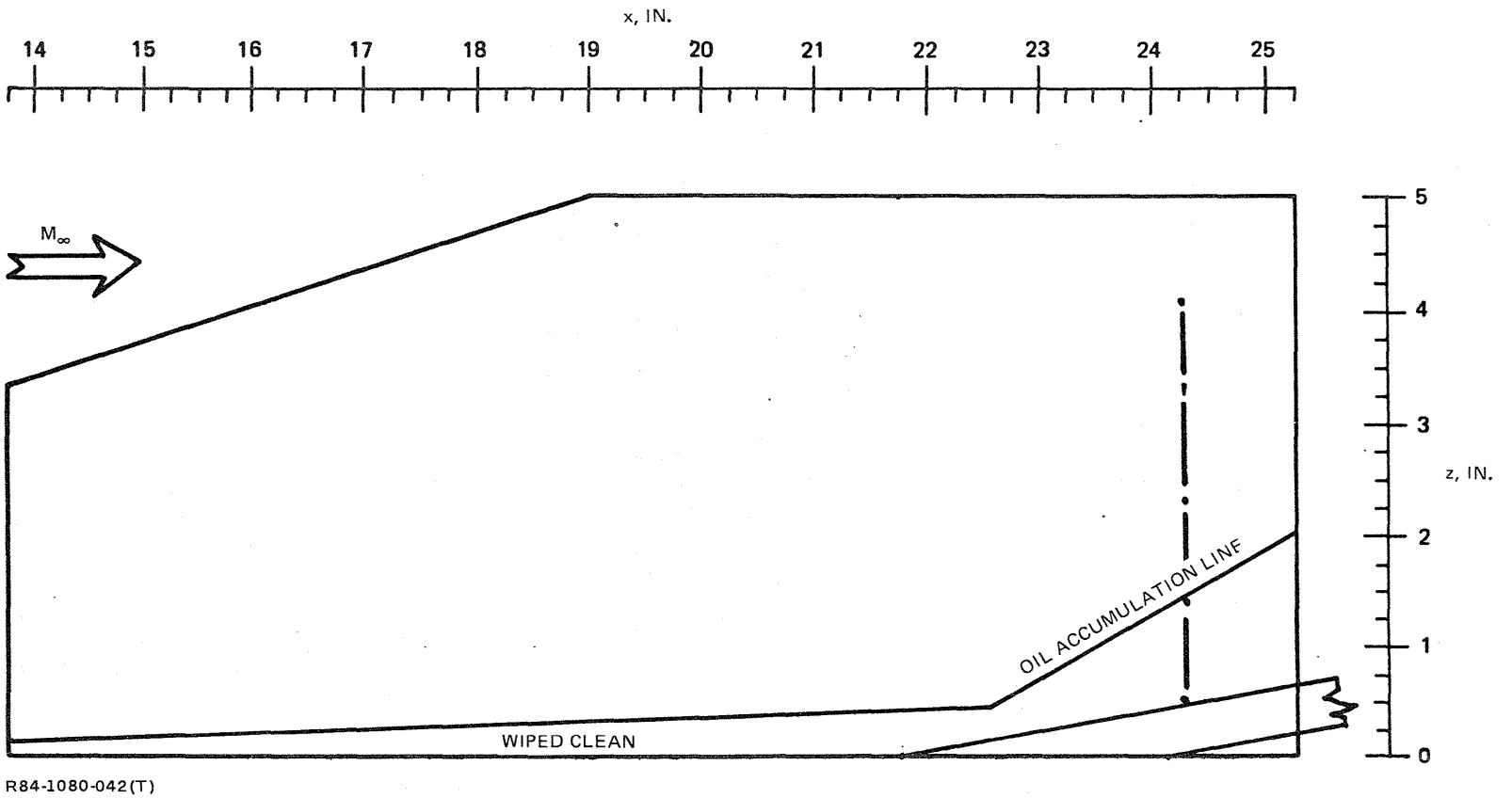

R84-1080-042(T)

Fig. 42 10° Long Elevon — Profile Oil Flow Results on End Plate Surface Indicating Region of High Shear and Oil Accumulation Line, Unswept Wing

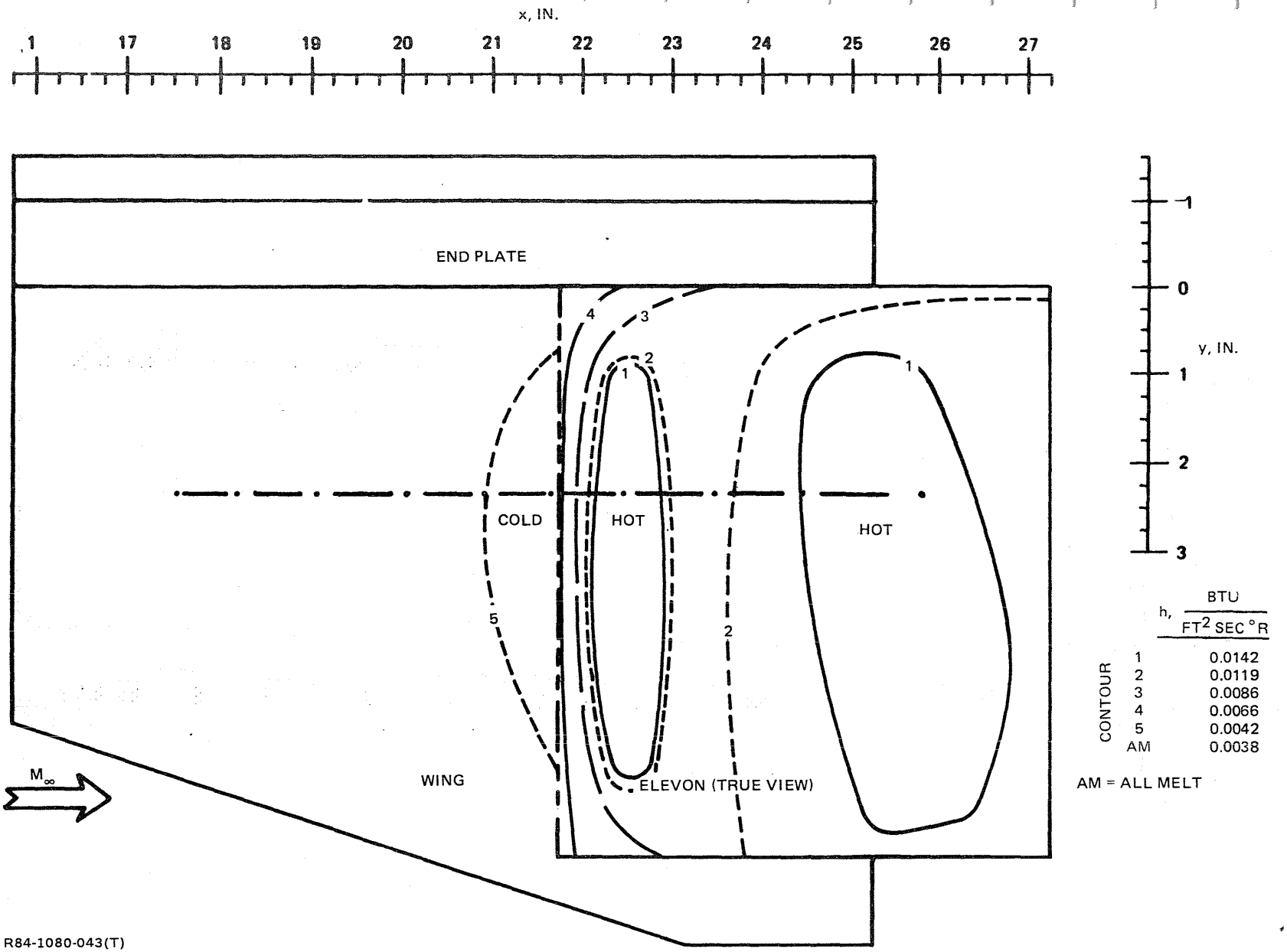

Fig. 43 10° Long Elevon — Planform Phase Change Results, Unswept Wing, End Plate

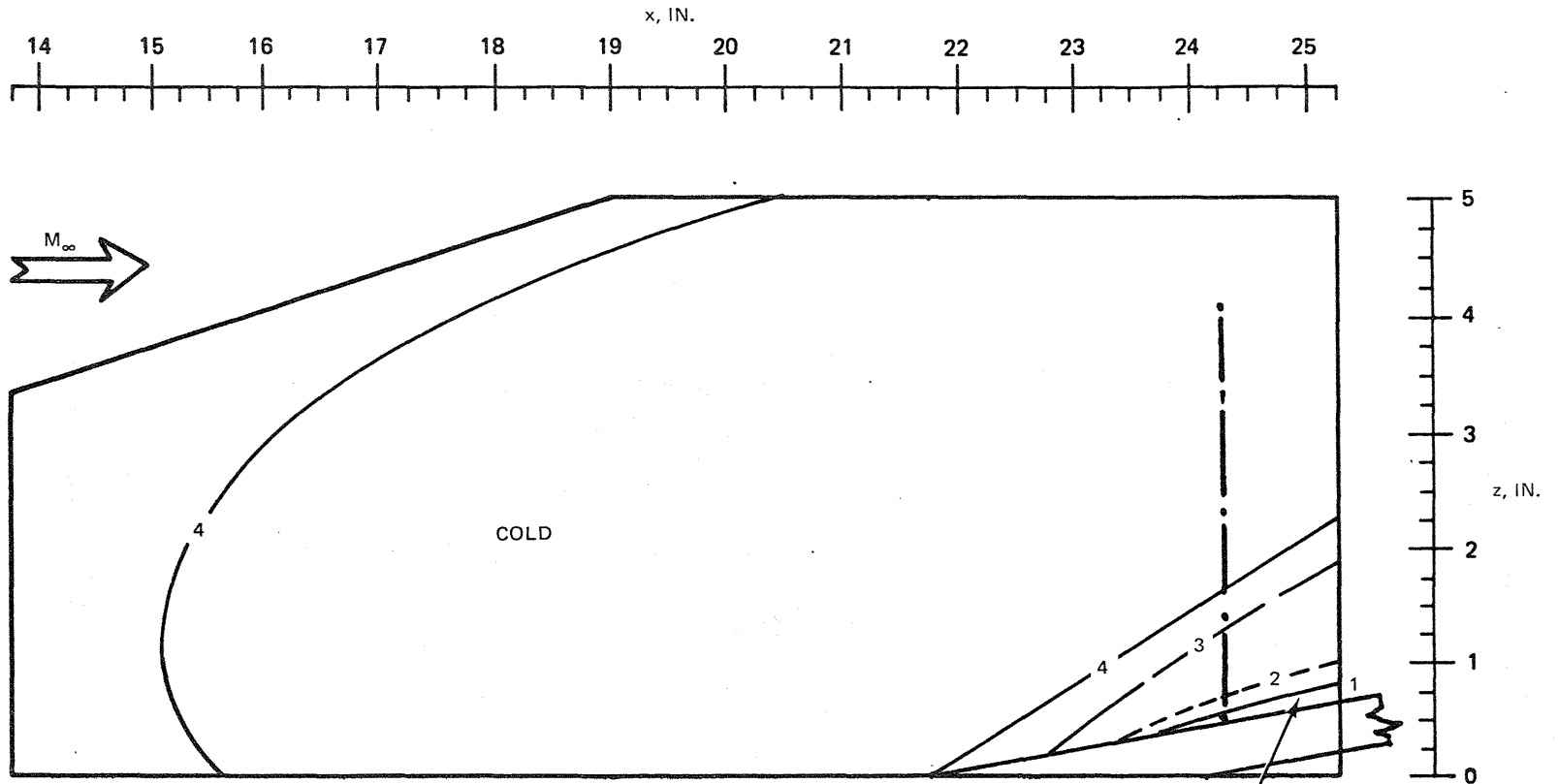

CONTOUR	h, BTU/FT^2 SEC °R
1	0.0119
2	0.0086
3	0.0066
4	0.0042
ALL MELT	0.0038

R84-1080-044(T)

Fig. 44 10° Long Elevon – Profile Phase Change Results, End Plate, Unswept Wing

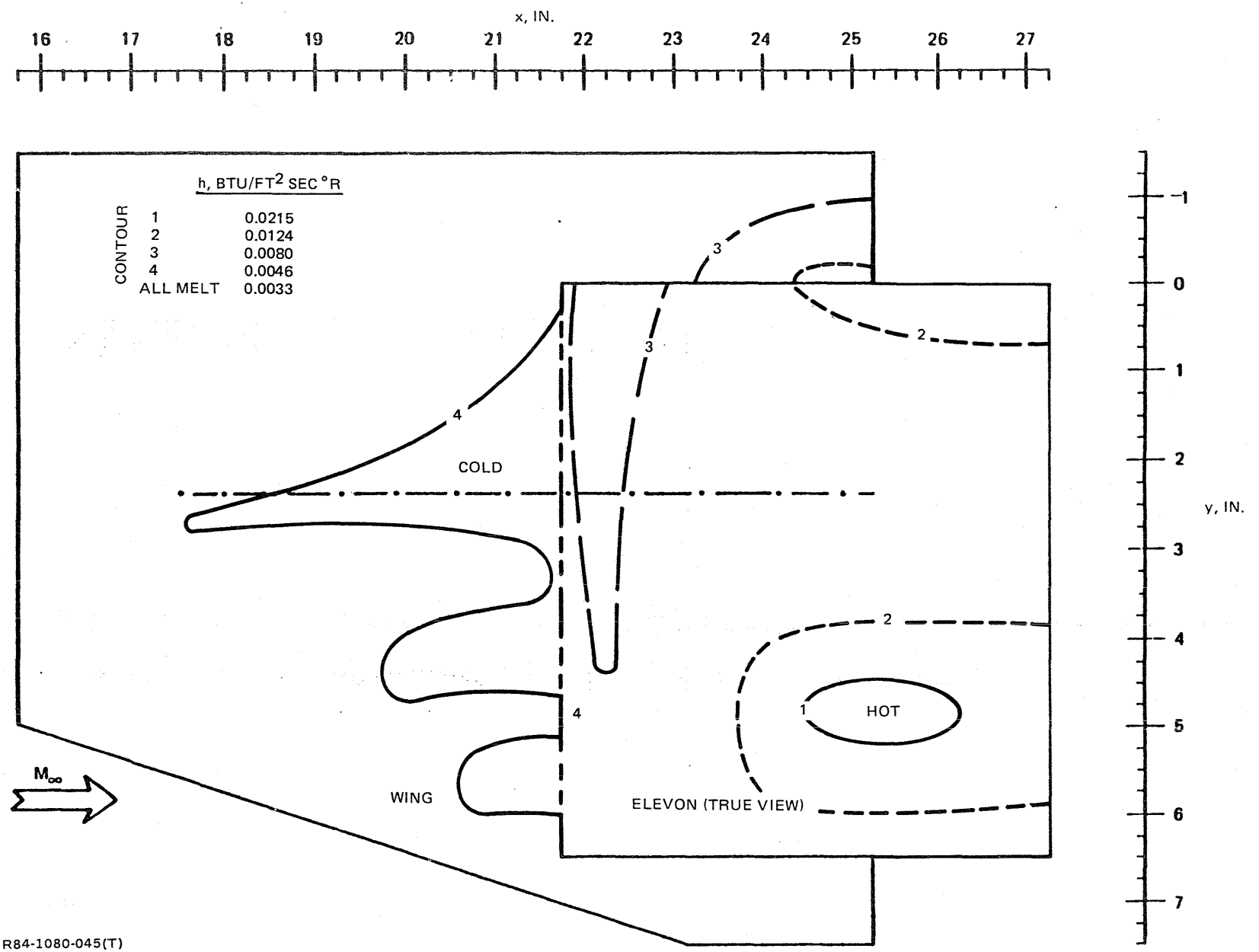

Fig. 45 10° Long Elevon — Planform Phase Change Results, 50° Swept Wing, No Center Body

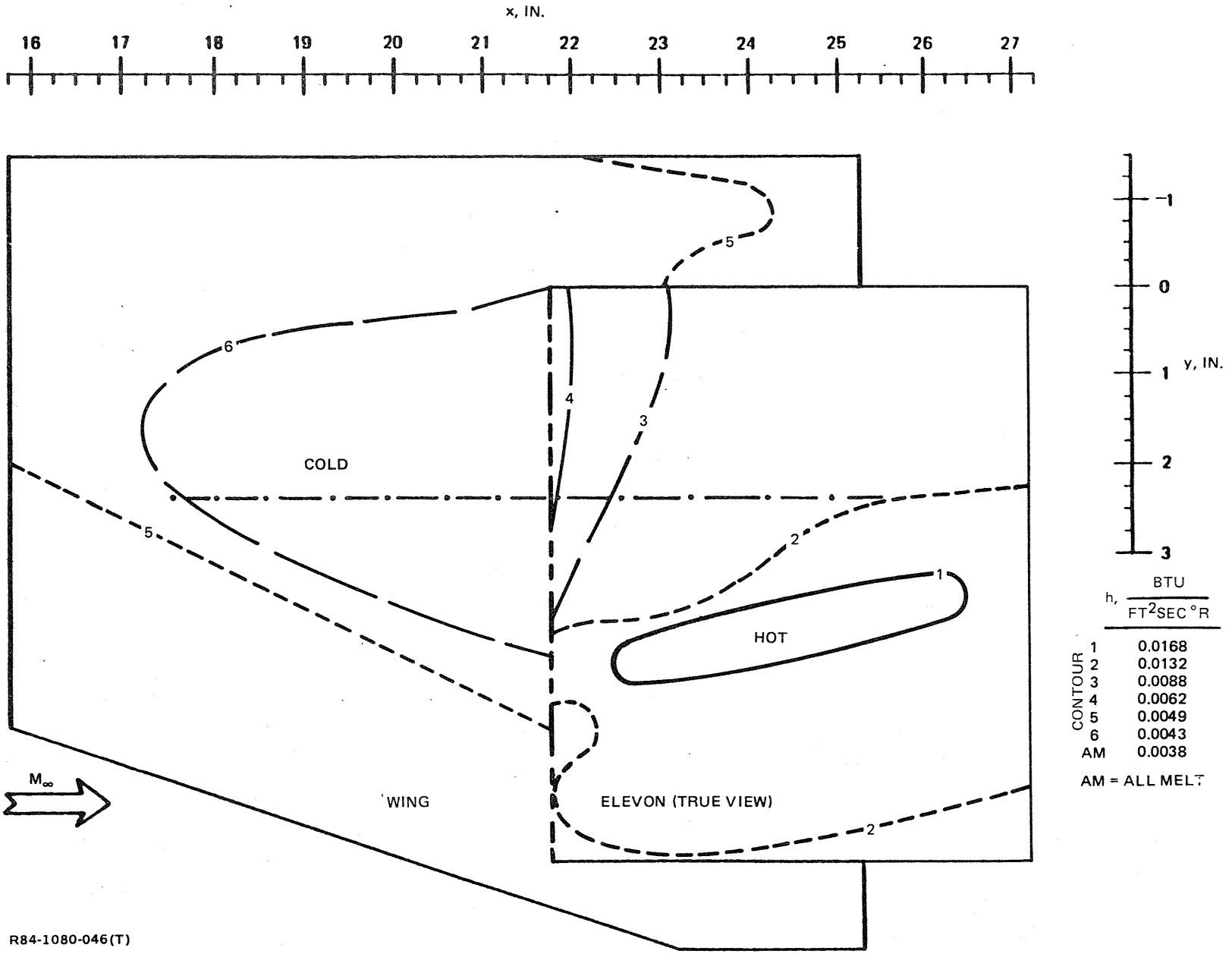

Fig. 46 10° Long Elevon — Planform Phase Change Results, 70° Swept Wing, No Center Body

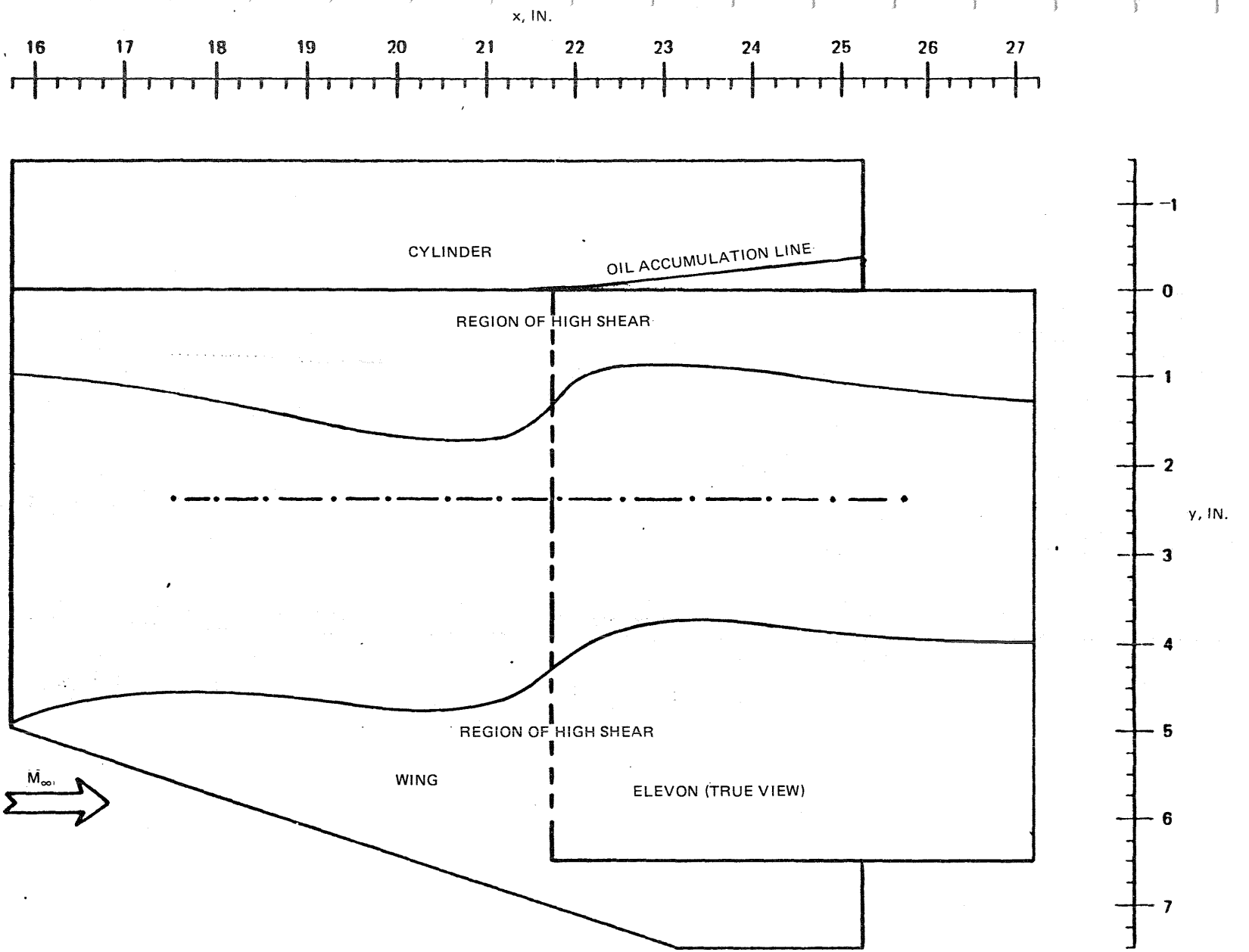

R84-1080-047(T)

Fig. 47 10° Long Elevon — Planform of Oil Flow Pattern, 70° Swept Wing, Cylindrical Center Body

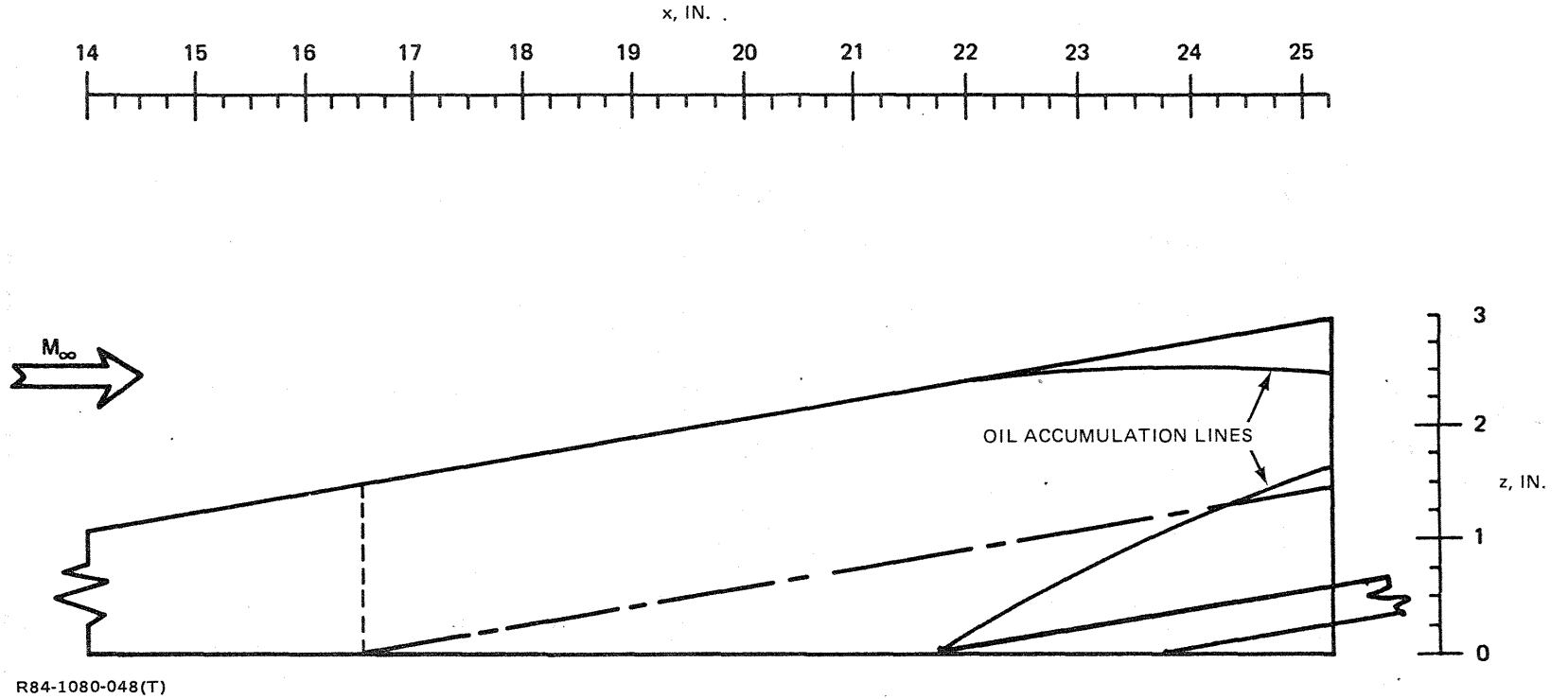

Fig. 48 10° Long Elevon — Profile Showing Oil Accumulation Lines on Cylindrical Body, 70° Swept Wing

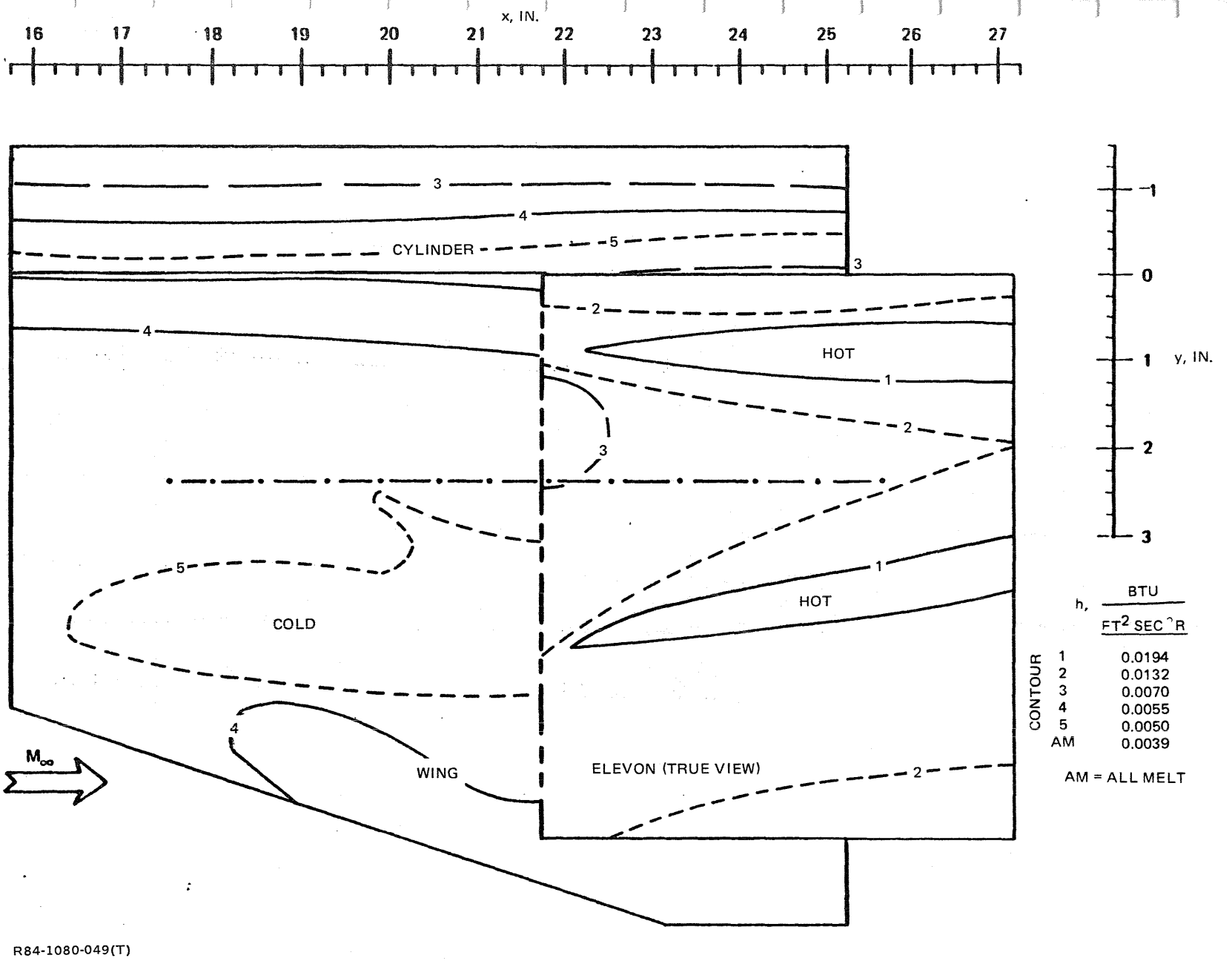

Fig. 49 10° Long Elevon — Planform Phase Change Results, 70° Swept Wing, Cylindrical Center Body

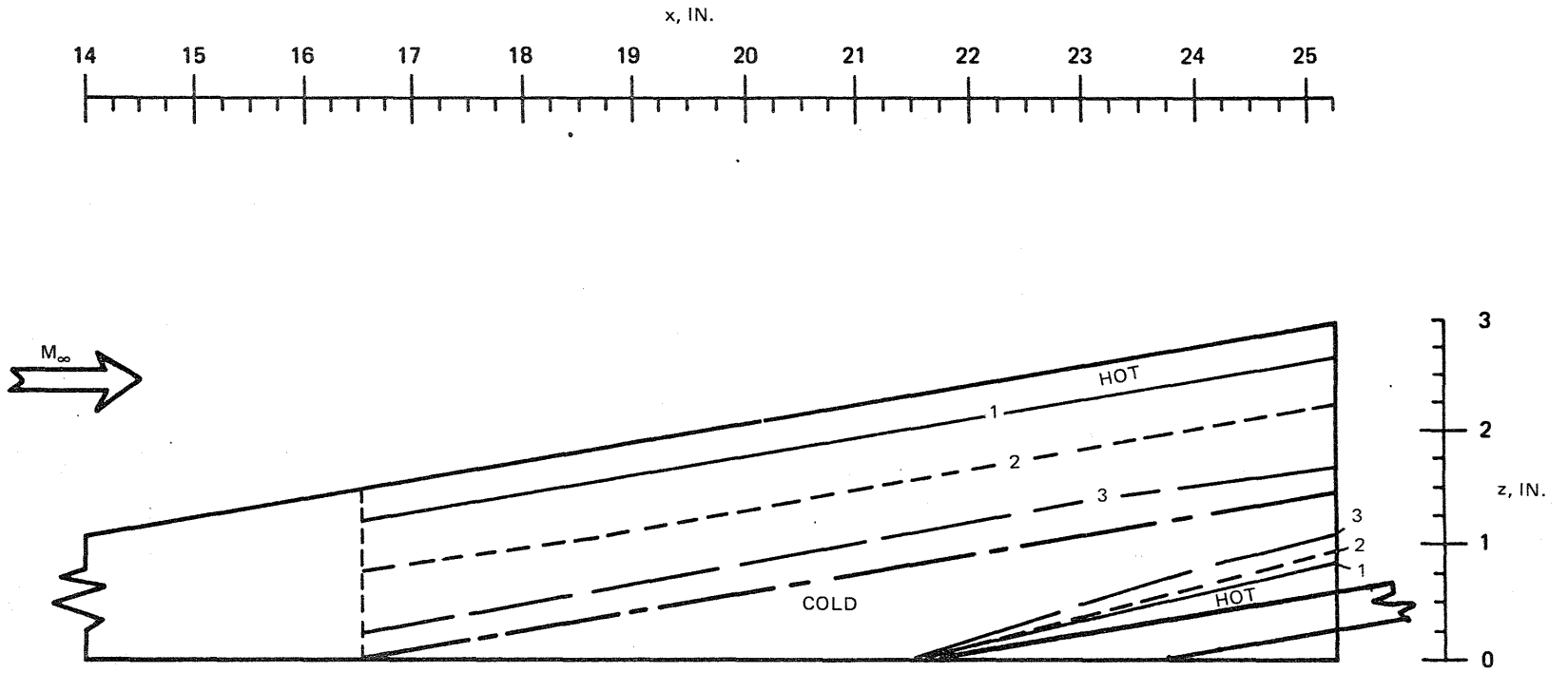

CONTOUR	h, BTU/FT^2 SEC °R
1	0.0070
2	0.0050
3	0.0040
ALL MELT	0.0039

R84-1080-050(T)

Fig. 50 10° Long Elevon — Profile Phase Change Results, Cylindrical Body, 70° Swept Wing

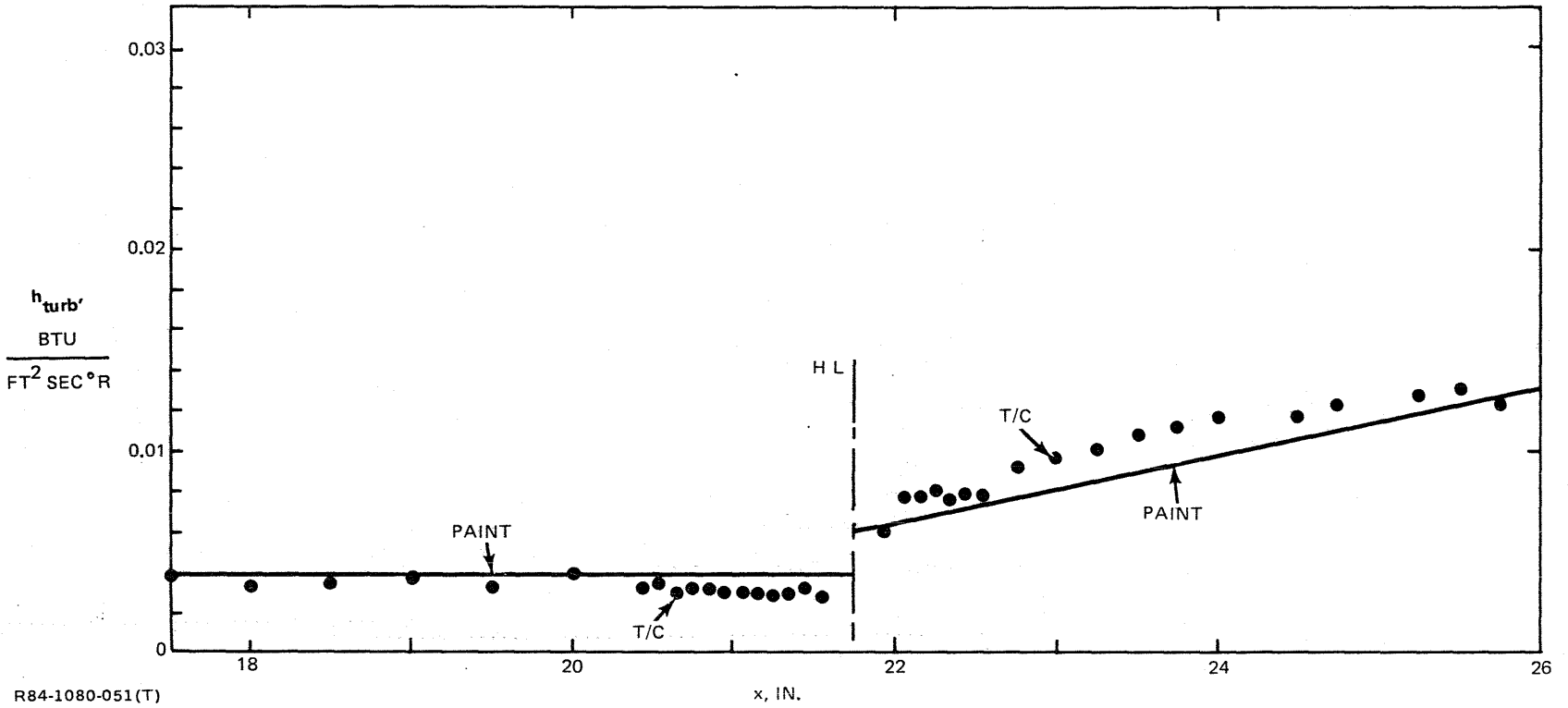

Fig. 51 10° Long Elevon – Comparison of Phase Change & Thermocouple Data, 70° Swept Wing, Cylindrical Center Body

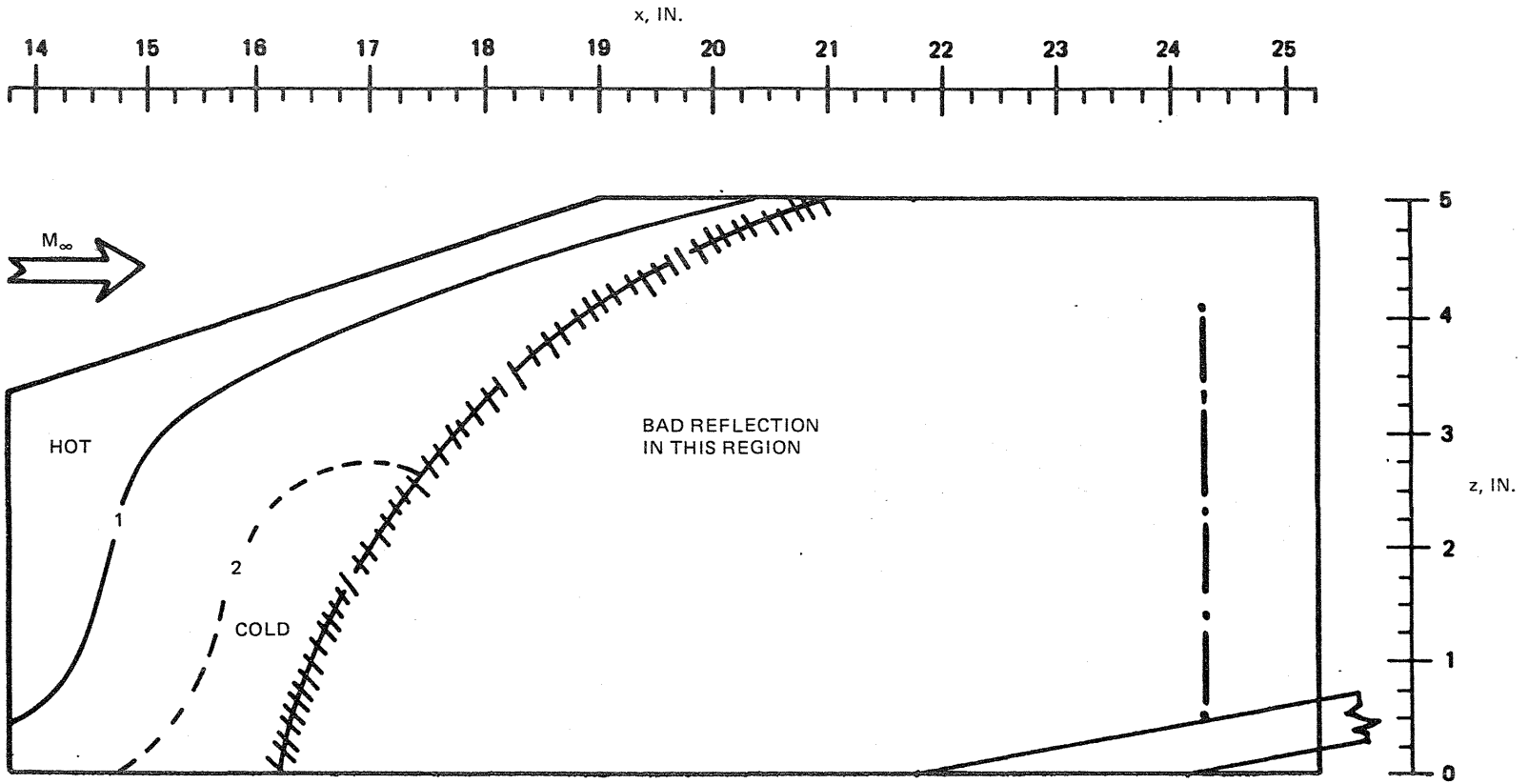

CONTOUR	h, BTU/FT^2 SEC °R
1	0.0042
2	0.0036
ALL MELT	0.0033

R84-1080-052(T)

Fig. 52 10° Long Elevon — Profile Phase Change Results, End Plate, 70° Swept Wing

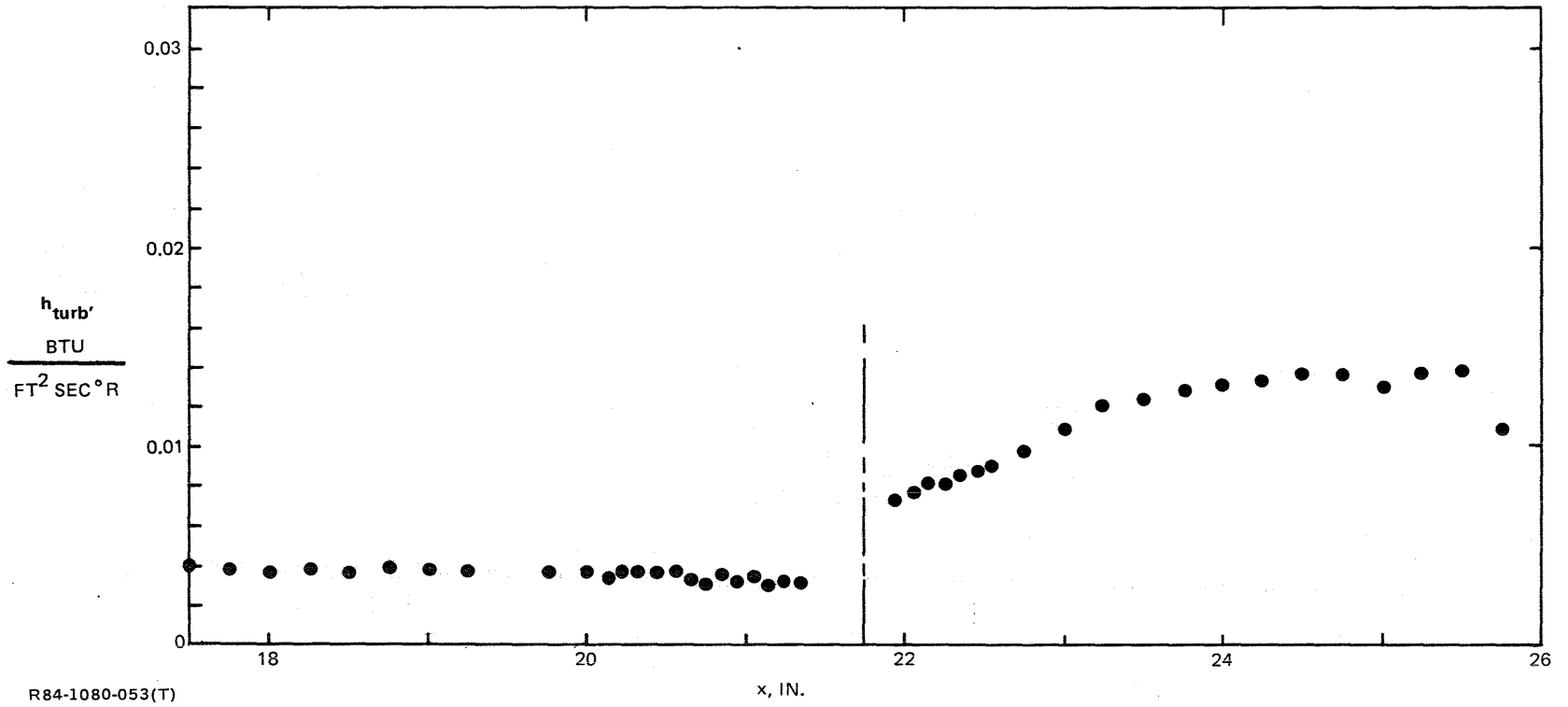

Fig. 53 10° Long Elevon — Thermocouple Data, 70° Swept Wing, End Plate

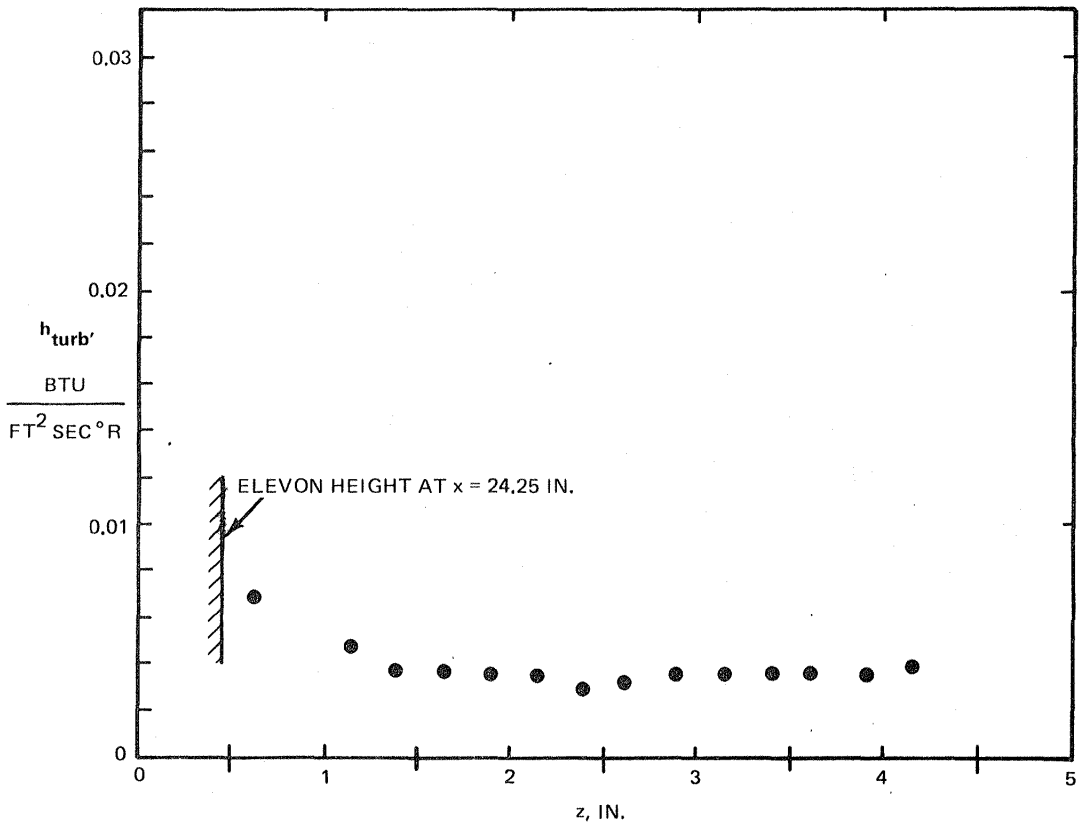

R84-1080-054(T)

Fig. 54 10° Long Elevon – Thermocouple Data, End Plate, 70° Swept Wing

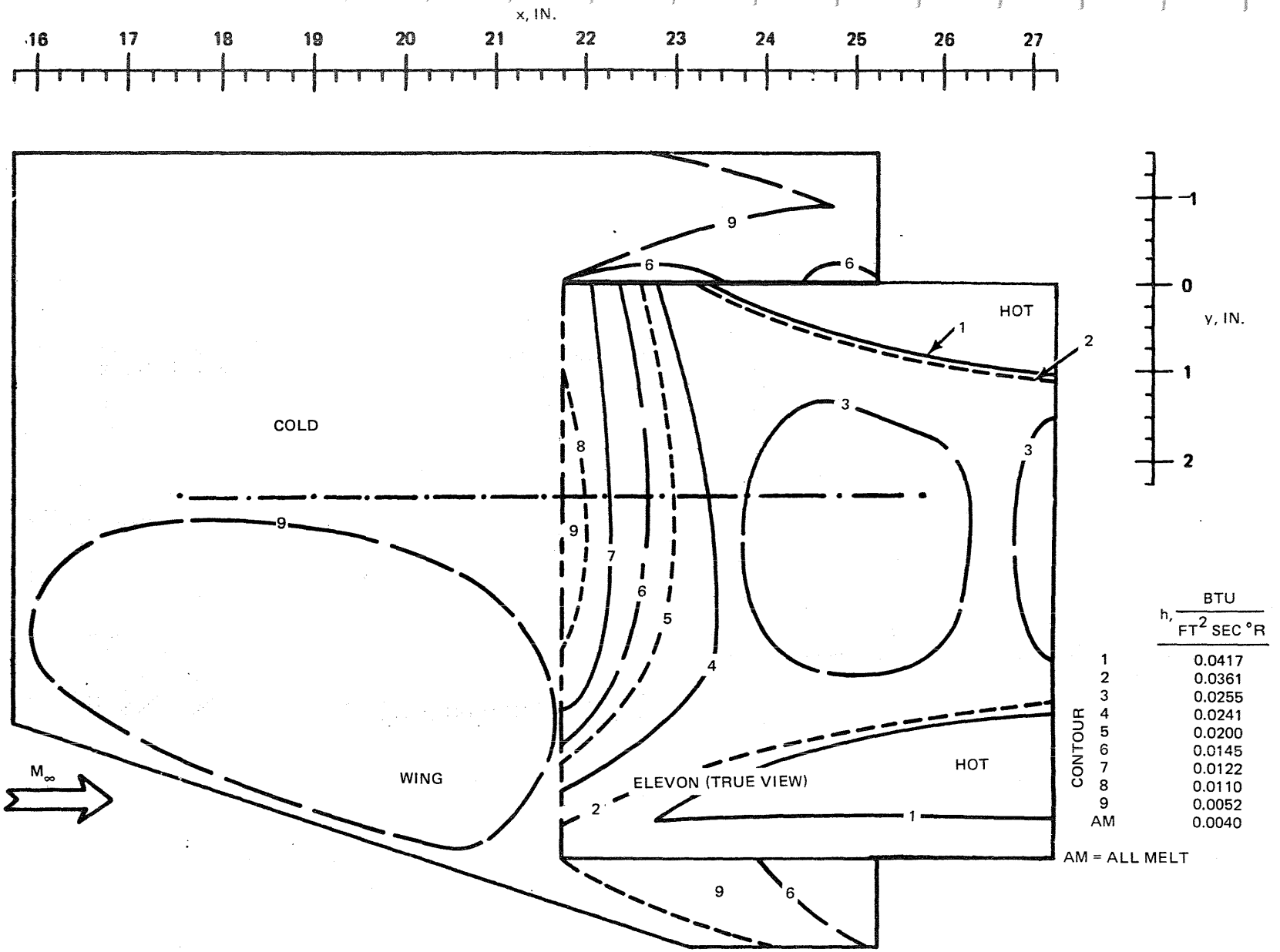

R84-1080-055(T)

Fig. 55 15° Long Elevon – Planform Phase Change Results, Unswept Wing, No Center Body

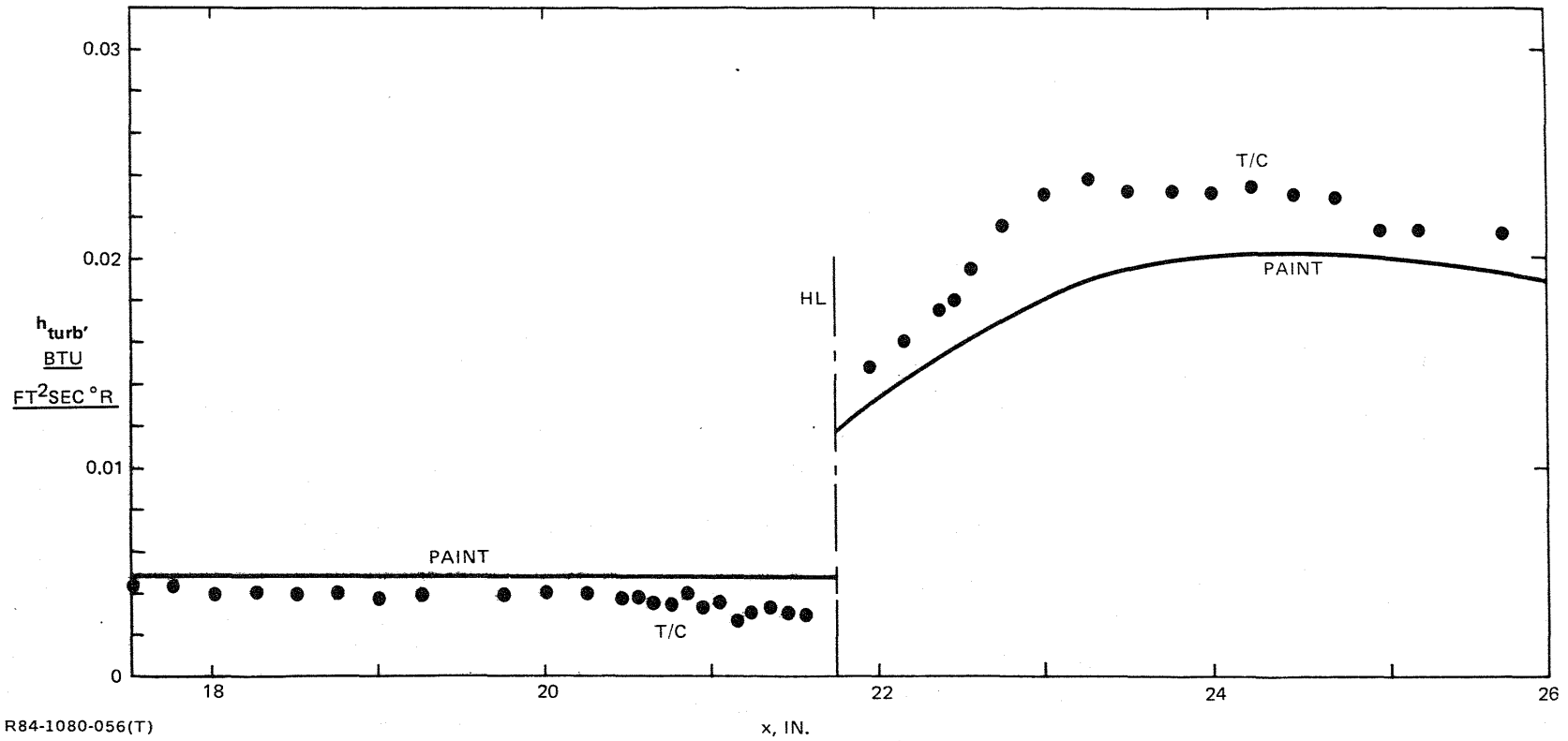

Fig. 56 15° Long Elevon – Comparison of Phase Change & Thermocouple Data, Unswept Wing, No Center Body

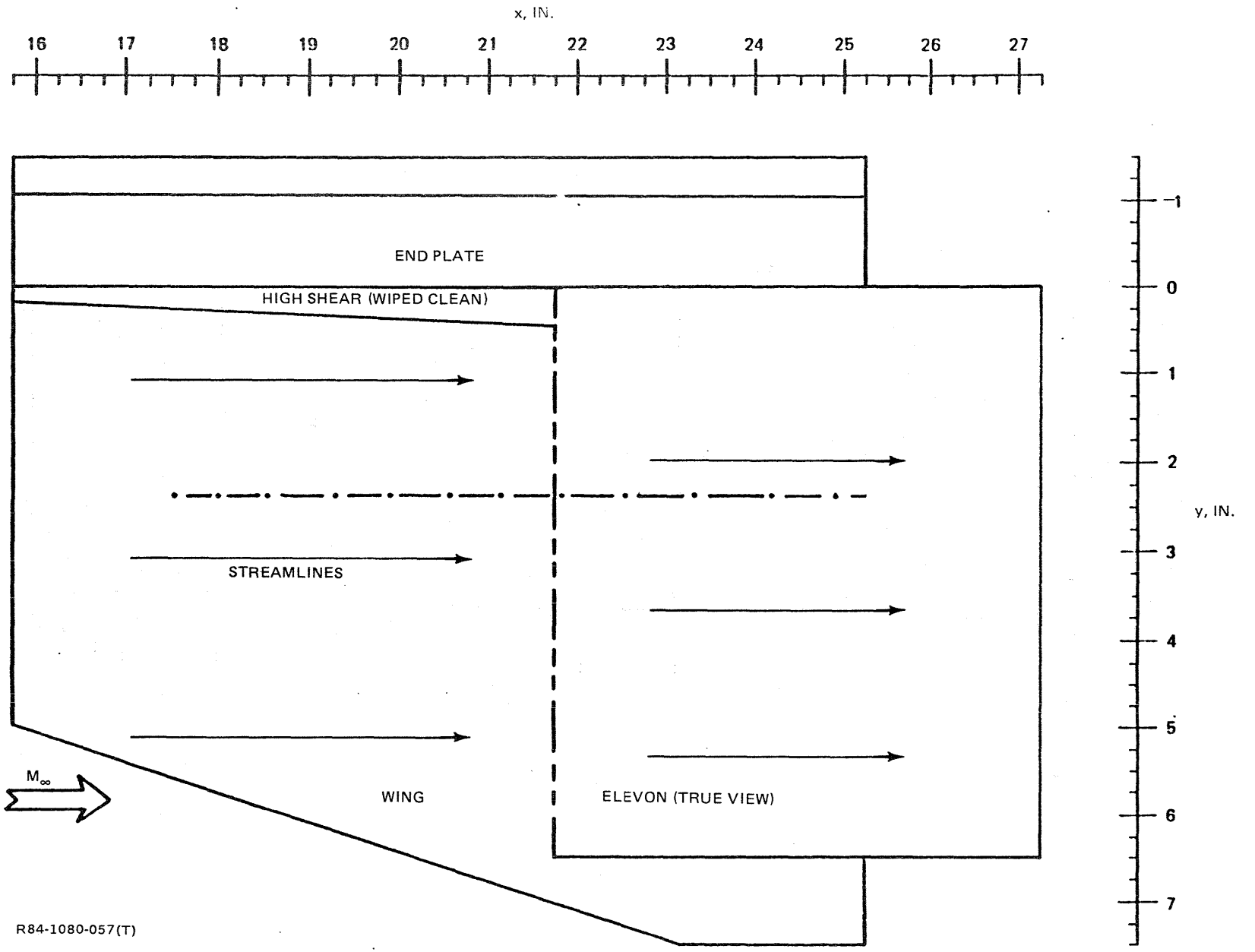

Fig. 57 15° Long Elevon -- Planform Oil Flow Pattern, Unswept Wing, End Plate

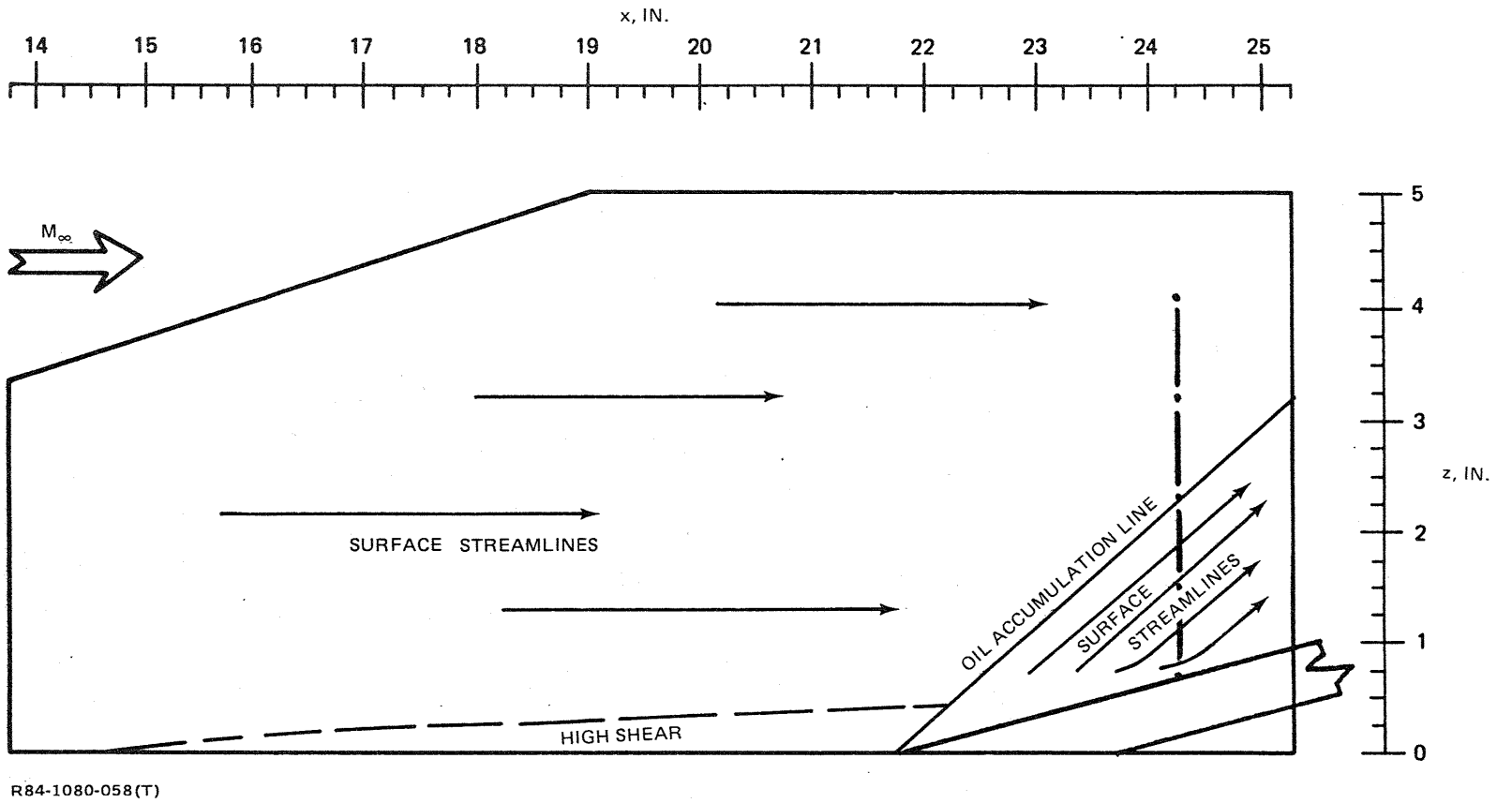

R84-1080-058(T)

Fig. 58 15° Long Elevon – Profile Oil Flow Pattern, End Plate, Unswept Wing

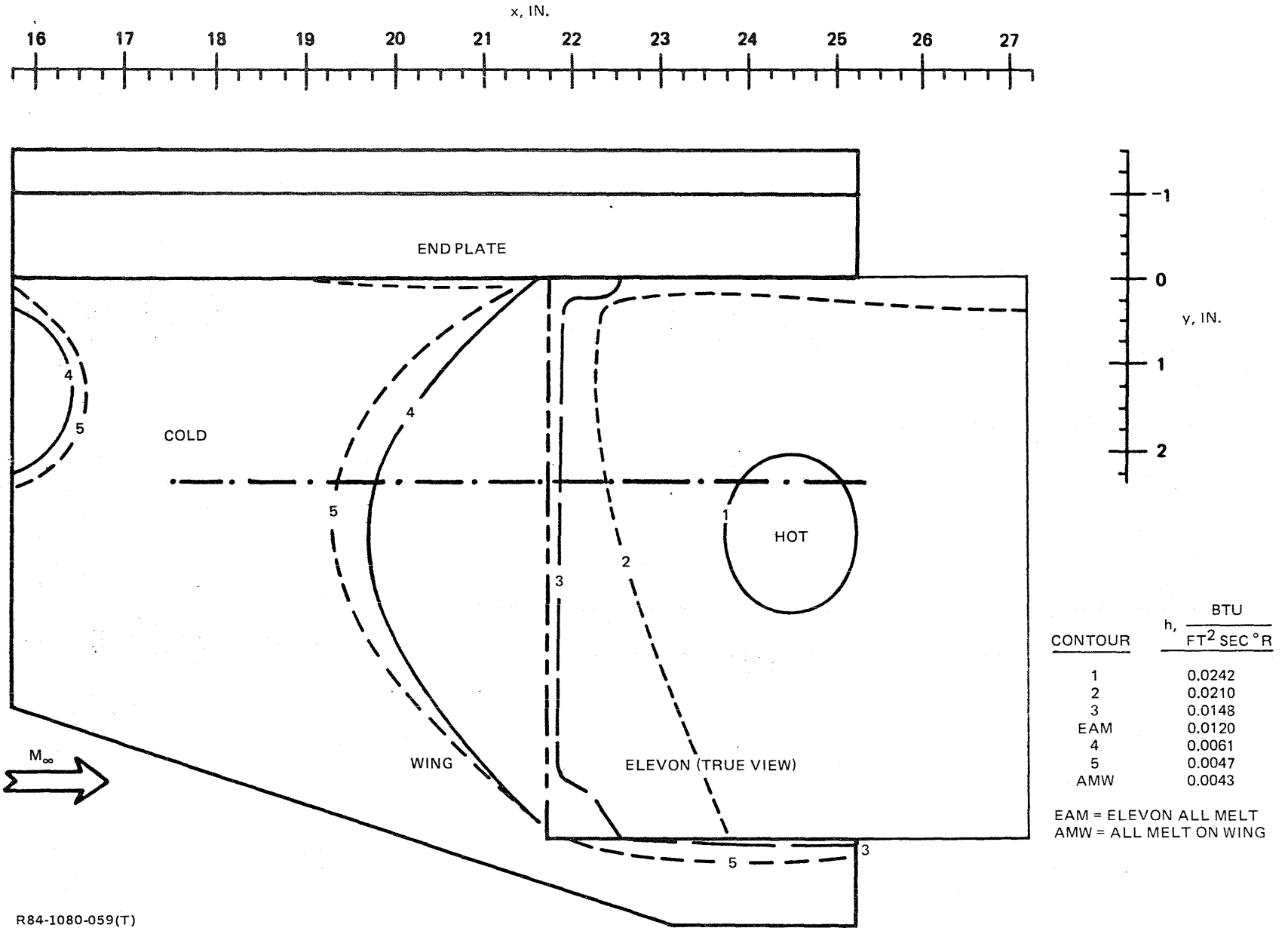

CONTOUR	h, BTU / FT^2 SEC °R
1	0.0242
2	0.0210
3	0.0148
EAM	0.0120
4	0.0061
5	0.0047
AMW	0.0043

EAM = ELEVON ALL MELT
AMW = ALL MELT ON WING

Fig. 59 15° Long Elevon — Planform Phase Change Results, Unswept Wing, End Plate

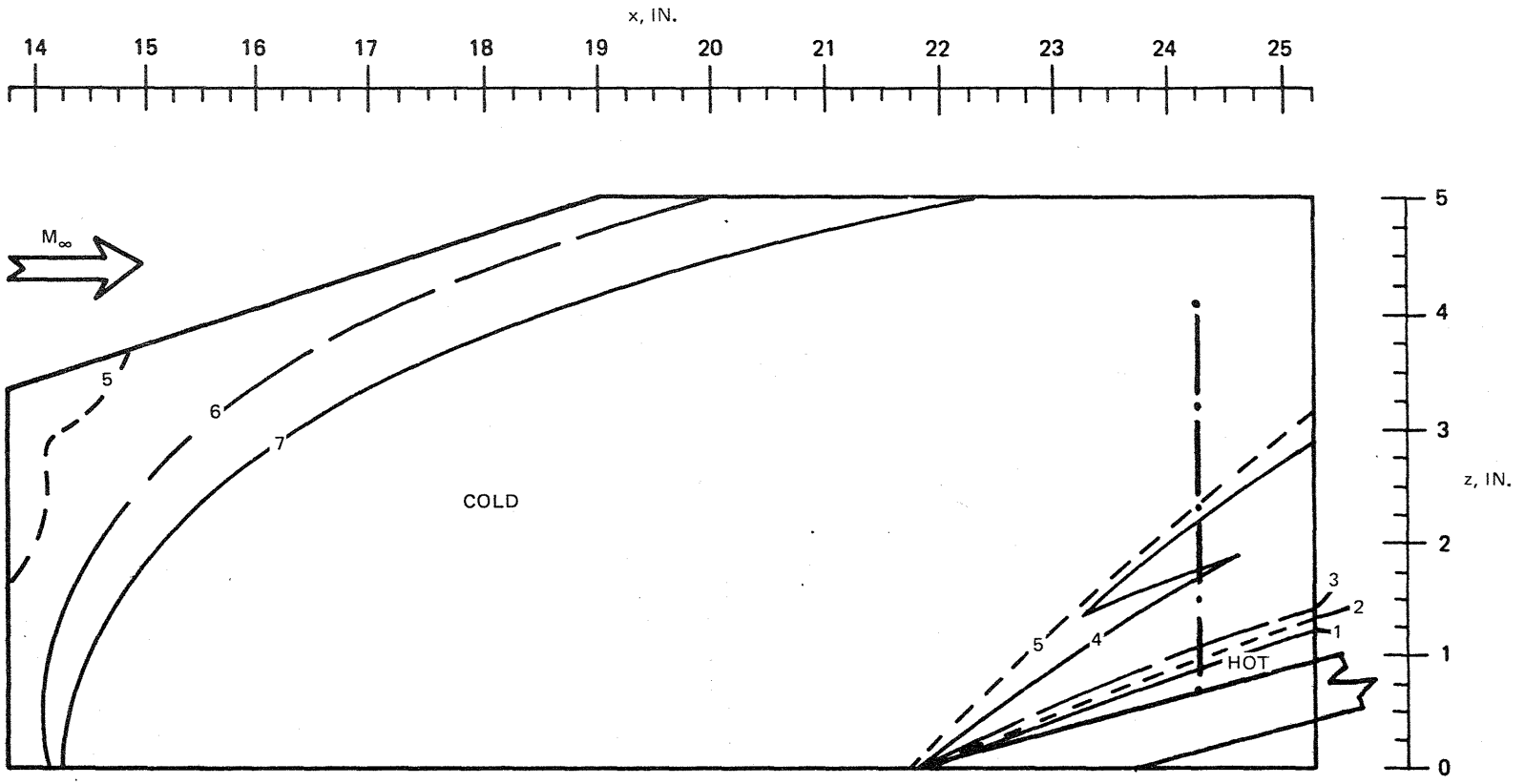

CONTOUR	h, BTU/FT^2 SEC °R
1	0.0242
2	0.0210
3	0.0148
4	0.0120
5	0.0061
6	0.0047
7	0.0043
ALL MELT	0.0036

R84-1080-060(T)

Fig. 60 15° Long Elevon — Profile Phase Change Results, End Plate, Unswept Wing

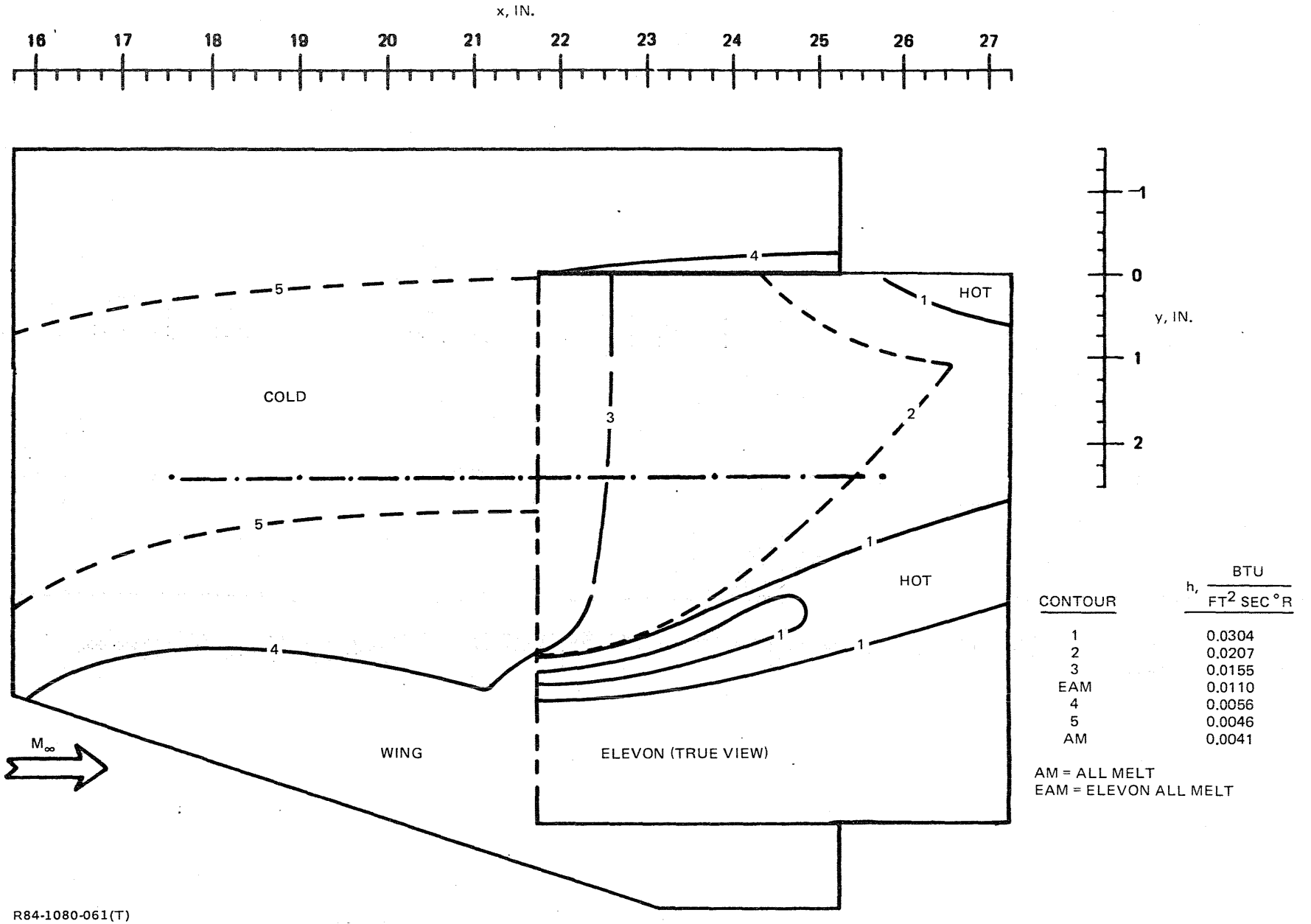

CONTOUR	h, BTU / FT^2 SEC °R
1	0.0304
2	0.0207
3	0.0155
EAM	0.0110
4	0.0056
5	0.0046
AM	0.0041

AM = ALL MELT
EAM = ELEVON ALL MELT

Fig. 61 15° Long Elevon – Planform Phase Change Results, 70° Swept Wing, No Center Body

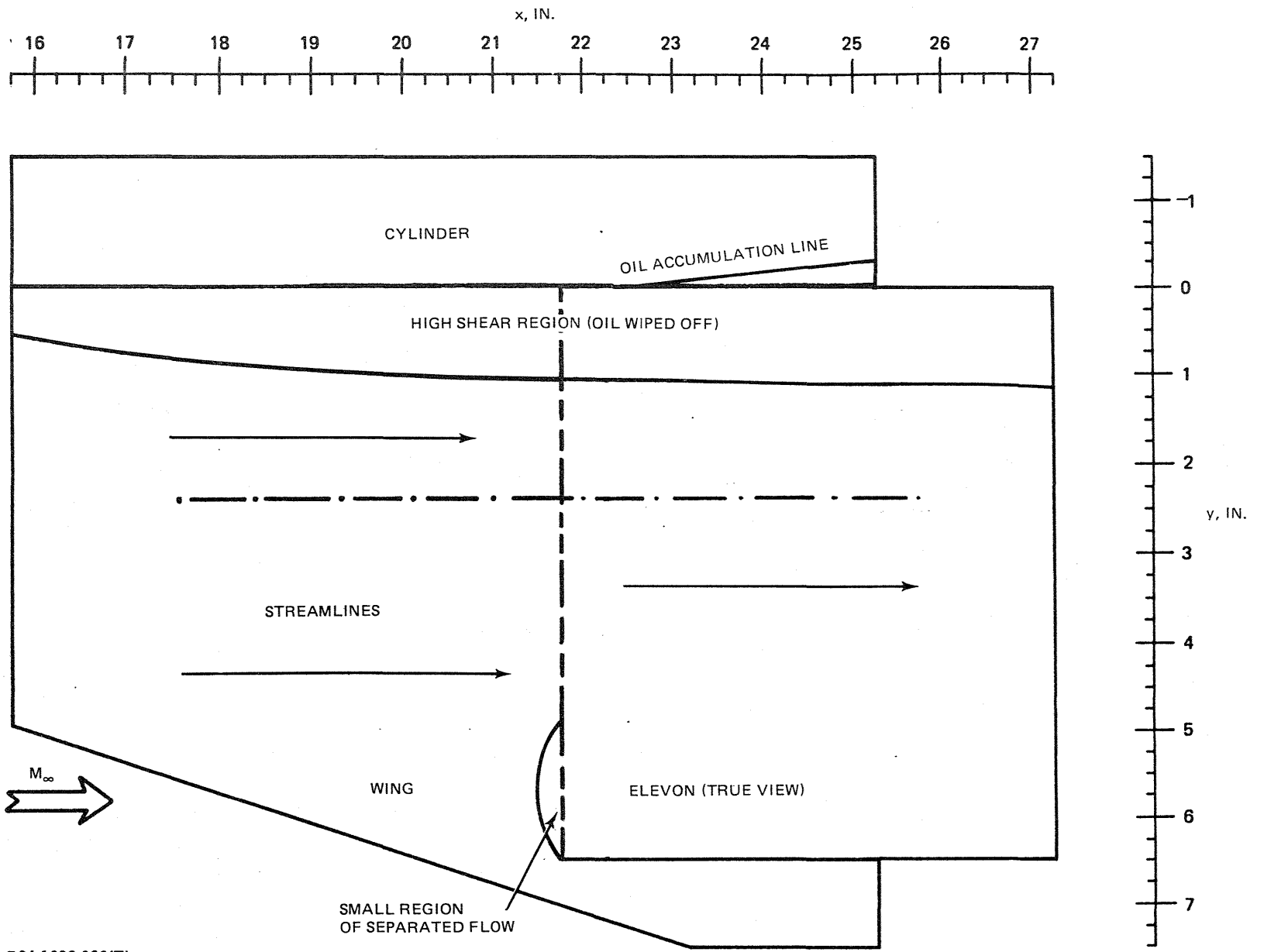

Fig. 62 15° Long Elevon – Planform Oil Flow Pattern, 70° Swept Wing, Cylindrical Center Body

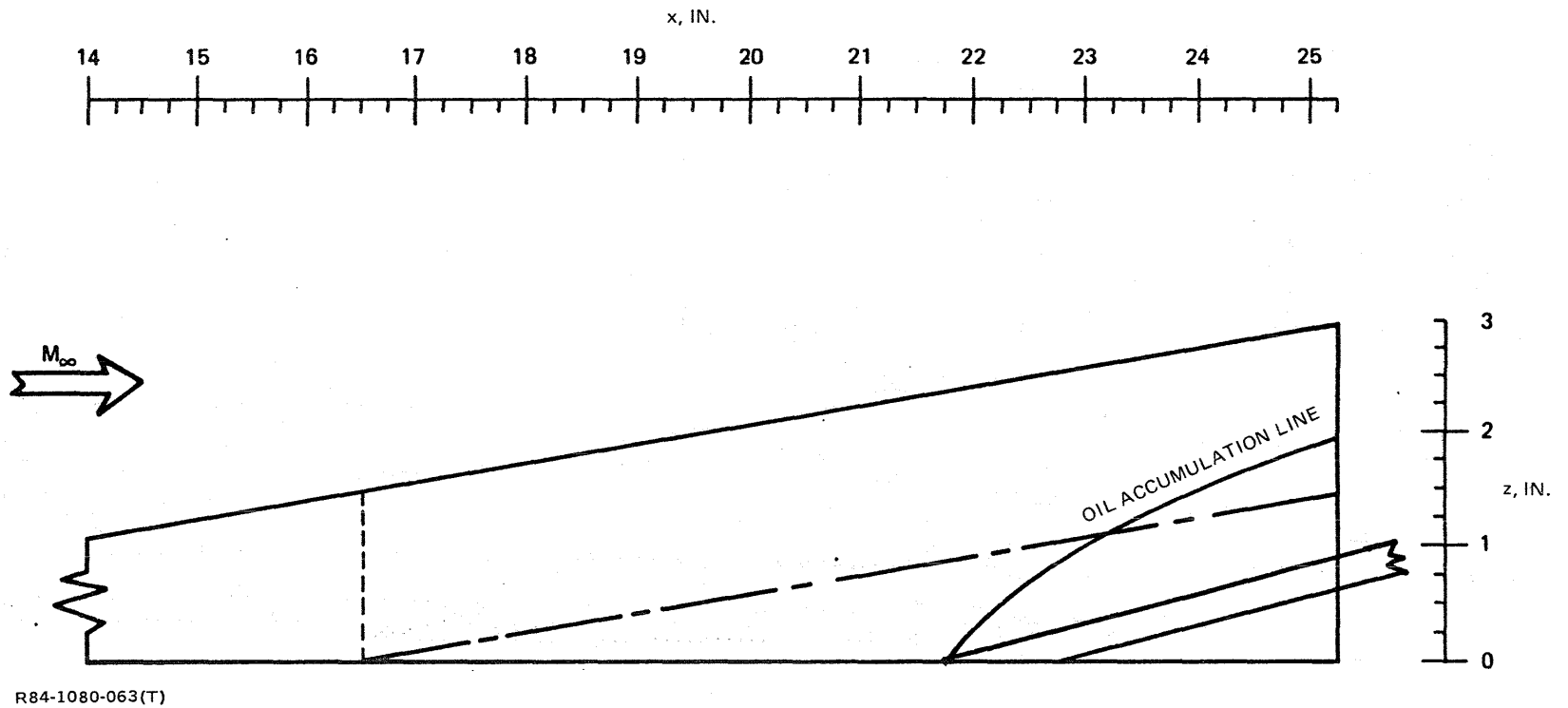

Fig. 63 15° Long Elevon – Profile Showing Oil Accumulation Line, Cylindrical Center Body, 70° Swept Wing

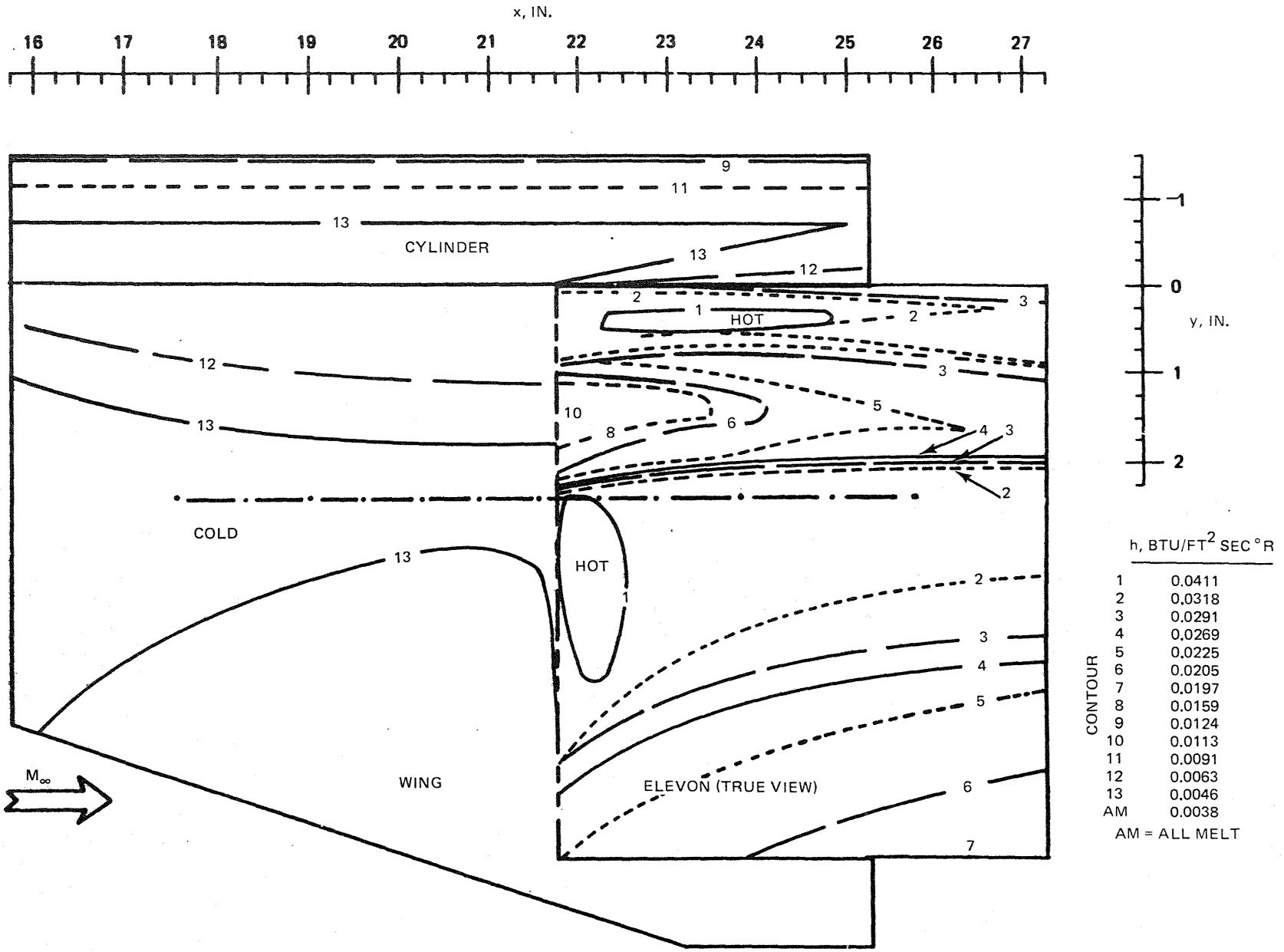

Fig. 64 15° Long Elevon Planform Phase Change Results, 70° Swept Wing, Cylindrical Center Body

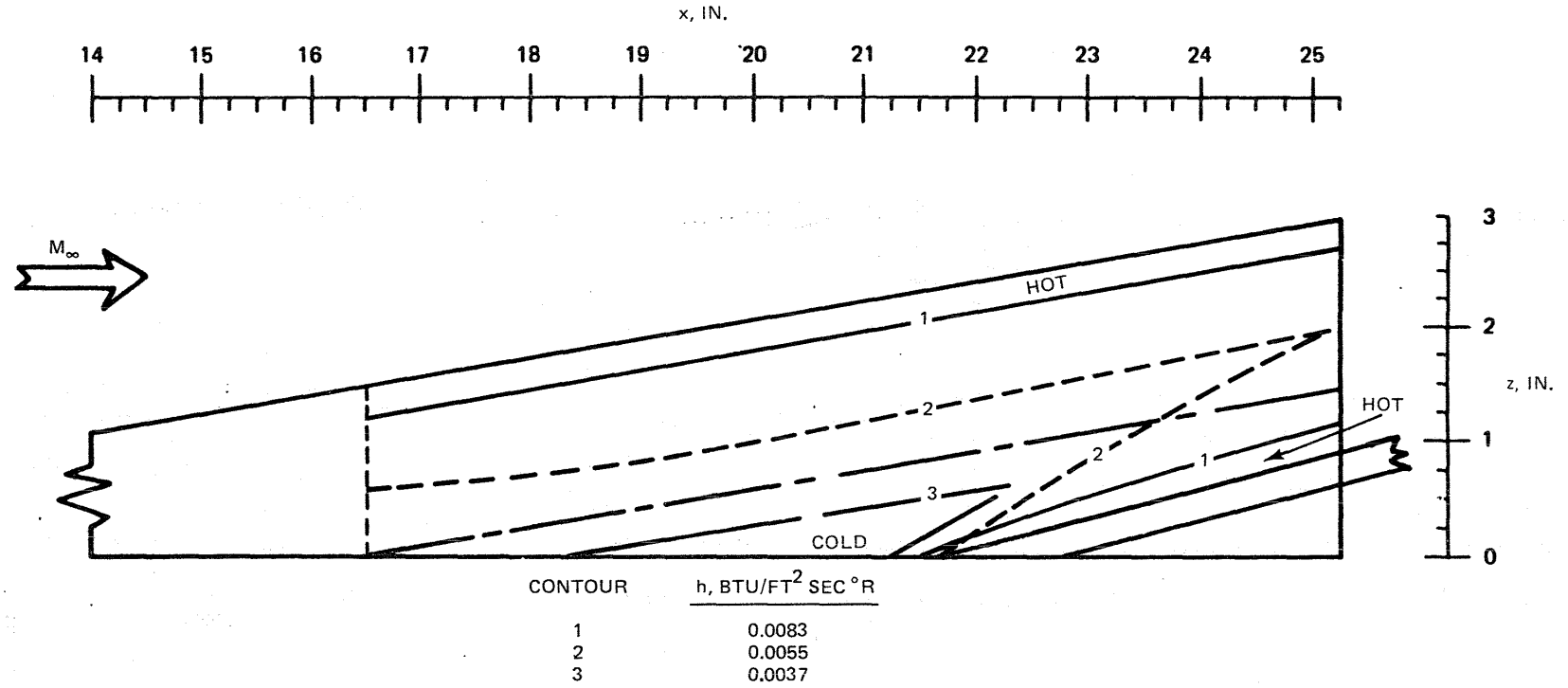

CONTOUR	h, BTU/FT^2 SEC °R
1	0.0083
2	0.0055
3	0.0037

R84-1080-065(T)

Fig. 65 15° Long Elevon – Profile Phase Change Results, Cylindrical Center Body, 70° Swept Wing

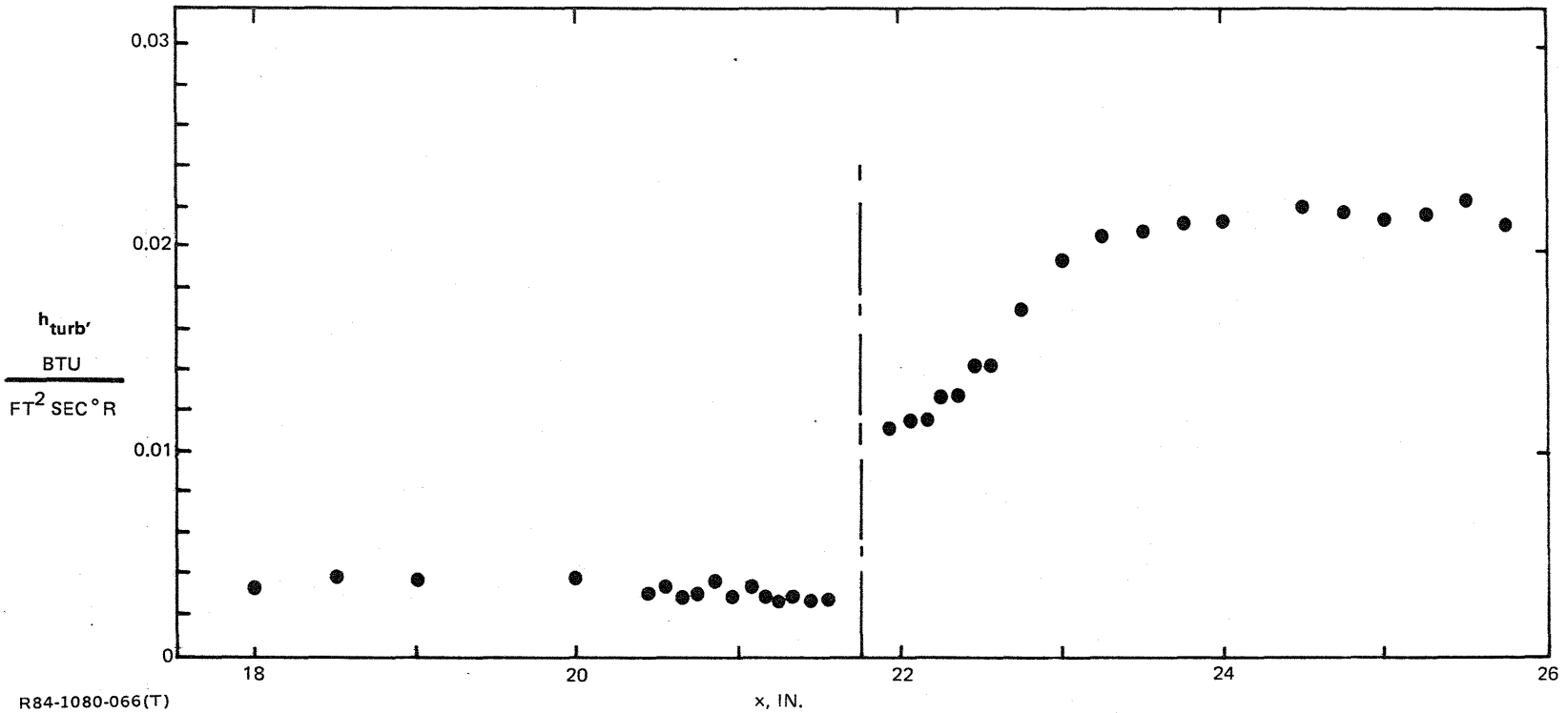

Fig. 66 15° Long Elevon — Thermocouple Data, 70° Swept Wing, Cylindrical Center Body

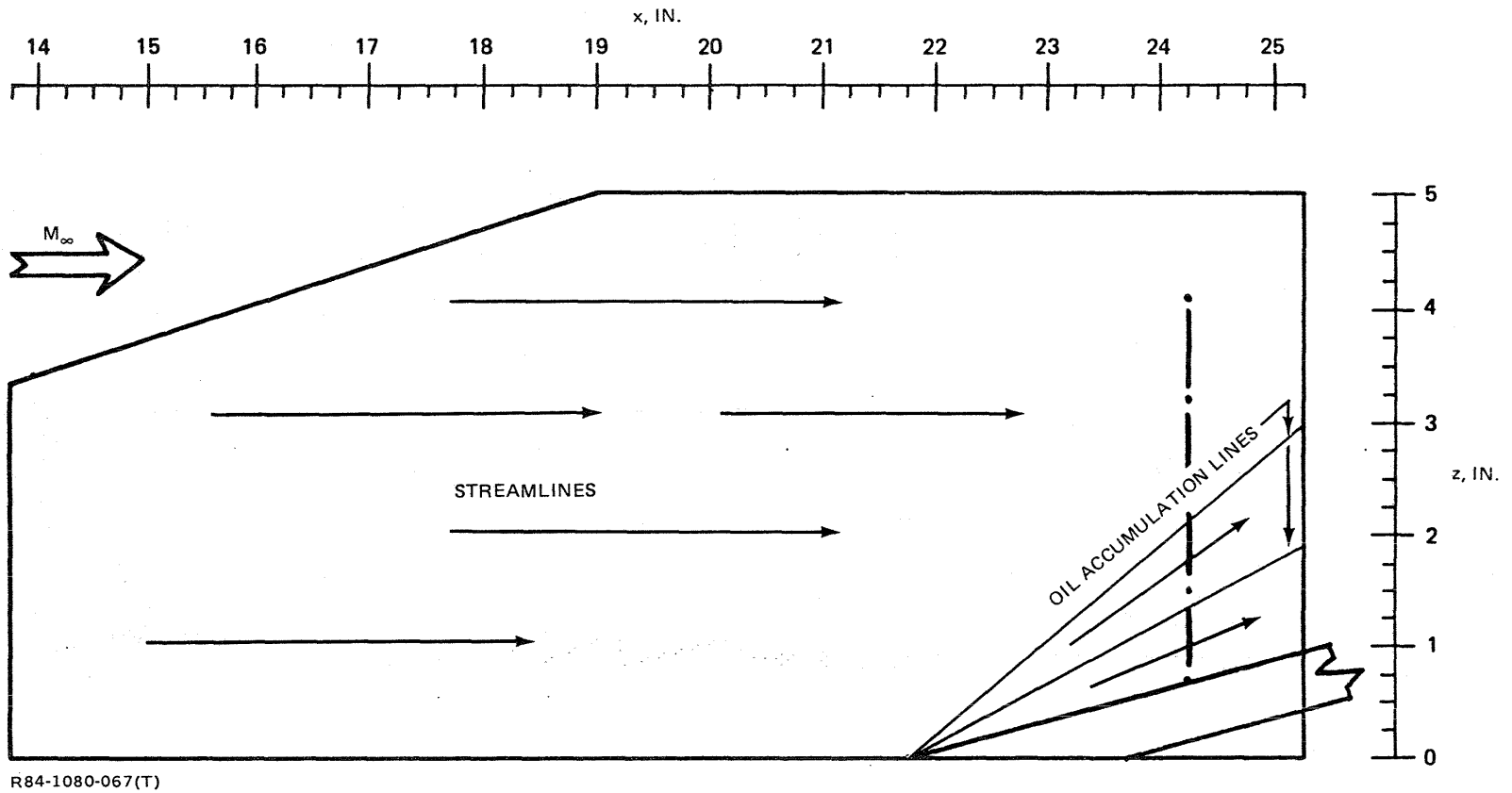

Fig. 67 15° Long Elevon – Oil Flow Pattern on End Plate, 70° Swept Wing

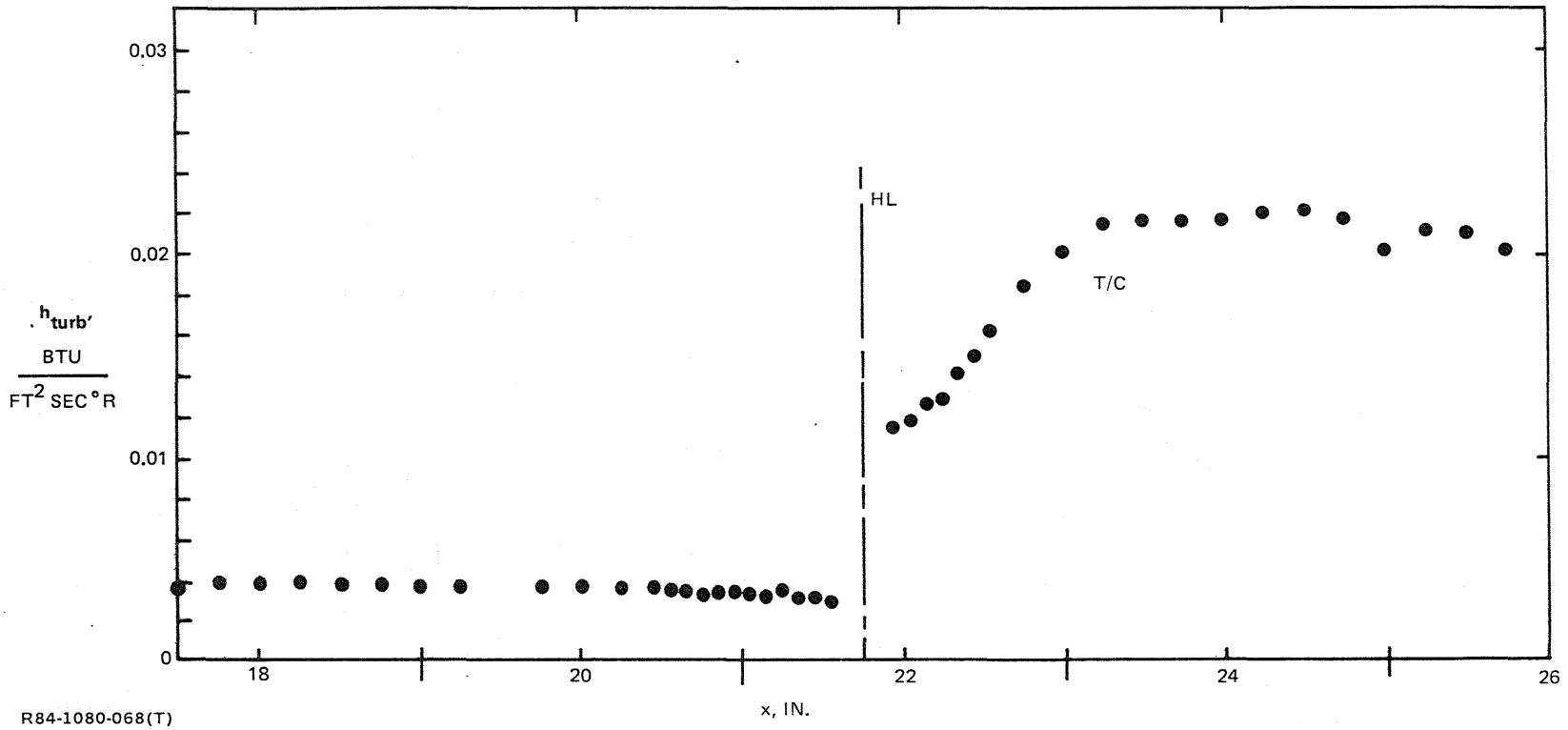

Fig. 68 15° Long Elevon – Thermocouple Data, 70° Swept Wing, End Plate

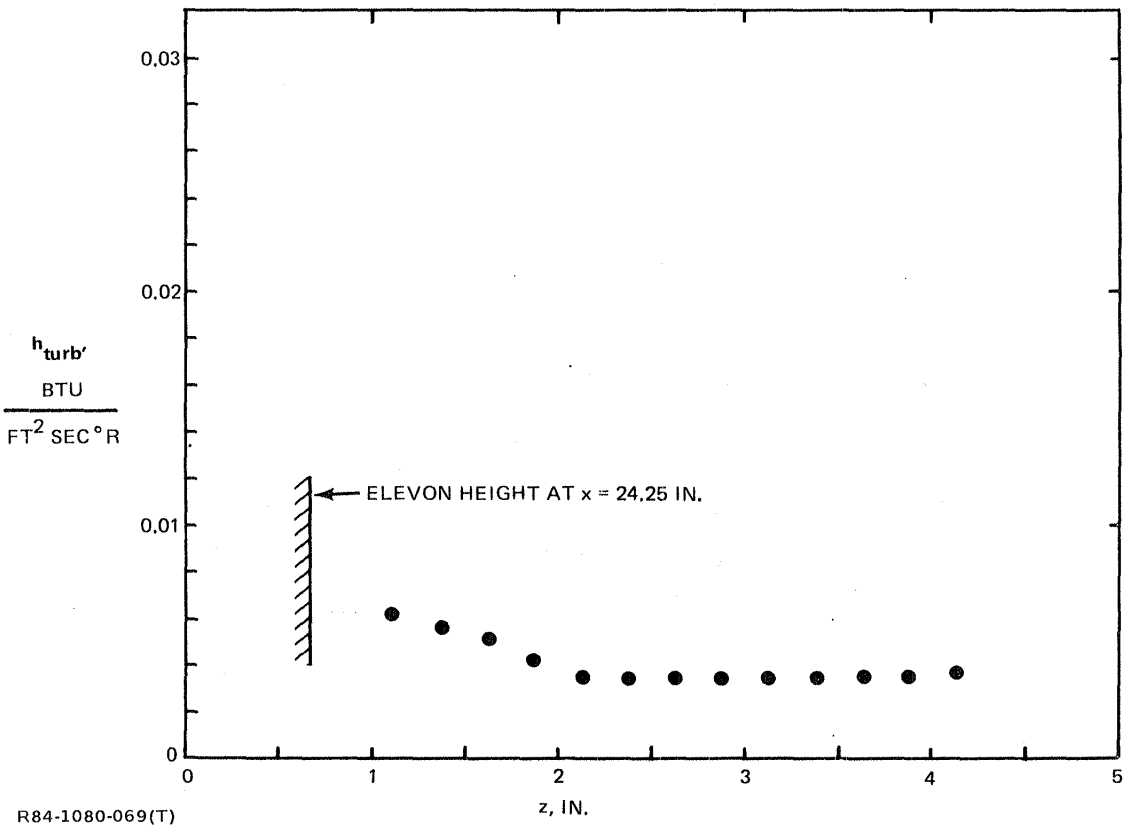

Fig. 69 15° Long Elevon – Thermocouple Data on End Plate, 70° Swept Wing

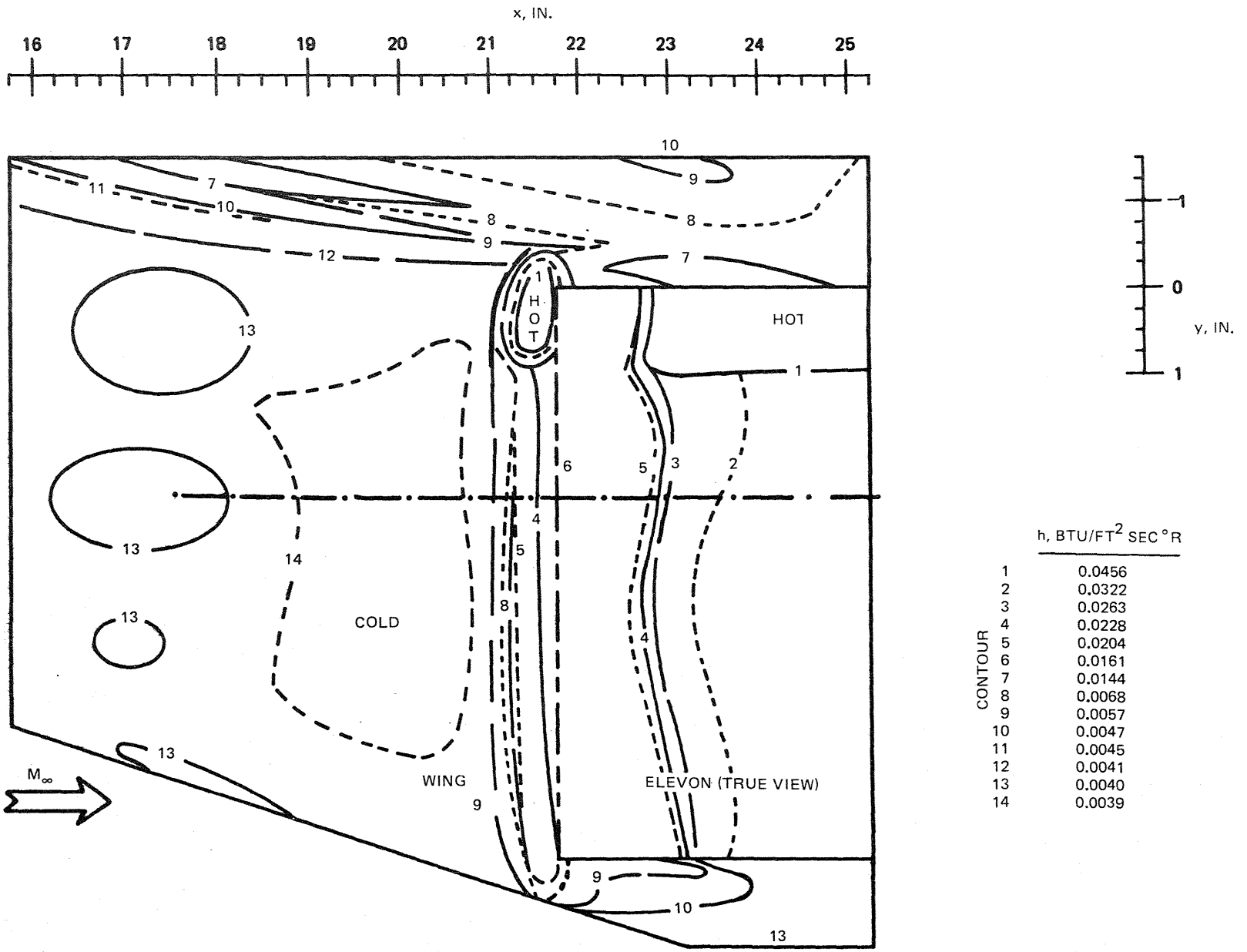

CONTOUR	h, BTU/FT^2 SEC °R
1	0.0456
2	0.0322
3	0.0263
4	0.0228
5	0.0204
6	0.0161
7	0.0144
8	0.0068
9	0.0057
10	0.0047
11	0.0045
12	0.0041
13	0.0040
14	0.0039

Fig. 70 20° Short Elevon — Planform Phase Change Results, Unswept Wing, No Center Body

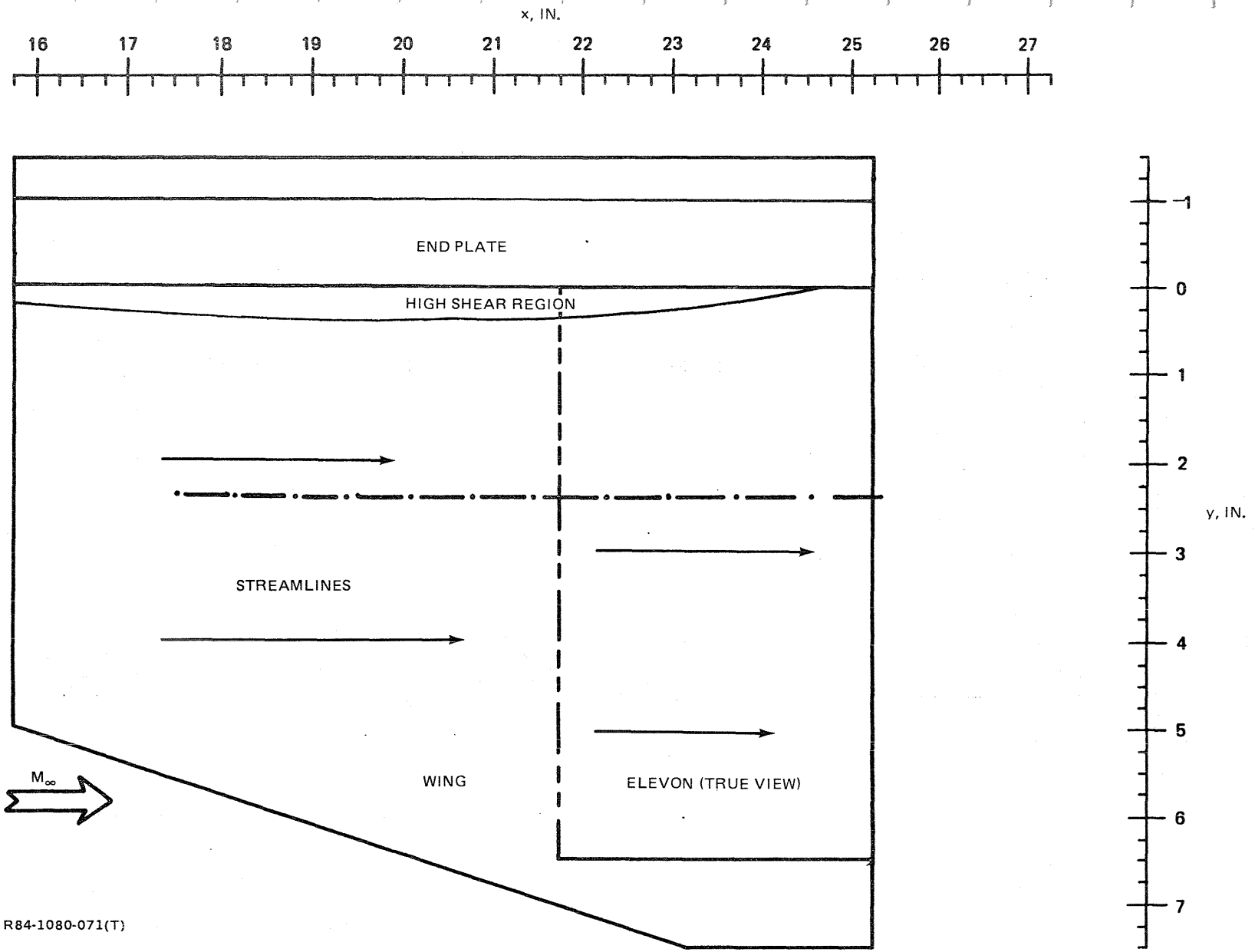

Fig. 71 20° Short Elevon – Oil Flow Pattern, Unswept Wing, End Plate

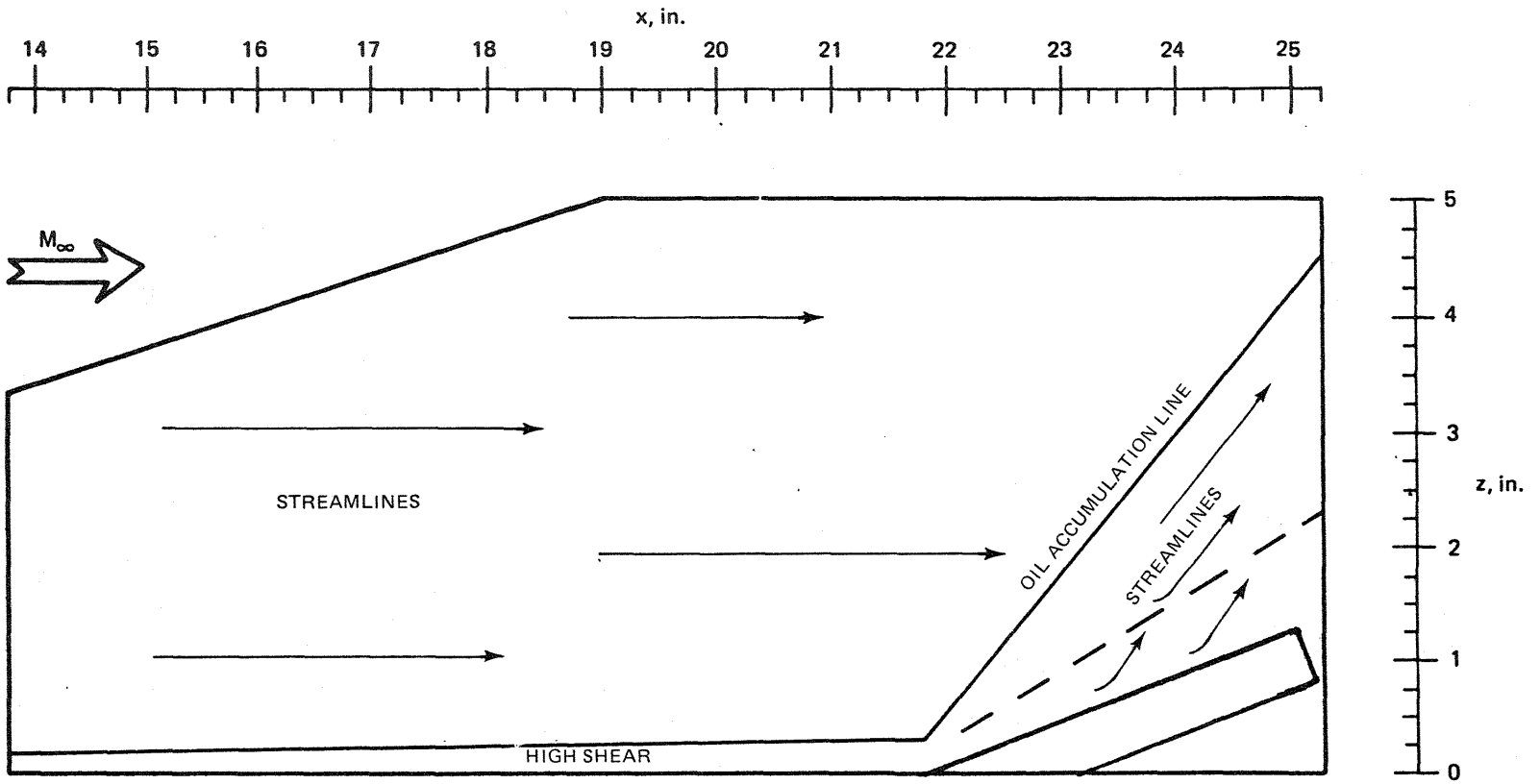

R84-1080-072(T)

Fig. 72 20° Short Elevon – Oil Flow Pattern, End Plate, Unswept Wing

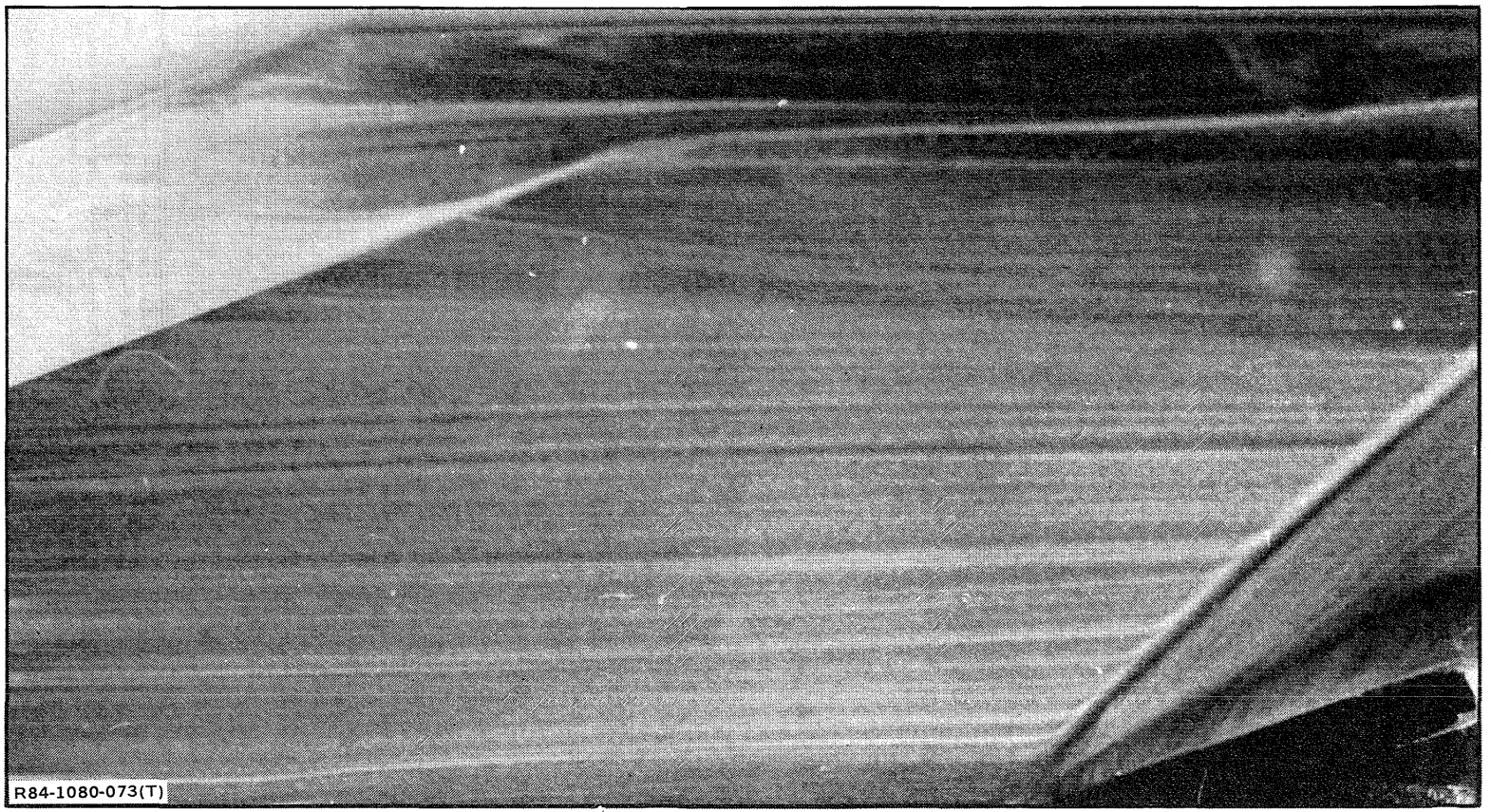

Fig. 73 20° Short Elevon – Photograph of Oil Flow Pattern on End Plate, Unswept Wing

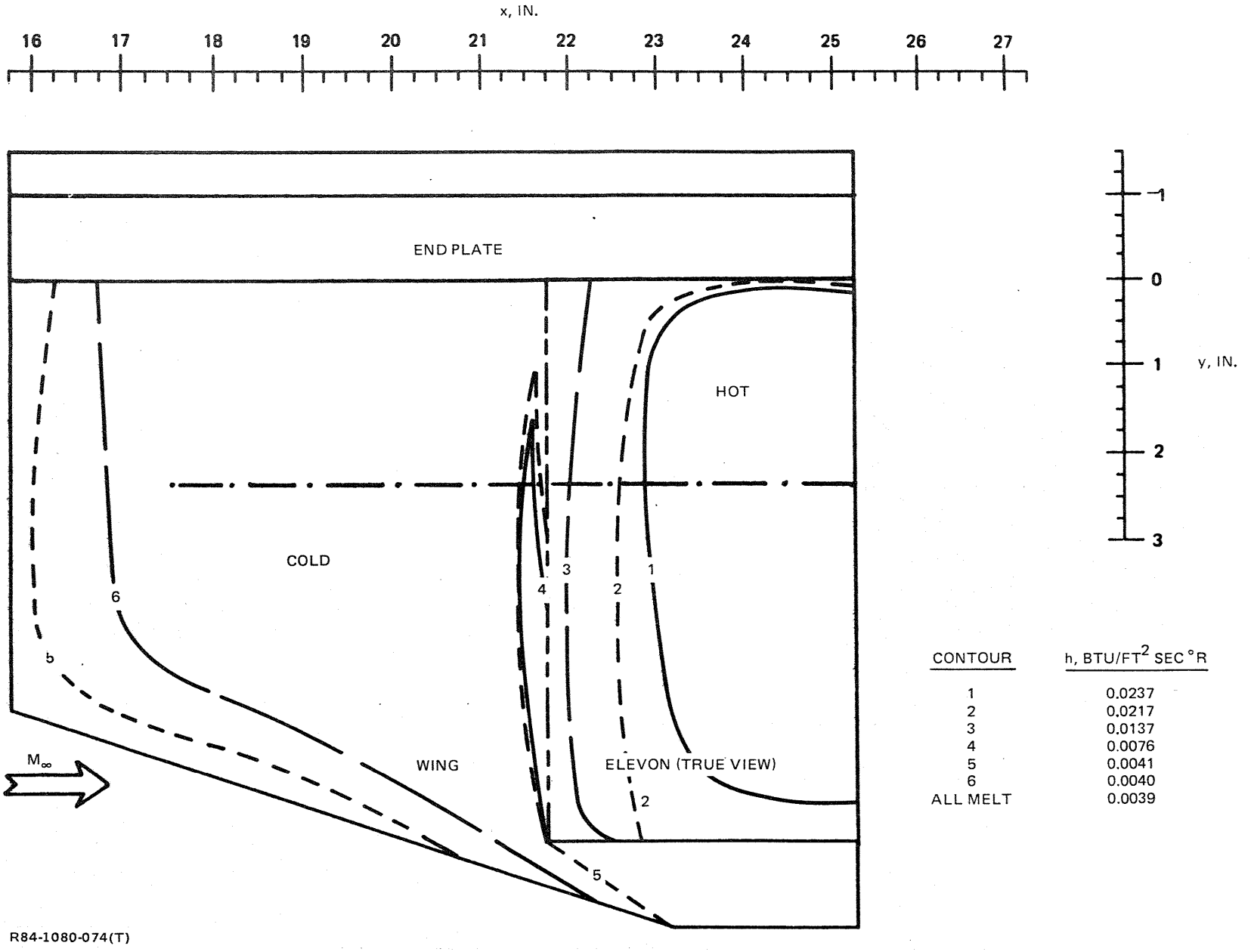

Fig. 74 20° Short Elevon — Phase Change Results, Unswept Wing, End Plate

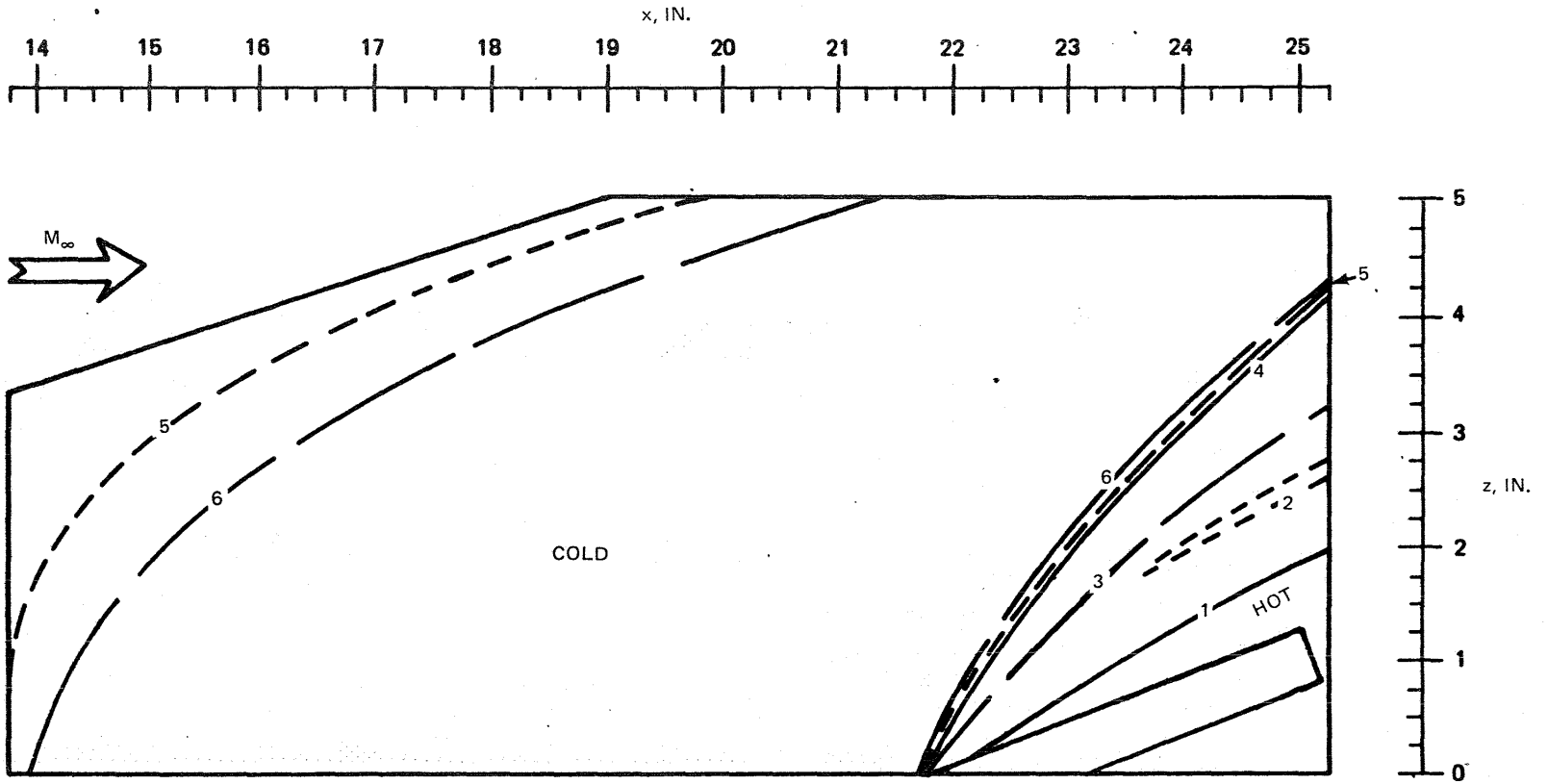

CONTOUR	h, BTU/FT^2 SEC °R
1	0.0217
2	0.0076
3	0.0064
4	0.0055
5	0.0041
6	0.0040
ALL MELT	0.0039

R84-1080-075(T)

Fig. 75 20° Short Elevon — Phase Change Results, End Plate, Unswept Wing

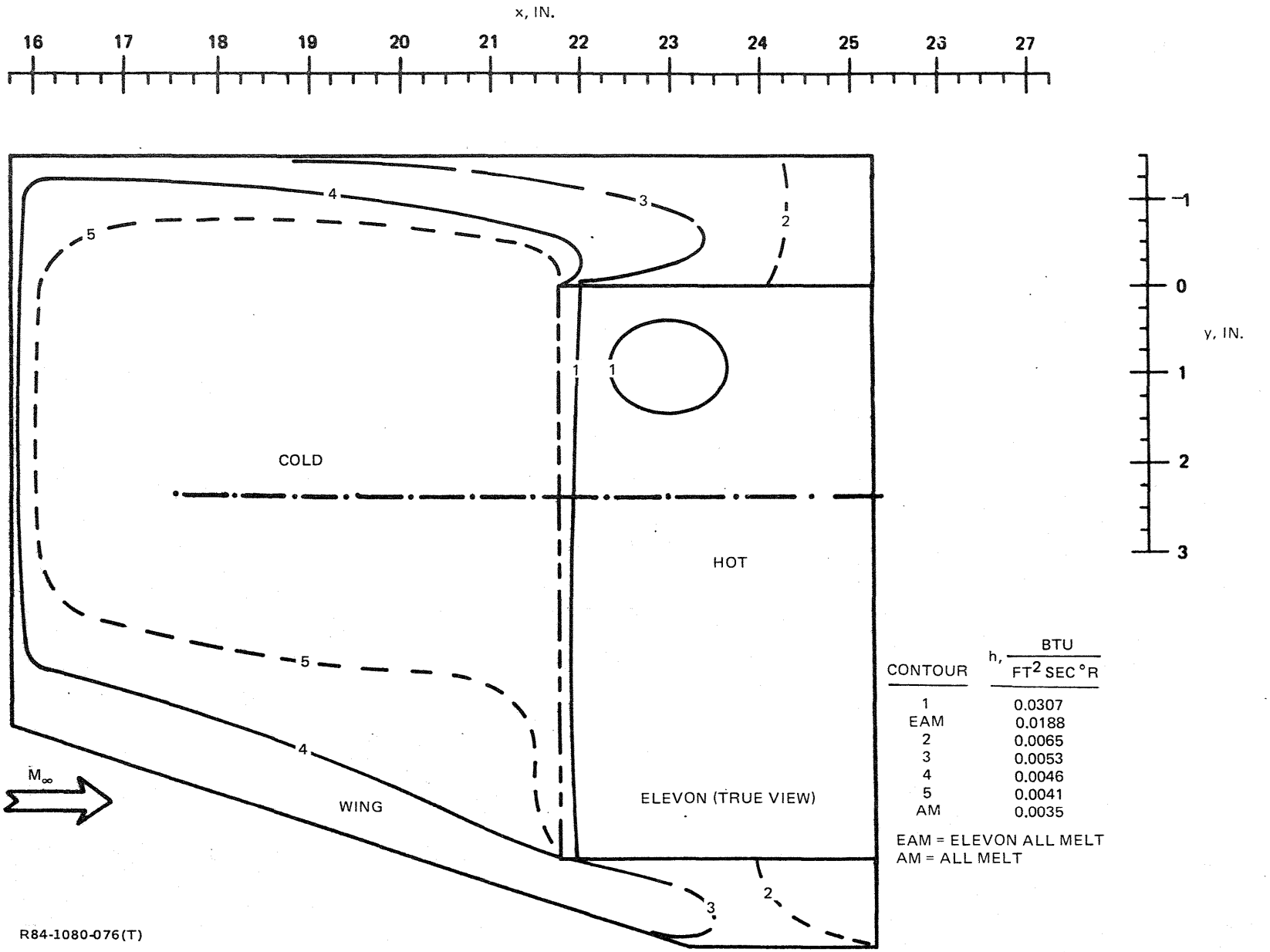

Fig. 76 20° Short Elevon — Phase Change Results, 50° Swept Wing, No Center Body

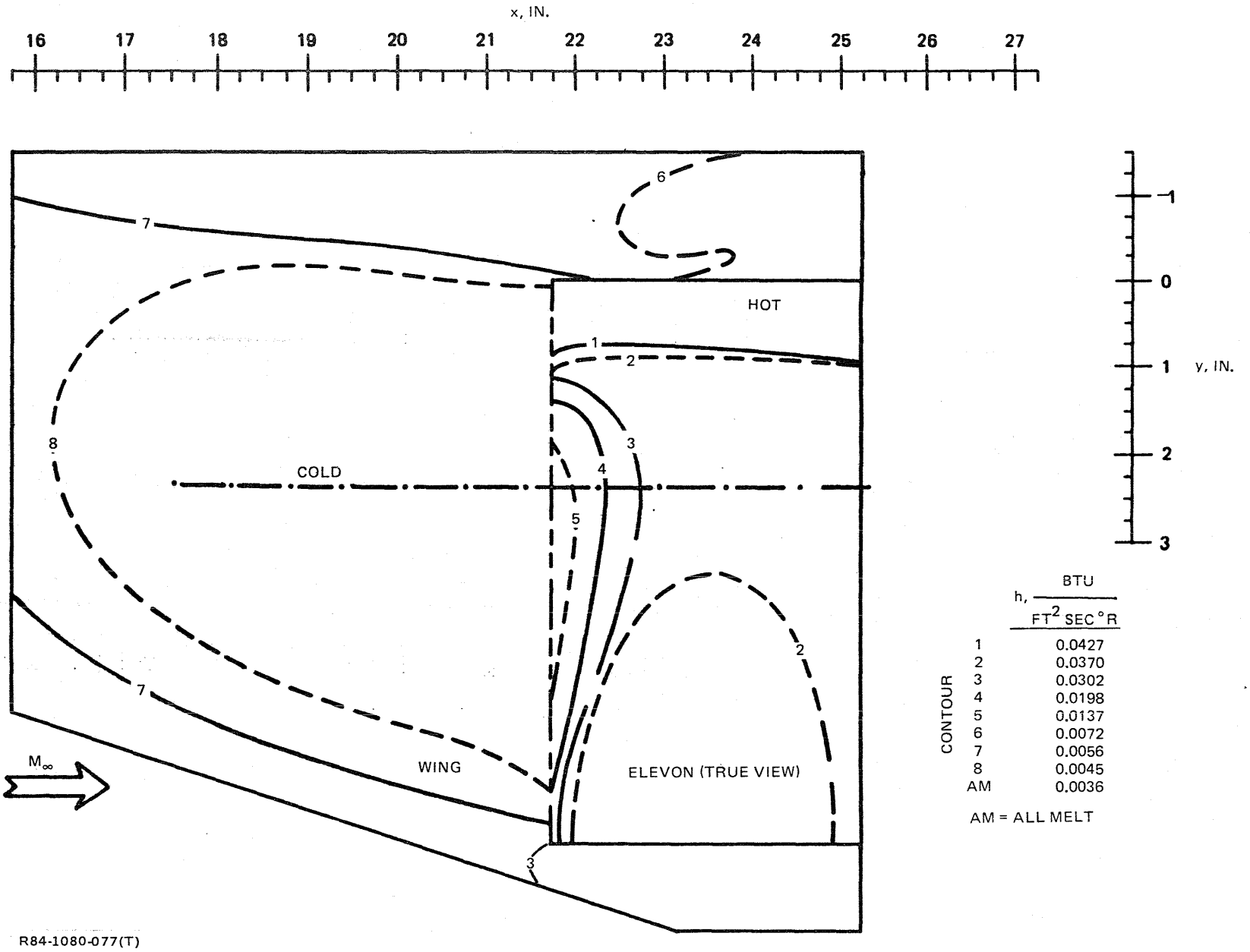

Fig. 77 20° Short Elevon – Phase Change Results, 70° Swept Wing, No Center Body

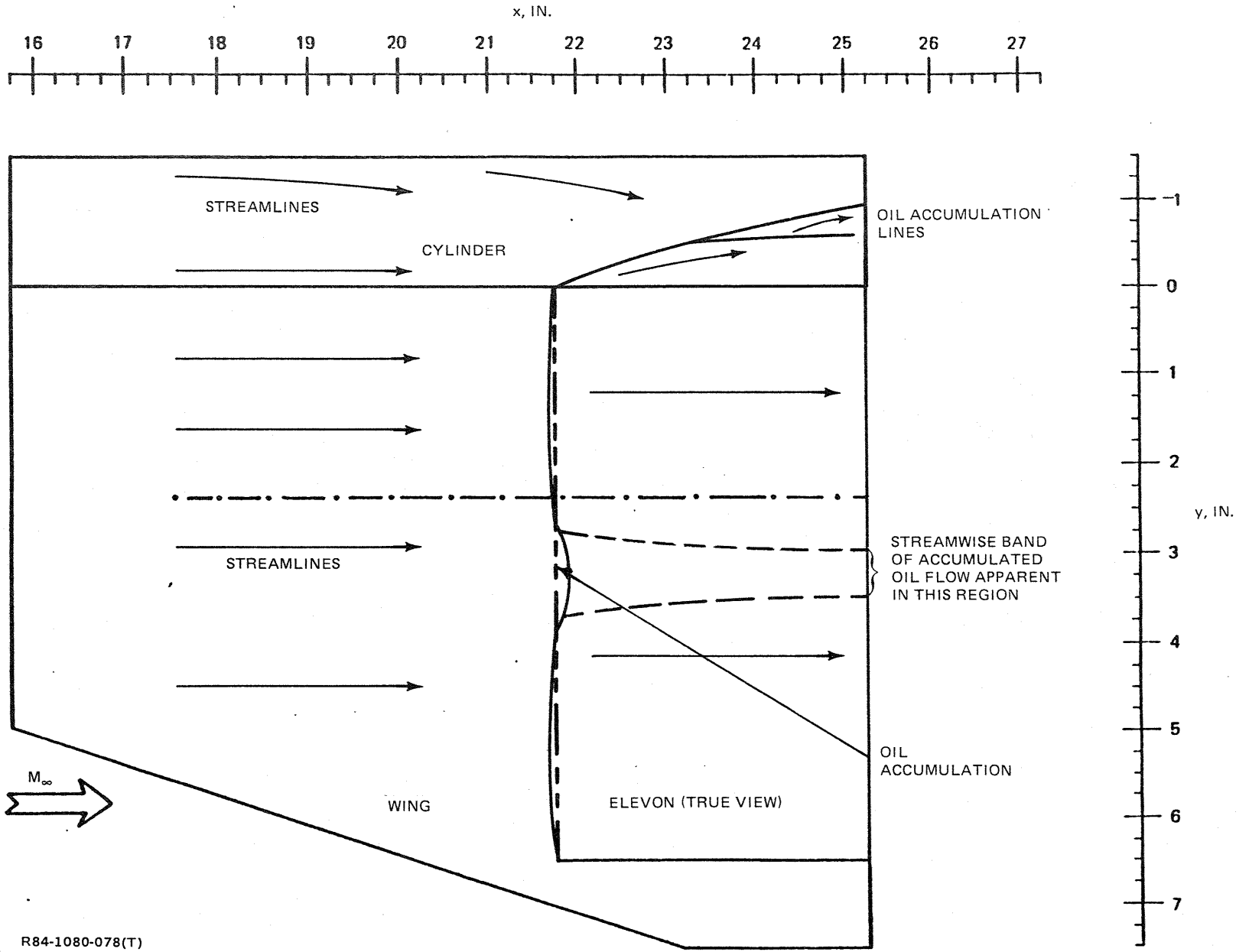

Fig. 78 20° Short Elevon – Oil Flow Pattern, 70° Swept Wing, Cylindrical Center Body

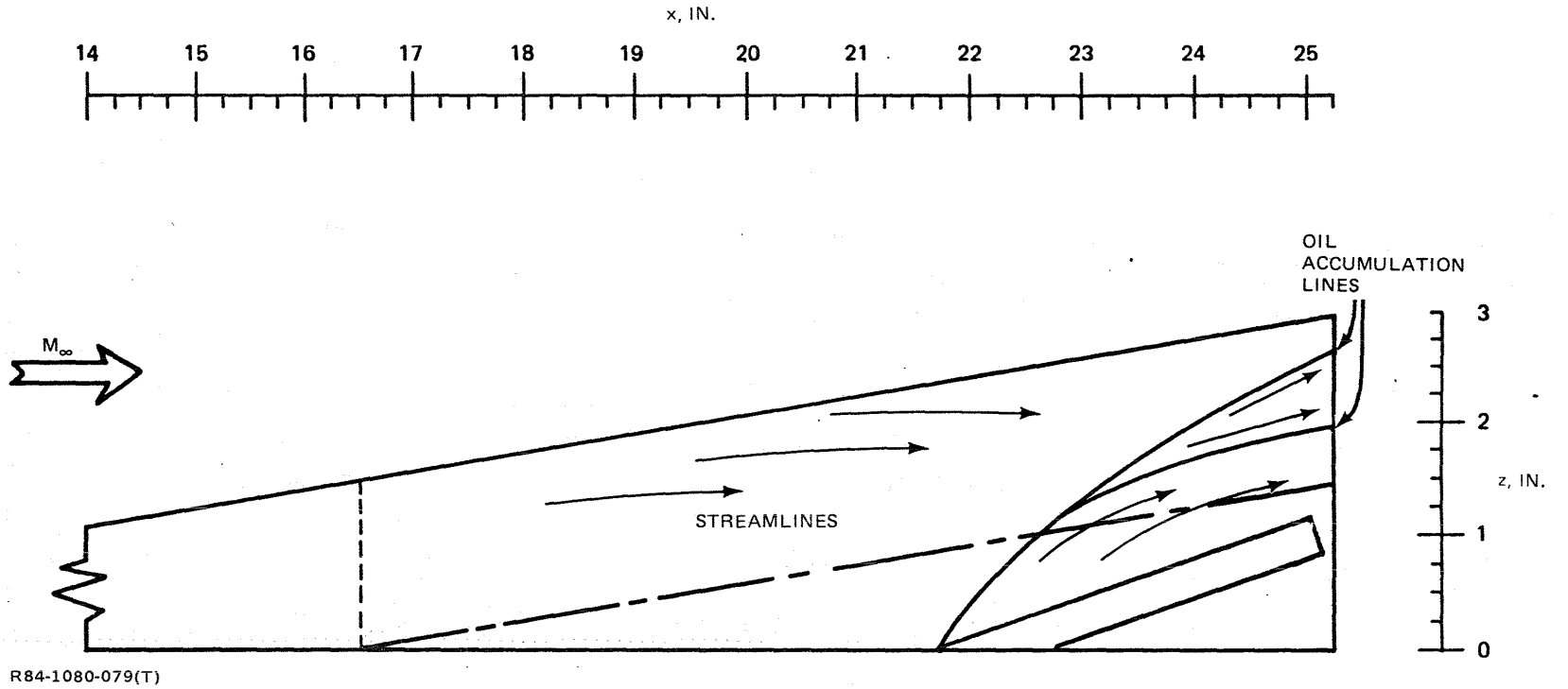

Fig. 79 20° Short Elevon – Oil Flow Pattern, Cylindrical Center Body, 70° Swept Wing

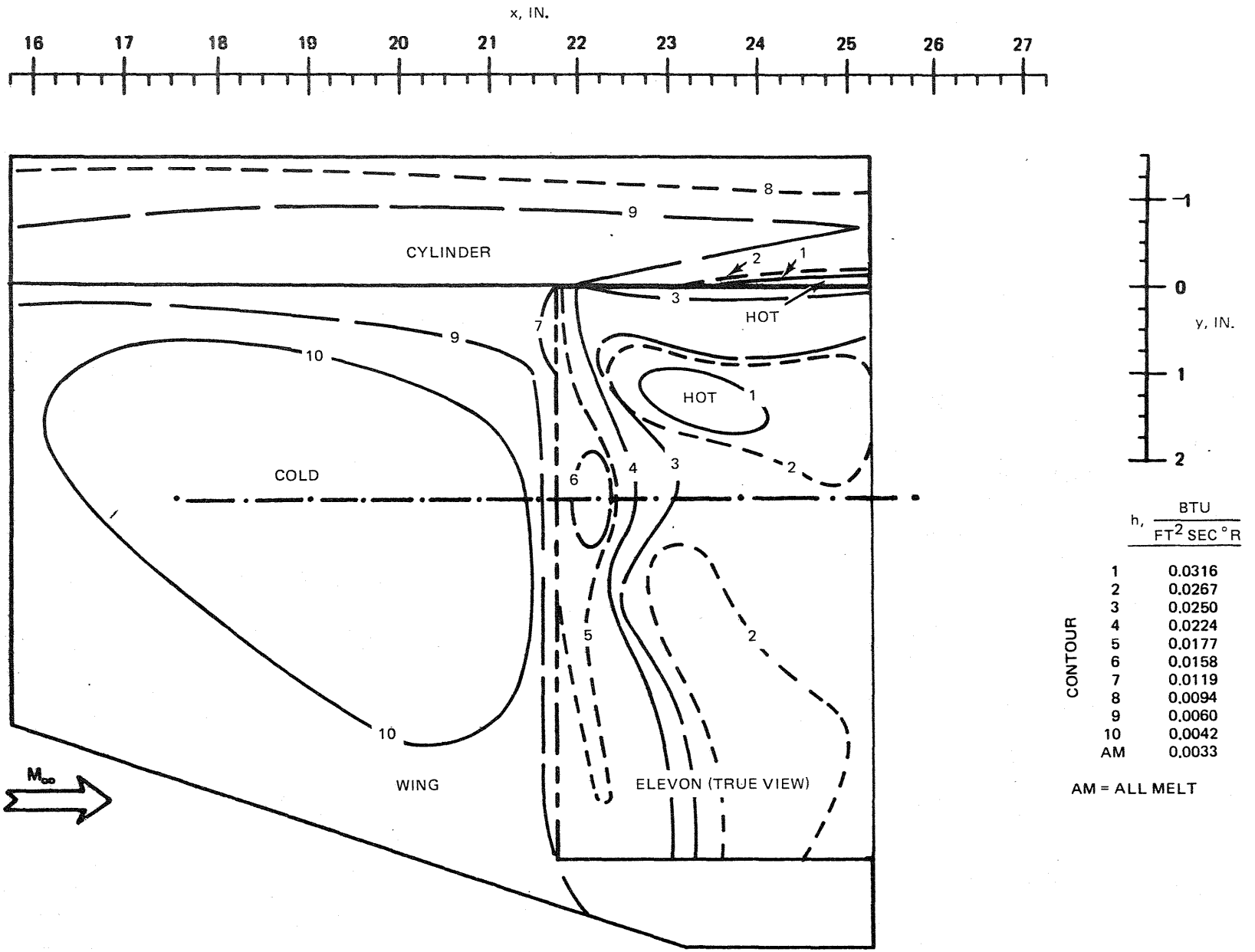

Fig. 80 20° Short Elevon — Phase Change Results, 70° Swept Wing, Cylindrical Center Body

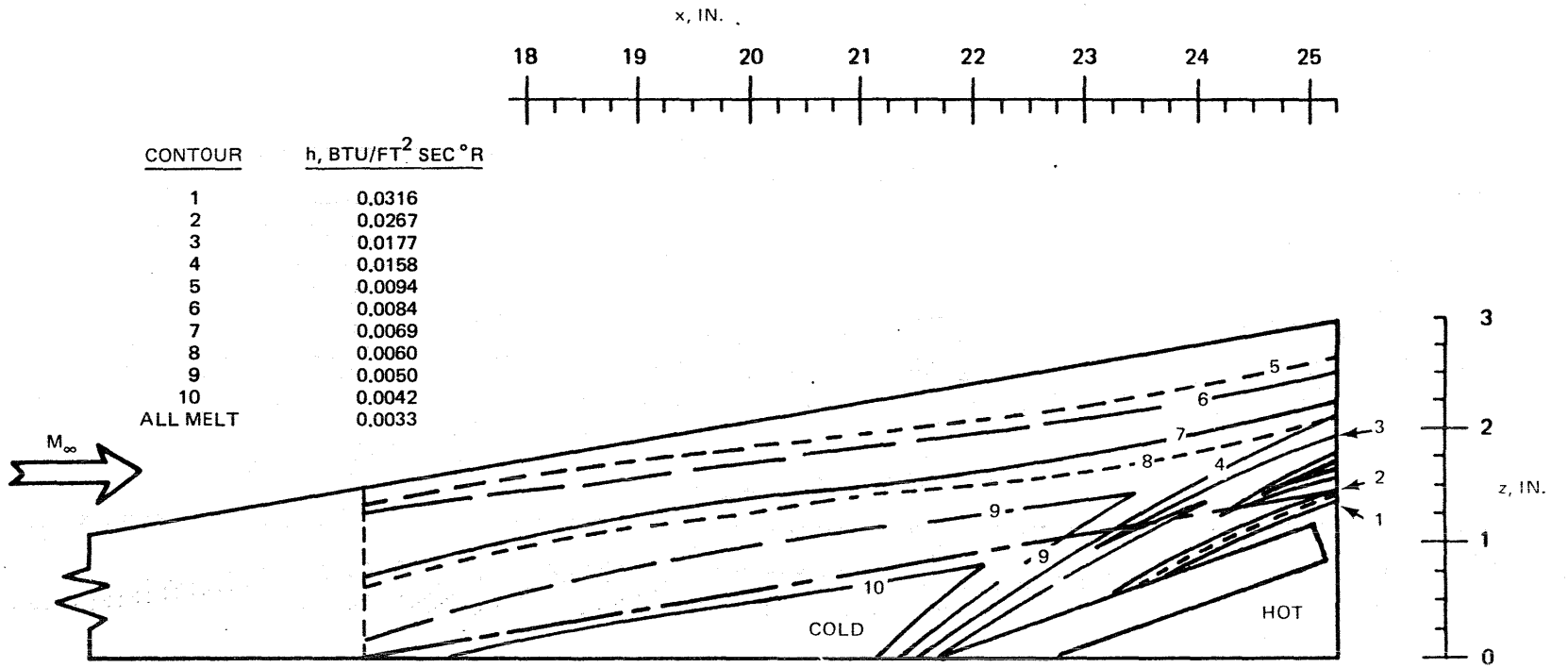

R84-1080-081(T)

Fig. 81 20° Short Elevon – Phase Change Results, Cylindrical Center Body, 70° Swept Wing

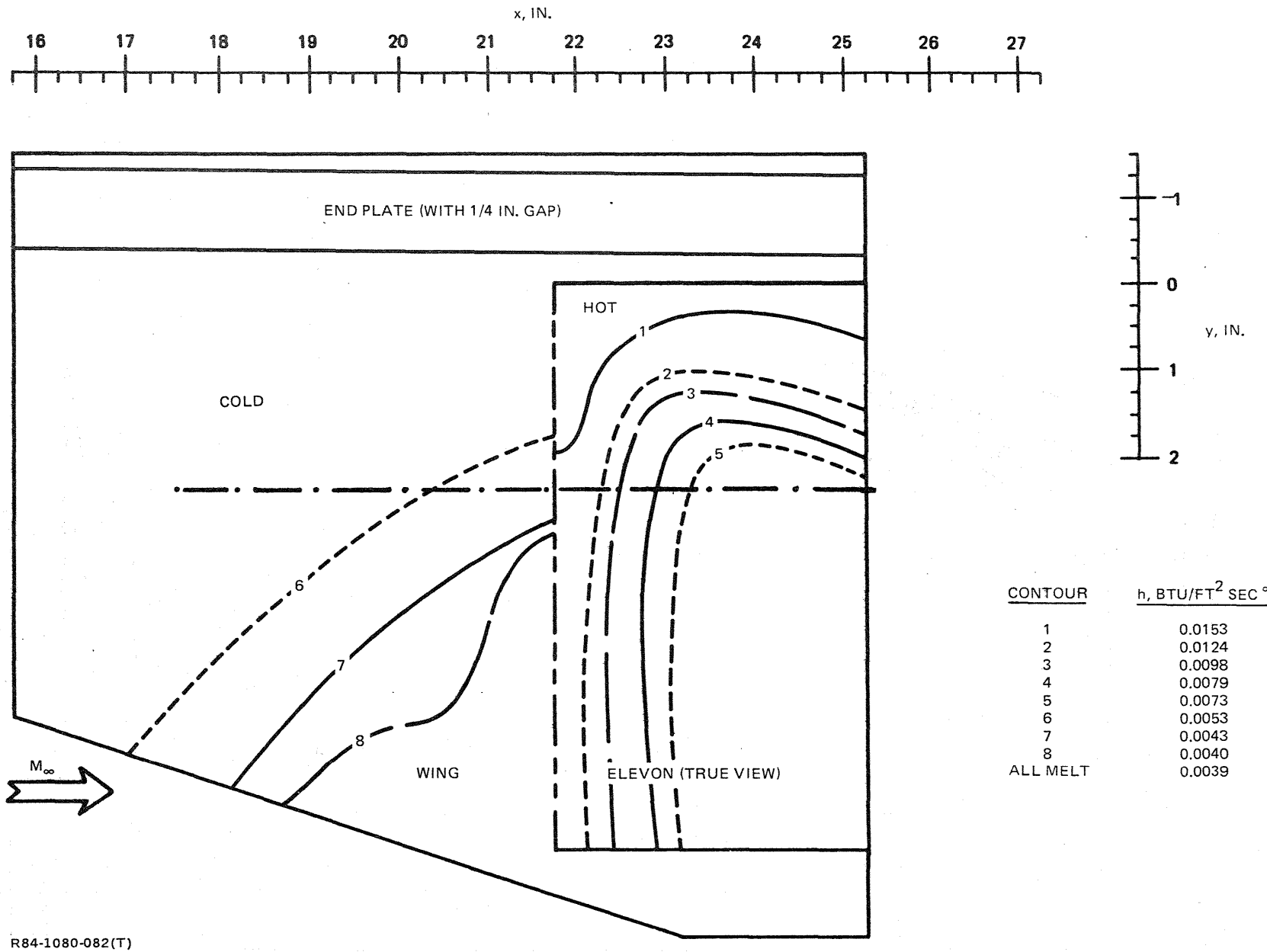

CONTOUR	h, BTU/FT^2 SEC °R
1	0.0153
2	0.0124
3	0.0098
4	0.0079
5	0.0073
6	0.0053
7	0.0043
8	0.0040
ALL MELT	0.0039

R84-1080-082(T)

Fig. 82 20° Short Elevon — Phase Change Results, 70° Swept Wing, End Plate Spaced ¼ in. Away from Elevon

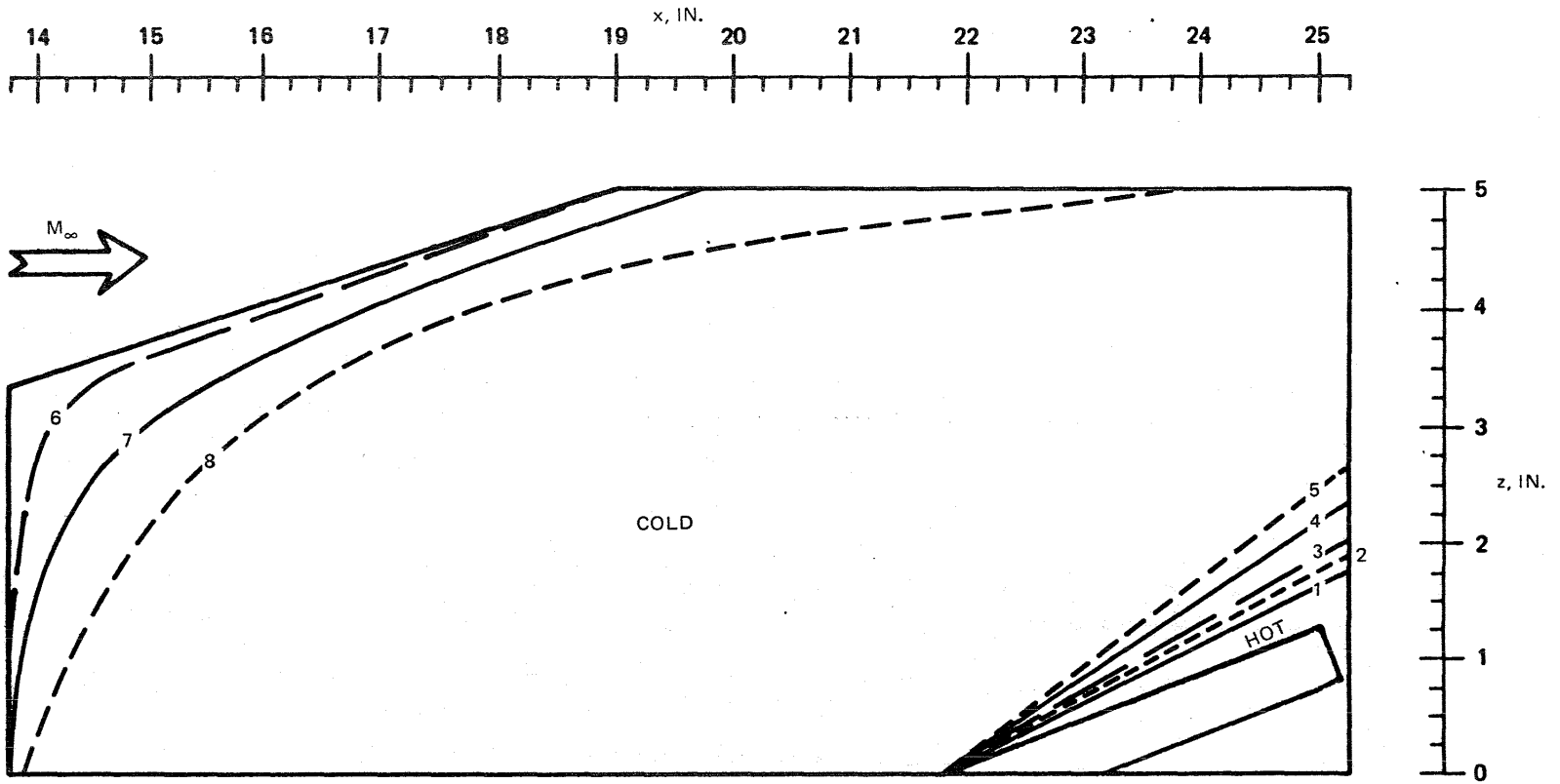

CONTOUR	h, BTU/FT^2 SEC °R
1	0.0612
2	0.0146
3	0.0120
4	0.0106
5	0.0093
6	0.0051
7	0.0046
8	0.0041
ALL MELT	0.0040

R84-1080-083(T)

Fig. 83 20° Short Elevon — Phase Change Results, End Plate Spaced ¼ in. Away from 70° Swept Wing

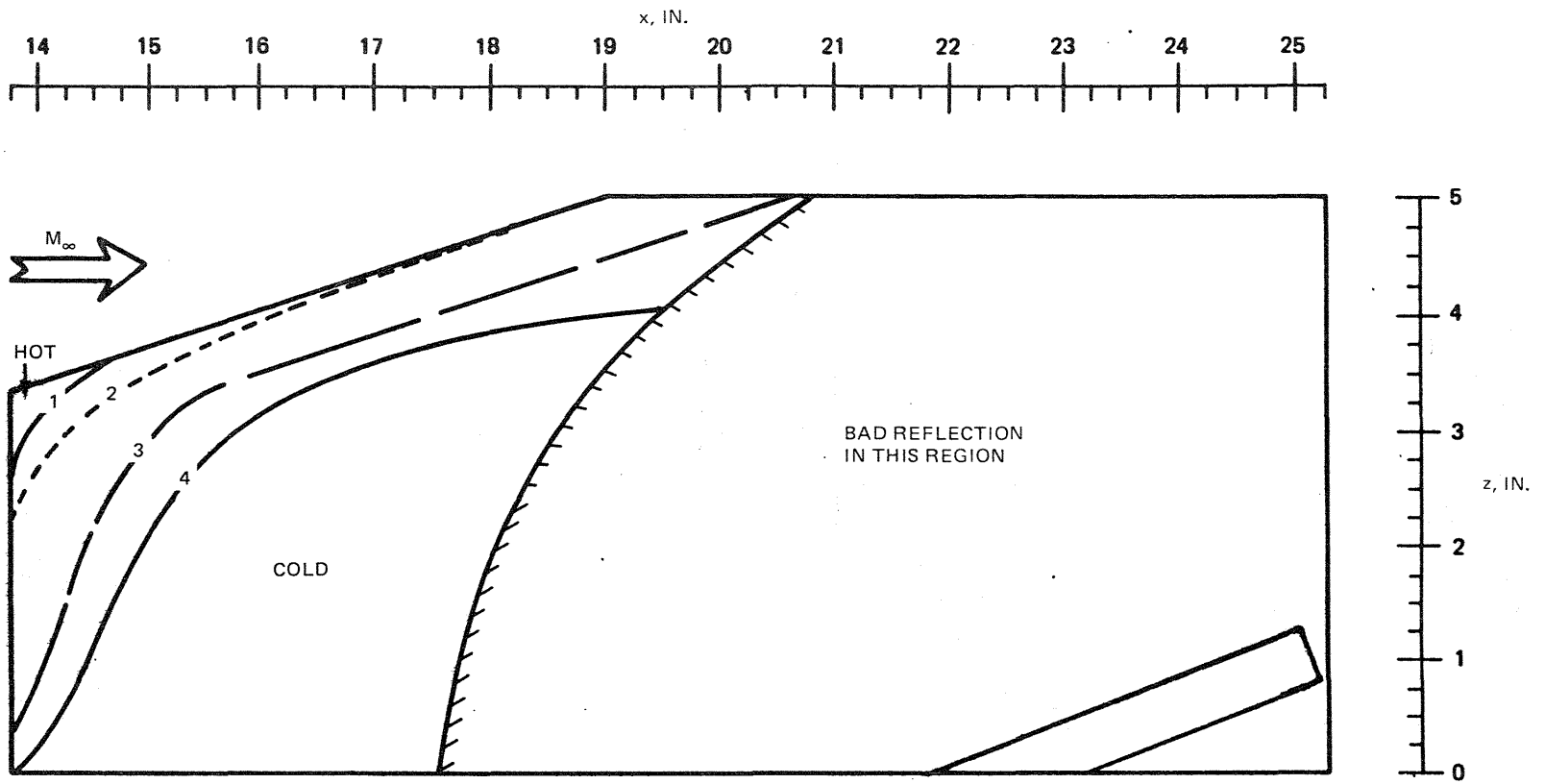

CONTOUR	h, BTU/FT^2 SEC °R
1	0.0056
2	0.0049
3	0.0043
4	0.0040

R84-1080-084(T)

Fig. 84 20° Short Elevon — Phase Change Results, End Plate, 70° Swept Wing

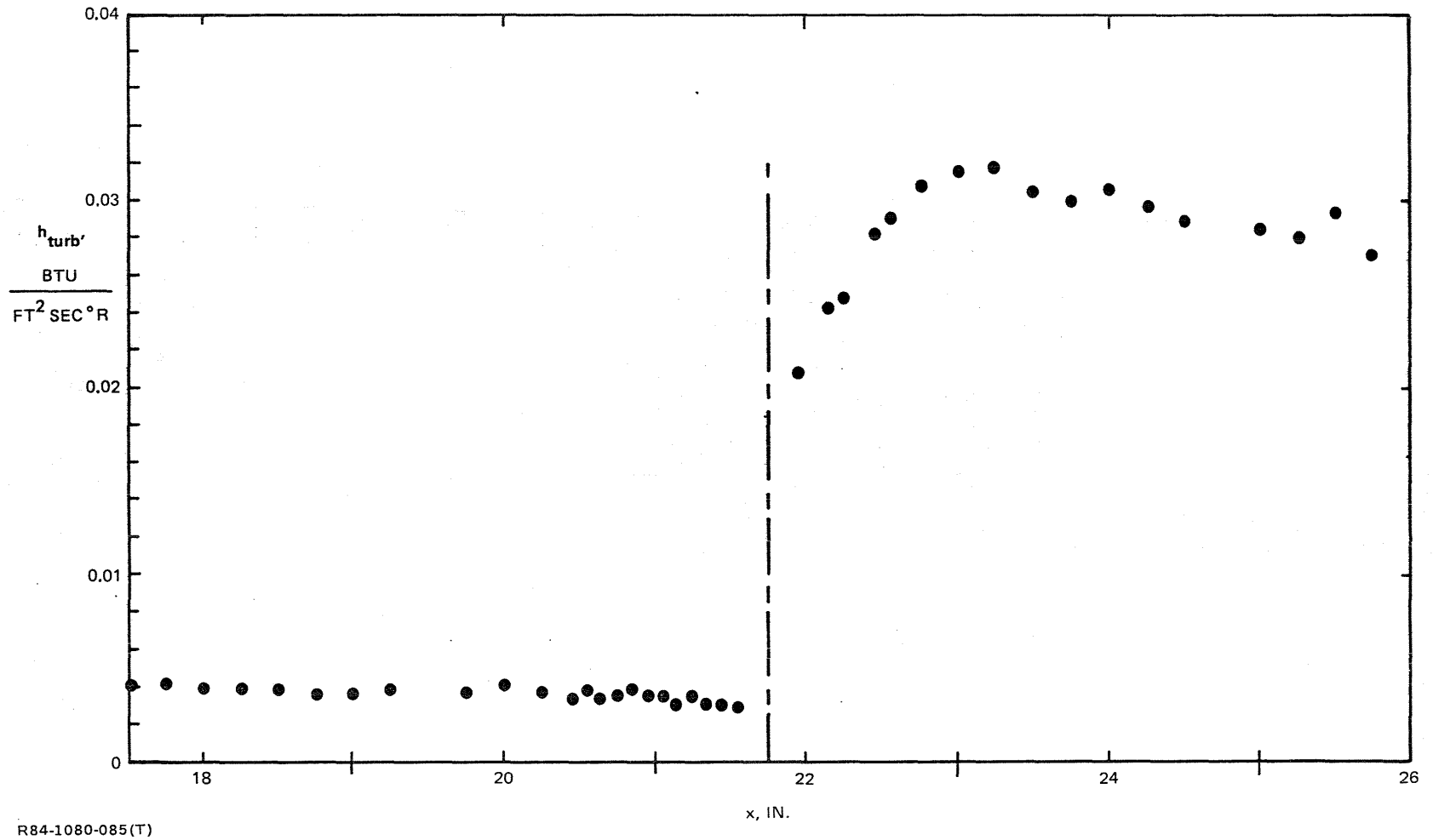

R84-1080-085(T)

Fig. 85 20° Long Elevon – Thermocouple Data, Unswept Wing, No Center Body

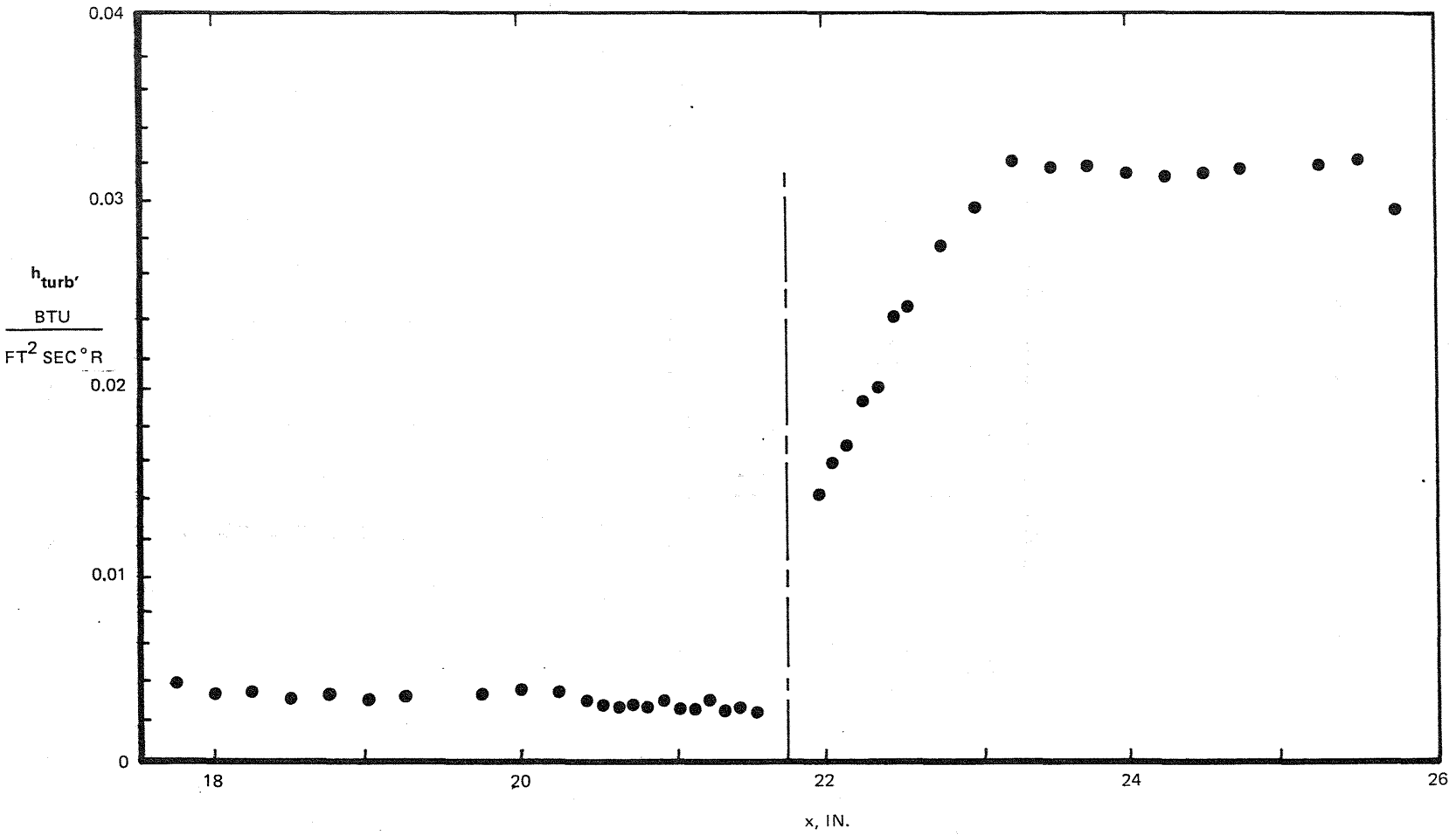

R84-1080-086(T)

Fig. 86 20° Long Elevon — Thermocouple Data, 70° Swept Wing, Cylindrical Center Body

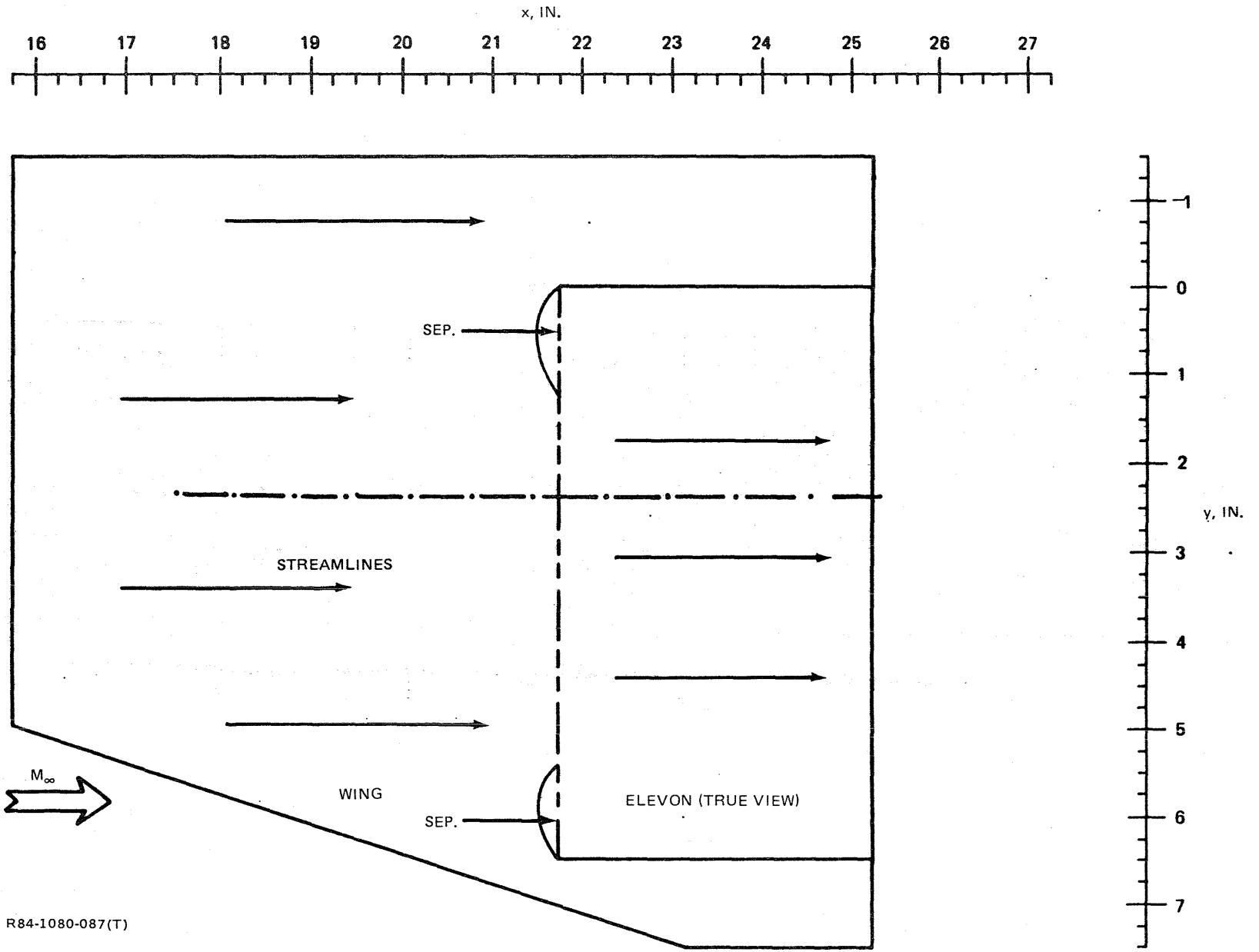

Fig. 87 25° Short Elevon – Oil Flow Pattern, Unswept Wing, No Center Body

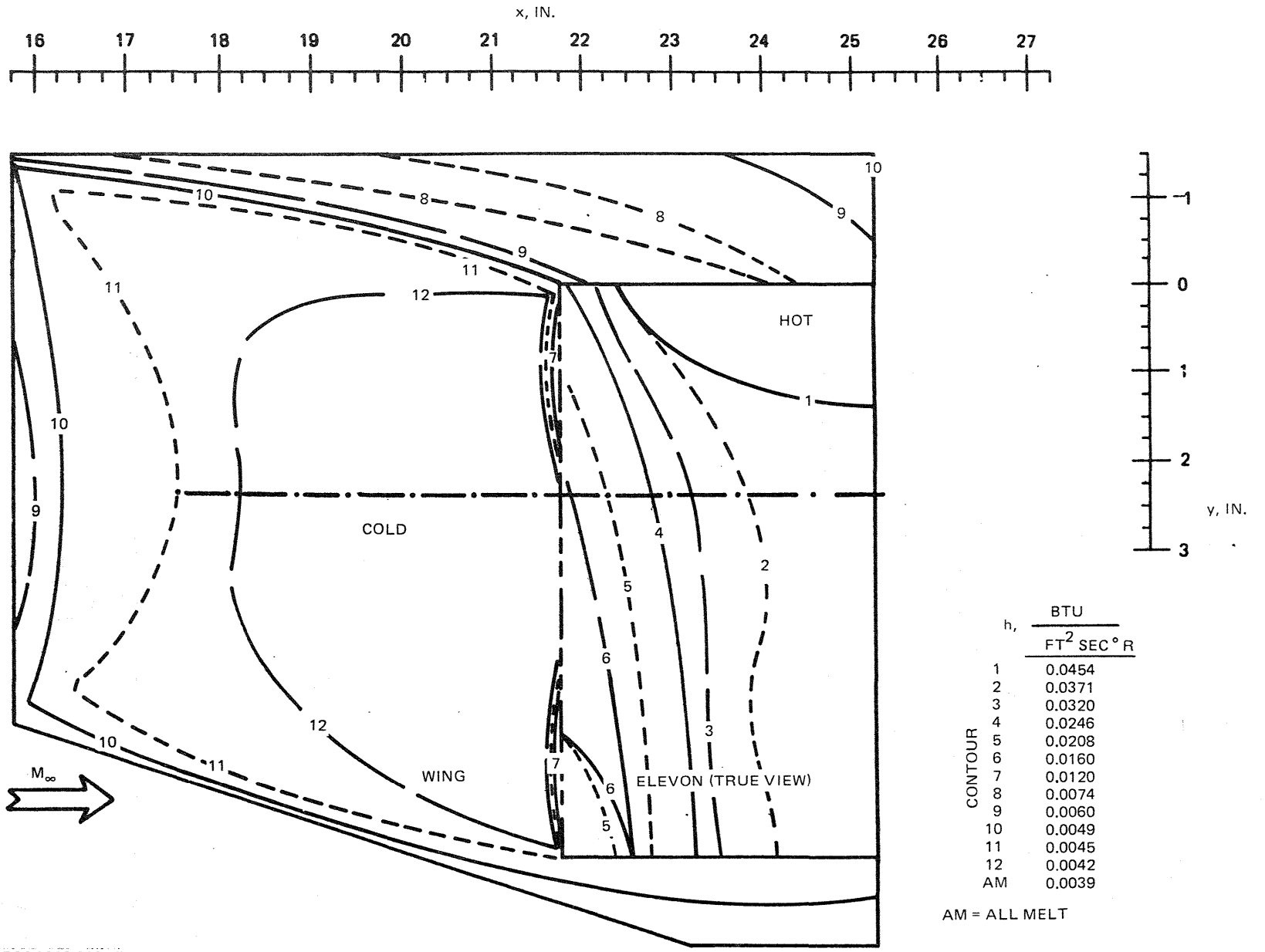

Fig. 88 25° Short Elevon — Phase Change Results, Unswept Wing, No Center Body, Composite of Contours Prepared for Tunnel Runs 093, 122 & 123

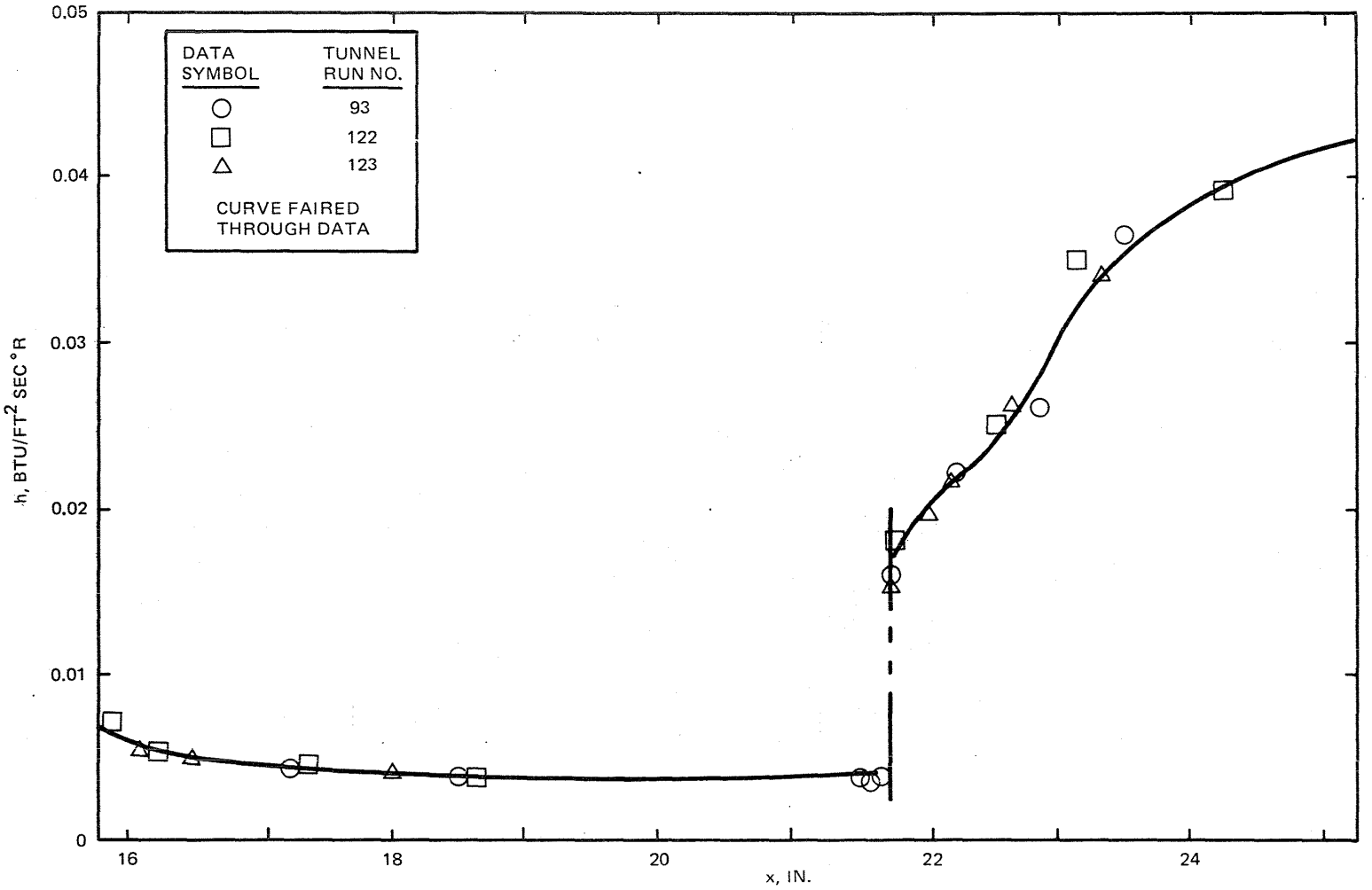

R84-1080-089(T)

Fig. 89 25° Short Elevon — Heat Transfer Coefficients on Wing and Elevon Surfaces, Obtained Using Phase Change Coating Technique, Unswept Wing No Center Body, Along a Streamwise Line at the y = 2.375 in. Spanwise Station for Tunnel Runs 093, 122 & 123

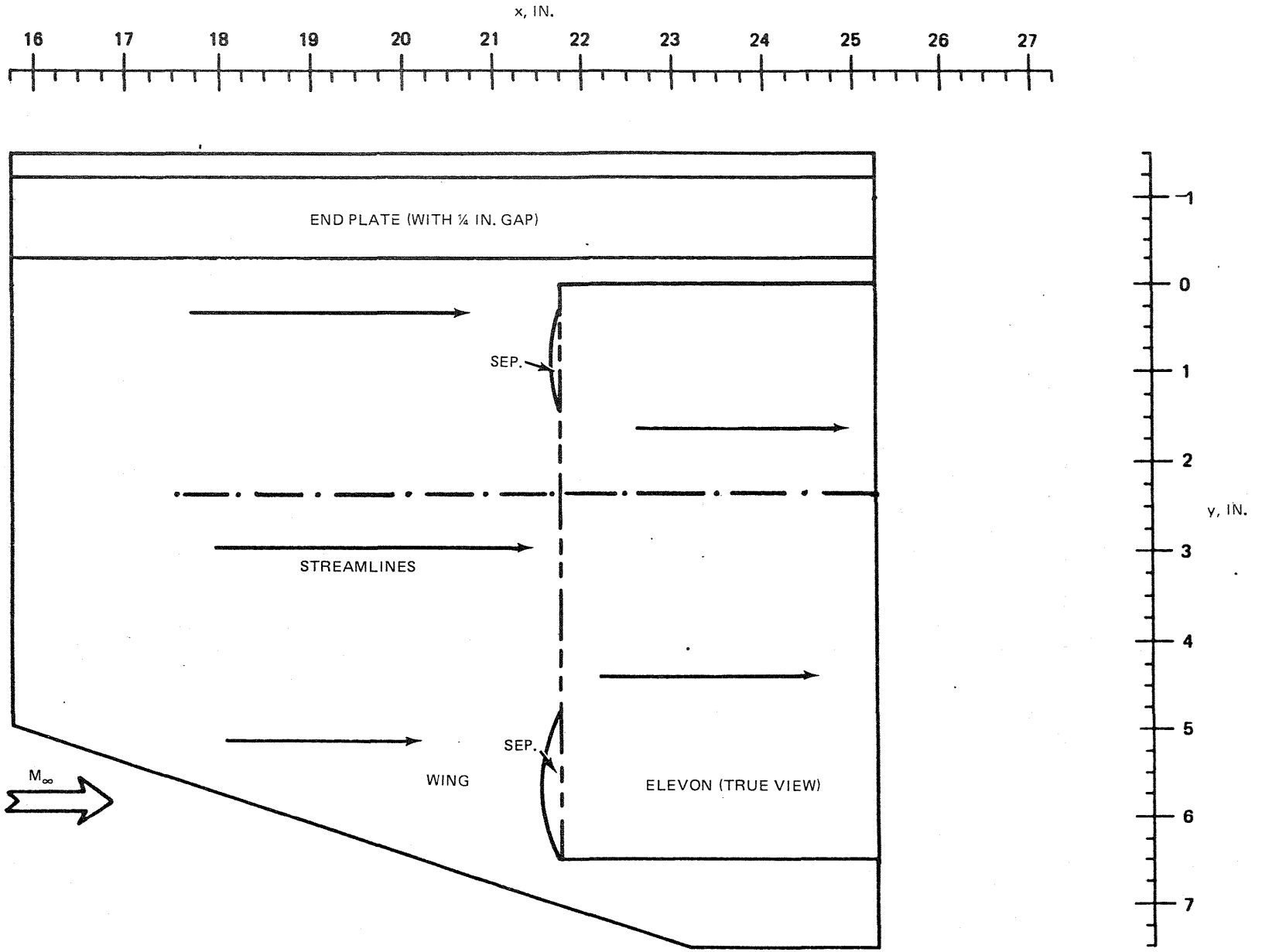

R84-1080-090(T)

Fig. 90 25° Short Elevon — Oil Flow Pattern, Unswept Wing, End Plate ¼ in. Away from Elevon

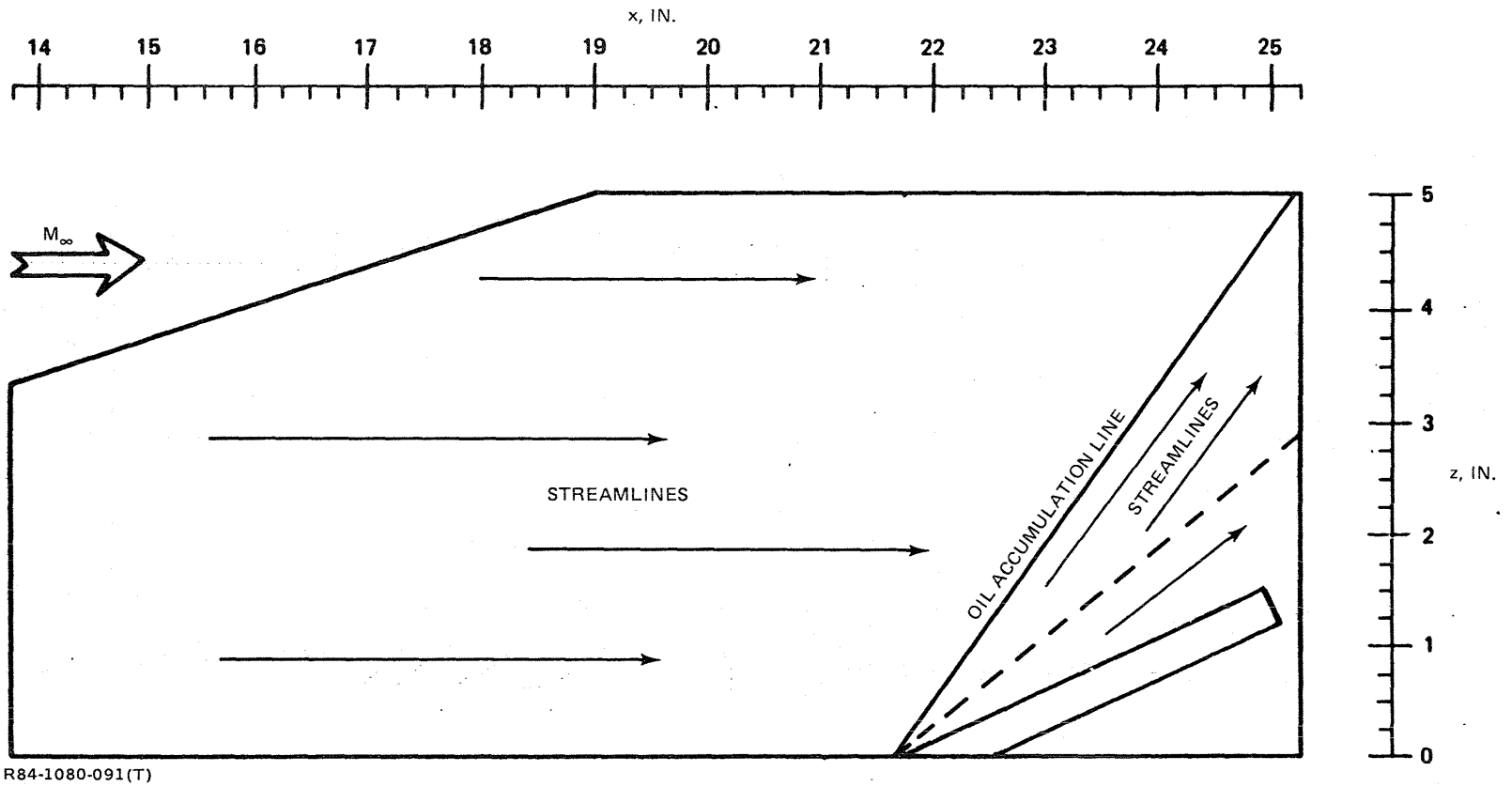

Fig. 91 25° Short Elevon — Oil Flow Pattern, End Plate Positioned ¼ in. Away from Elevon, Unswept Wing

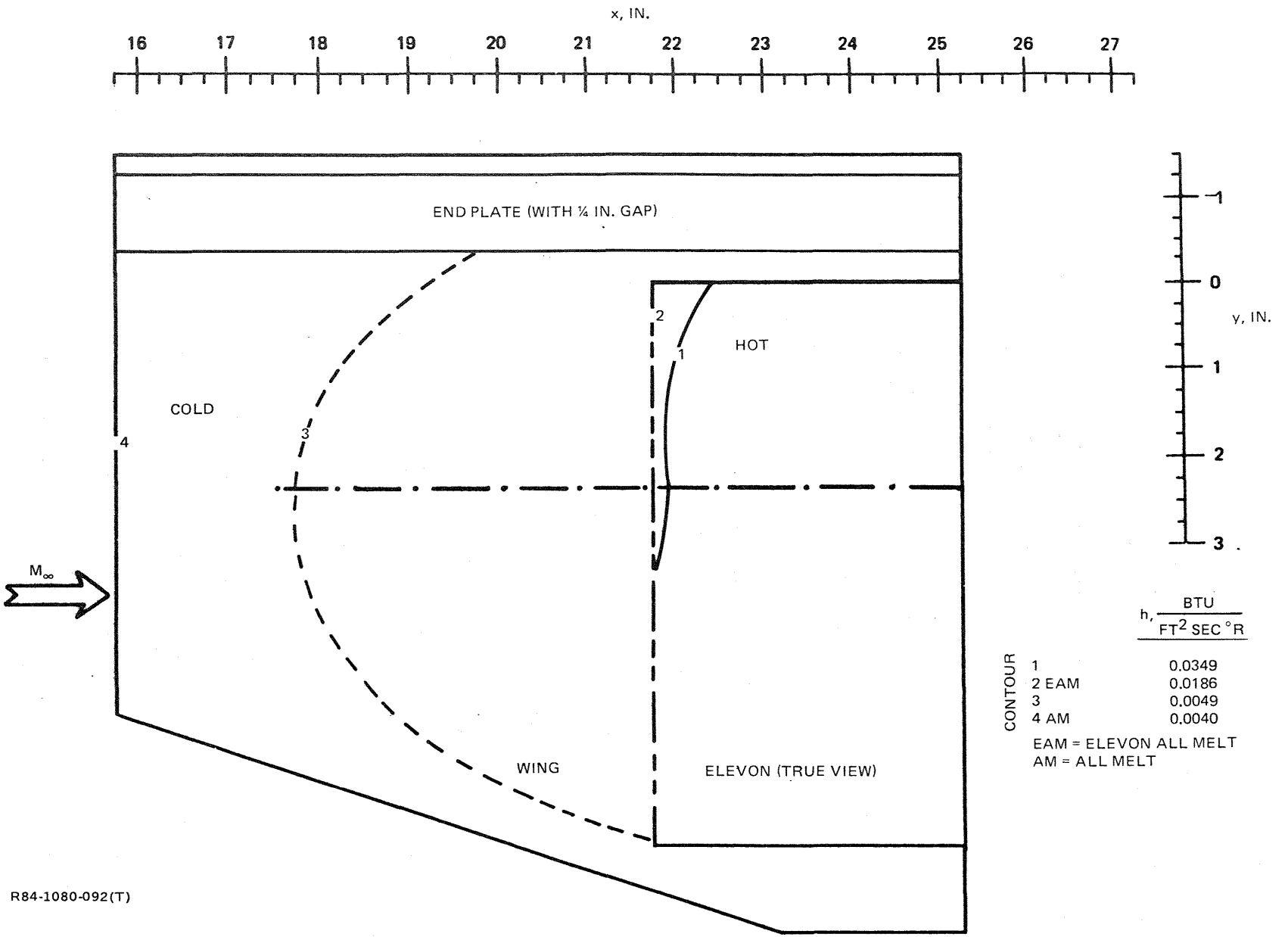

Fig. 92 25° Short Elevon — Phase Change Results, Unswept Wing, End Plate ¼ in. Away from Elevon

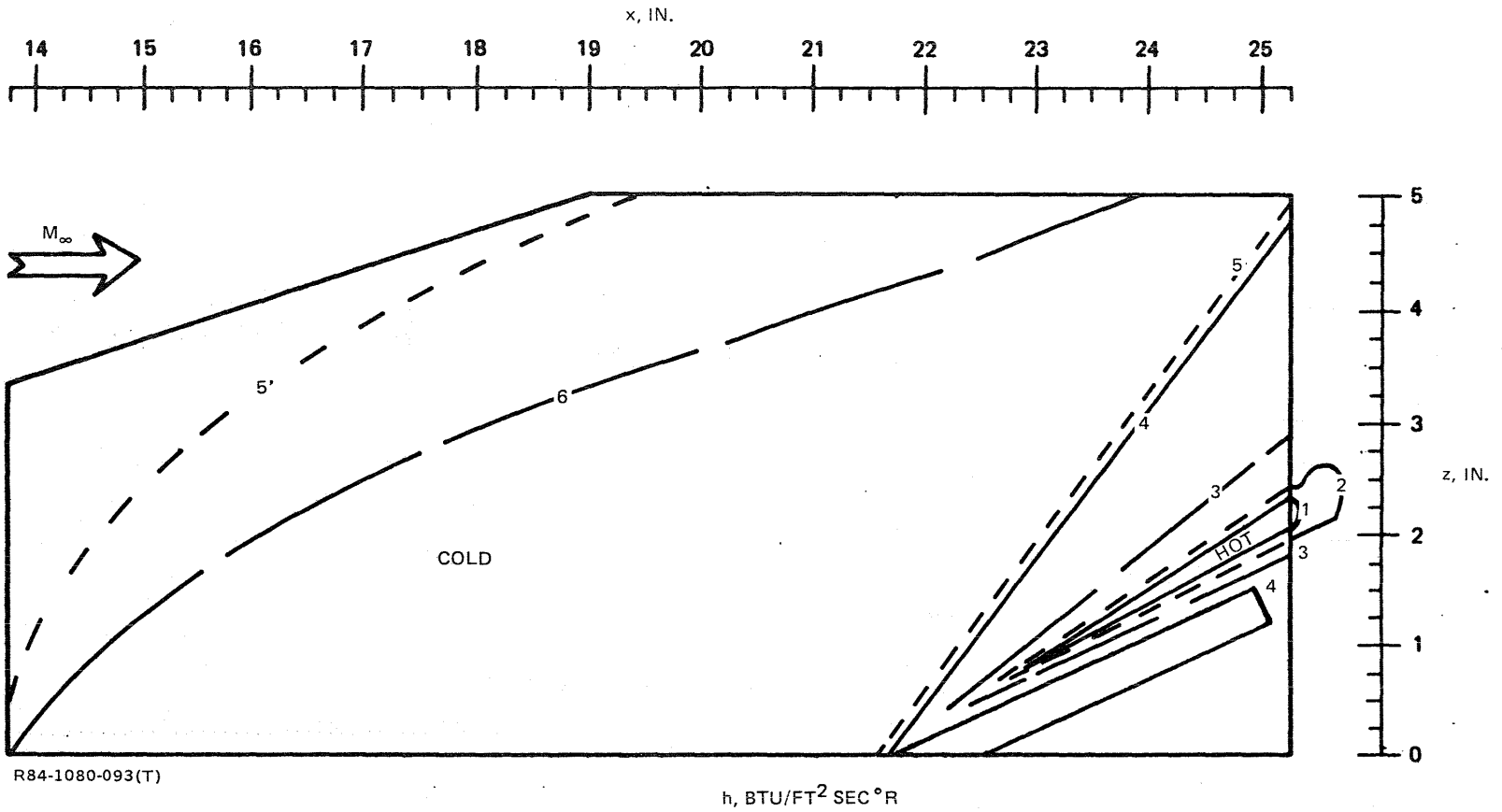

h, BTU/FT^2 SEC °R

CONTOUR	1	0.0270
	2	0.0191
	3	0.0102
	4	0.0071
	5	0.0049
	6	0.0042
	ALL MELT	0.0038

Fig. 93 25° Short Elevon – Phase Change Results, End Plate Positioned ¼ in. Away from Elevon, Unswept Wing

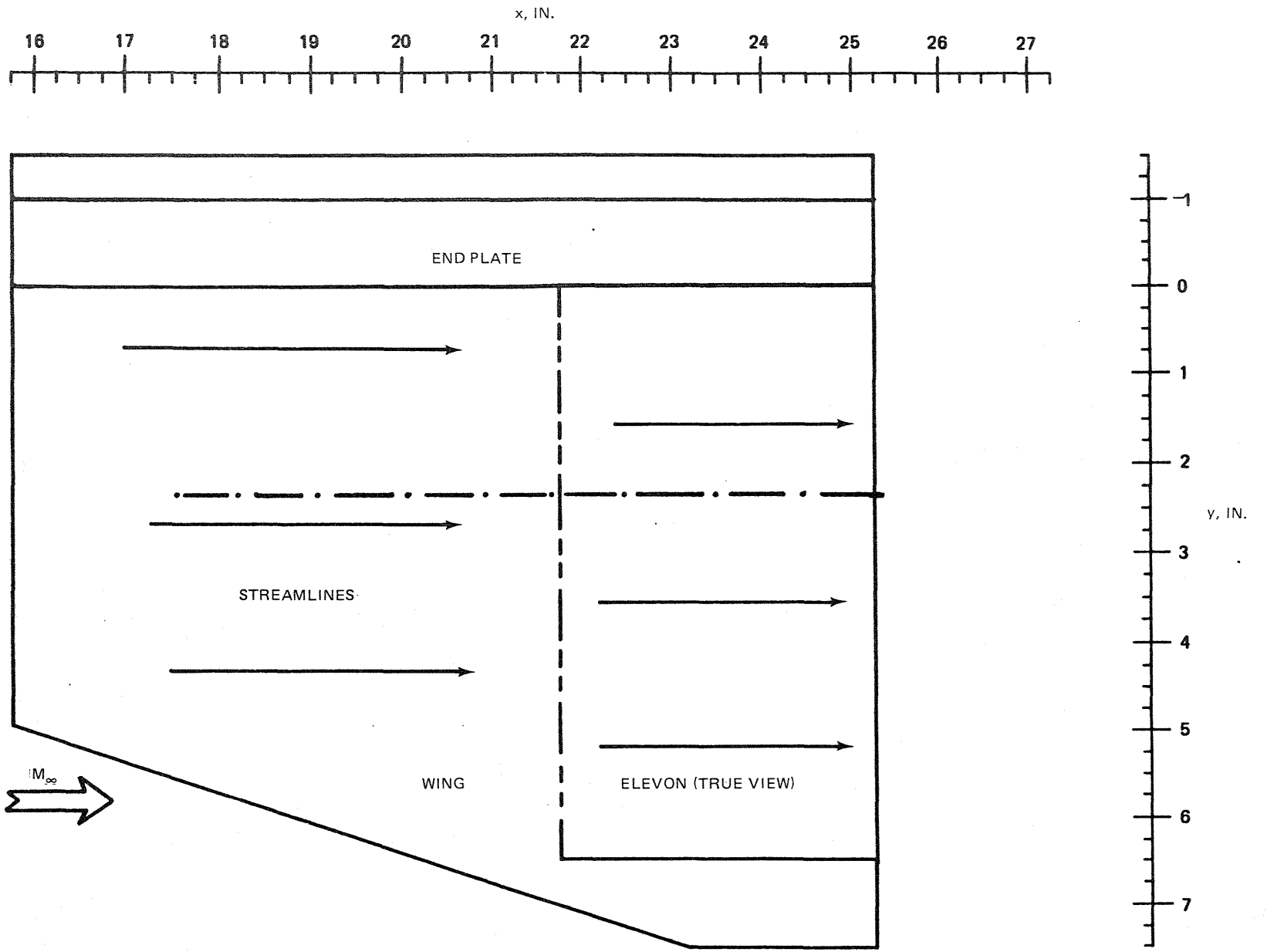

R84-1080-094(T)

Fig. 94 25° Short Elevon — Oil Flow Pattern, Unswept Wing, End Plate

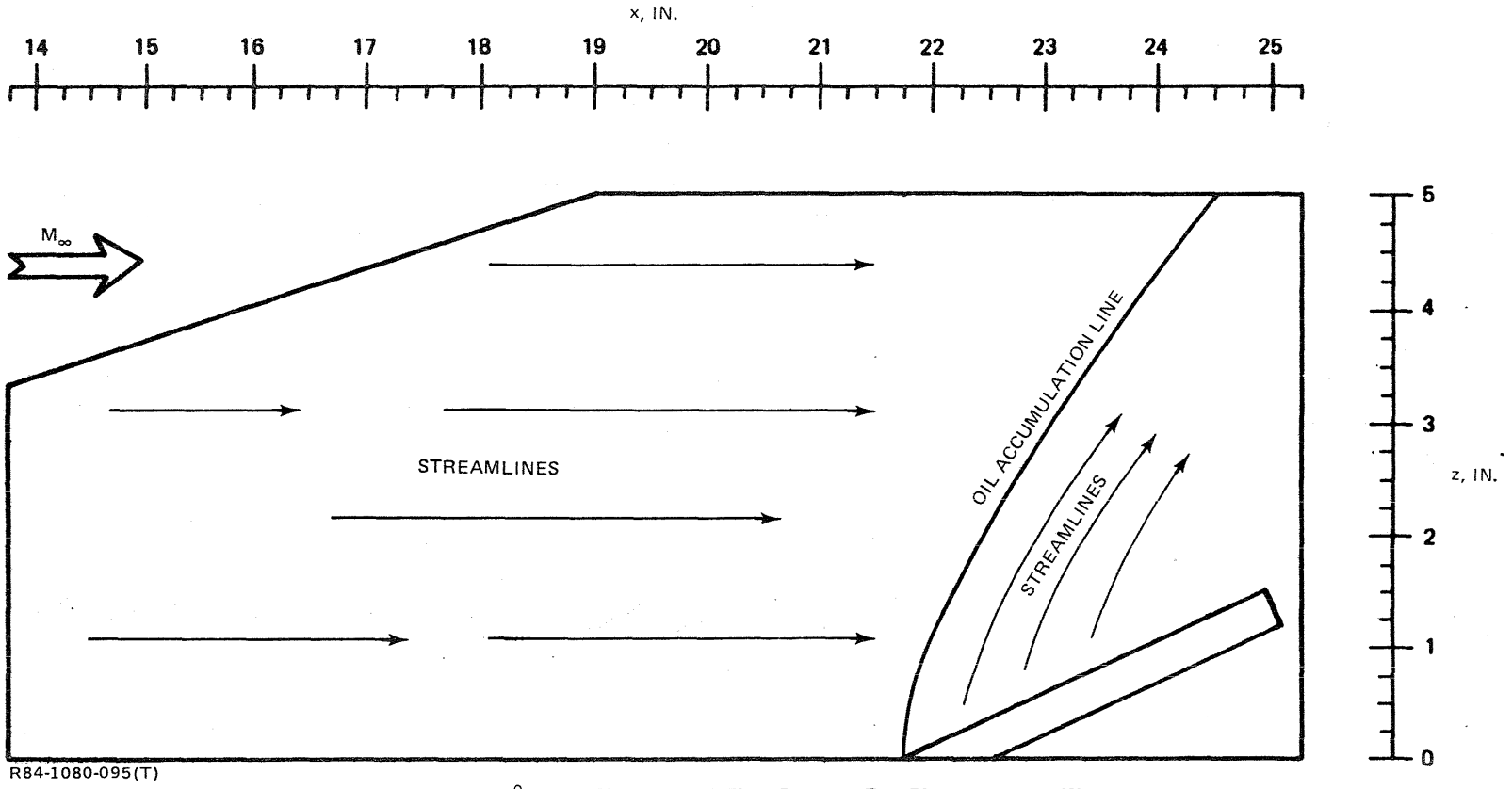

R84-1080-095(T)

Fig. 95 25° Short Elevon – Oil Flow Pattern, End Plate, Unswept Wing

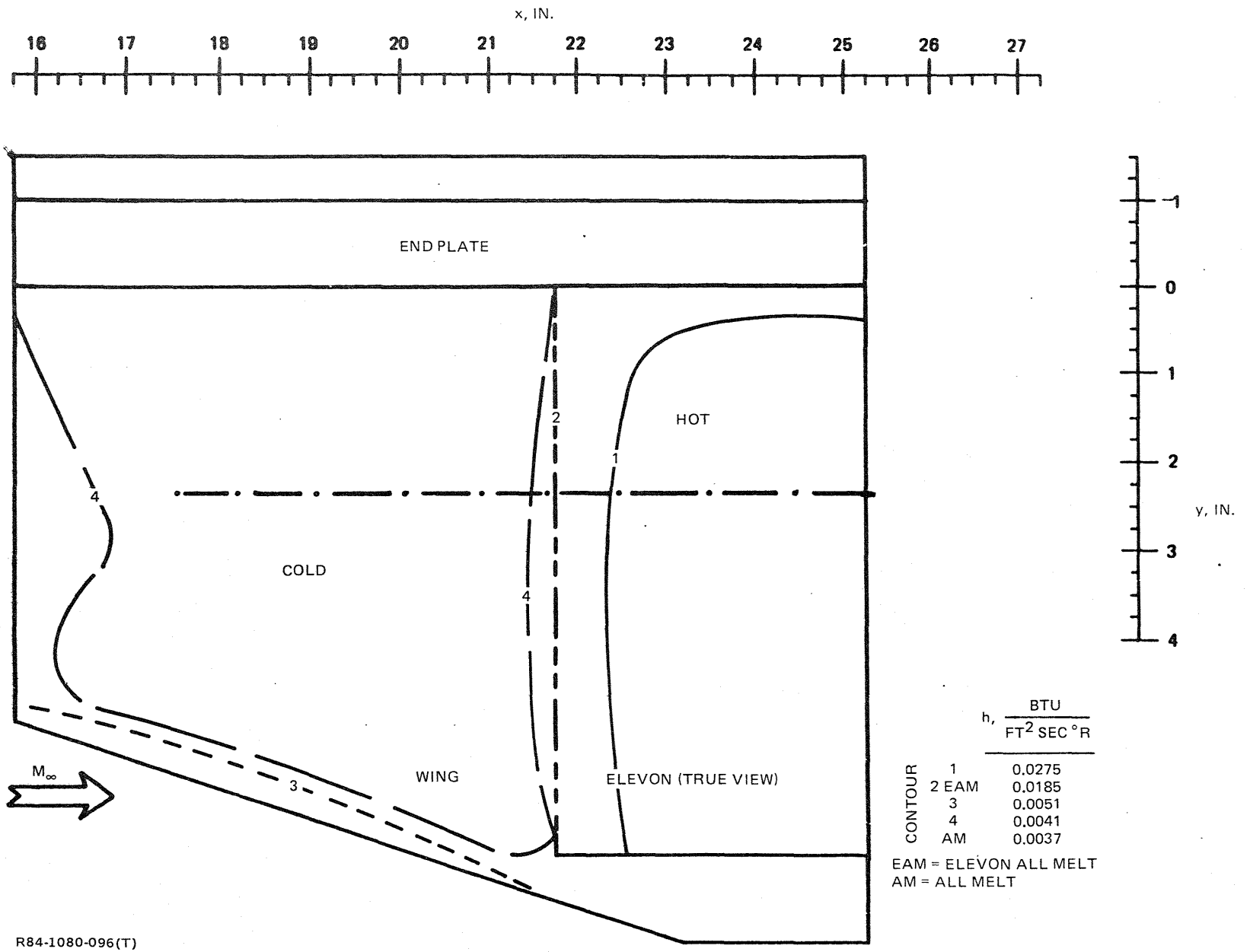

Fig. 96 25° Short Elevon — Phase Change Results, Unswept Wing, End Plate

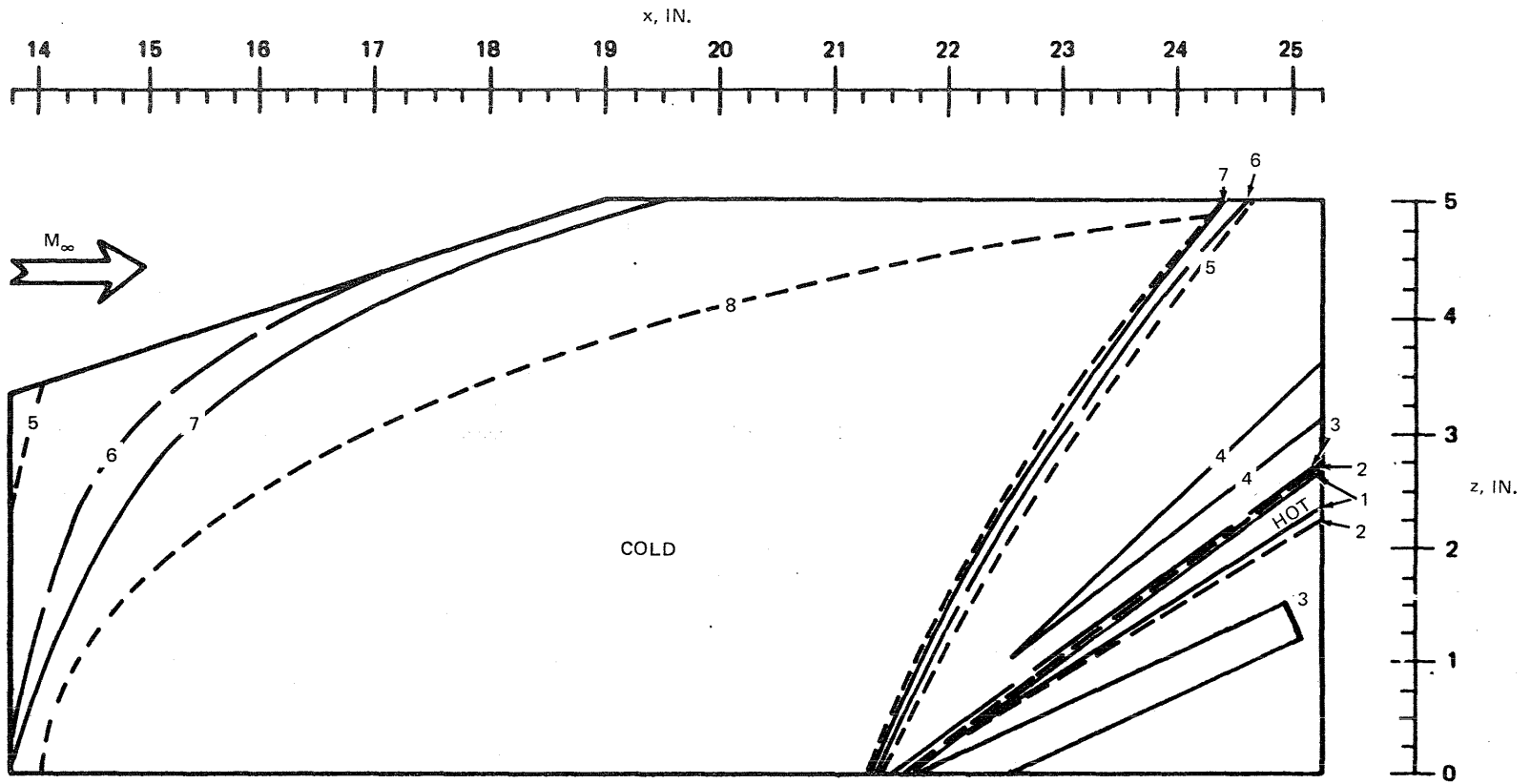

CONTOUR	h, BTU/FT^2 SEC °R
1	0.0275
2	0.0185
3	0.0151
4	0.0083
5	0.0069
6	0.0051
7	0.0041
8	0.0037
ALL MELT	0.0034

R84-1080-097(T)

Fig. 97 25° Short Elevon — Phase Change Results, End Plate, Unswept Wing

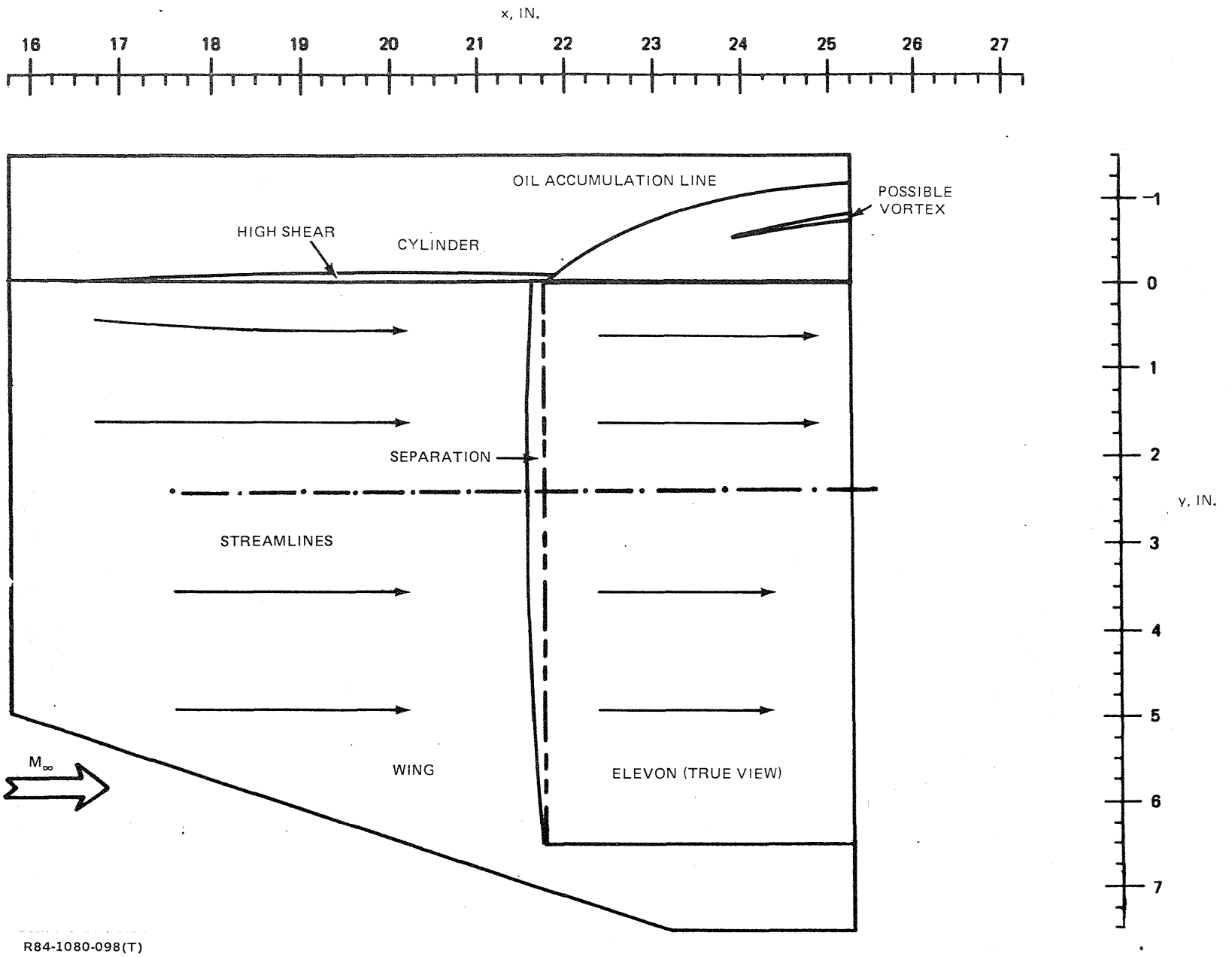

Fig. 98 25° Short Elevon – Oil Flow Pattern, 70° Swept Wing, Cylindrical Center Body

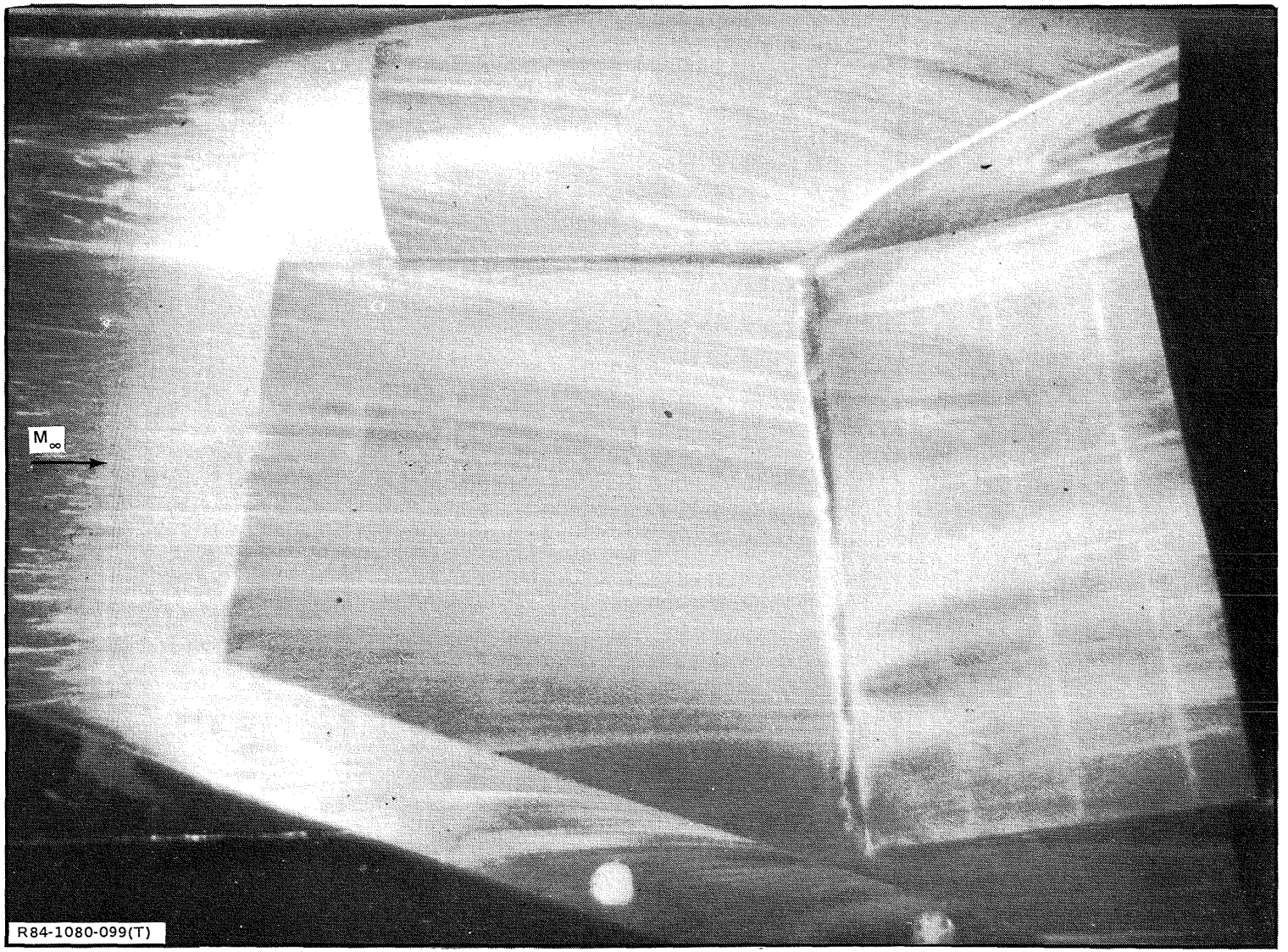

Fig. 99 25° Short Elevon — Photograph of Oil Flow Pattern, 70° Swept Wing, Cylindrical Center Body

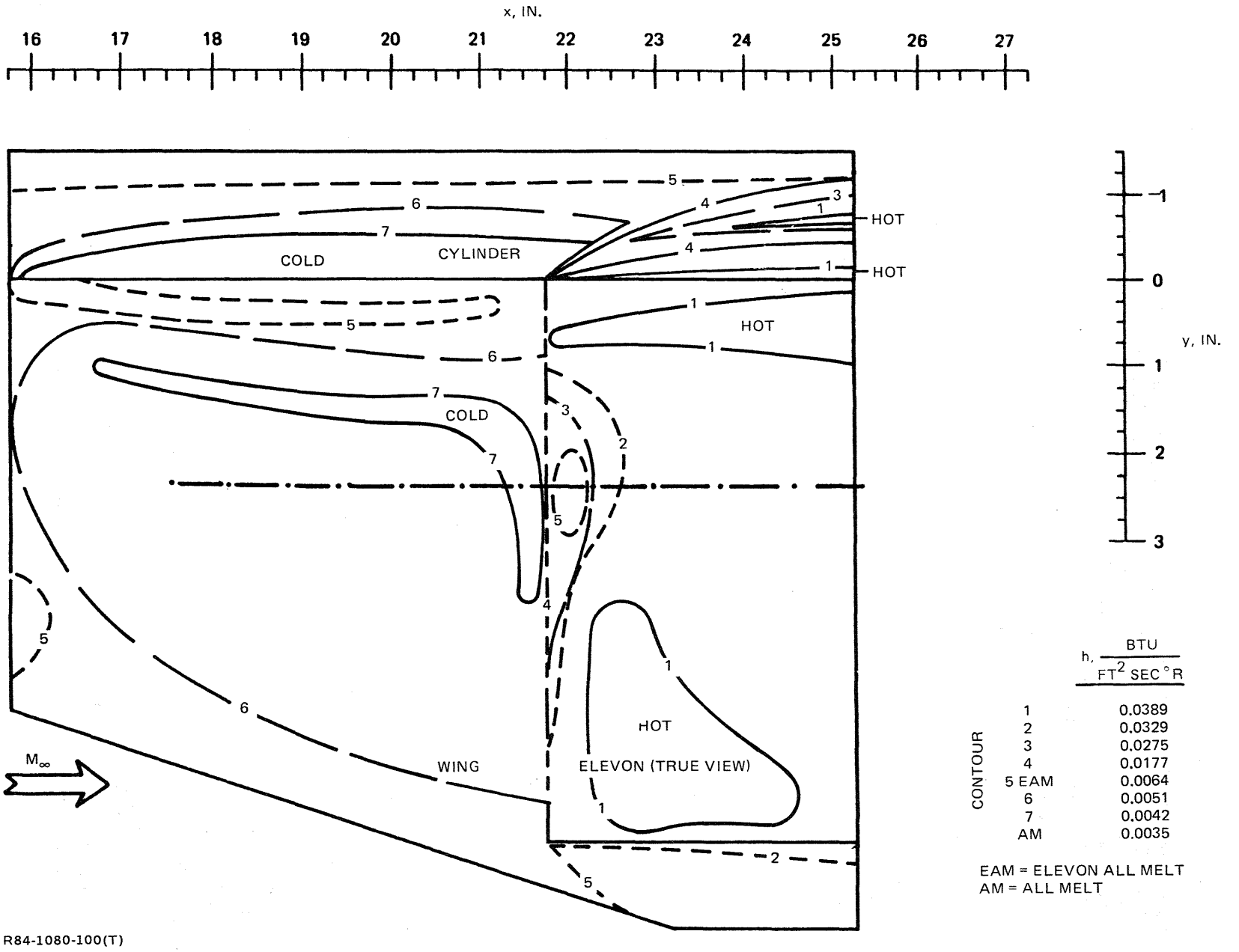

Fig. 100 25° Short Elevon — Phase Change Results, 70° Swept Wing, Cylindrical Center Body

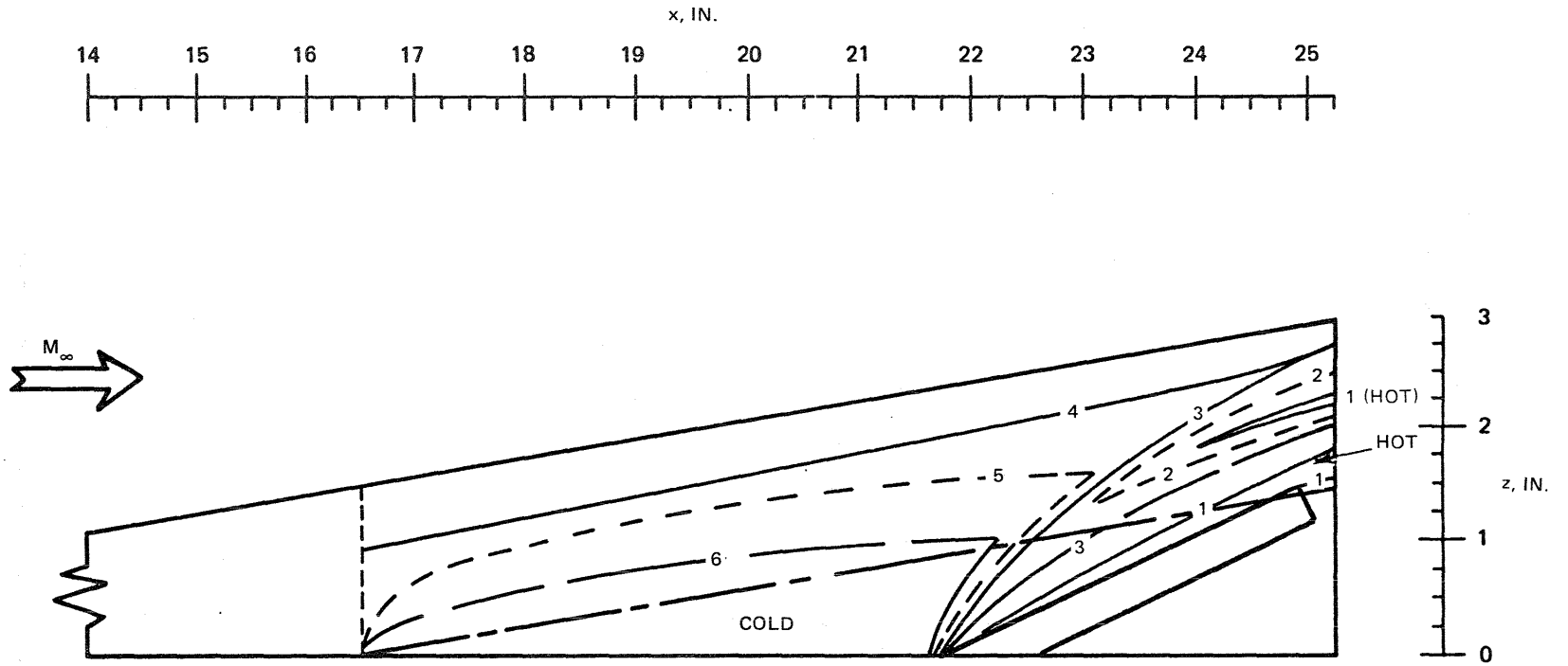

CONTOUR	h, BTU / FT² SEC °R
1	0.0389
2	0.0275
3	0.0177
4	0.0064
5	0.0051
6	0.0042
ALL MELT	0.0035

R84-1080-101(T)

Fig. 101 25° Short Elevon — Phase Change Results, Cylindrical Center Body, 70° Swept Wing

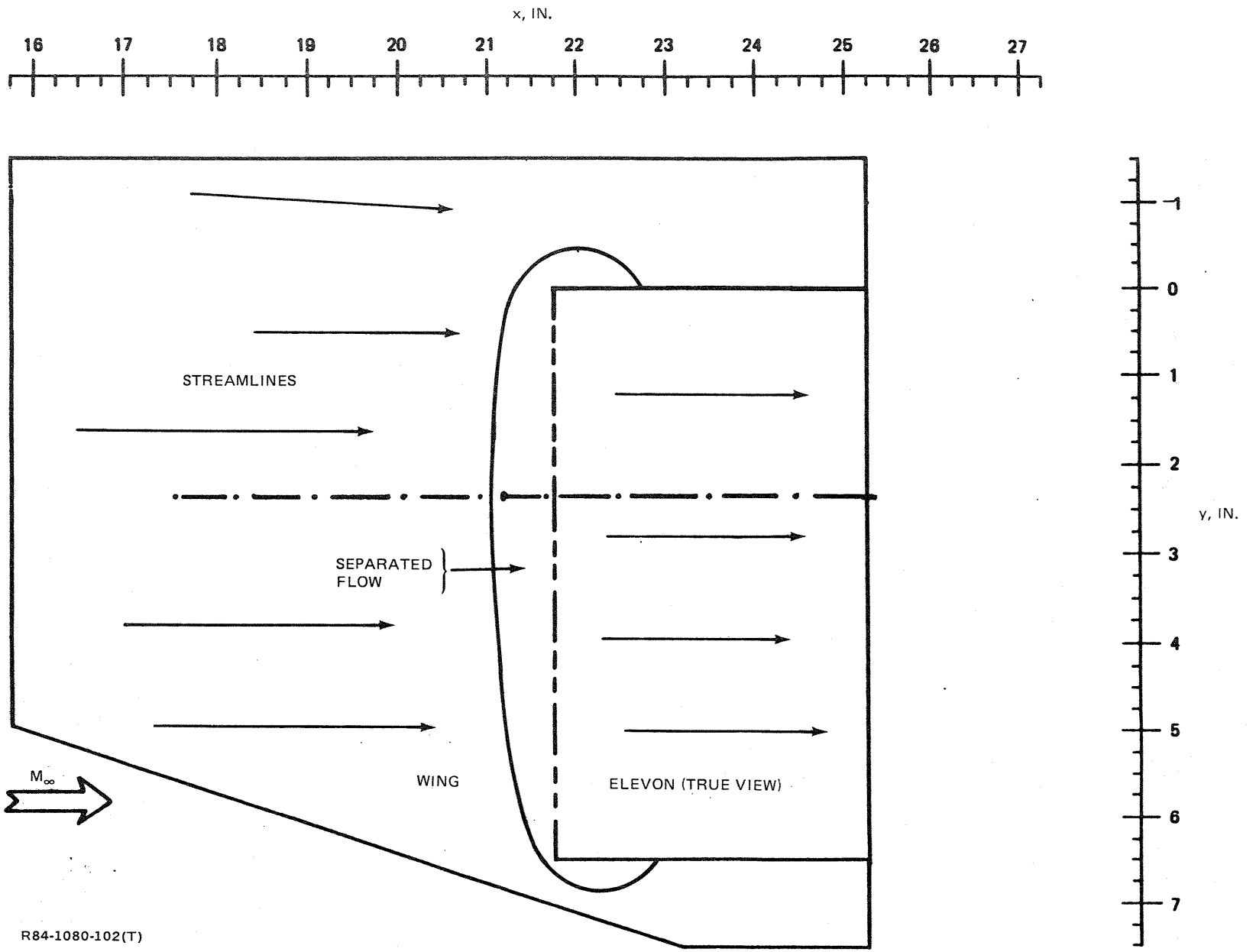

Fig. 102 30° Short Elevon — Oil Flow Pattern, Unswept Wing, No Center Body

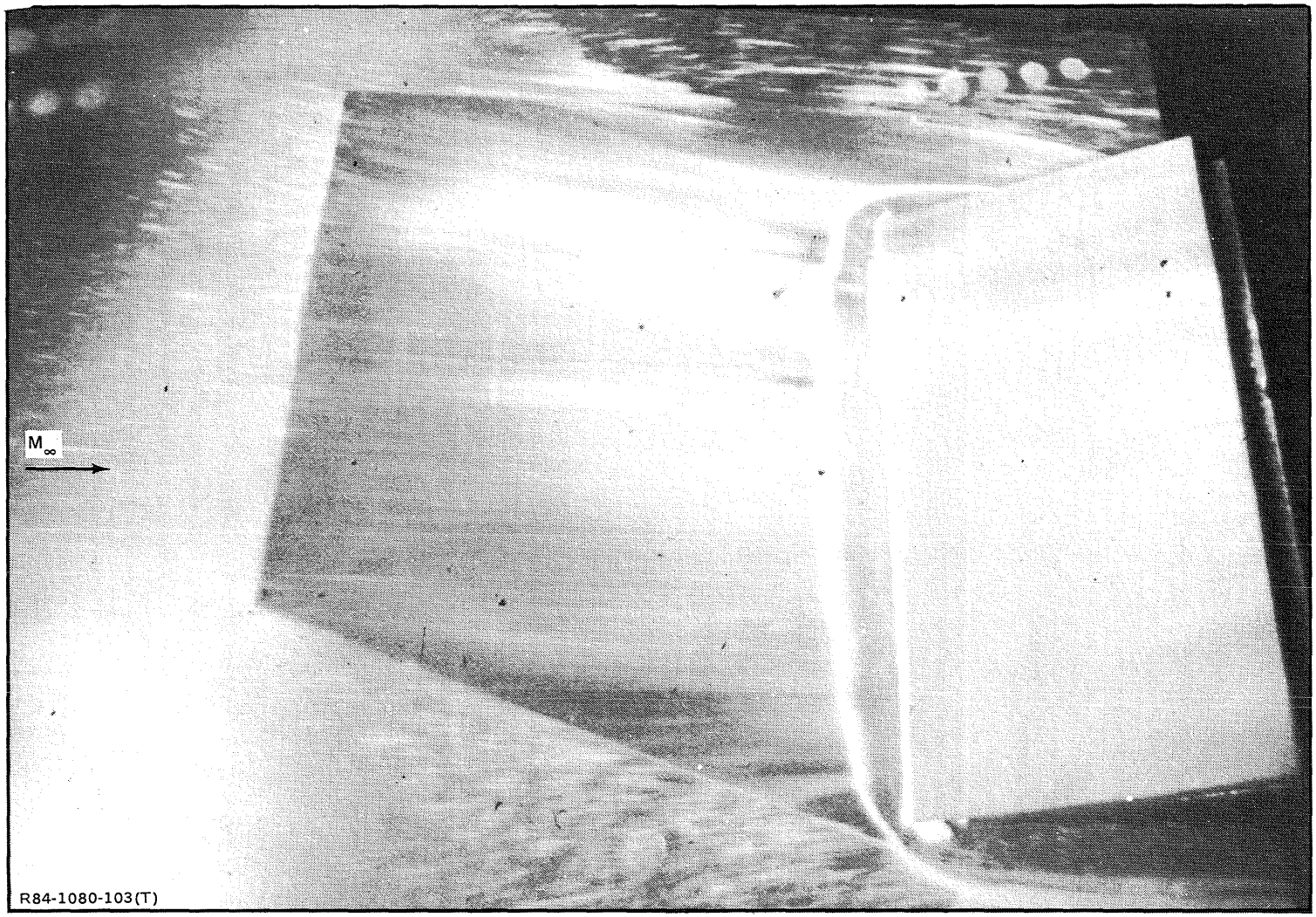

Fig. 103 30° Short Elevon – Photograph of Oil Flow Pattern, Unswept Wing, No Center Body

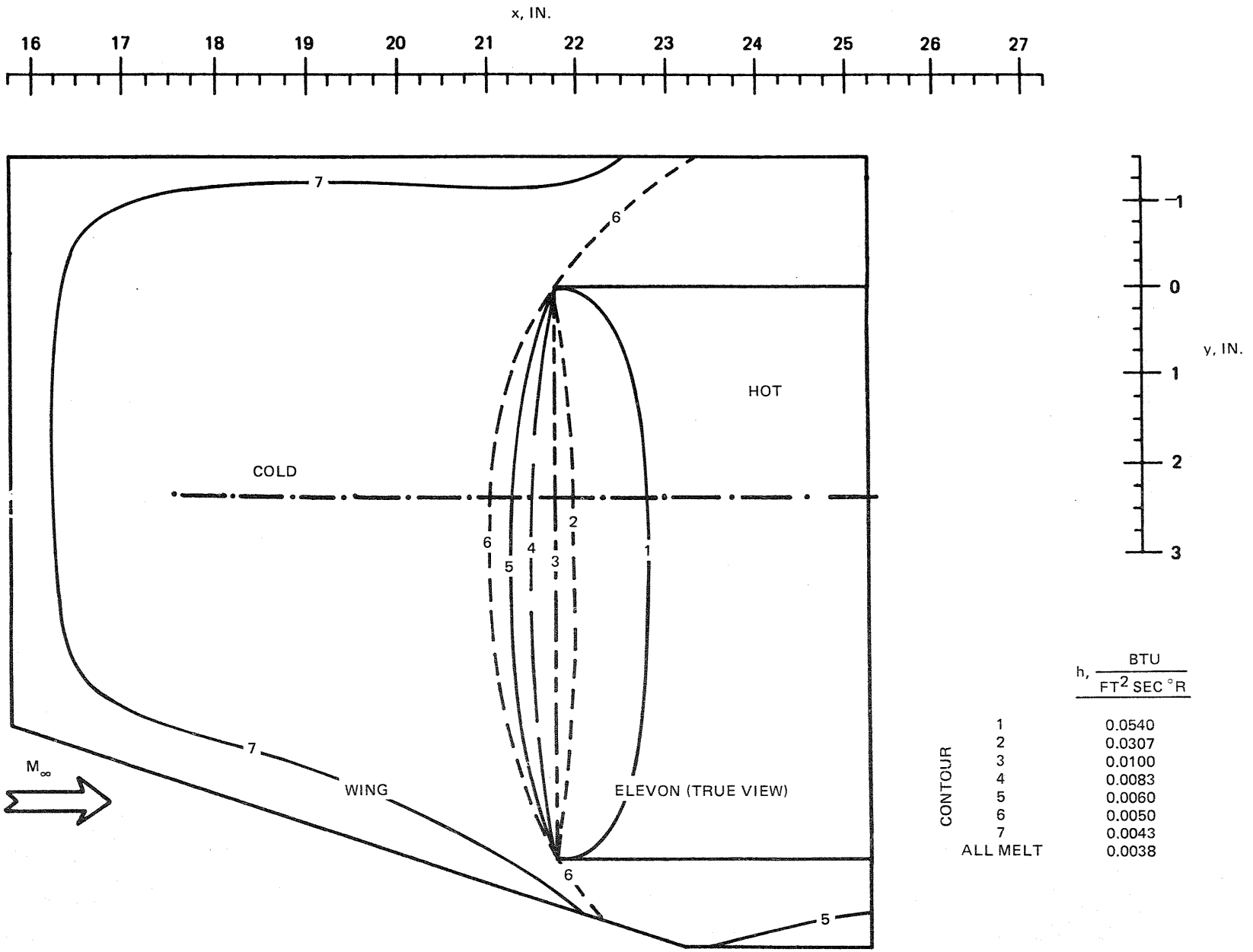

Fig. 104 30° Short Elevon — Phase Change Results, Unswept Wing, No Center Body

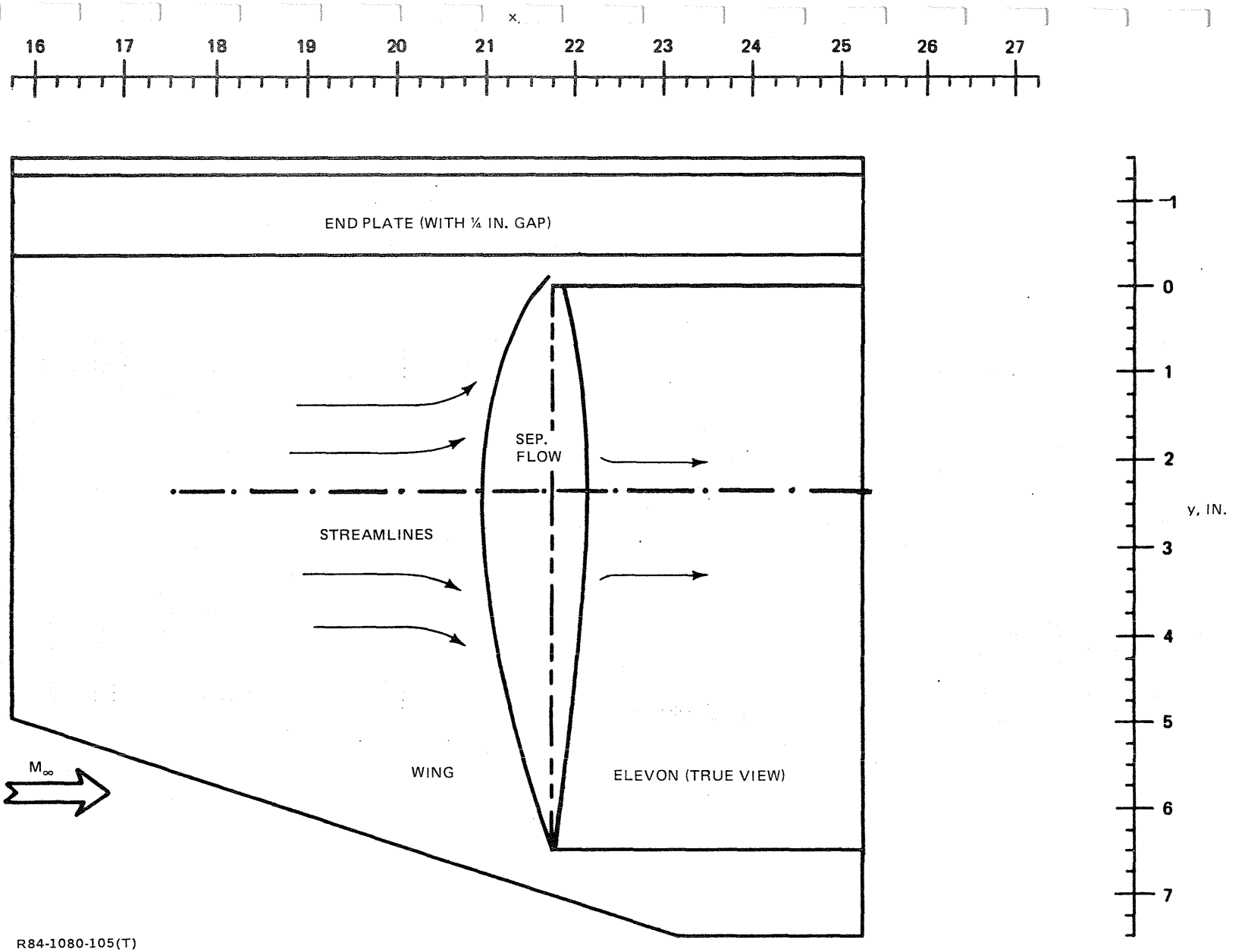

R84-1080-105(T)

Fig. 105 30° Short Elevon – Oil Flow Pattern, 70° Swept Wing, End Plate ¼ in. Away from Elevon

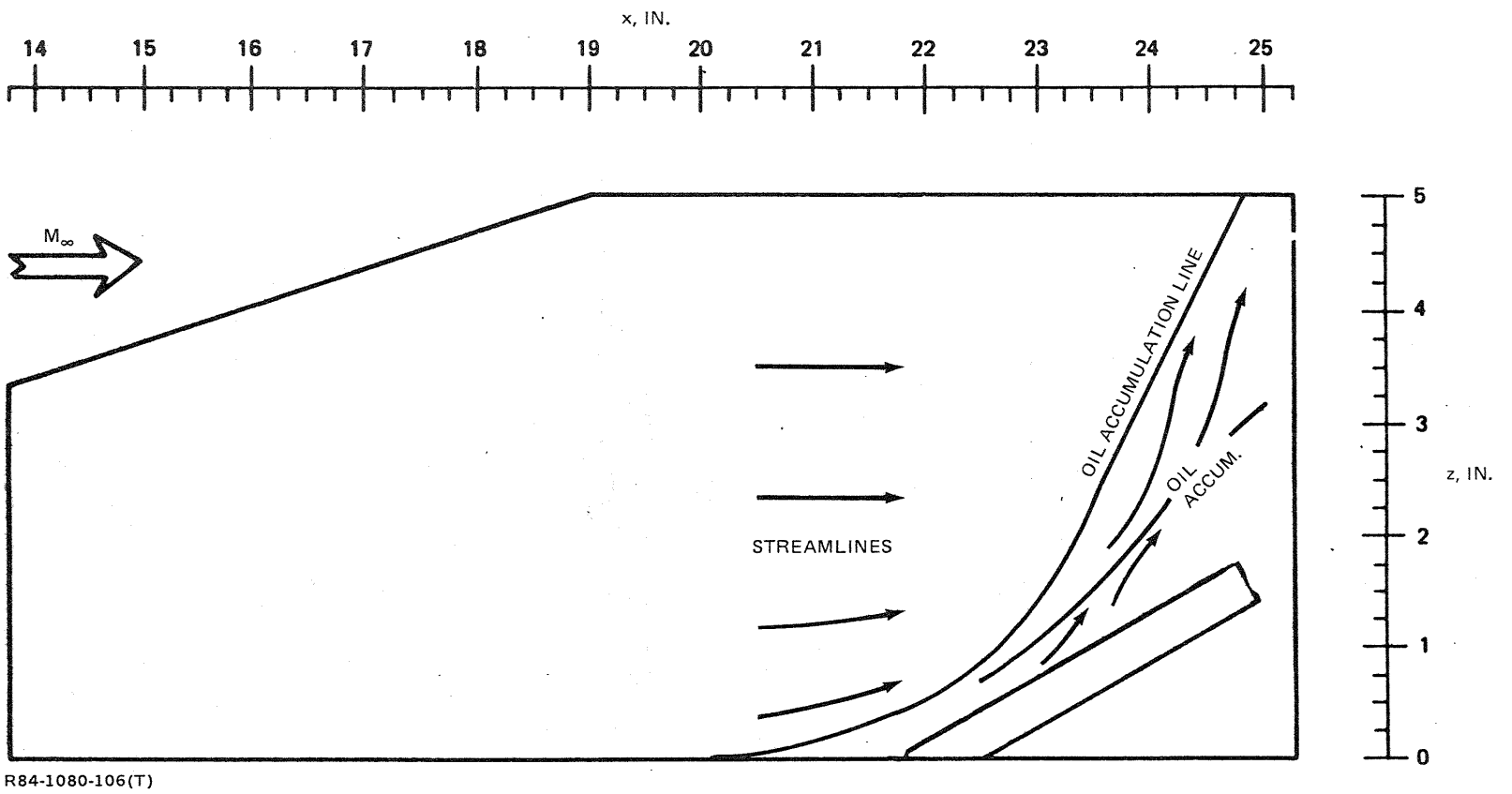

Fig. 106 30° Short Elevon — Oil Flow Pattern, End Plate Positioned ¼ in. Away from Elevon, 70° Swept Wing

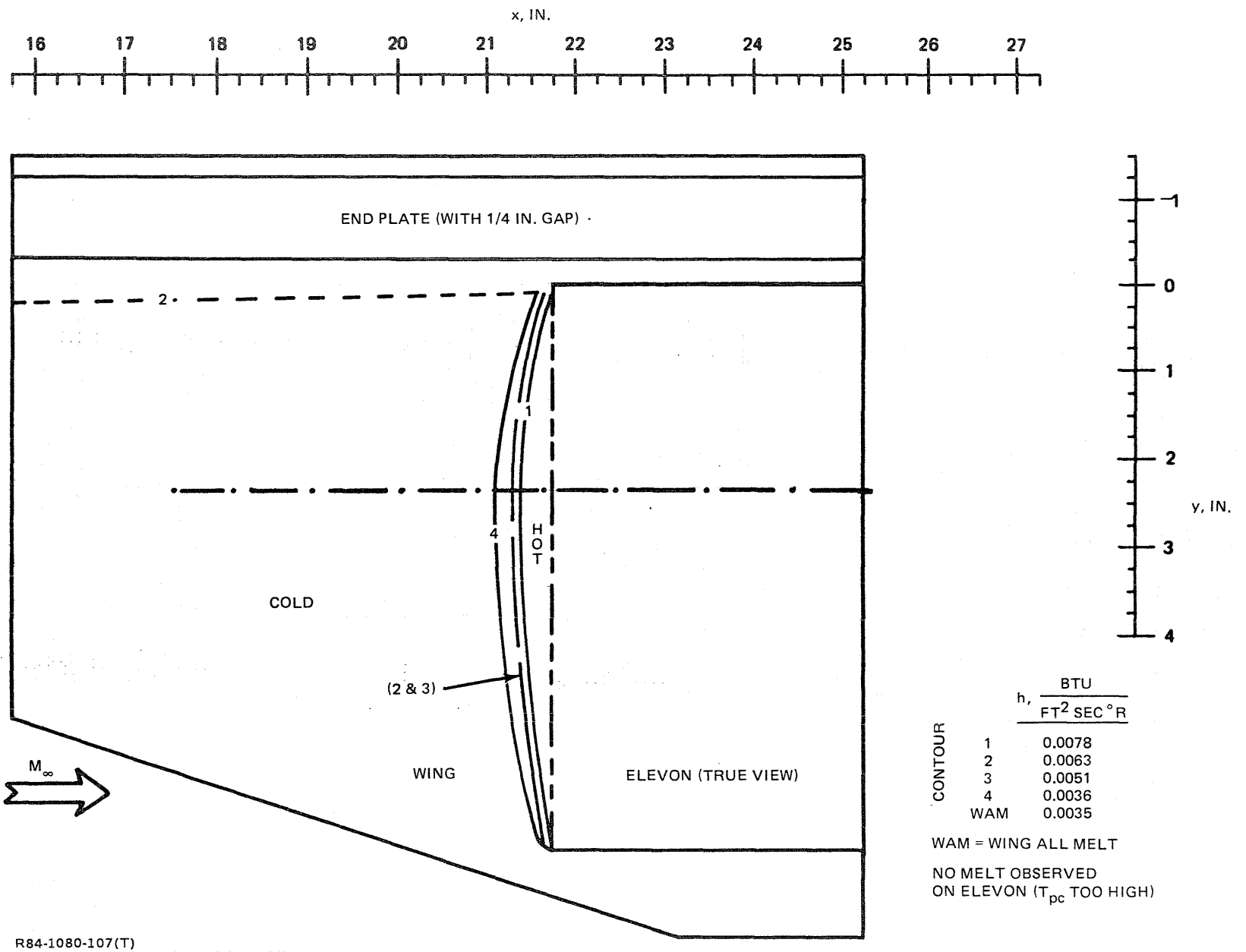

R84-1080-107(T)

Fig. 107 30° Short Elevon — Phase Change Results, 70° Swept Wing, End Plate Positioned ¼ in. Away from Elevon

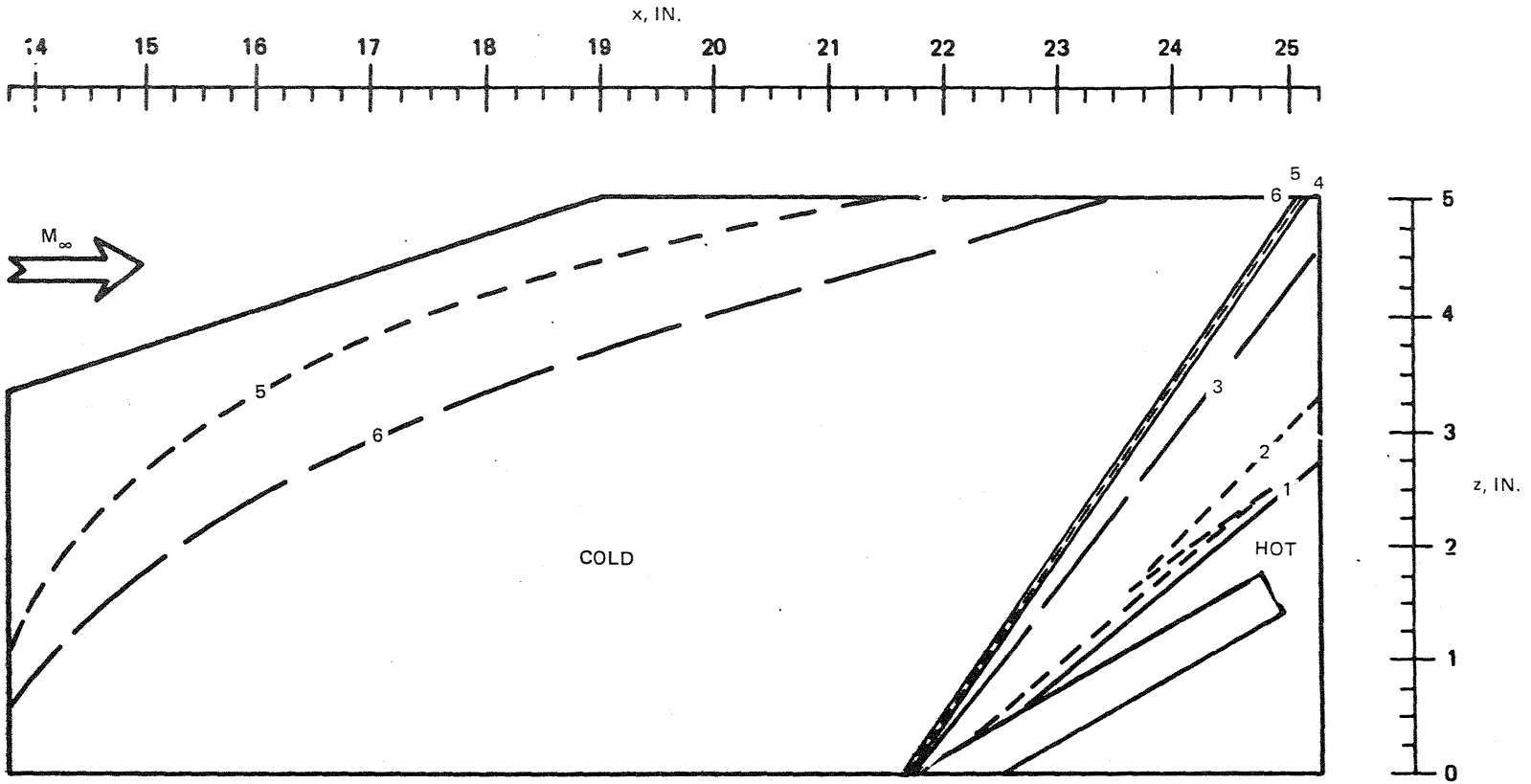

h, $\frac{BTU}{FT^2\ SEC\ °R}$	
CONTOUR 1	0.0195
2	0.0087
3	0.0062
4	0.0047
5	0.0037
6	0.0036
ALL MELT	0.0035

R84-1080-108(T)

Fig. 108 30° Short Elevon – Phase Change Results, End Plate ¼ in. Away from Elevon, 70° Swept Wing

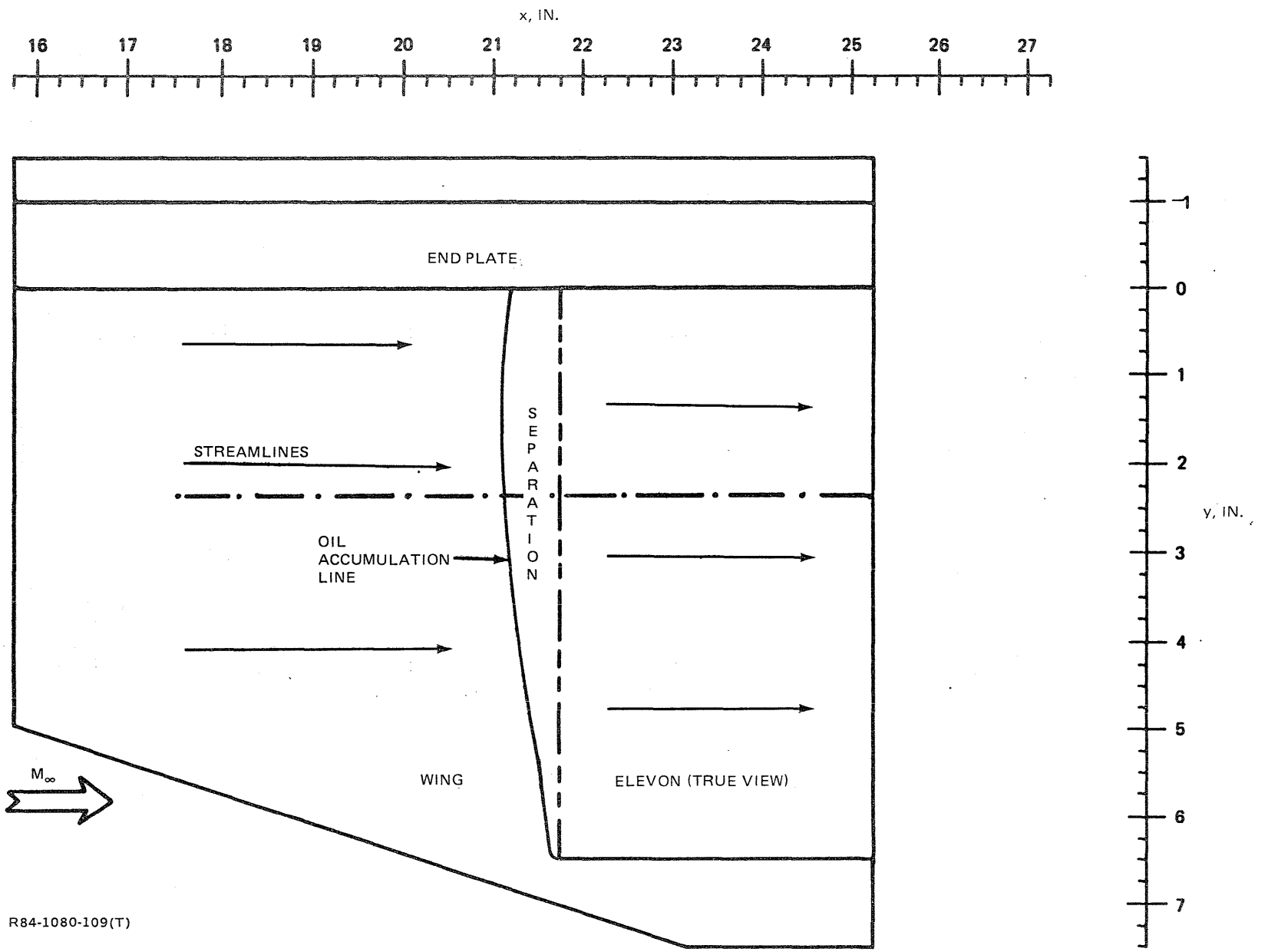

Fig. 109 30° Short Elevon – Oil Flow Pattern, 70° Swept Wing, End Plate

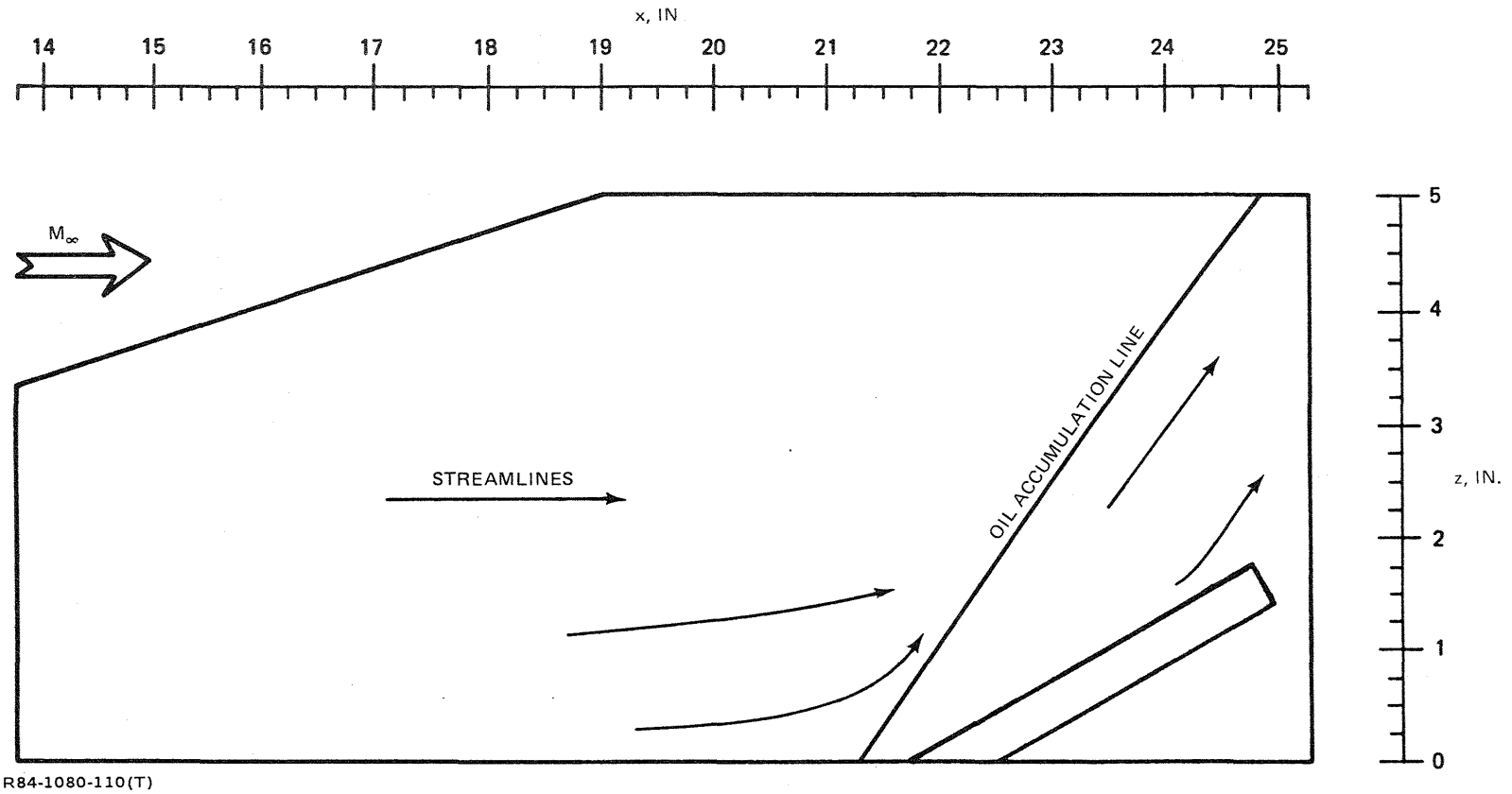

Fig. 110 30° Short Elevon — Oil Flow Pattern, End Plate, 70° Swept Wing

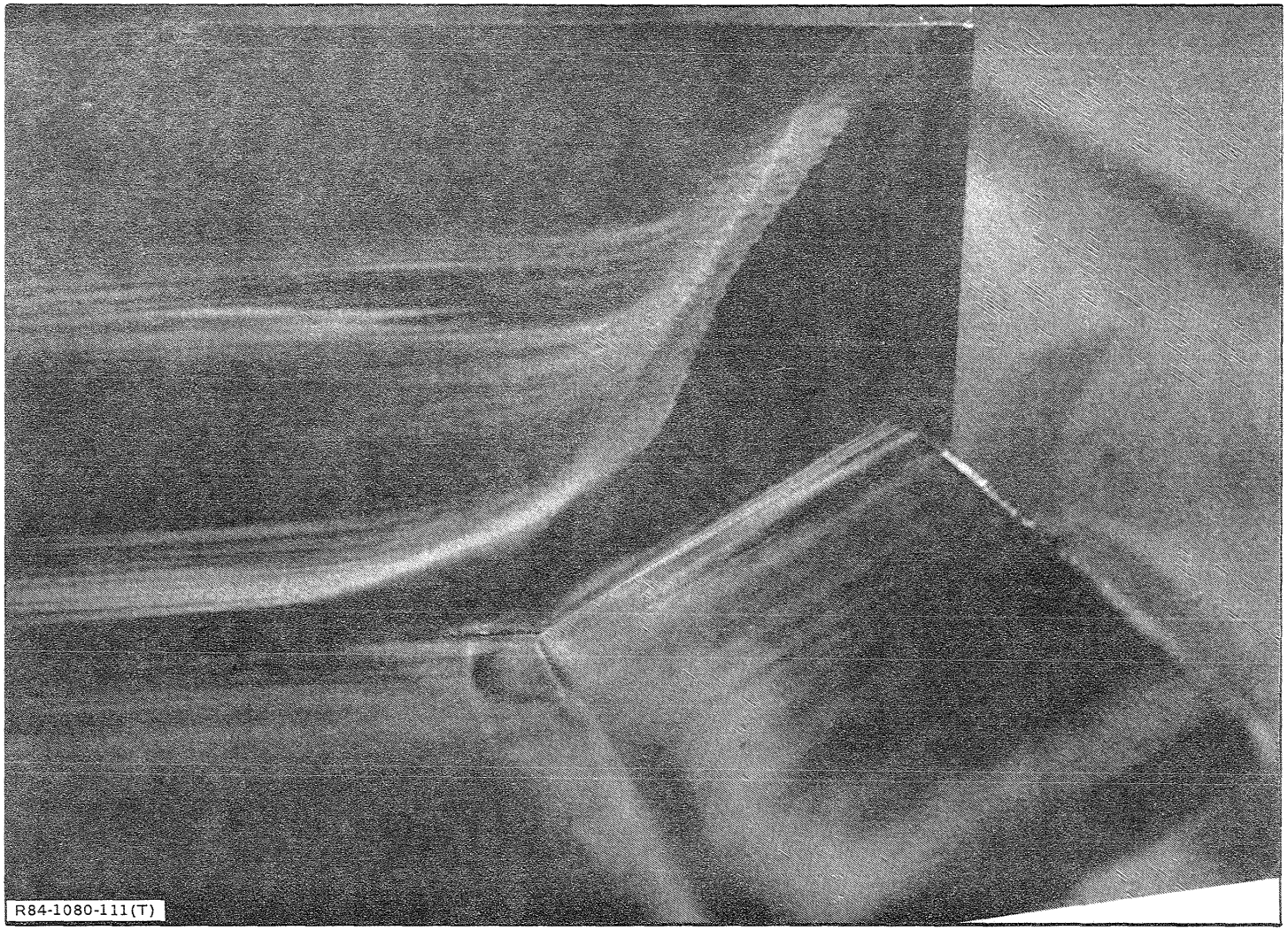

Fig. 111 30° Short Elevon – Photograph of Oil Flow Pattern, 70° Swept Wing, End Plate

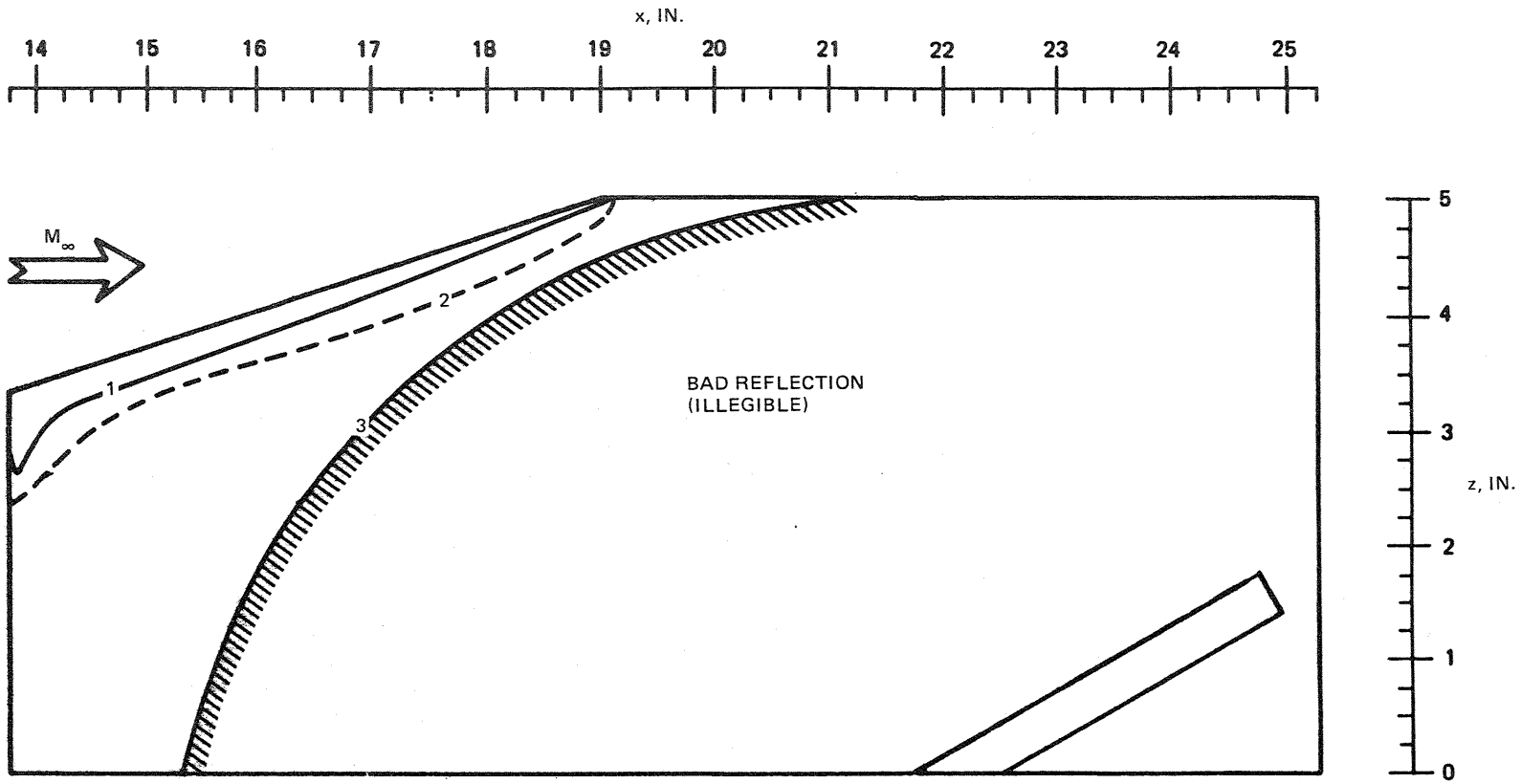

CONTOUR	h, BTU/FT^2 SEC °R
1	0.0053
2	0.0049
3	0.0048

R84-1080-112(T)

Fig. 112 30° Short Elevon – Phase Change Results for Forward Portion of End Plate, 70° Swept Wing

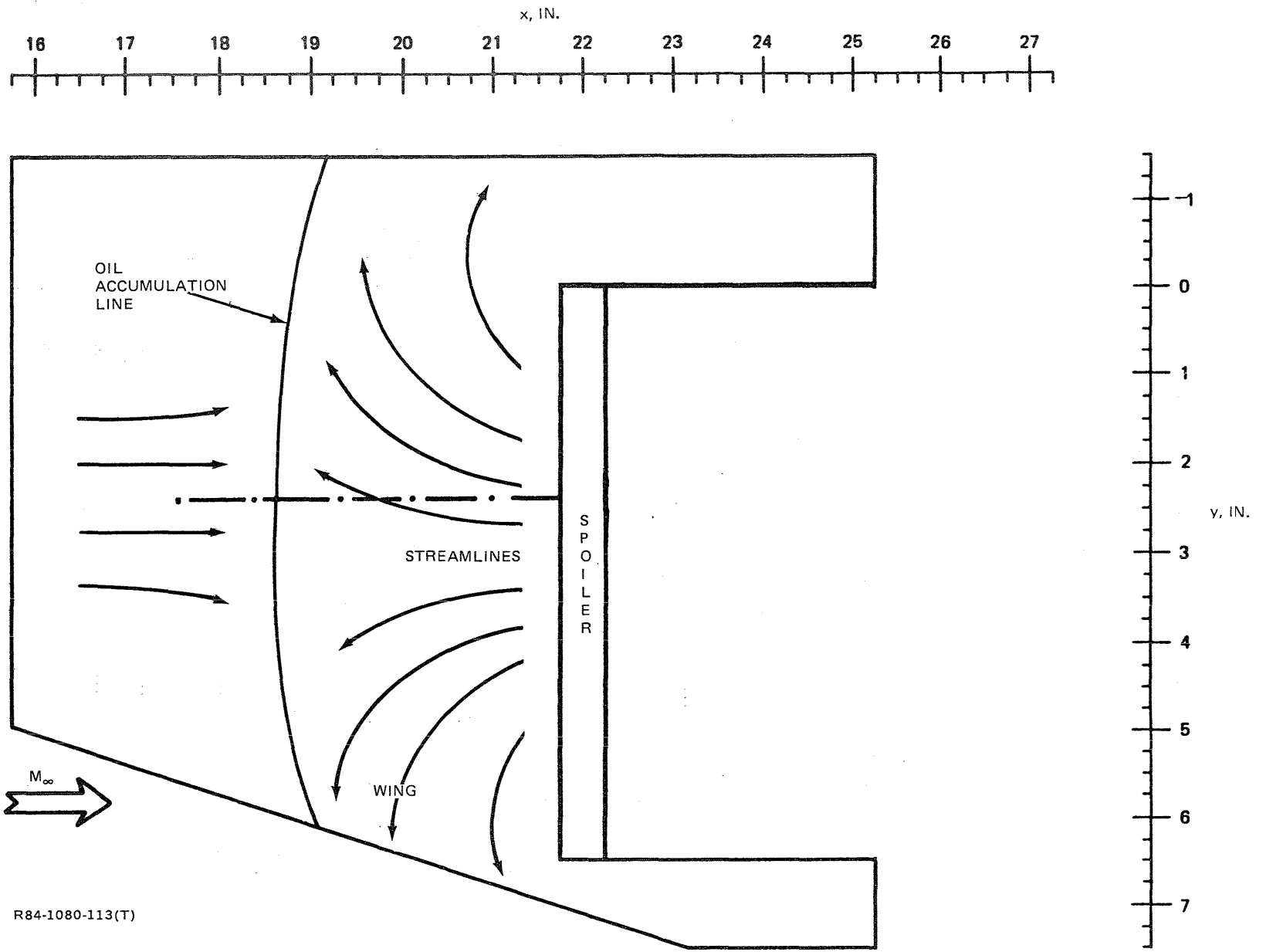

Fig. 113 Low Spoiler – Oil Flow Pattern, Unswept Wing, No Center Body

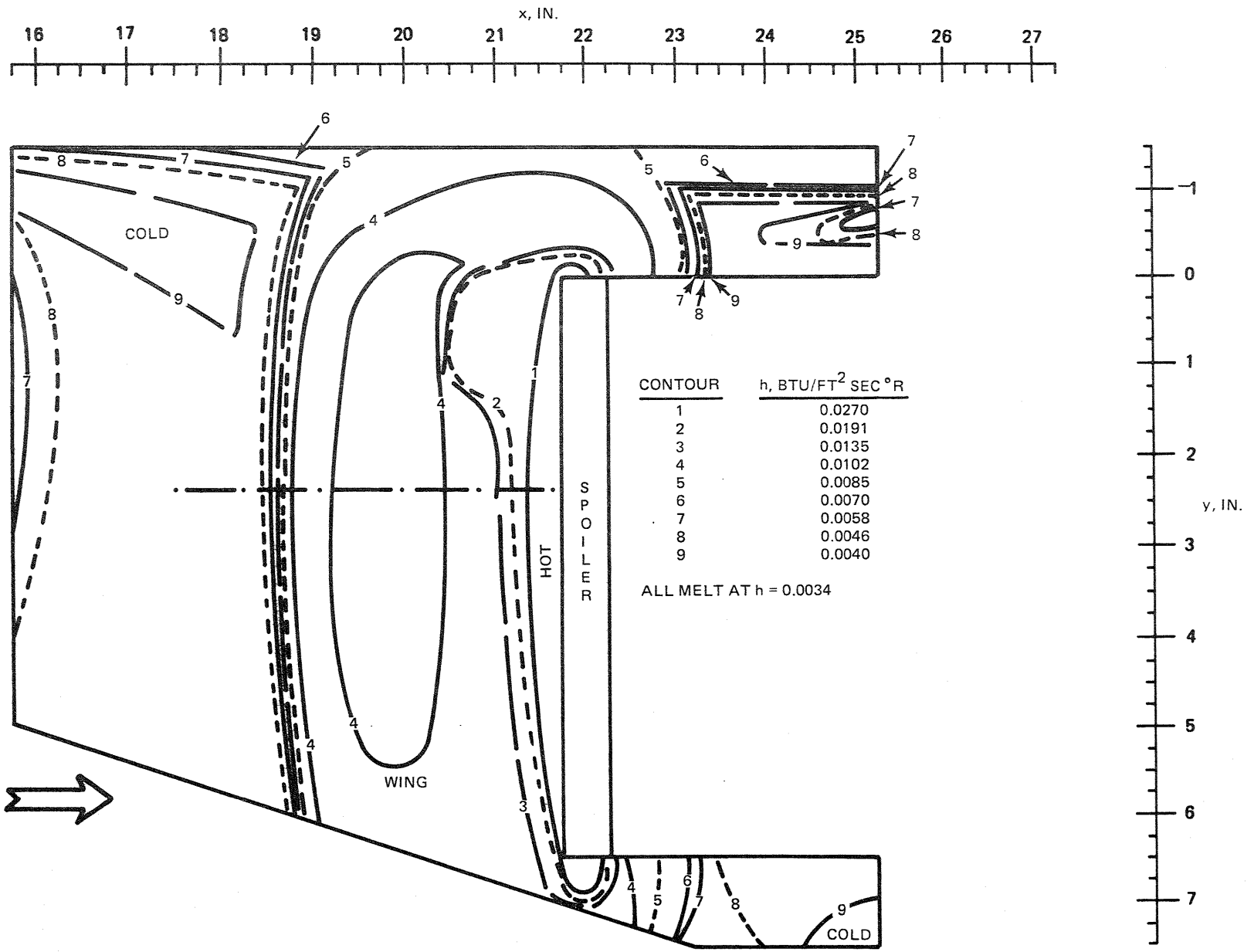

R84-1080-114(T)

Fig. 114 Low Spoiler — Phase Change Results, Unswept Wing, No Center Body

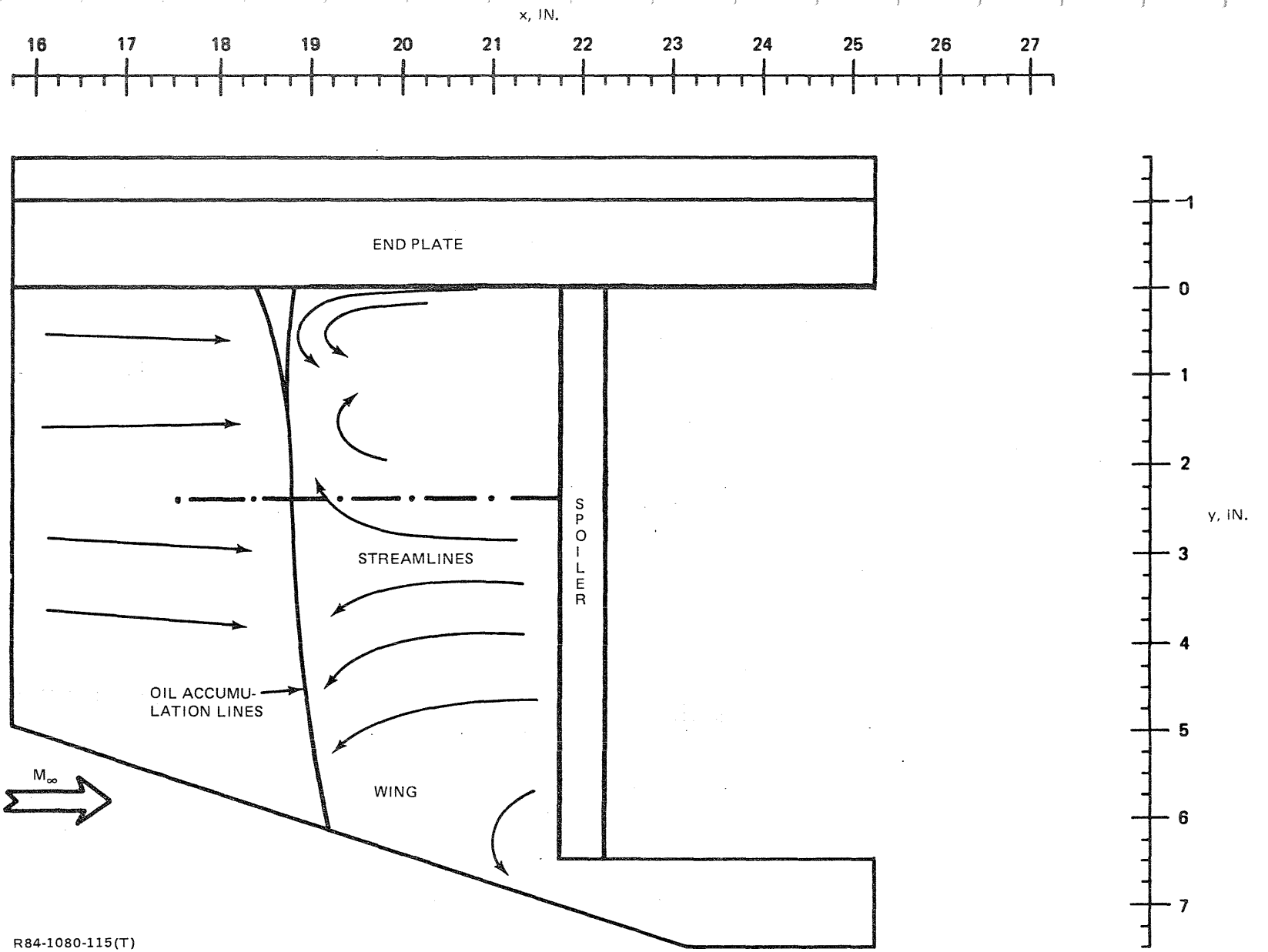

Fig. 115 Low Spoiler — Oil Flow Pattern, Unswept Wing, End Plate

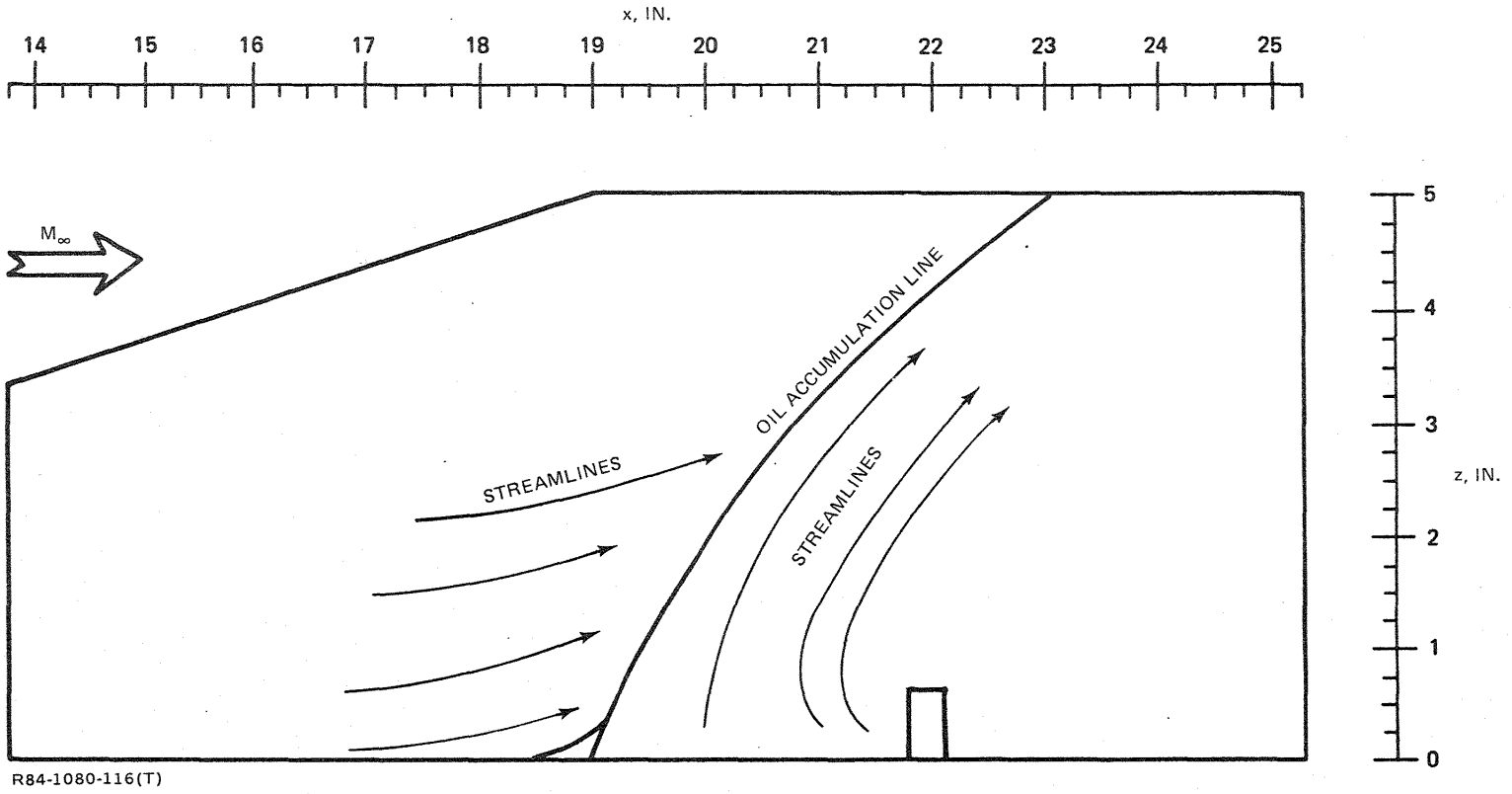

Fig. 116 Low Spoiler – Oil Flow Pattern, End Plate, Unswept Wing

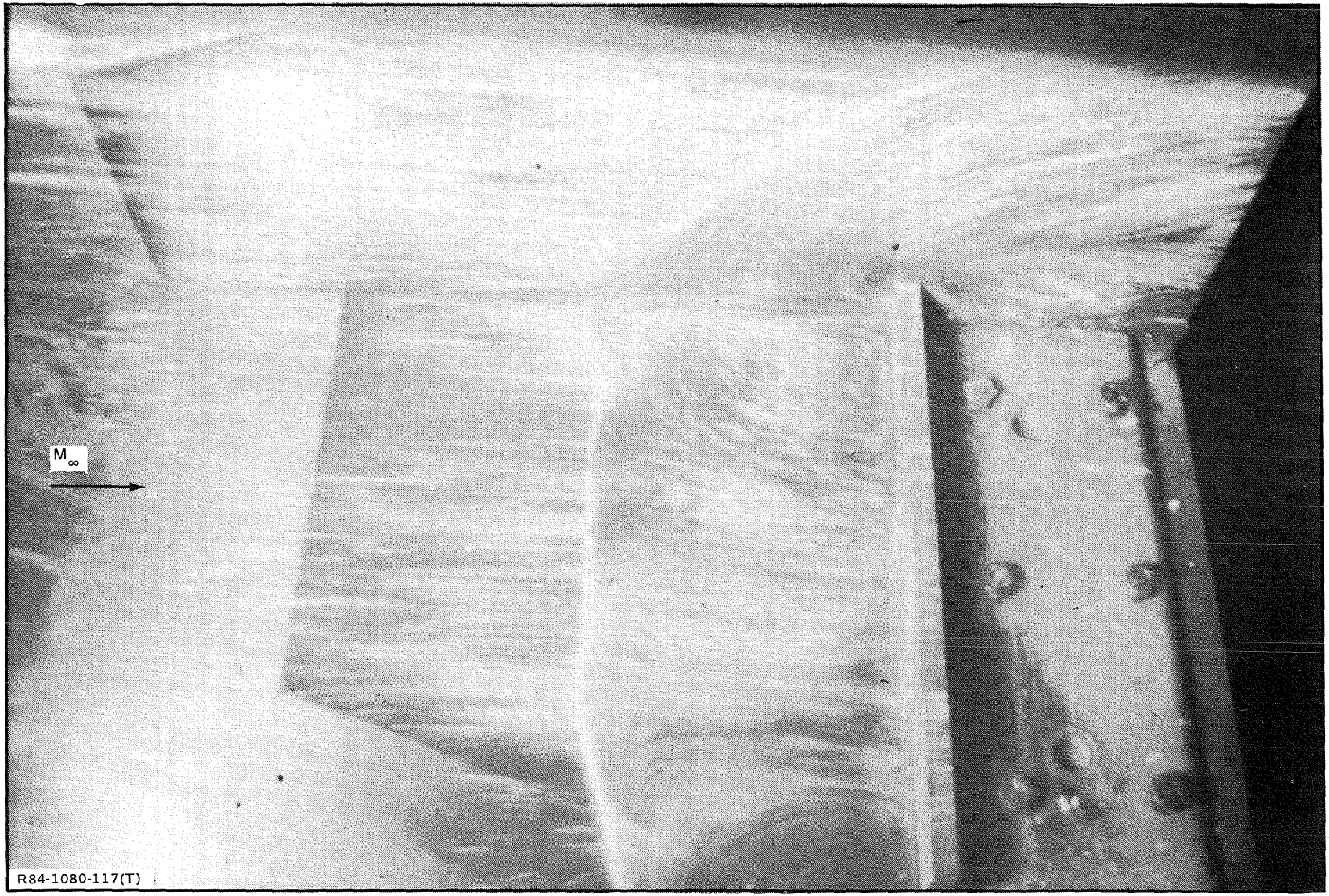

Fig. 117 Low Spoiler — Frame from Oil Flow Run Motion Picture, Unswept Wing, End Plate

Fig. 118 Low Spoiler – Photograph of Oil Flow Pattern on End Plate Taken After Tunnel Run 119, Unswept Wing

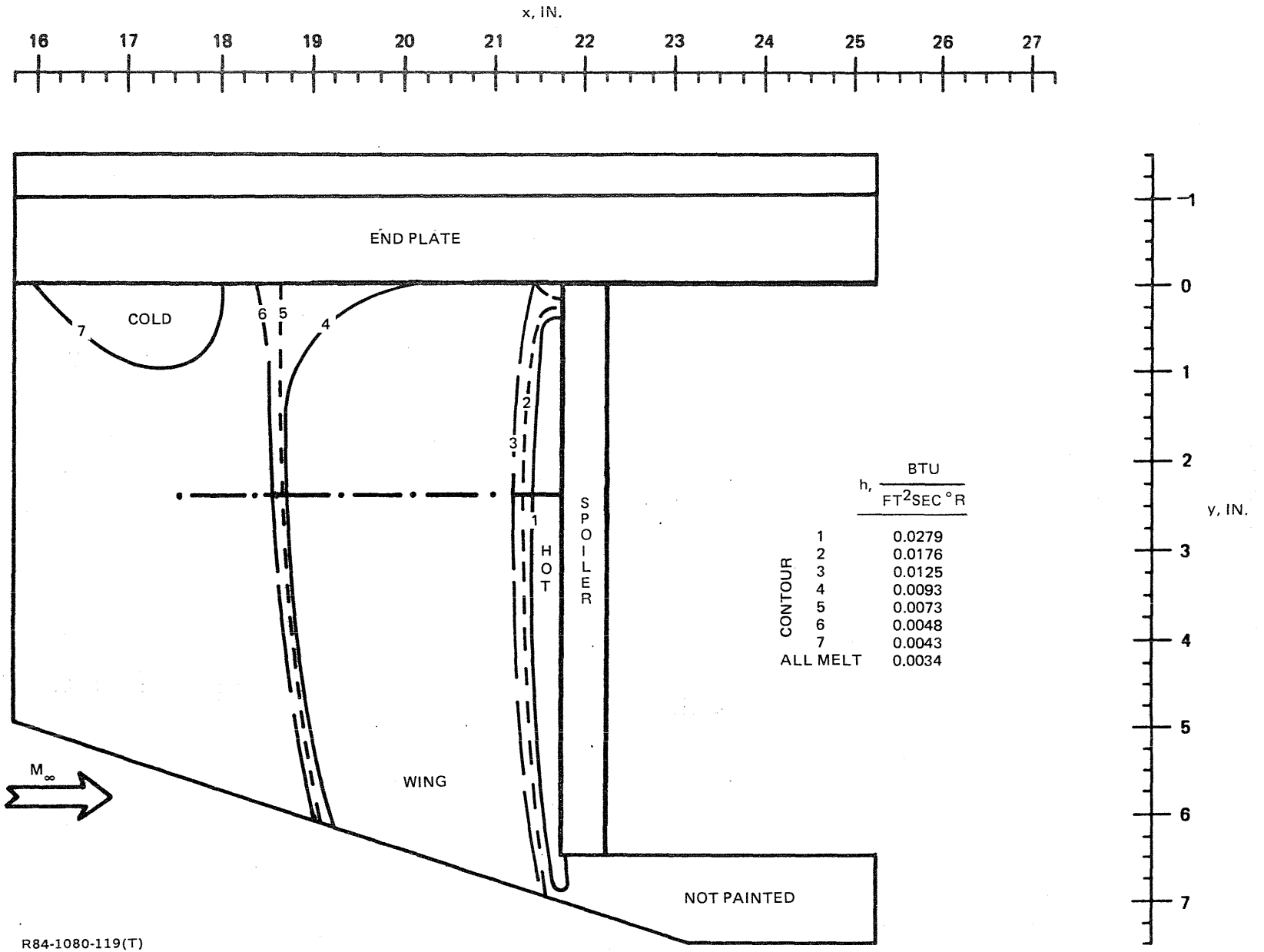

Fig. 119 Low Spoiler — Phase Change Results, Unswept Wing, End Plate

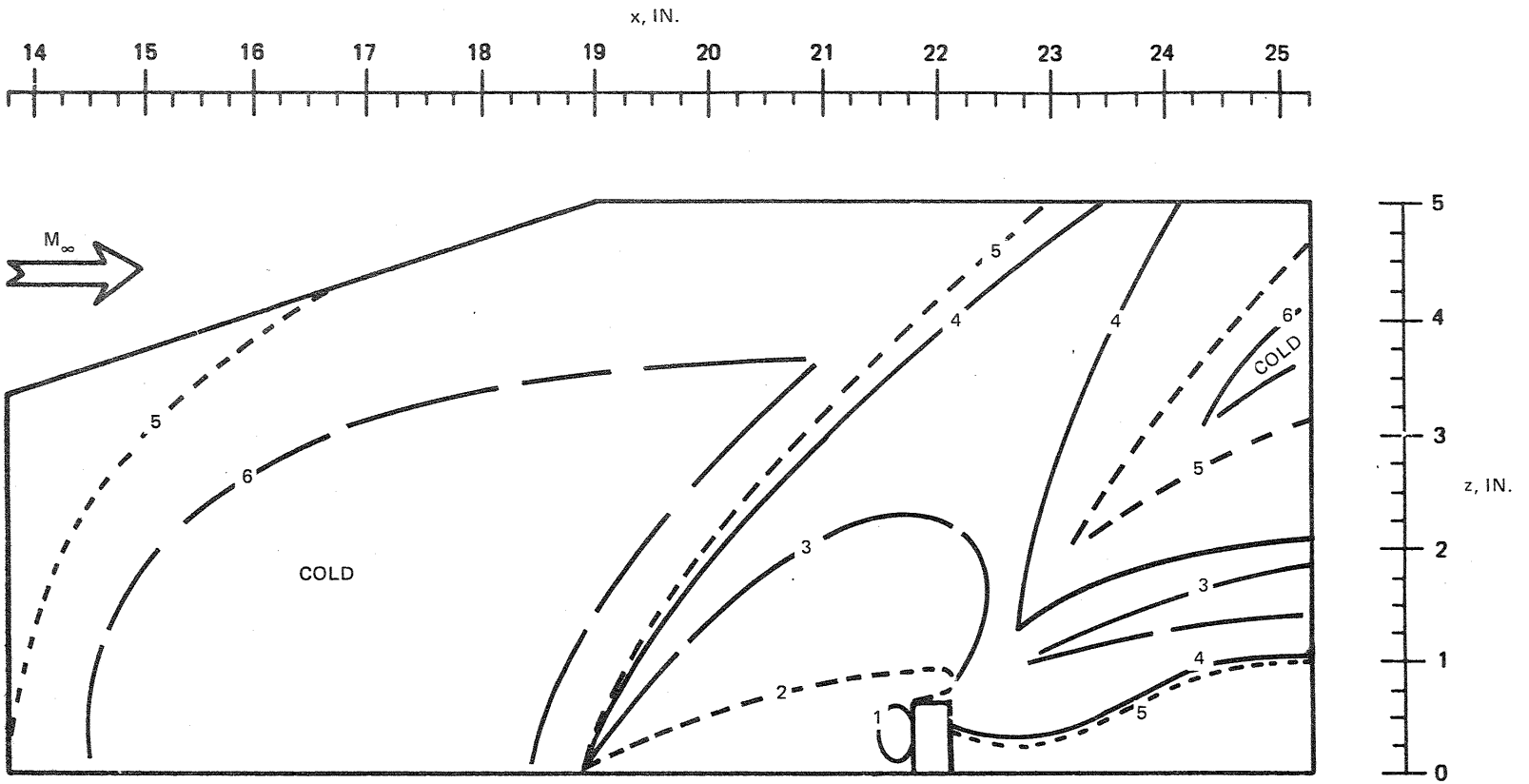

CONTOUR	h, BTU/FT^2 SEC °R
1	0.0176
2	0.0093
3	0.0073
4	0.0048
5	0.0043
6	0.0039
ALL MELT	0.0034

R84-1080-120(T)

Fig. 120 Low Spoiler – Phase Change Results, End Plate, Unswept Wing

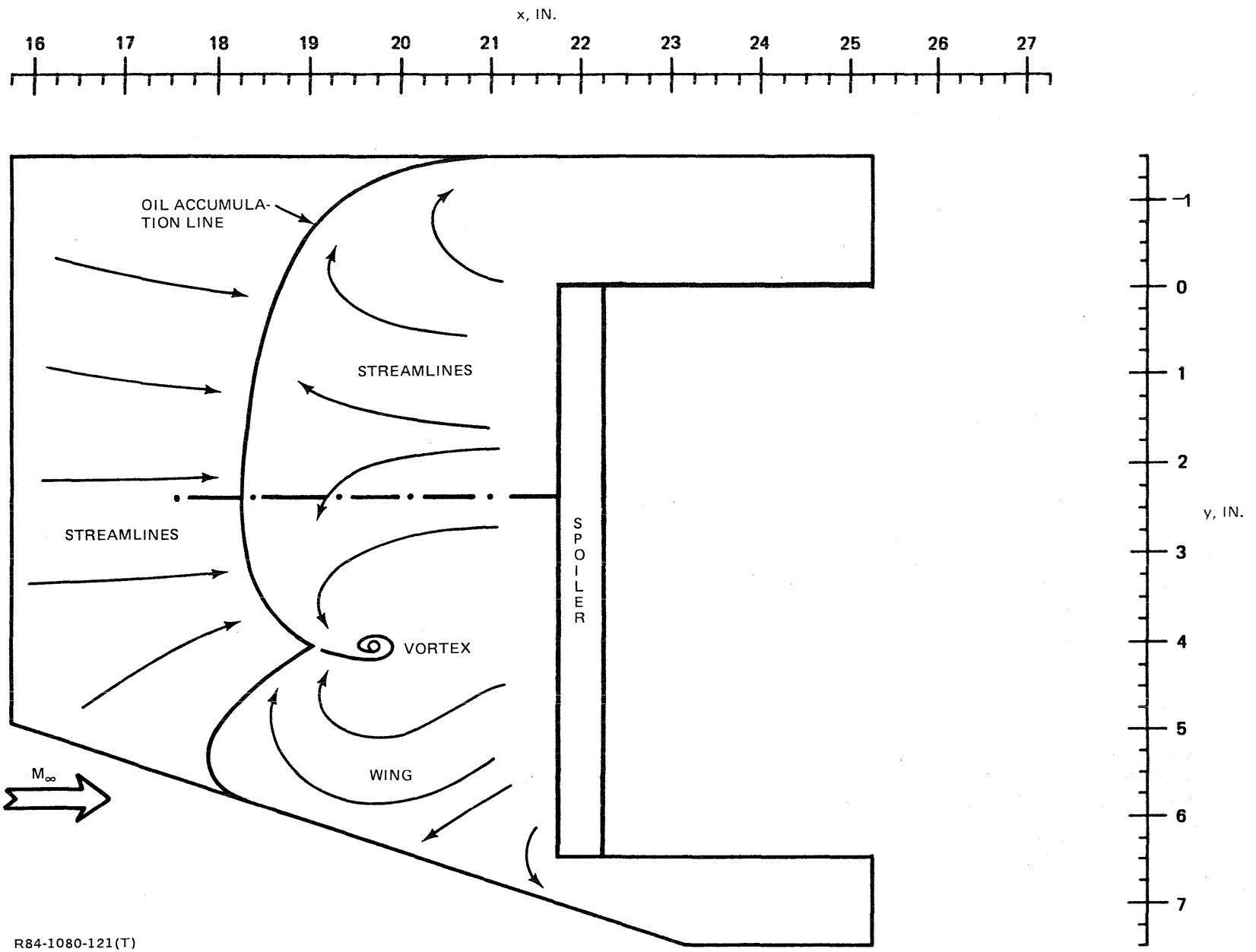

Fig. 121 Low Spoiler – Oil Flow Pattern, 70° Swept Wing, No Center Body

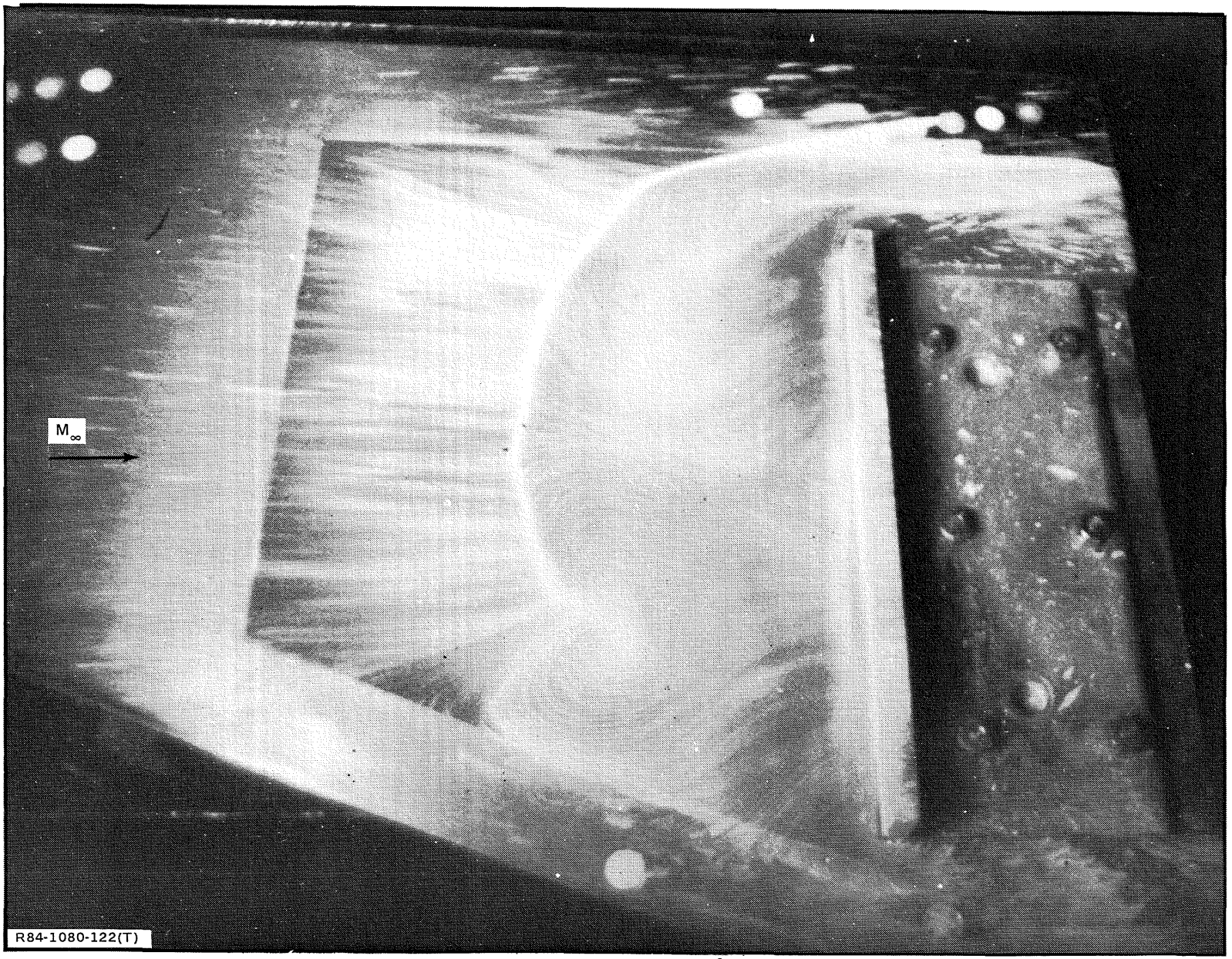

Fig. 122 Low Spoiler – Photograph of Oil Flow Pattern, 70° Swept Wing, No Center Body

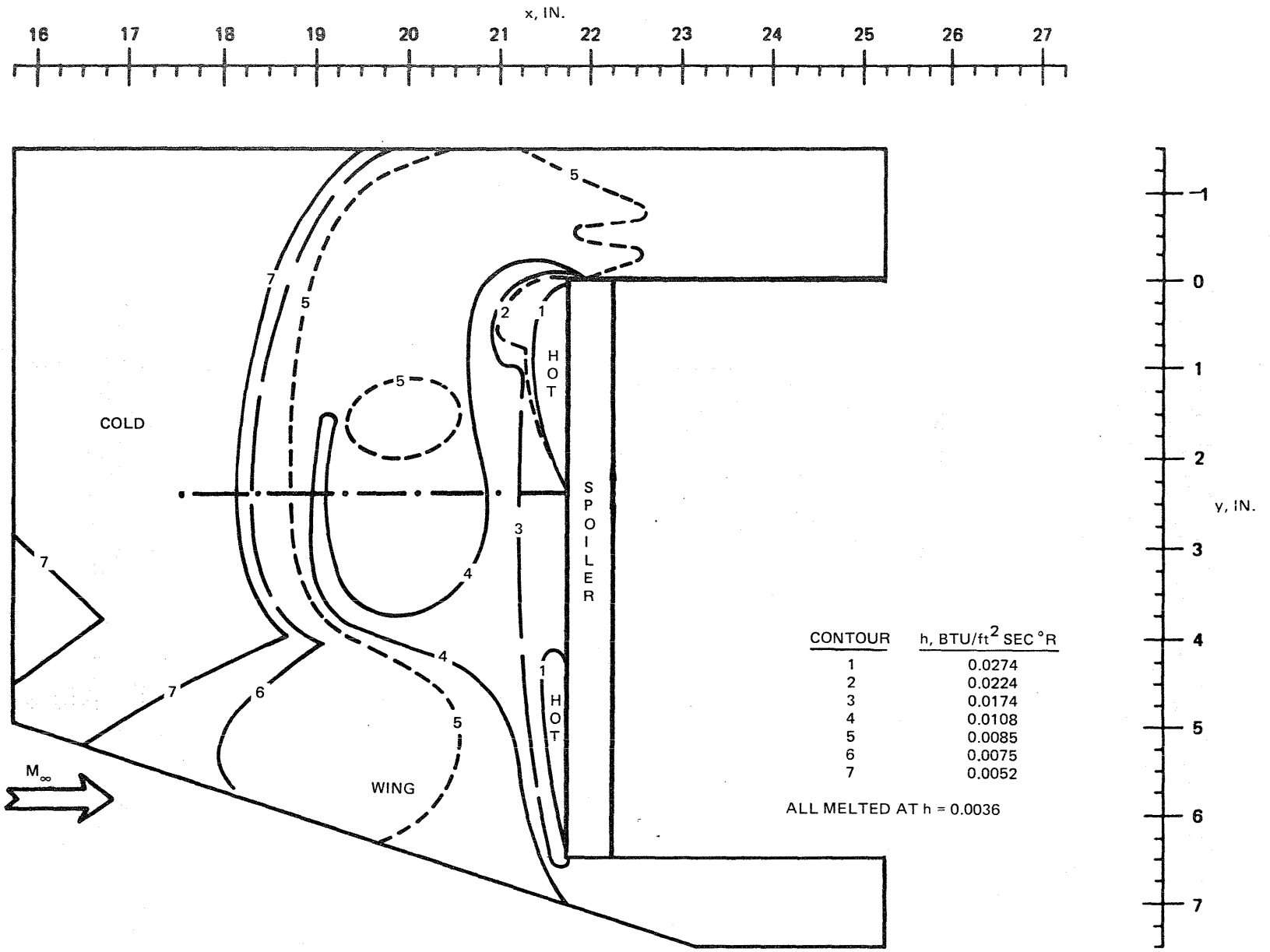

Fig. 123 Low Spoiler – Phase Change Results, 70° Swept Wing, No Center Body

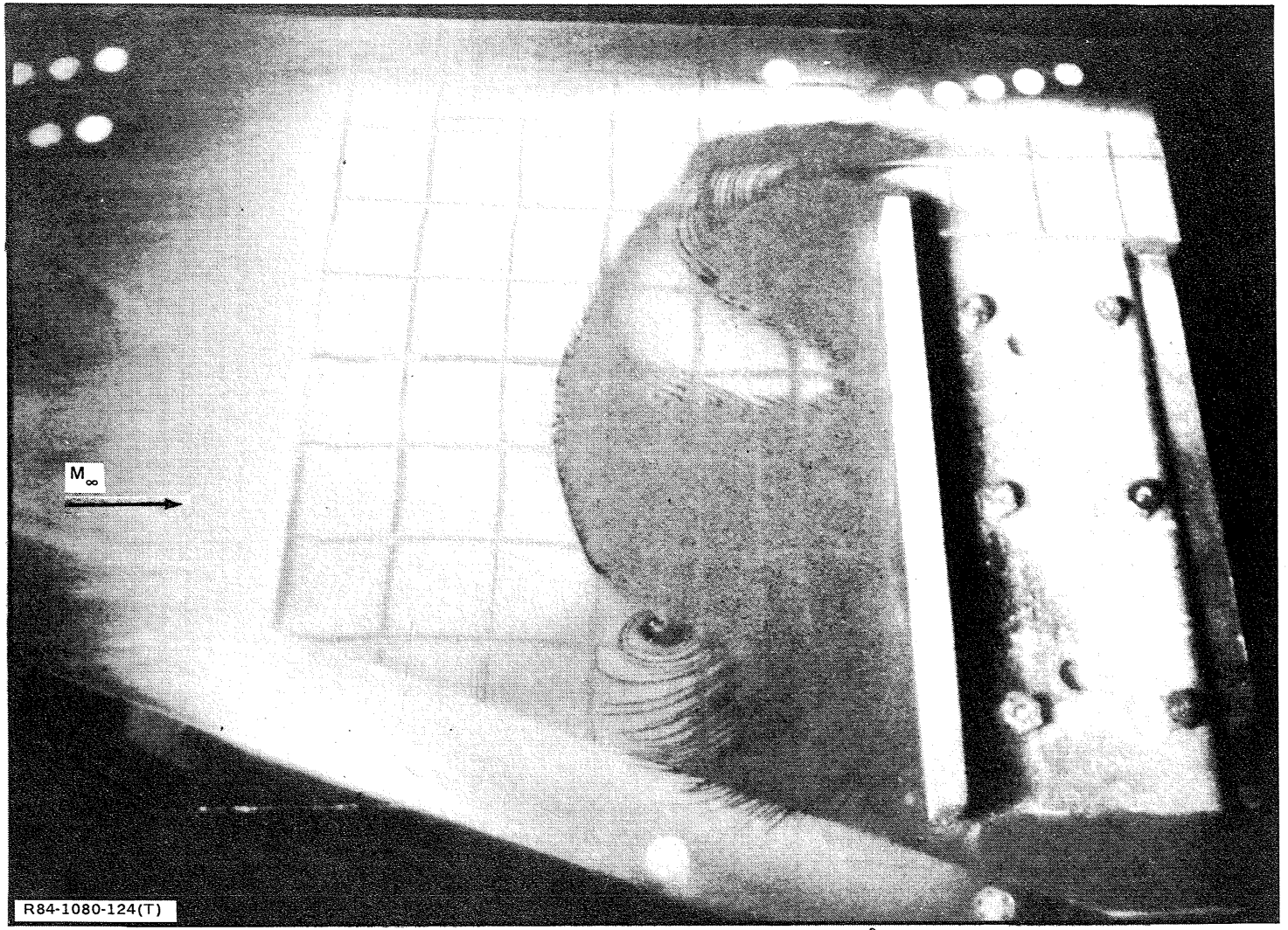

Fig. 124 Low Spoiler — Frame from Motion Picture of Phase Change Coating, 70° Swept Wing, No Center Body

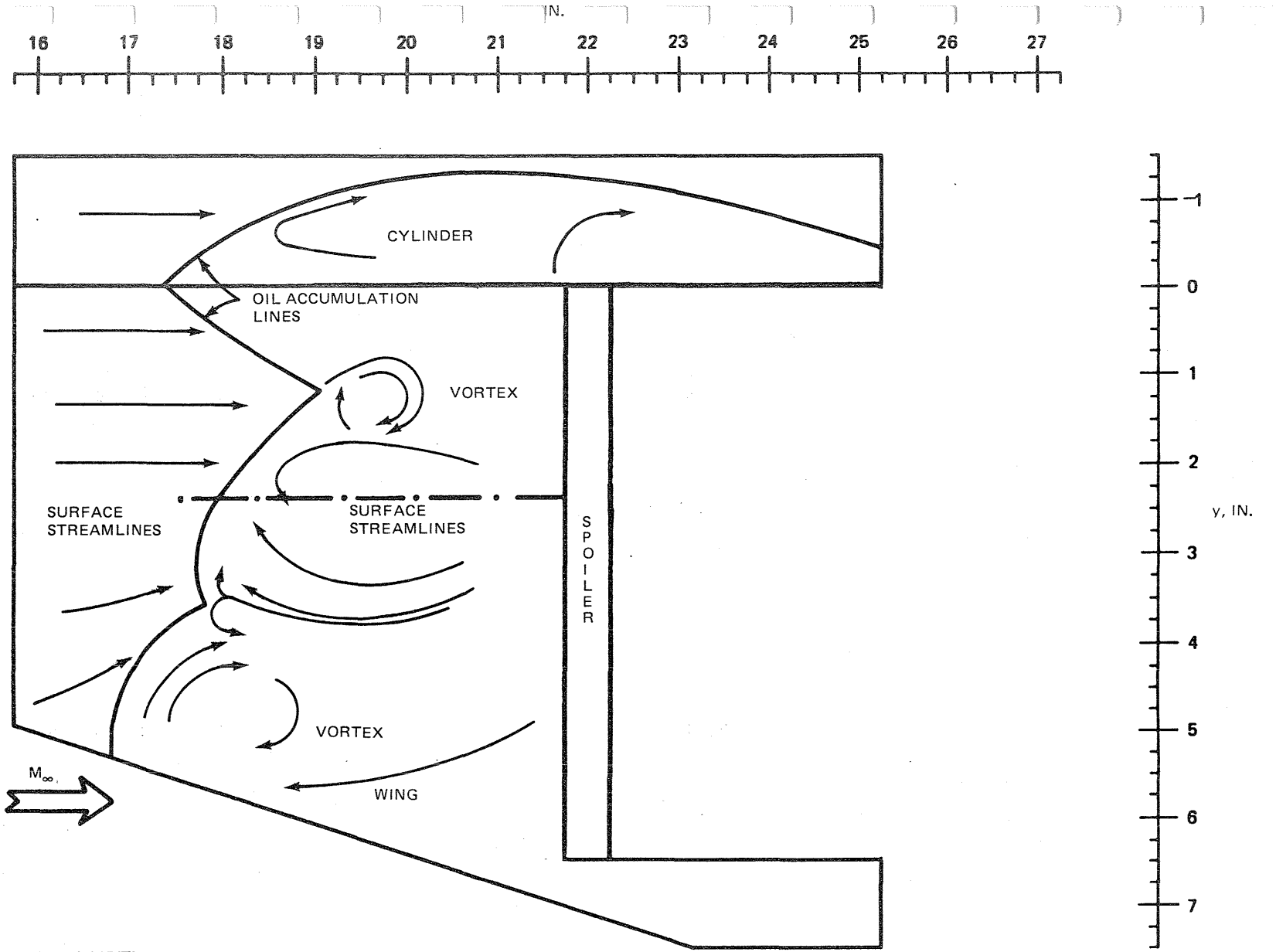

Fig. 125 Low Spoiler – Oil Flow Pattern, 70° Swept Wing, Cylindrical Center Body

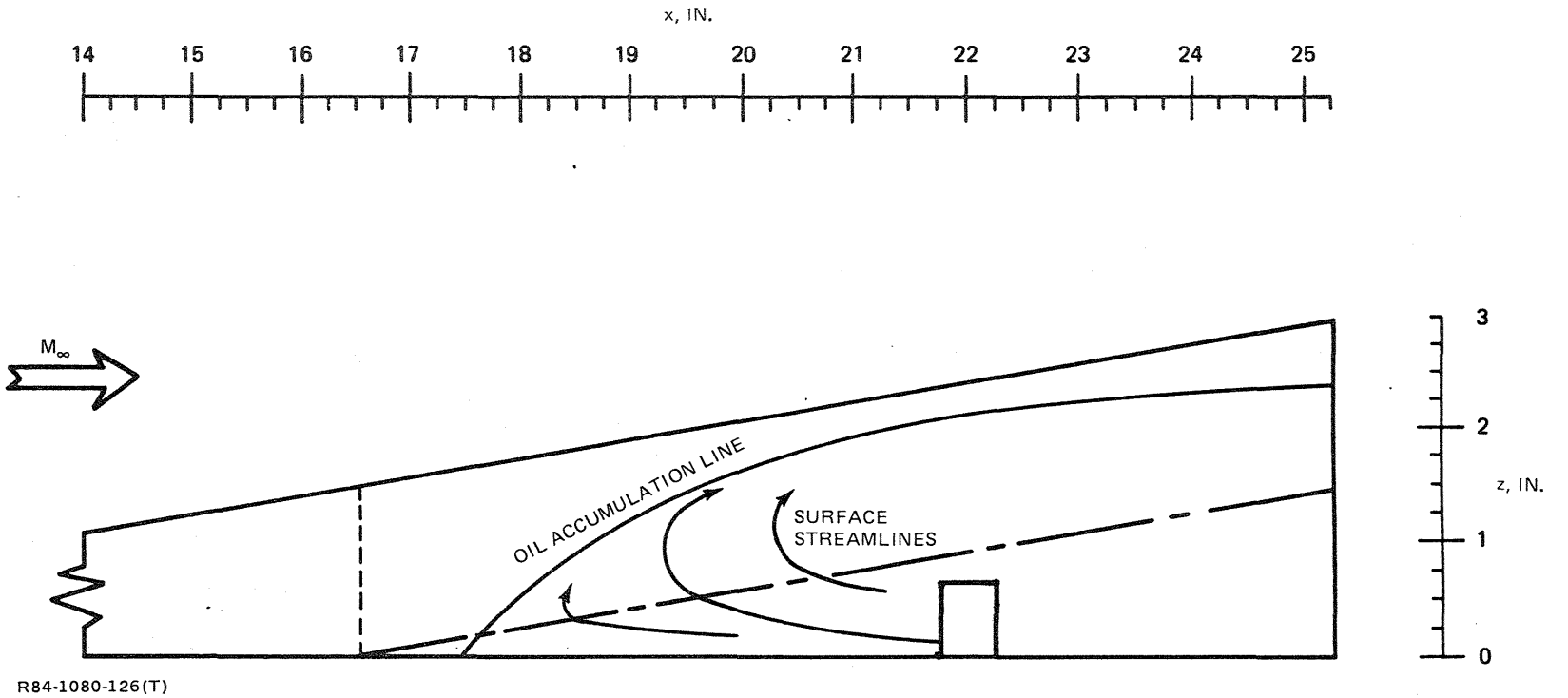

Fig. 126 Low Spoiler – Oil Flow Pattern, Cylindrical Center Body, 70° Swept Wing

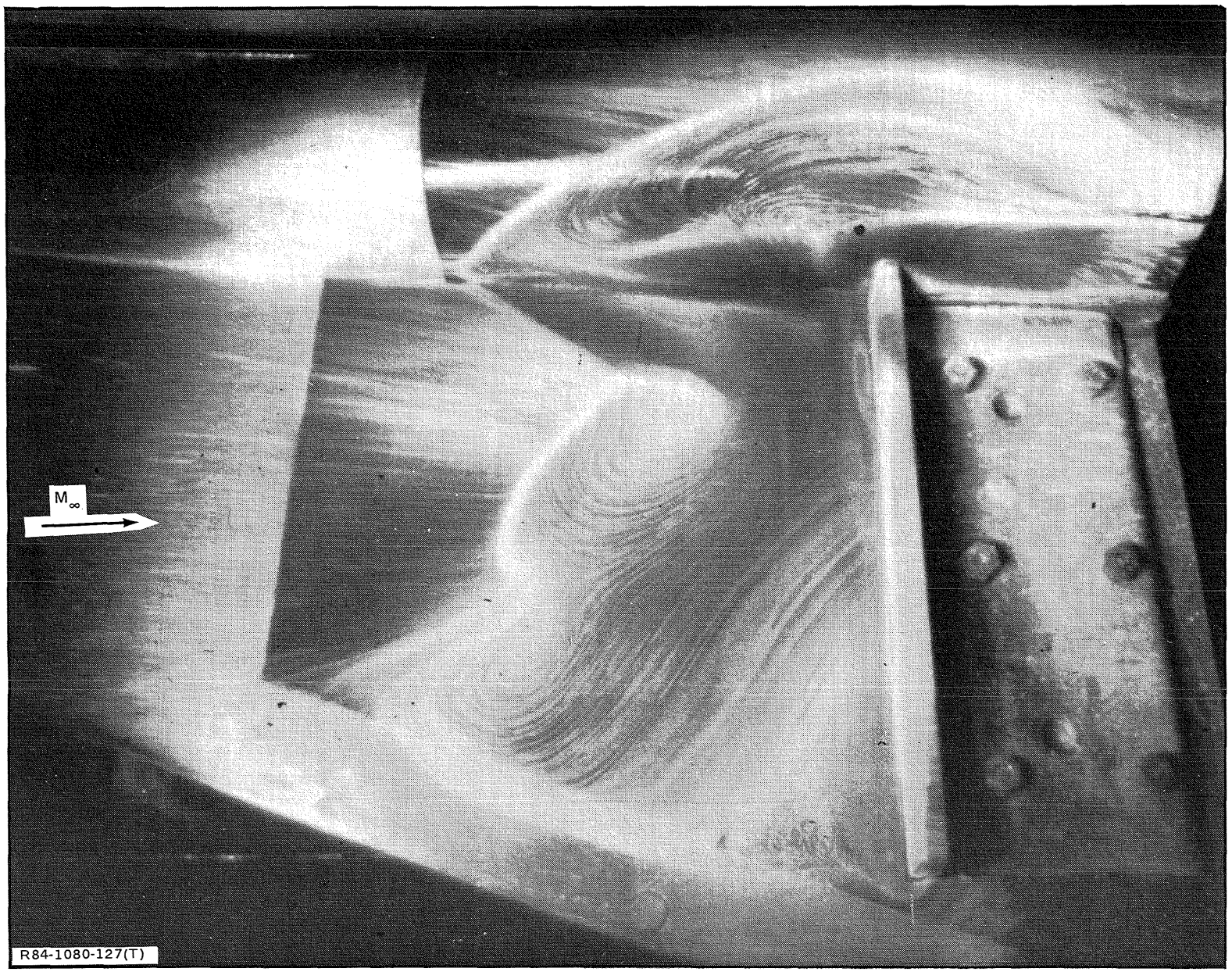

Fig. 127 Low Spoiler – Photograph of Oil Flow Pattern, 70° Swept Wing, Cylindrical Center Body

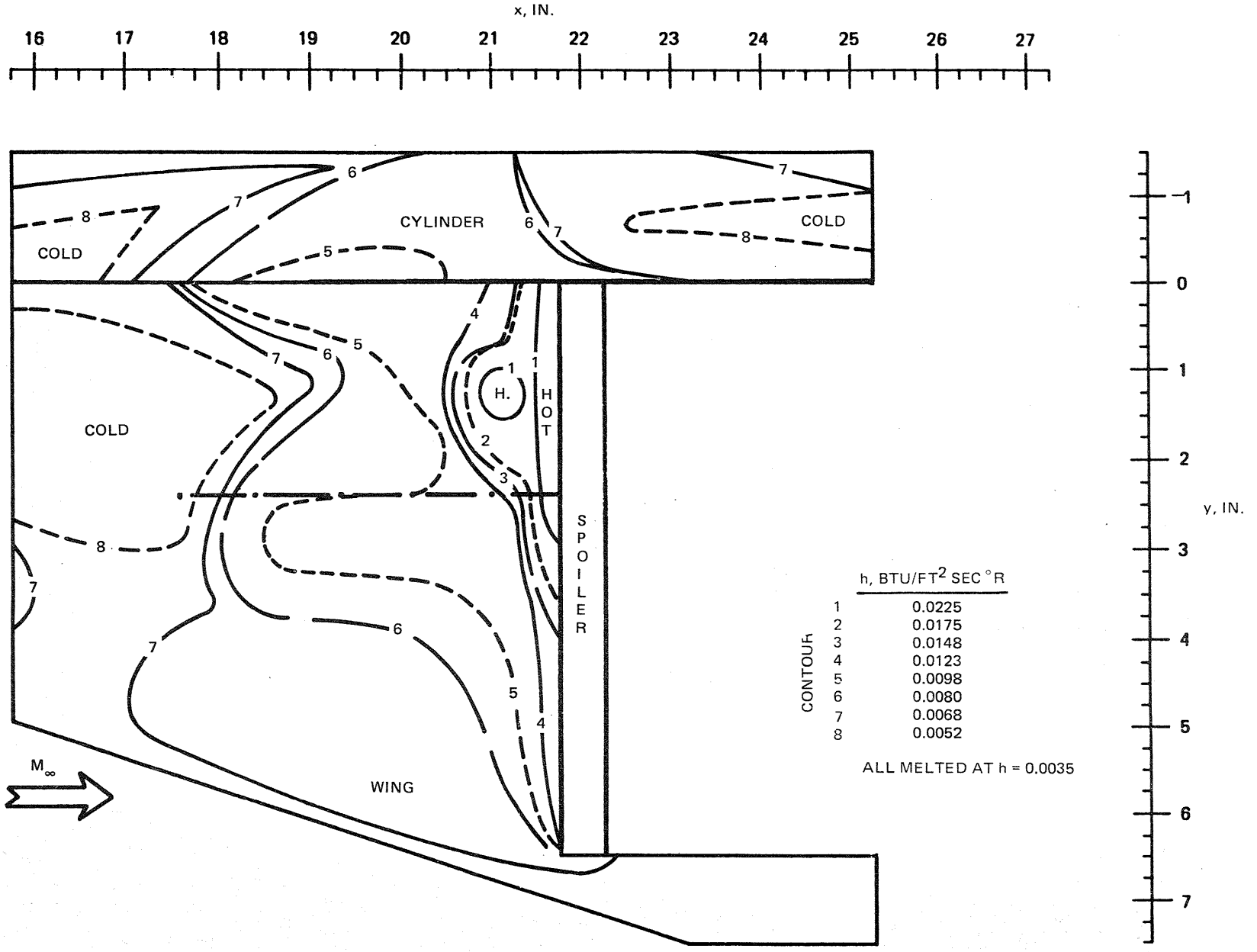

R84-1080-128(T)

Fig. 128 Low Spoiler — Phase Change Results, 70° Swept Wing, Cylindrical Center Body

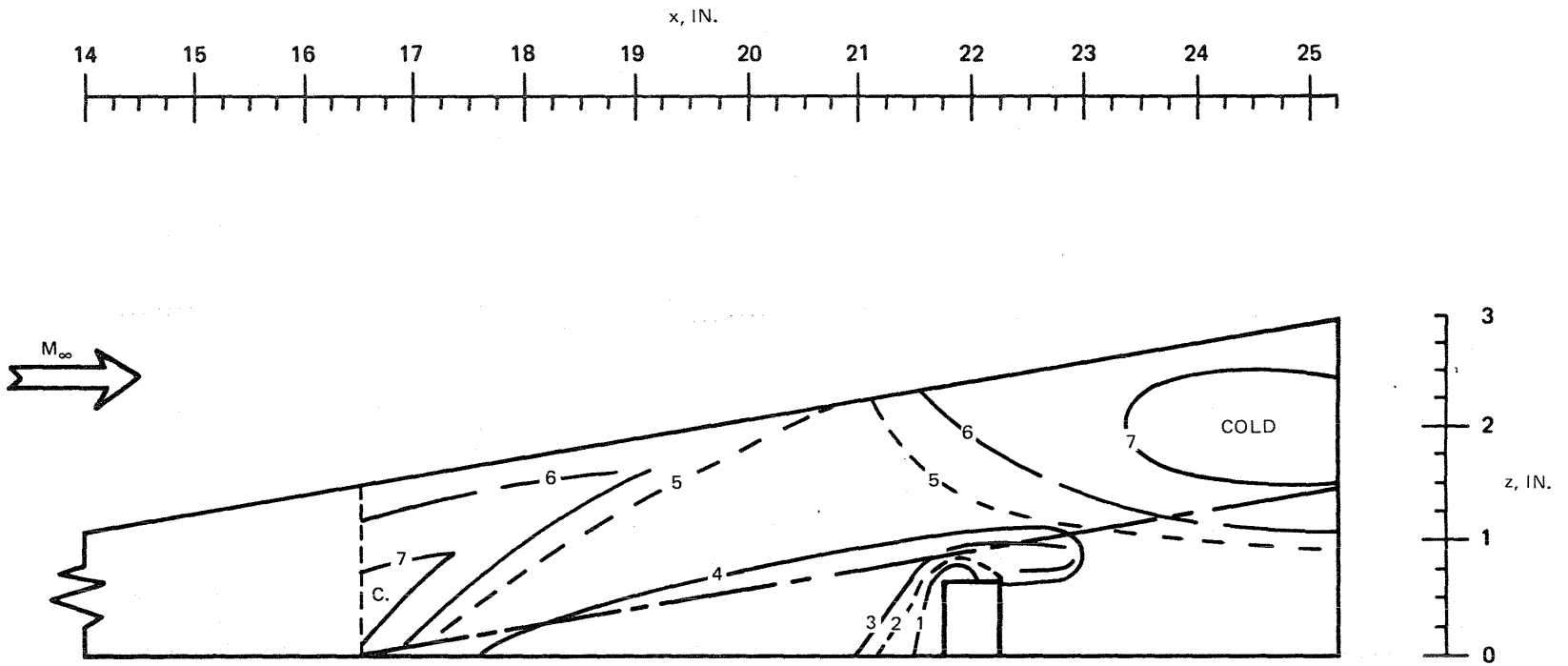

CONTOUR	h, BTU/FT^2 SEC °R
1	0.0225
2	0.0161
3	0.0123
4	0.0098
5	0.0080
6	0.0068
7	0.0052
ALL MELT	0.0035

R84-1080-129(T)

Fig. 129 Low Spoiler – Phase Change Results, Cylindrical Center Body, 70° Swept Wing

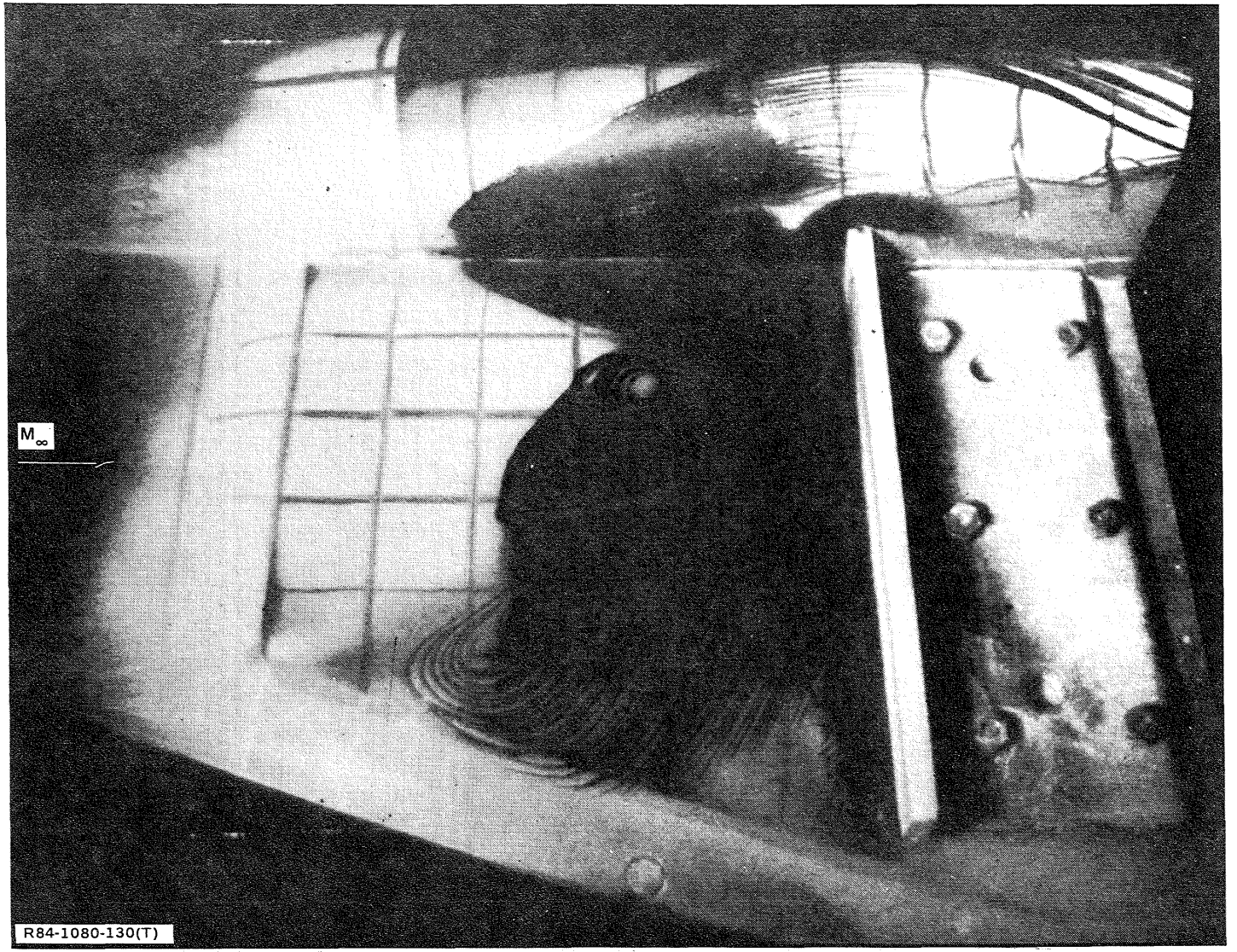

Fig. 130 Low Spoiler — Frame from Motion Picture of Phase Change Coating, 70° Swept Wing, Cylindrical Center Body

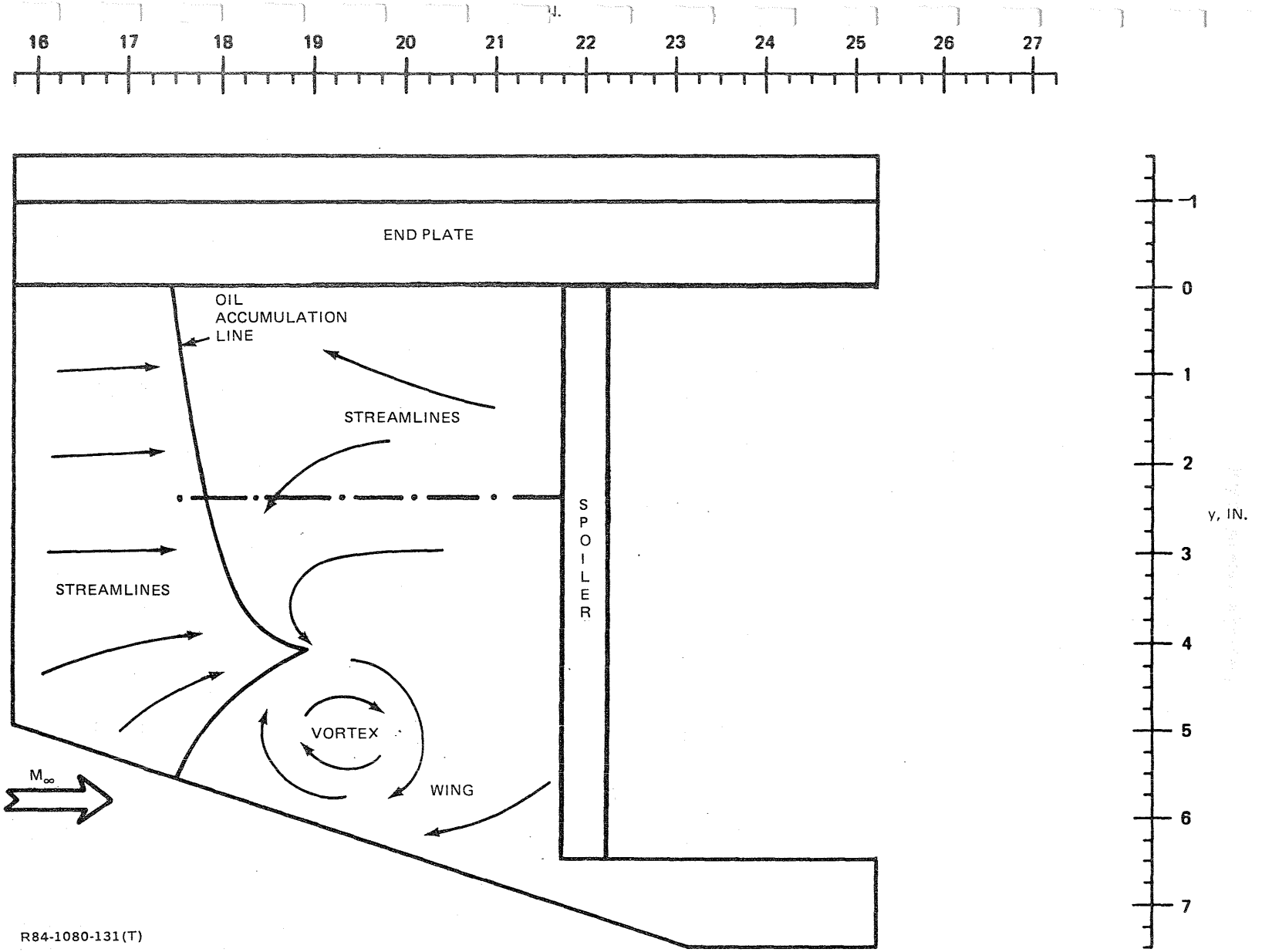

Fig. 131 Low Spoiler – Oil Flow Pattern, 70° Swept Wing, End Plate

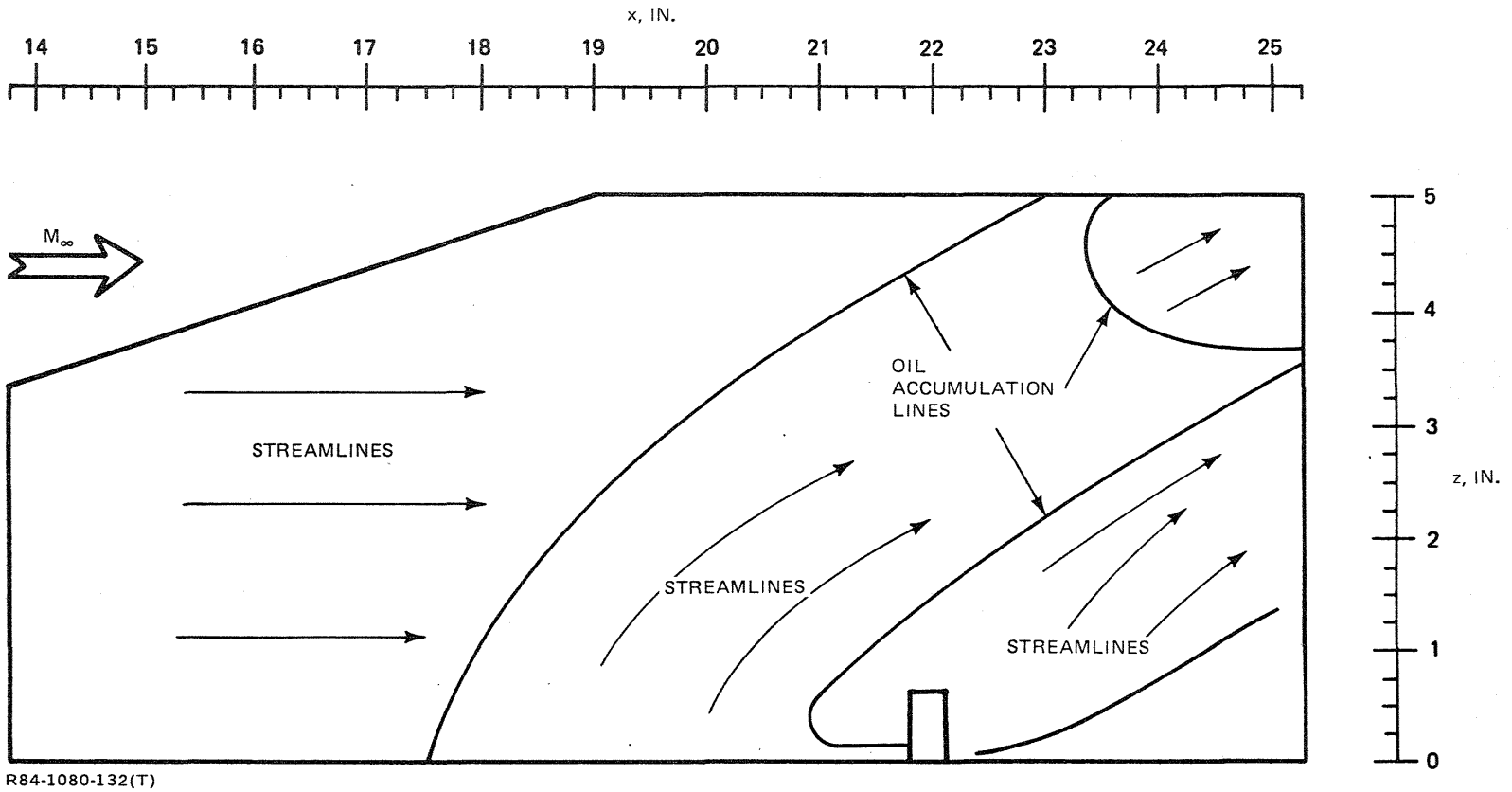

R84-1080-132(T)

Fig. 132 Low Spoiler — Oil Flow Pattern, End Plate, 70° Swept Wing

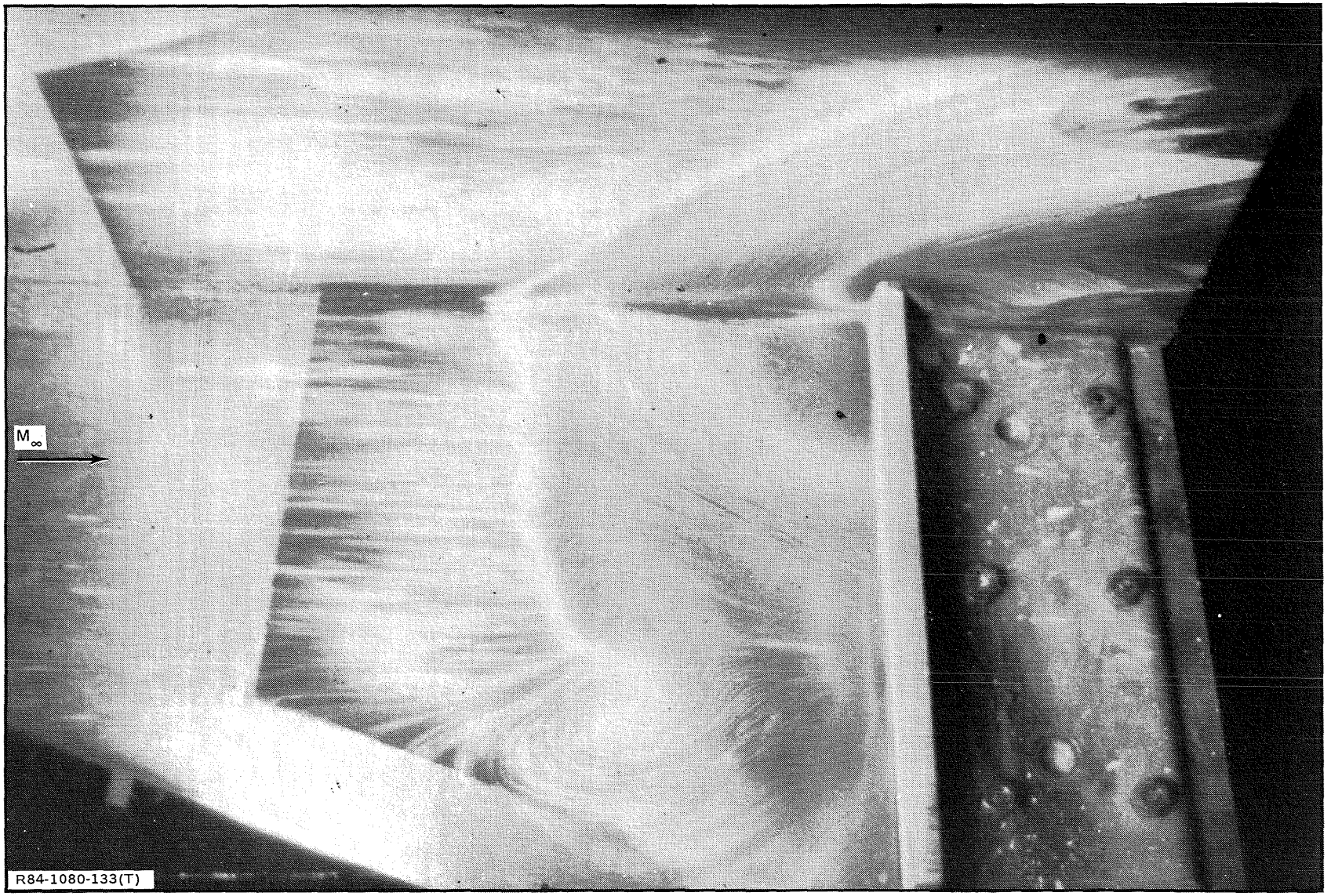

Fig. 133 Low Spoiler – Photograph of Oil Flow Pattern, 70° Swept Wing, End Plate

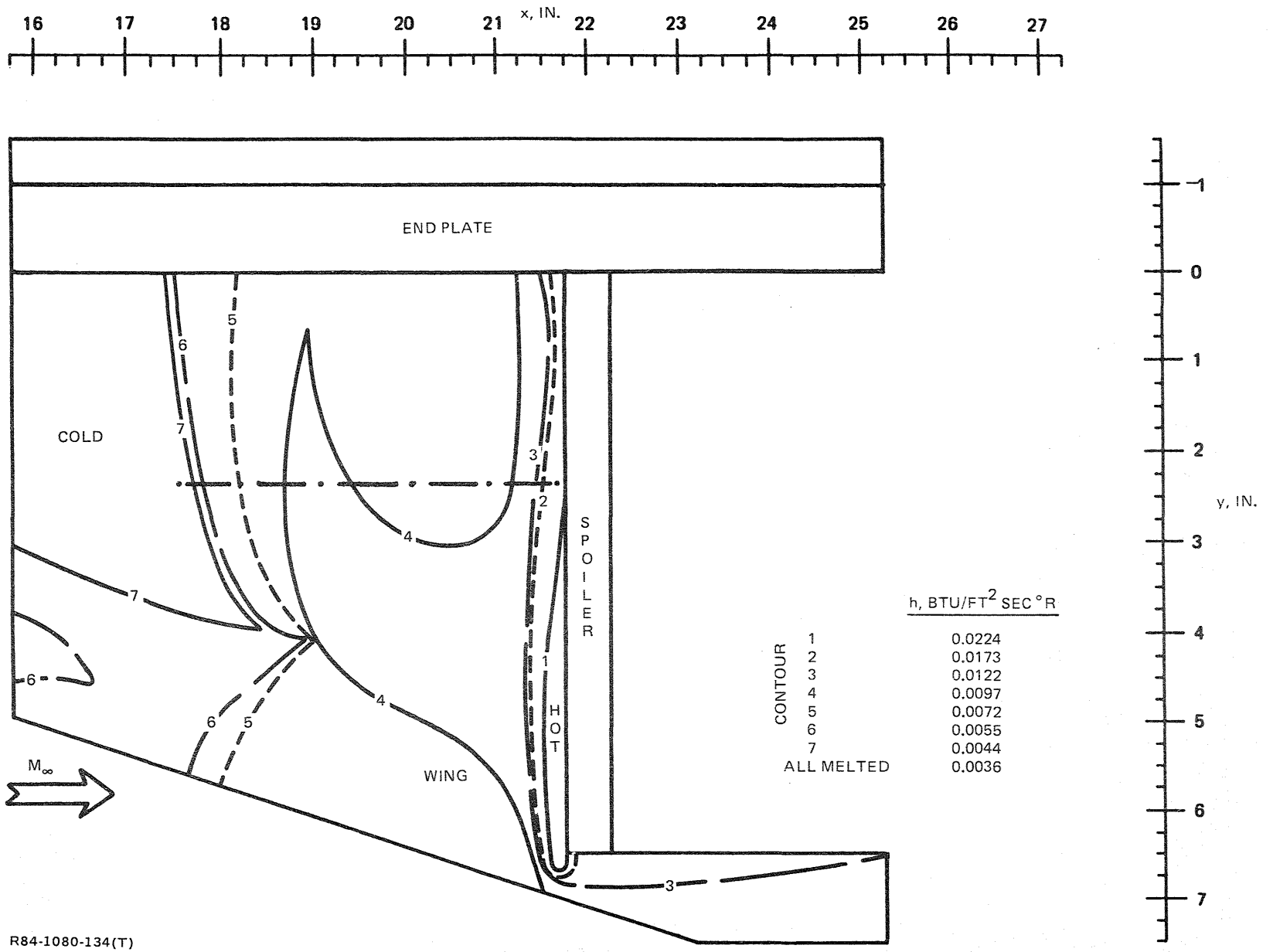

Fig. 134 Low Spoiler — Phase Change Results, 70° Swept Wing, End Plate

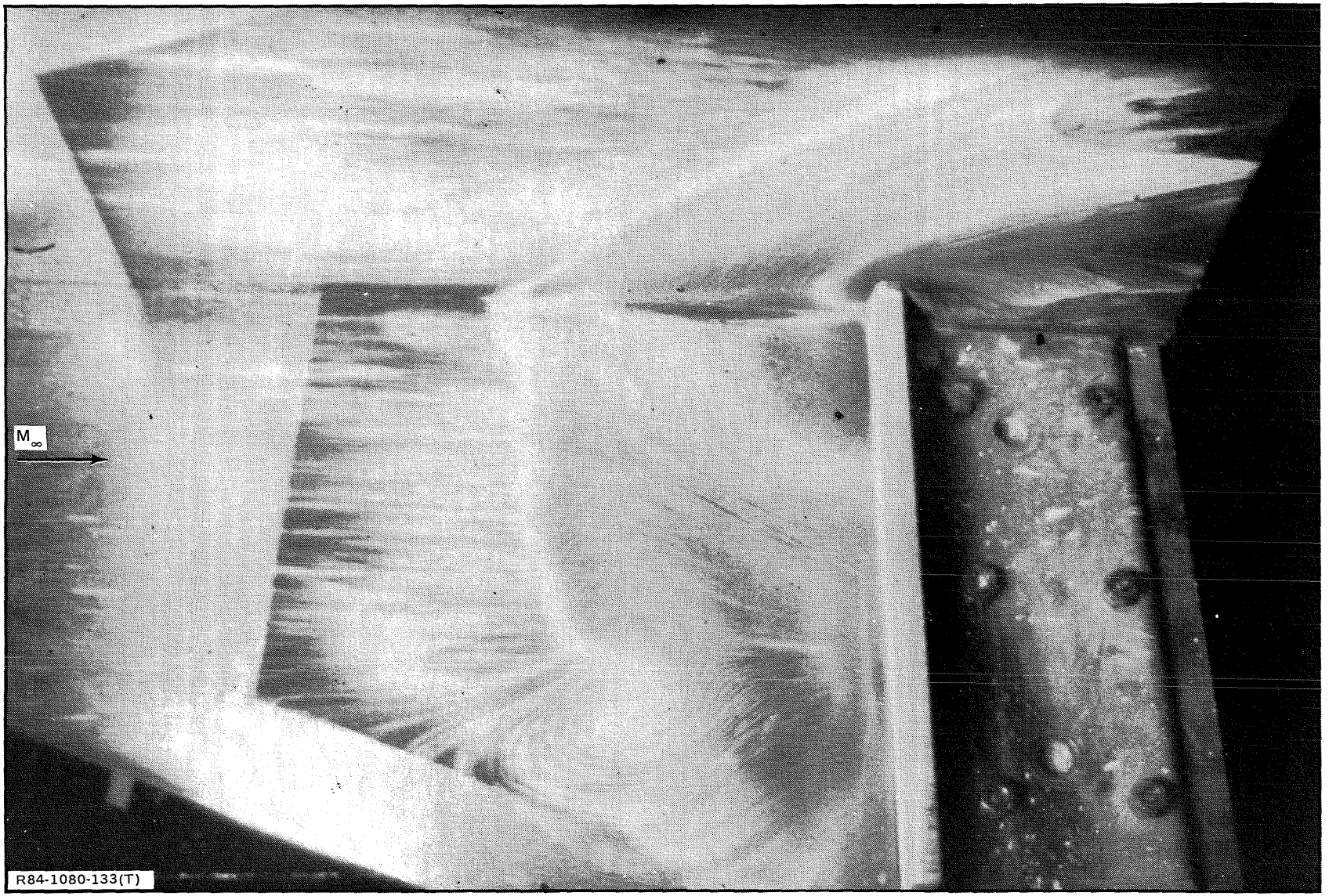

Fig. 133 Low Spoiler – Photograph of Oil Flow Pattern, 70° Swept Wing, End Plate

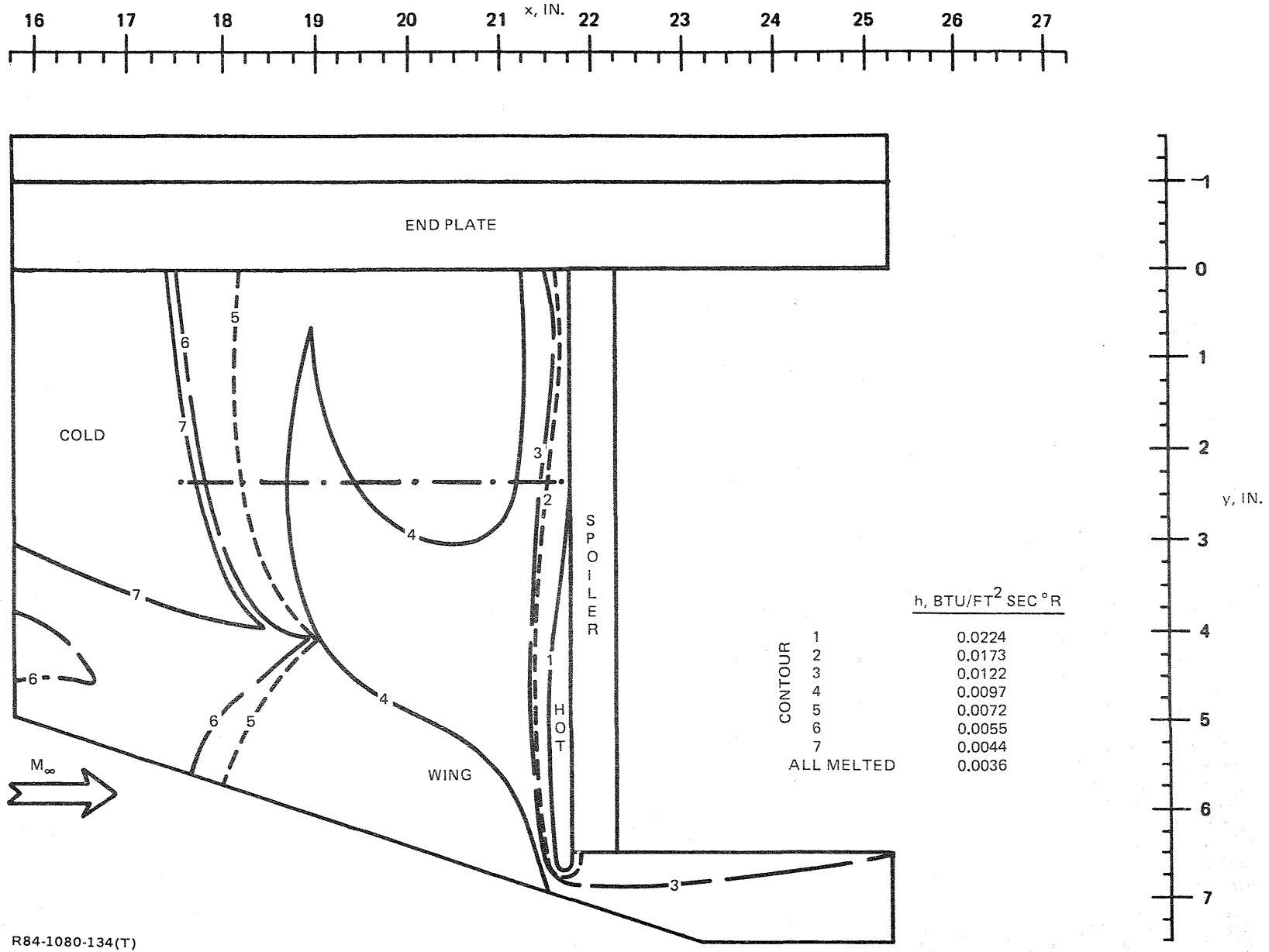

Fig. 134 Low Spoiler – Phase Change Results, 70° Swept Wing, End Plate

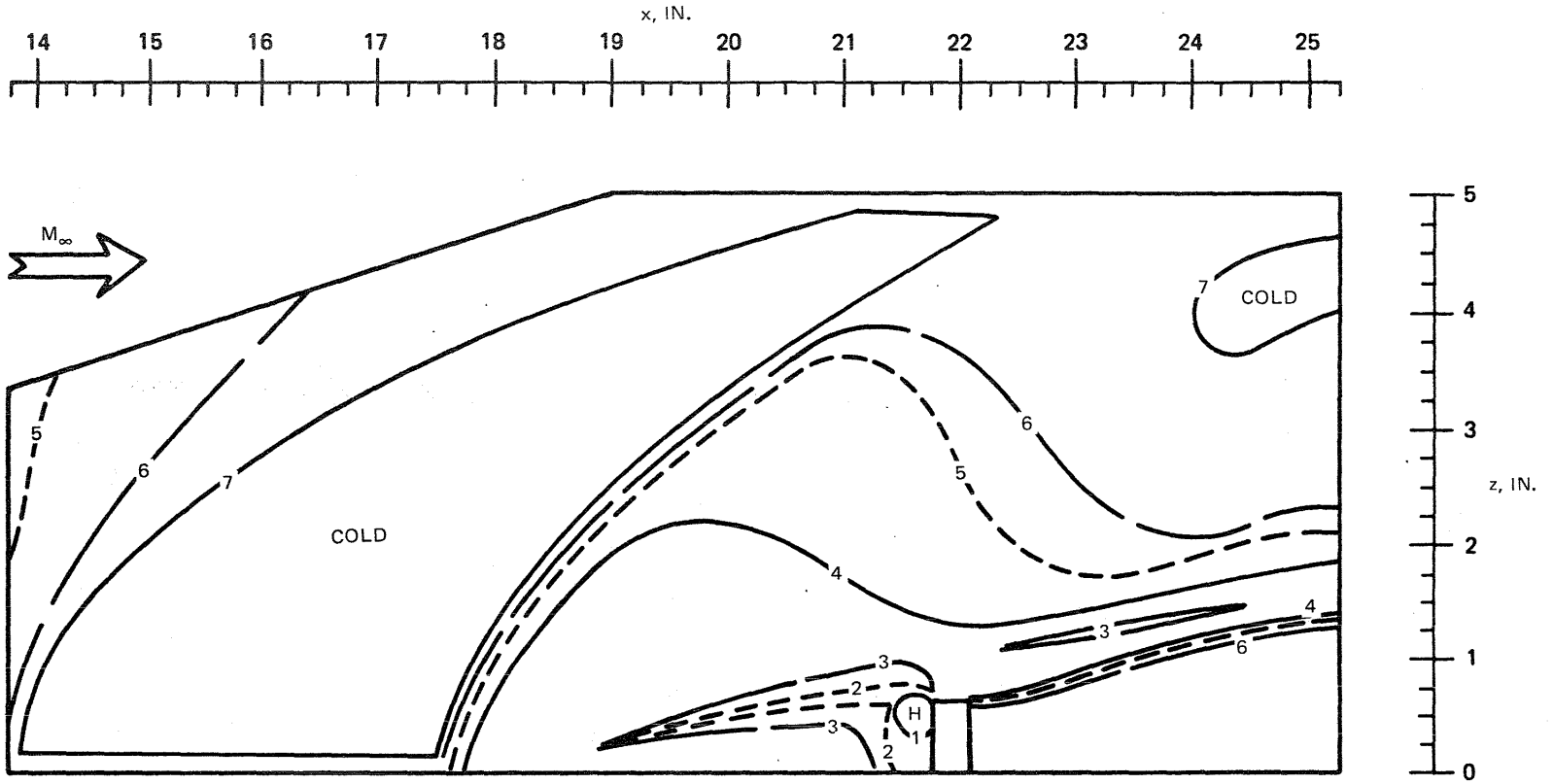

h, BTU/FT^2 SEC °R

CONTOUR	
1	0.0173
2	0.0122
3	0.0097
4	0.0072
5	0.0055
6	0.0044
7	0.0038
ALL MELT	0.0036

R84-1080-135(T)

Fig. 135 Low Spoiler – Phase Change Results, End Plate, 70° Swept Wing

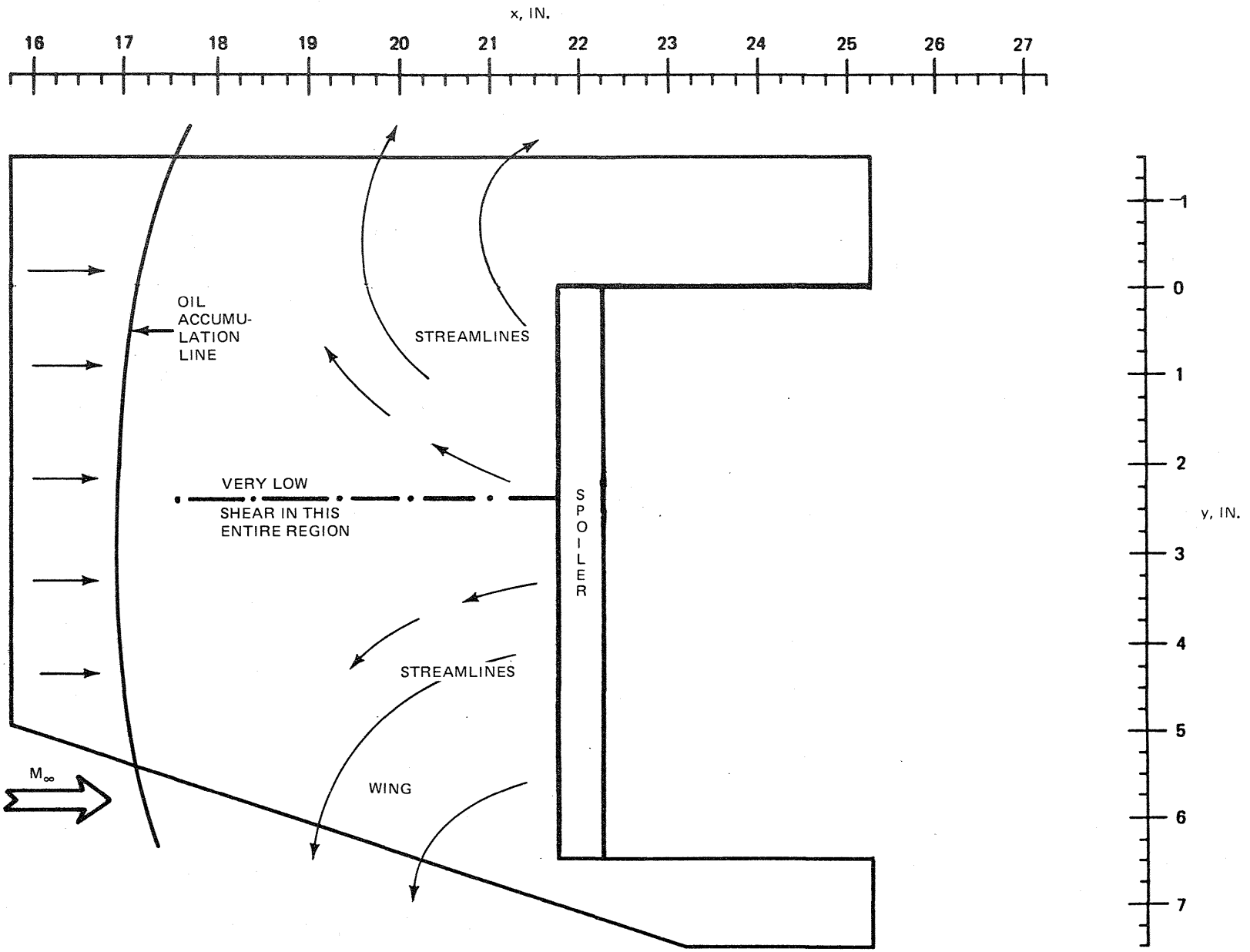

Fig. 136 High Spoiler — Oil Flow Pattern, Unswept Wing, No Center Body

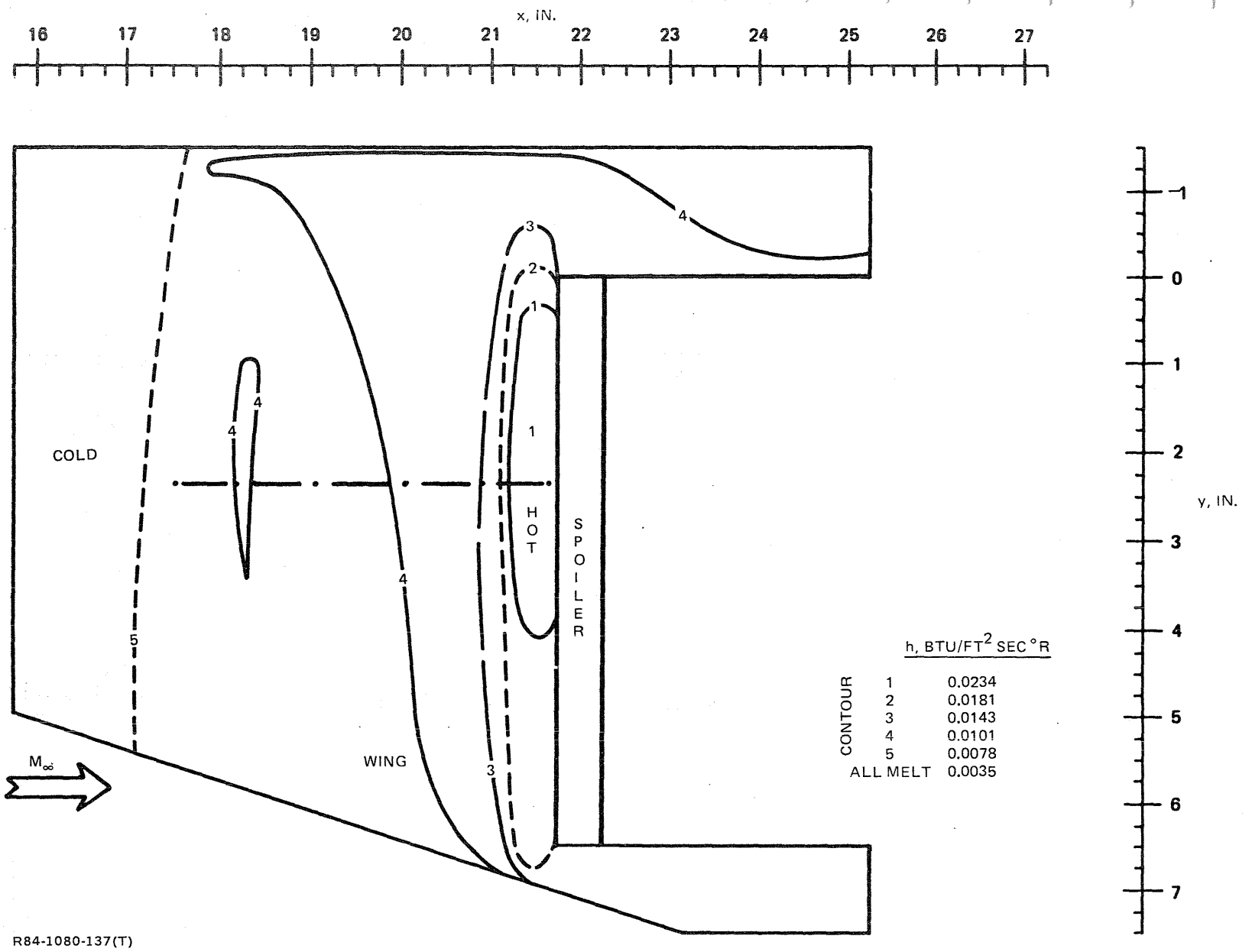

Fig. 137 High Spoiler — Phase Change Results, Unswept Wing, No Center Body

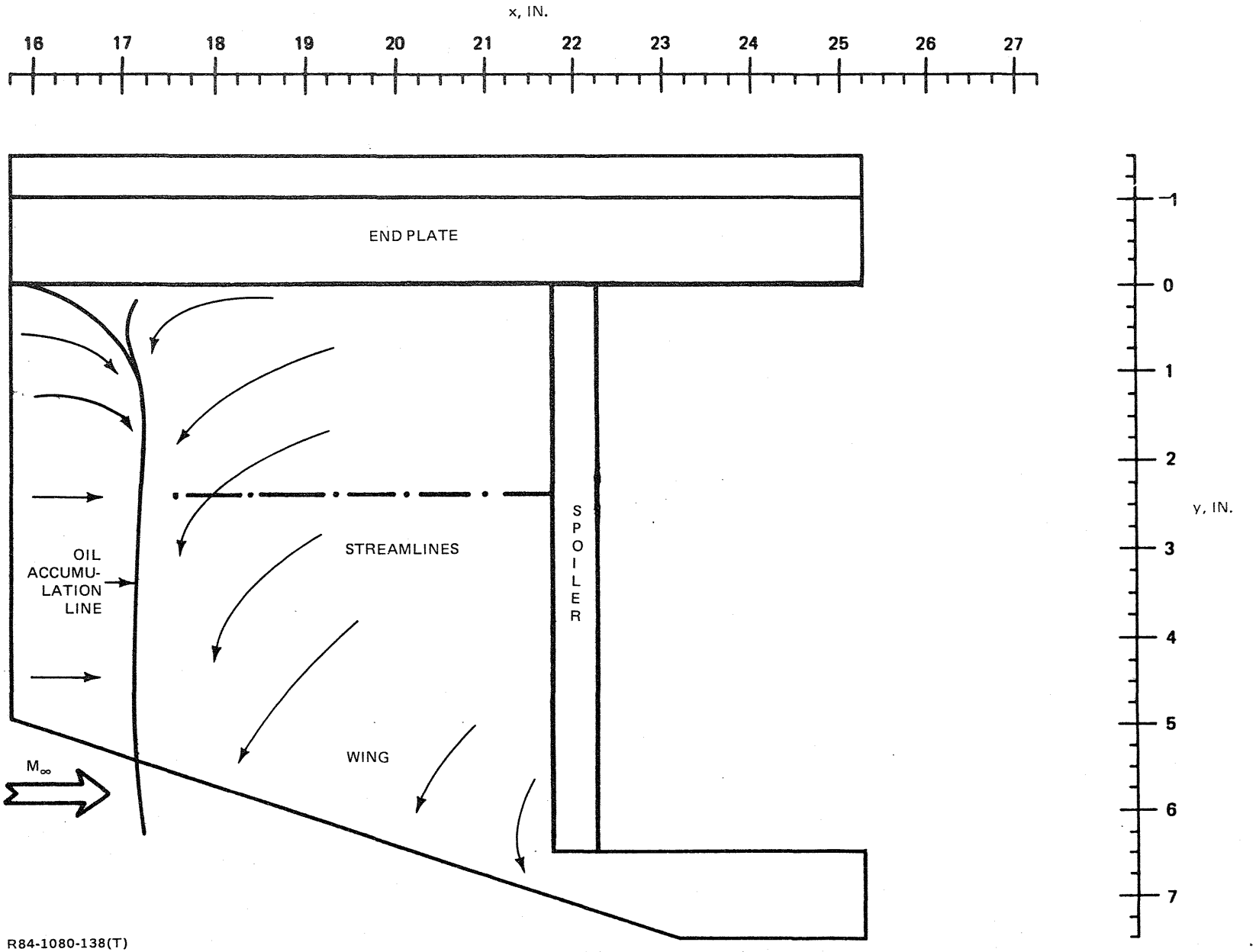

Fig. 138 High Spoiler – Oil Flow Pattern, Unswept Wing, End Plate

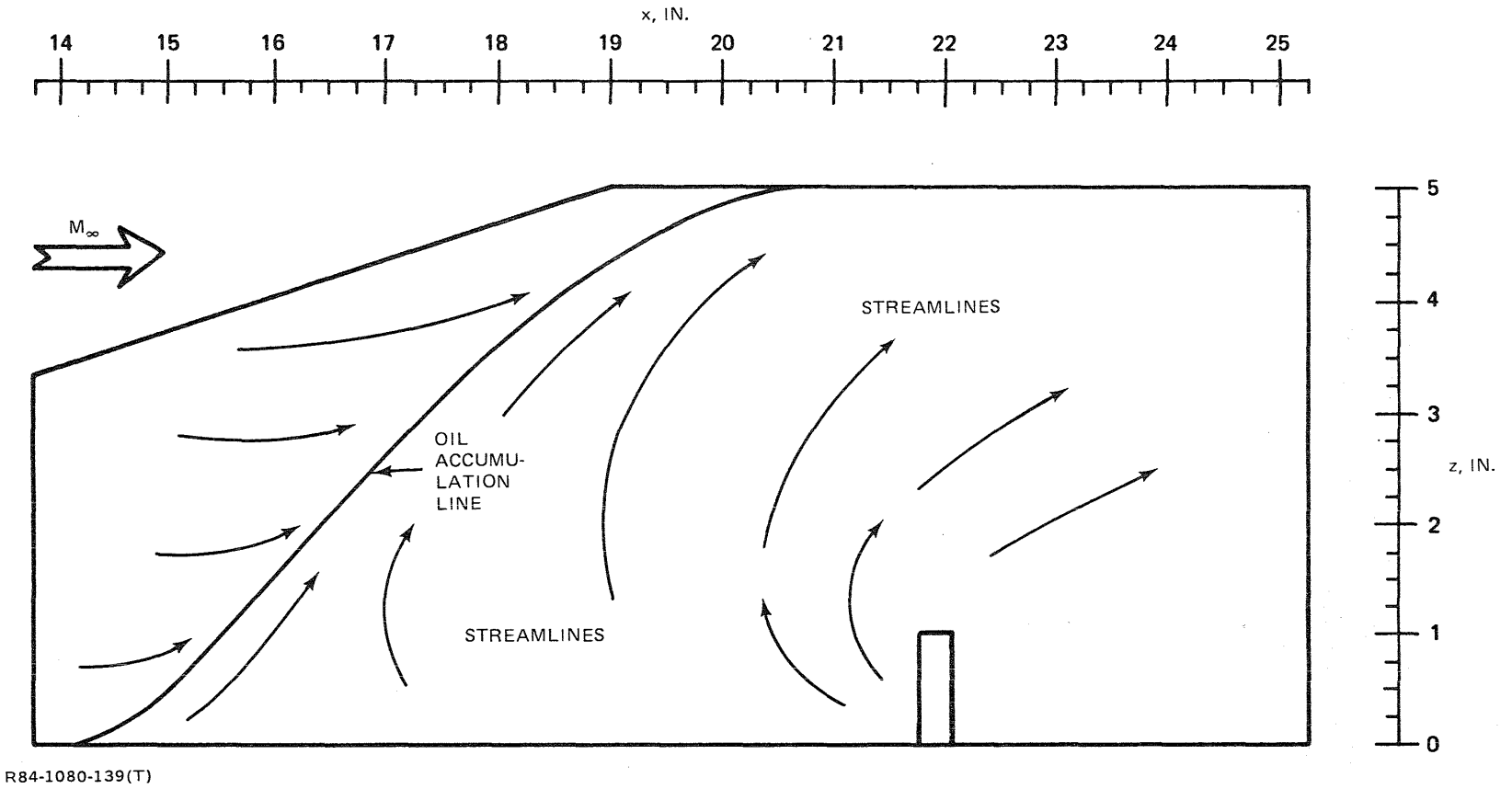

Fig. 139 High Spoiler — Oil Flow Pattern, End Plate, Unswept Wing

Fig. 140 High Spoiler — Photograph of Oil Flow, Unswept Wing, End Plate

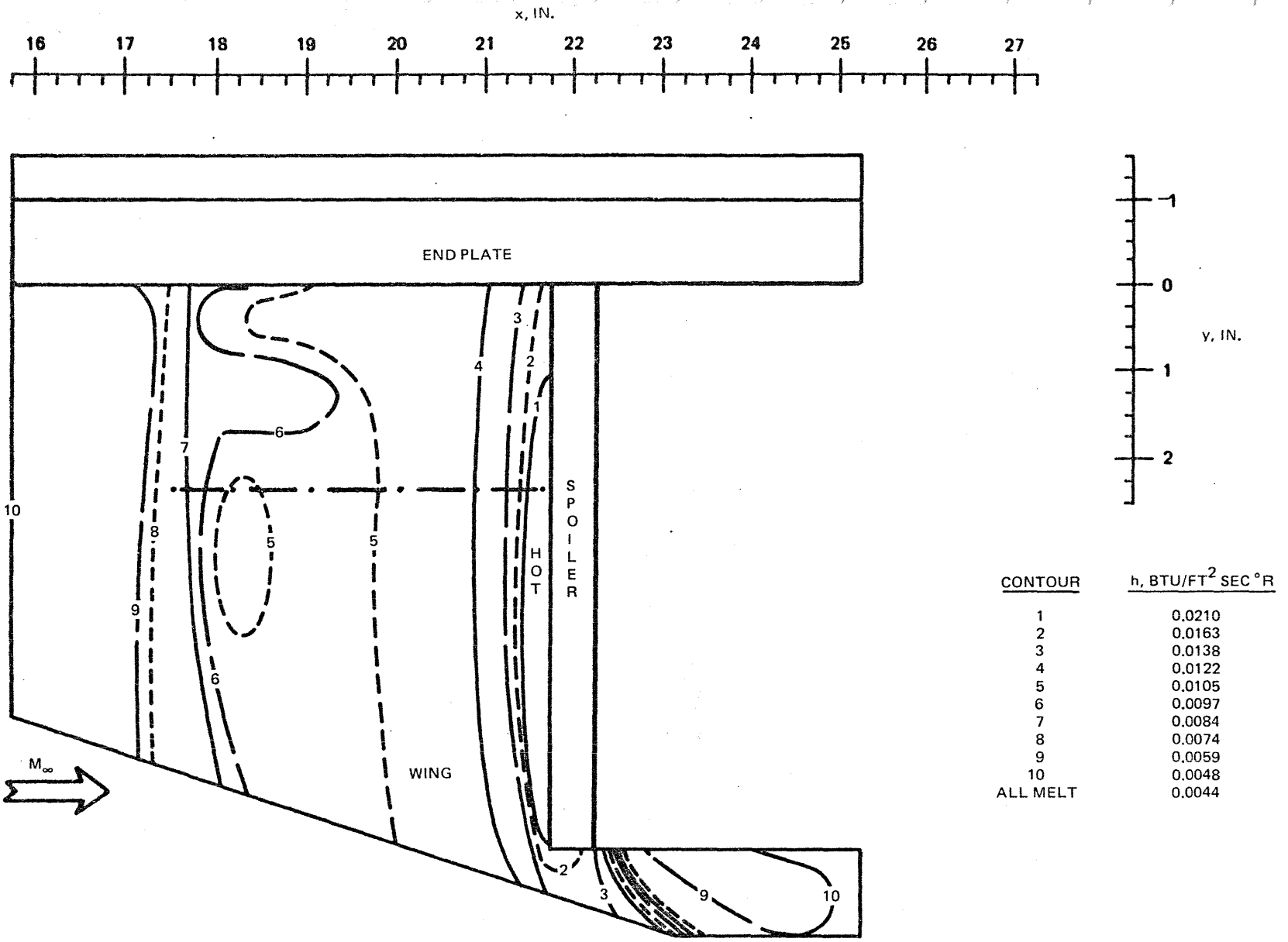

Fig. 141 High Spoiler – Phase Change Result, Unswept Wing, End Plate

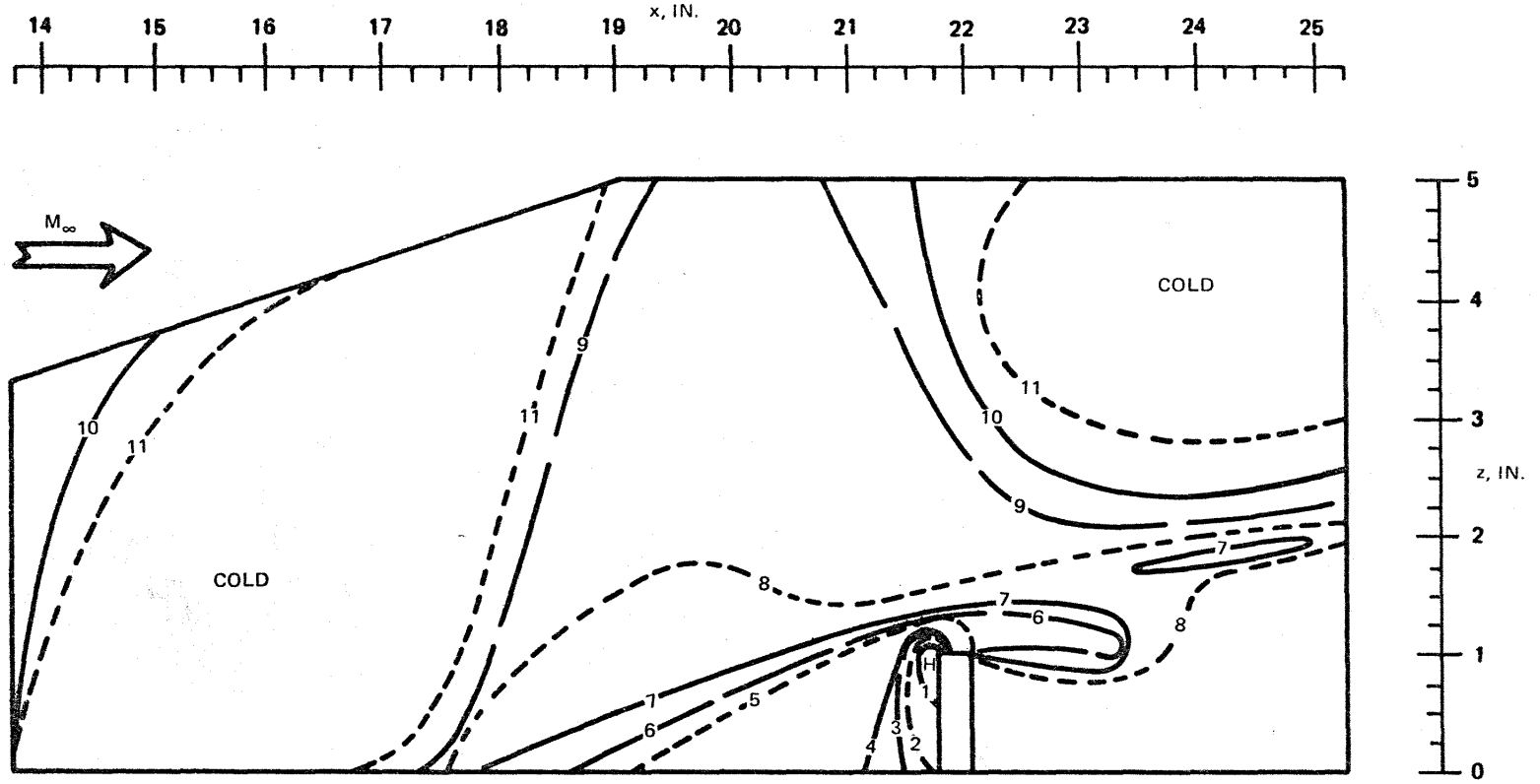

CONTOUR	h, BTU/FT^2 SEC °R
1	0.0210
2	0.0163
3	0.0138
4	0.0122
5	0.0105
6	0.0097
7	0.0084
8	0.0074
9	0.0059
10	0.0053
11	0.0048

ALL MELTED
AT h = 0.0044

R84-1080-142(T)

Fig. 142 High Spoiler – Phase Change Results, End Plate, Unswept Wing

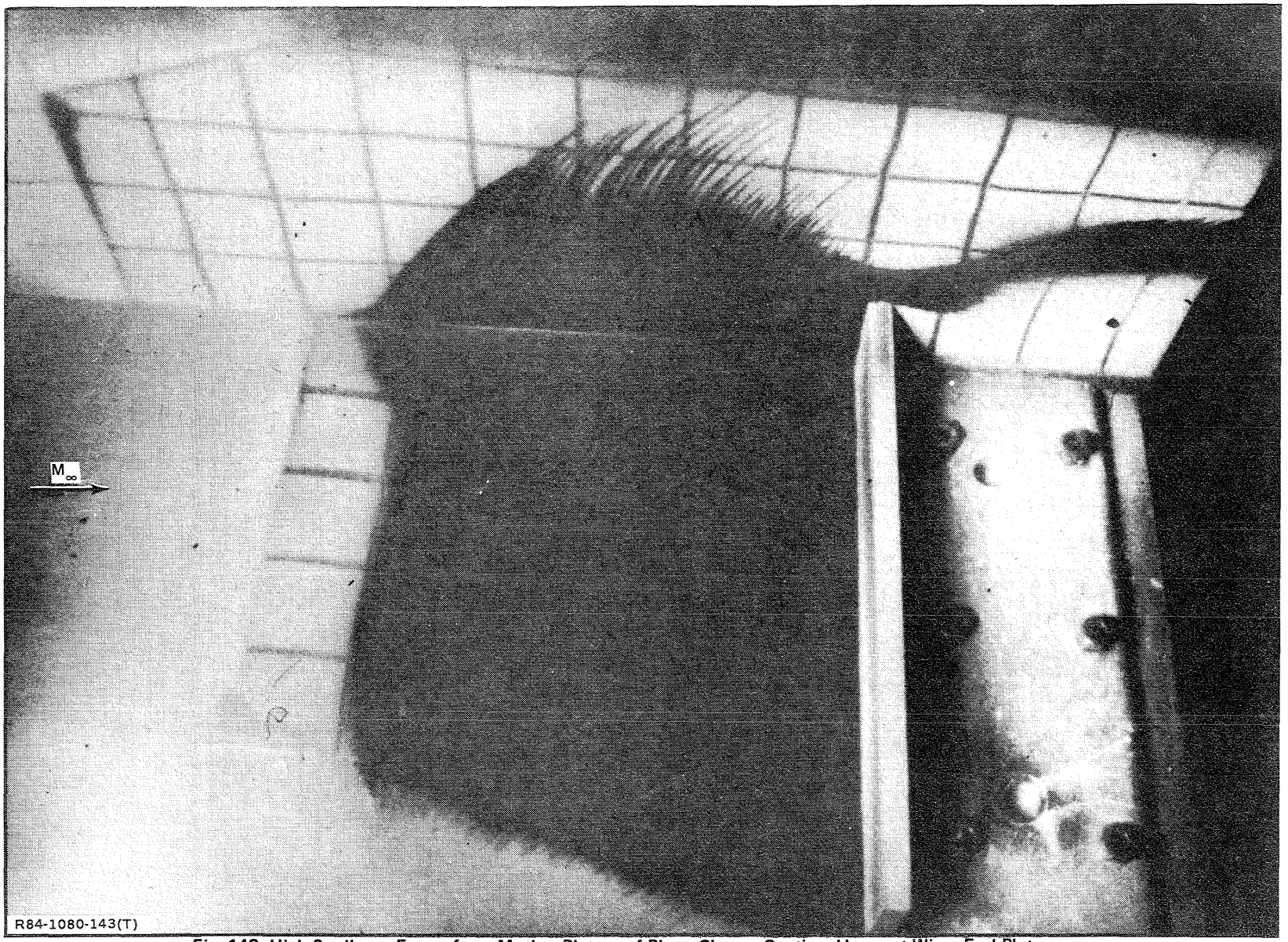

Fig. 143 High Spoiler — Frame from Motion Picture of Phase Change Coating, Unswept Wing, End Plate

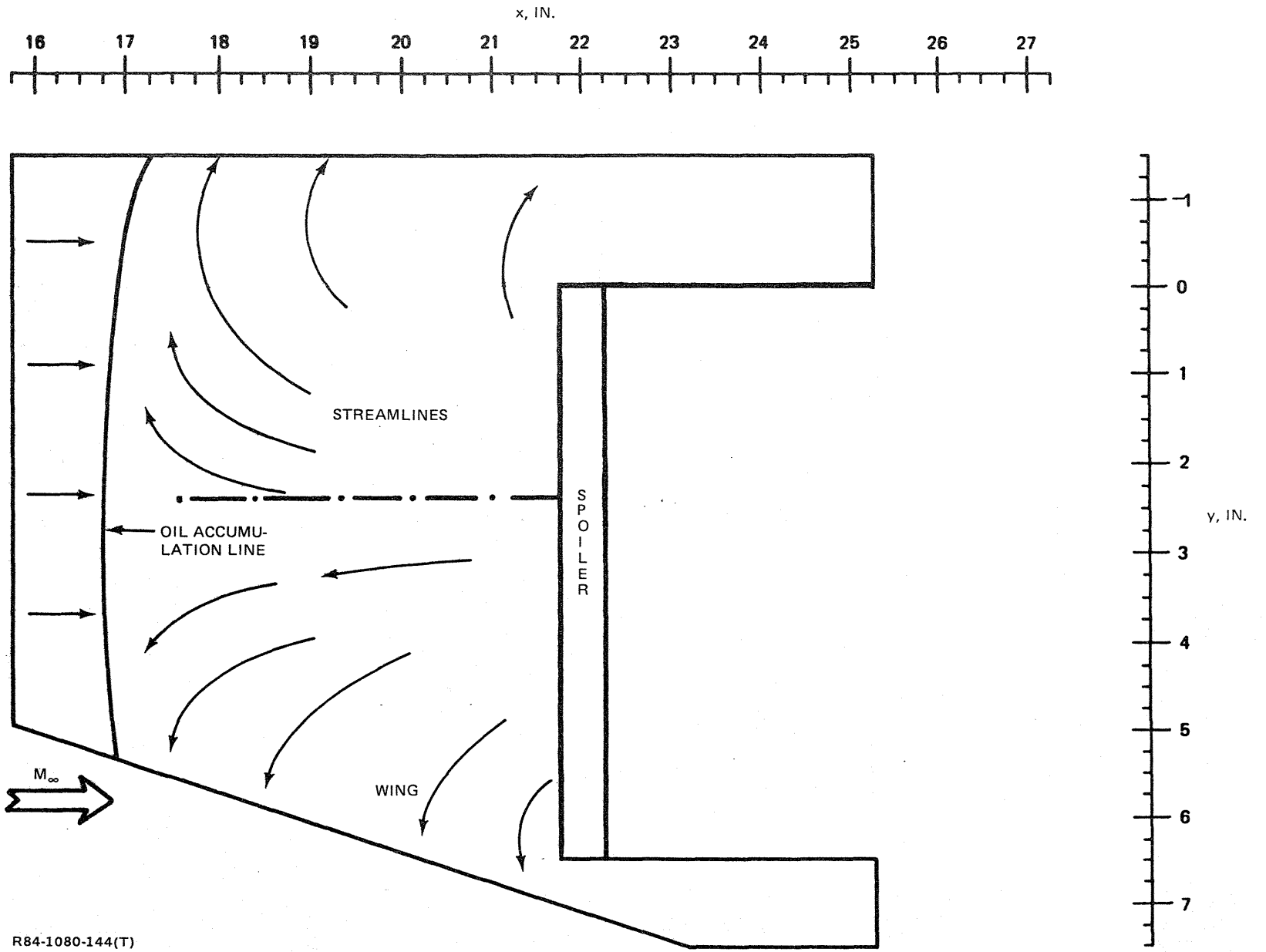

Fig. 144 High Spoiler – Oil Flow Pattern, 50° Swept Wing, No Center Body

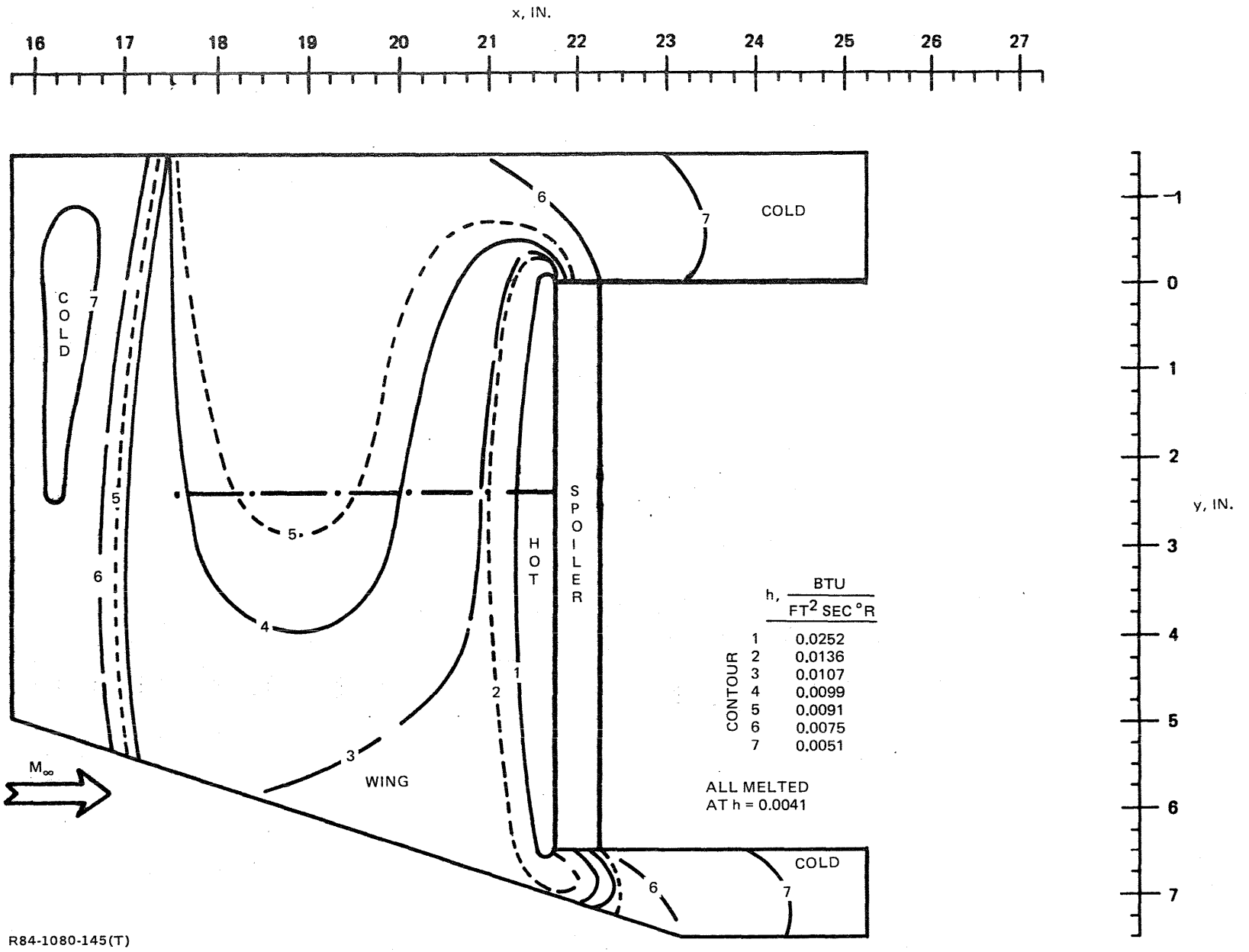

Fig. 145 High Spoiler – Phase Change Results, 50° Swept Wing, No Center Body

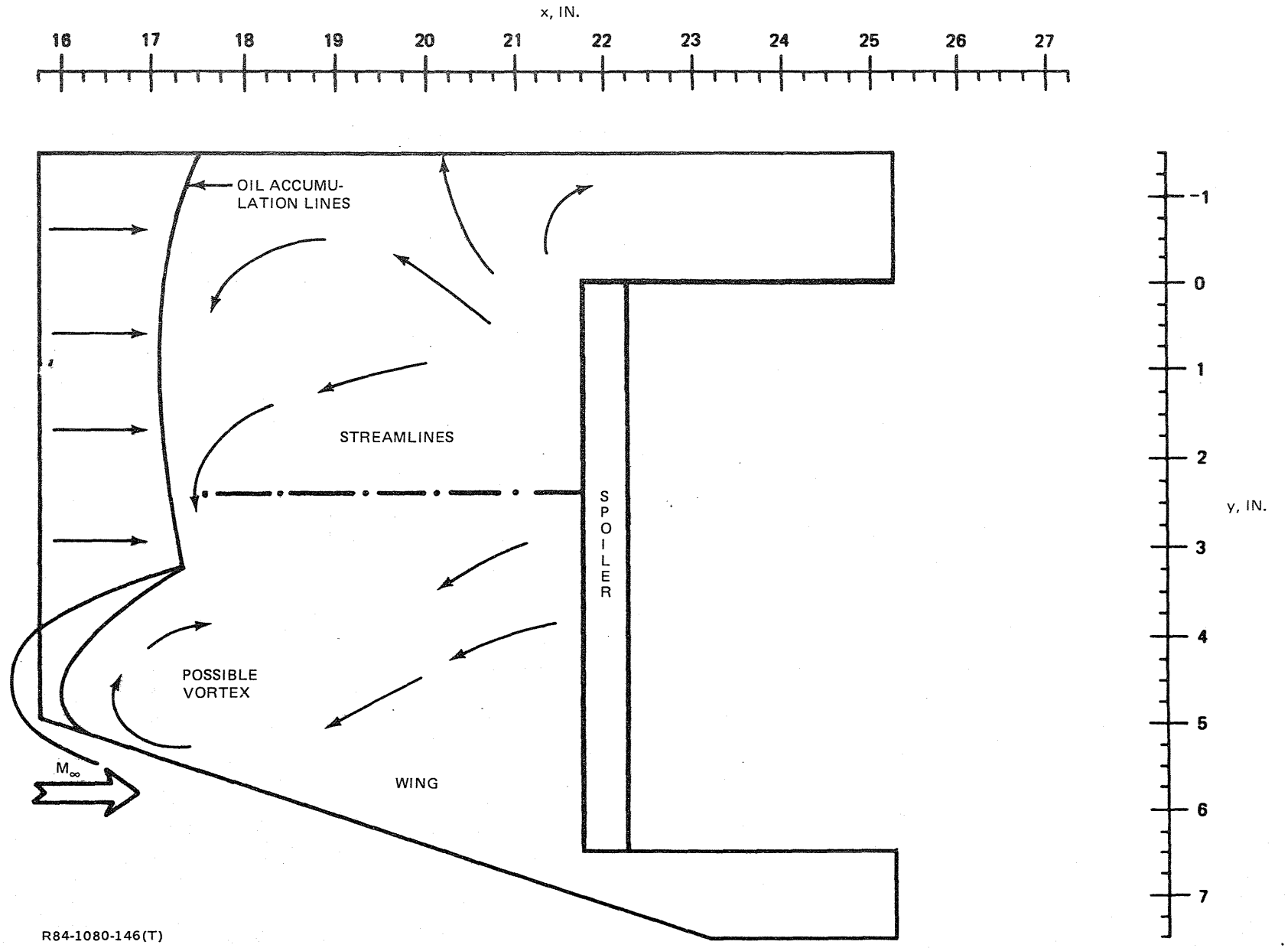

Fig. 146 High Spoiler – Oil Flow Pattern, 70° Swept Wing, No Center Body

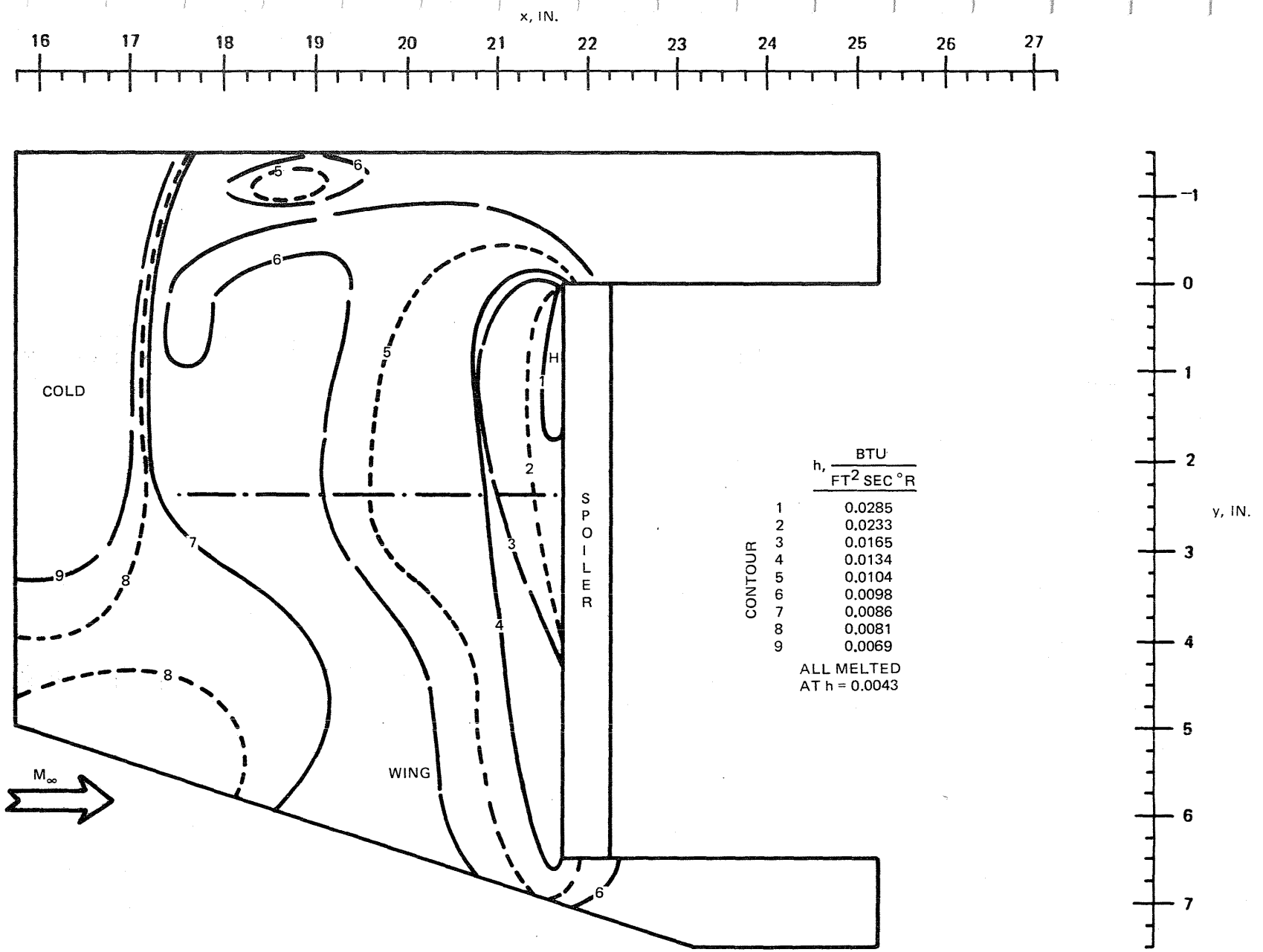

R84-1080-147(T)

Fig. 147 High Spoiler — Phase Change Results, 70° Swept Wing, No Center Body

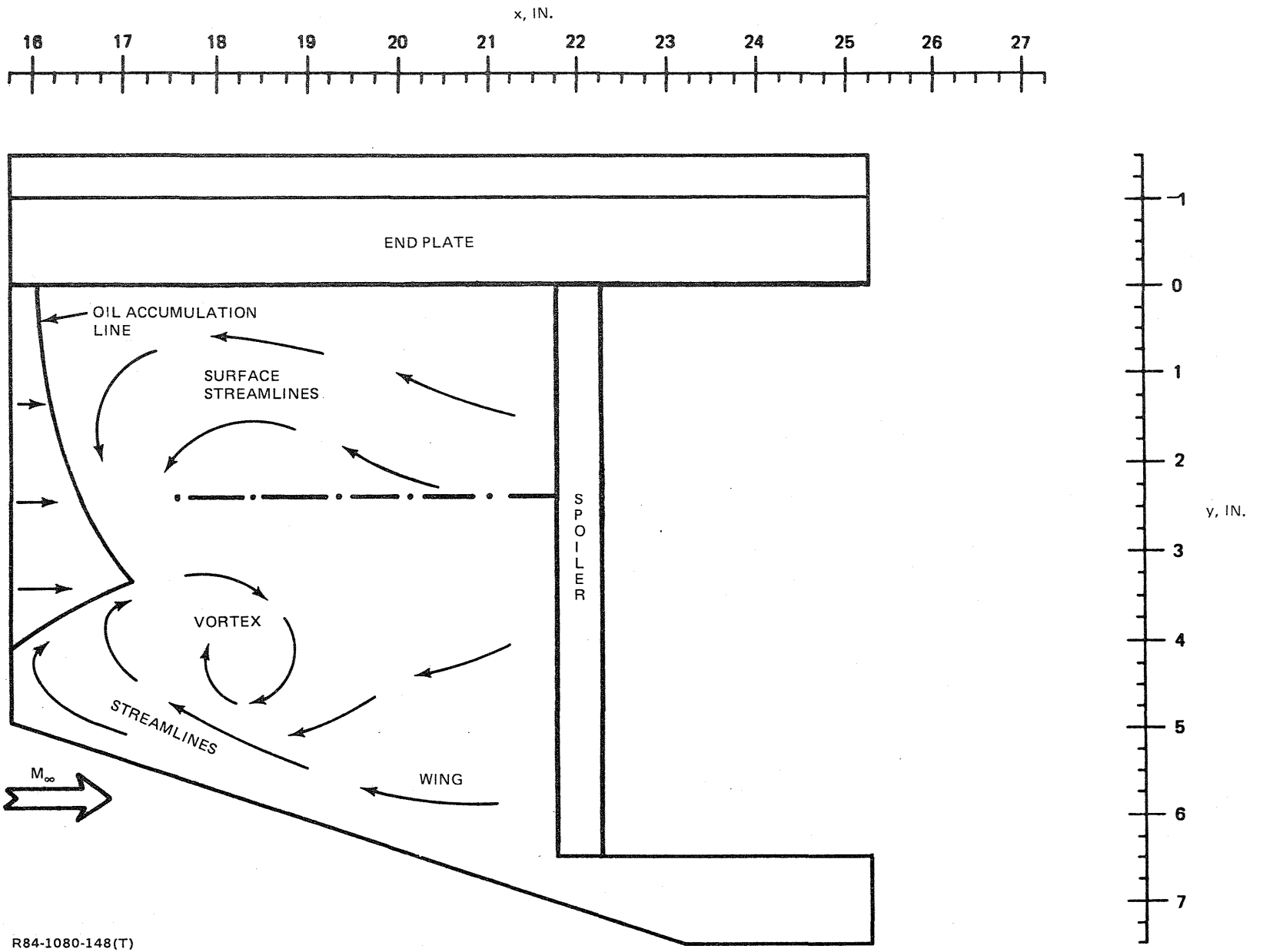

Fig. 148 High Spoiler – Oil Flow Pattern, 70° Swept Wing, End Plate

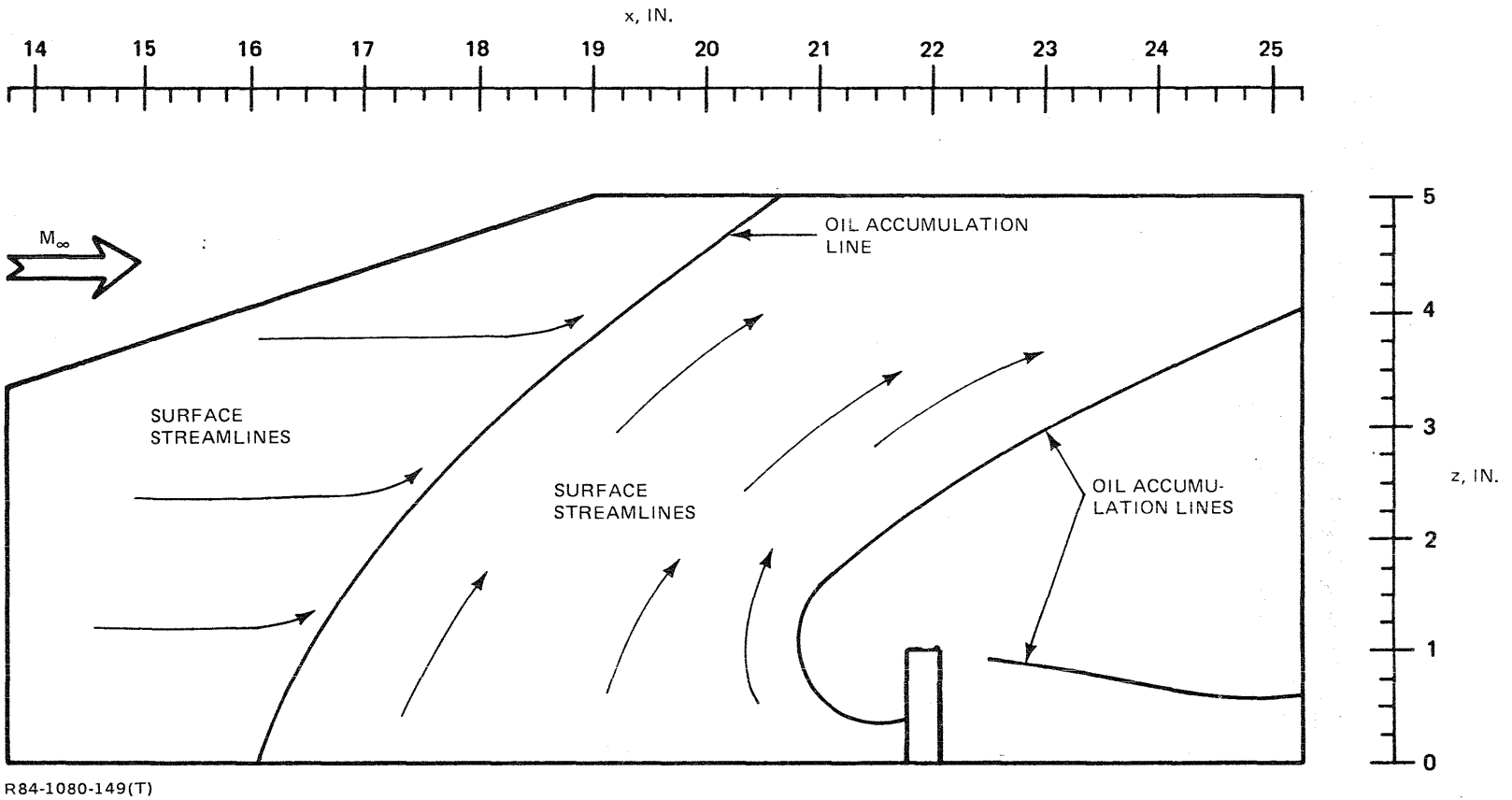

R84-1080-149(T)

Fig. 149 High Spoiler — Oil Flow Pattern, End Plate, 70° Swept Wing

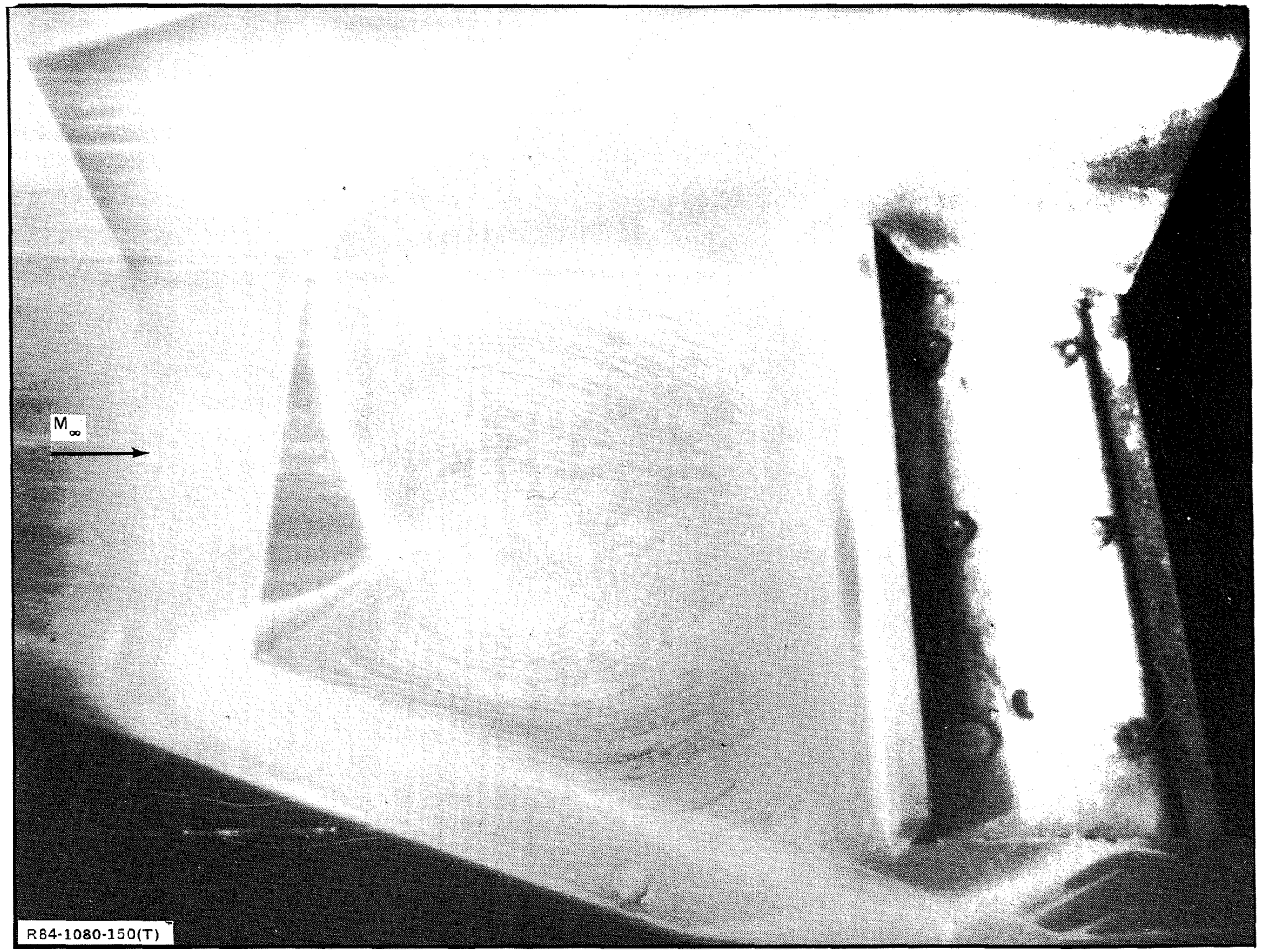

Fig. 150 High Spoiler — Photograph of Oil Flow Pattern, 70° Swept Wing, End Plate

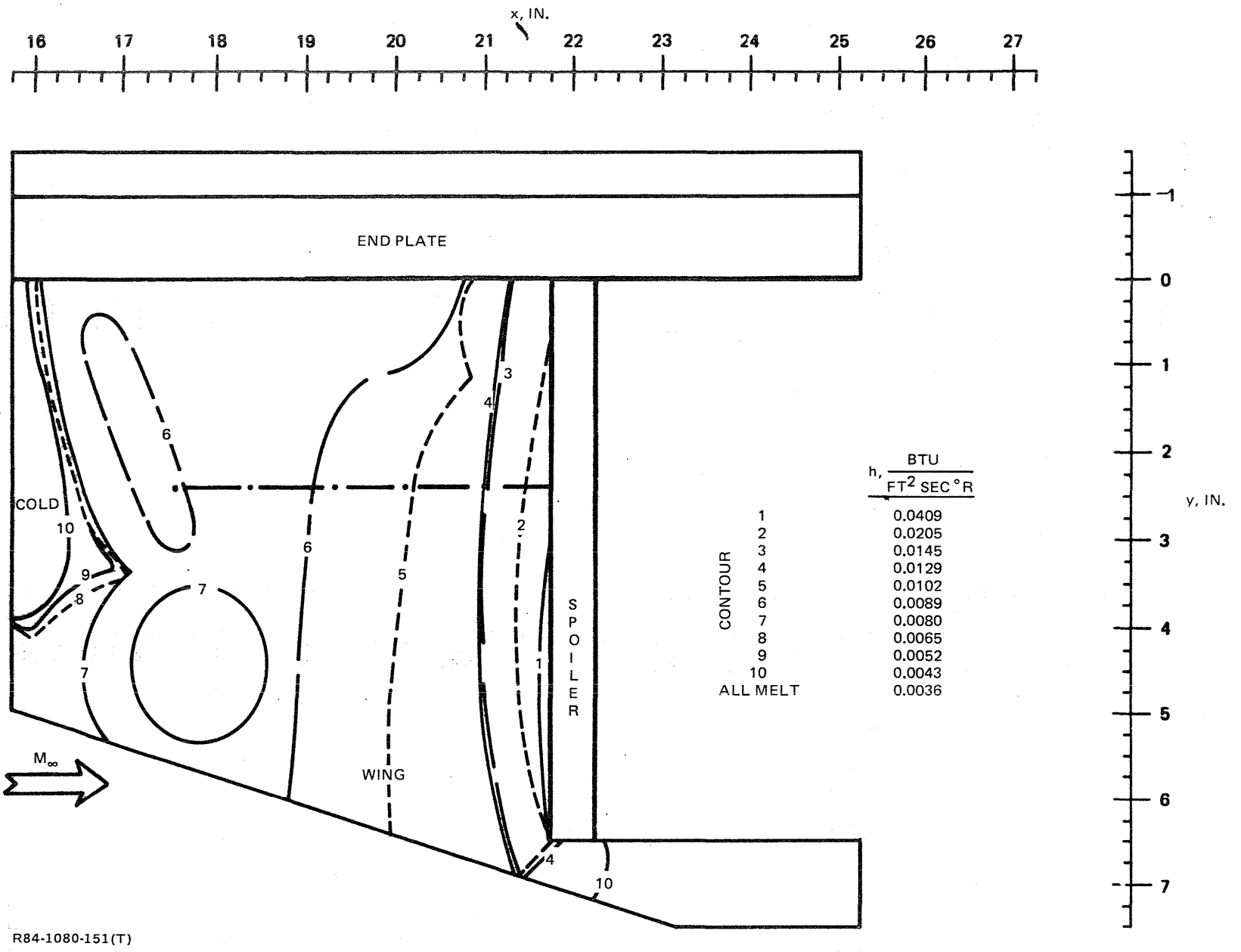

Fig. 151 High Spoiler — Phase Change Results, 70° Swept Wing, End Plate

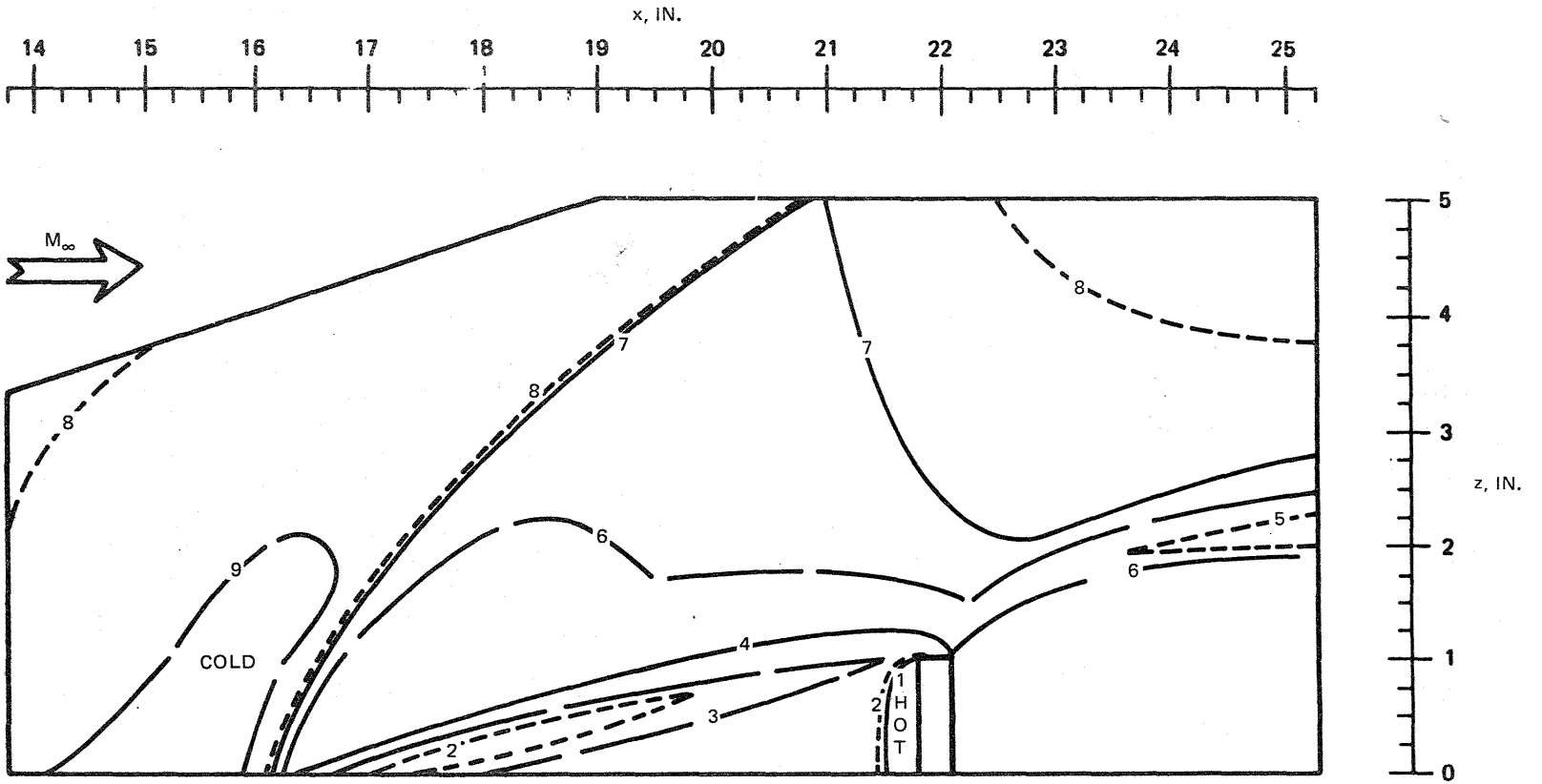

CONTOUR	h, BTU/FT^2 SEC °R
1	0.0145
2	0.0129
3	0.0102
4	0.0089
5	0.0080
6	0.0065
7	0.0052
8	0.0043
9	0.0038
ALL MELT	0.0035

R84-1080-152(T)

Fig. 152 High Spoiler – Phase Change Results, End Plate, 70° Swept Wing

End of Document